Functional characterisation of the activities and interactions of Gram-negative penicillin-binding proteins PBP1b and PBP3

Katie Smart

A thesis submitted in partial fulfilment of the requirements for the degree of Doctor of Philosophy

University of Warwick
Warwick Medical School

September 2019

Table of Contents

List of tables

List of figures

Acknowledgements

I would firstly like to thank the Warwick MRC-DTP and the MRC for providing me with both the opportunity and the funding to complete this PhD. I am also hugely thankful to my supervisors Professor Chris Dowson and Professor Jozef Lewandowski who designed me such a great project. I would like to thank Chris for his encouragement and guidance throughout my PhD, and for allowing me to freely explore new ideas and techniques. Chris, thank you for also providing me with so many opportunities to grow as a scientist outside of the lab setting.

The research carried out in this thesis would not have been possible without the efforts of the Dowson Roper Lloyd group. Special thanks go to Dr Adrian Lloyd who laid the foundations for this work. I cannot thank you enough for your continued support throughout my PhD, your scientific insights and your patience explaining so many concepts, particularly "chemistry". Thank you for always being so enthusiastic about my work and making me feel like I had achieved something worth being very proud of. A big thanks also go to Anita Catherwood and Julie Tod for teaching me the ways of Lipid II synthesis, and providing me with so many reagents and invaluable knowledge.

To the past and present students of the Dowson Roper Lloyd group, and Tom and Beki from my DTP cohort, you have become my best friends, and I cannot thank you enough for making this challenge so enjoyable and memorable! I will miss you all!

Finally, I would like to thank my family, particularly Winston, for their continued understanding, support and encouragement throughout the ups and downs of my PhD. Thank you for being the people I could always rely on.

Declaration

I hereby declare that I personally have carried out the work submitted in this thesis under the supervision of Professor Christopher Dowson (School of Life Sciences) and Professor Jozef Lewandowski (Department of Chemistry) at the University of Warwick. Where work has been contributed to by other individuals it is specifically stated in the text.

No part of this work has previously been submitted to be considered for a degree or qualification. All sources of information are specifically acknowledged in the form of references.

Abstract

The clinical introduction of antibiotics revolutionised medicine, however the emergence of resistant bacteria is threatening their use. Of particular worry are multi-drug resistant Gram-negative bacteria that have evaded the development of any new treatment classes since the 1960's, making them particularly difficult to treat. Penicillin and other β-lactams have been one of the most clinically important classes of antibiotics, not least because they inhibit multiple targets simultaneously, but also because of their broad-spectrum profile. β-lactams target penicillin-binding proteins (PBPs), enzymes which synthesise the bacterial cell wall. As the need for novel antibiotics intensifies, understanding these validated targets is invaluable.

PBPs work in multi-protein complexes (elongasome and divisome) that coordinate cell wall synthesis and hydrolysis with membrane growth and constriction, to allow bacterial elongation and division. This work investigates how members of the *Escherichia coli*, *Pseudomonas aeruginosa* and *Yersinia pestis* divisome interact with PBPs and affect their activity. Using continuous and SDS-PAGE glycosyltransferase assays and a novel continuous transpeptidase assay with near-native substrates, this work presents the first report of *Y. pestis* PBP1b *in vitro* activity, and has allowed the investigation of its substrate specificity. This work establishes the essentiality of LpoB, an outer-membrane lipoprotein, for *Y. pestis* and *E. coli* PBP1b transpeptidase activity *in vitro*, and demonstrates how divisome protein FtsN, but not CpoB, affect activated PBP1b activity, although both were shown to interact with PBP1b by analytical ultracentrifugation.

This work also reports the first observations of *P. aeruginosa* PBP3 *in vitro* activity with native substrates. Activity assays and LCMS analysis confirmed glycan chains produced by transpeptidase inactive *E. coli* PBP1b were substrates for *P. aeruginosa* PBP3, and substrate modifications biased PBP3 towards a particular activity. These findings highlight essential interactions and present new platforms which can be utilised for novel inhibitor discovery.

Abbreviations

4P	L-alanyl-γ-D-glutamyl-meso-diaminopimelyl-D-alanine
5P	L-alanyl-γ-D-glutamyl-meso-diaminopimelyl-D-alanyl-D-alanine
Amp	Ampicillin
APS	Ammonium persulfate
ATP	Adenosine tri-phosphate
AUC	Analytical ultracentrifugation
A_x	Absorbance at x wavelength
bp	Base pairs
C-terminus	Carboxy-terminus
C_8E_5	Pentaethylene Glycol Monooctyl Ether
CAA	Chloroacetamide
CAPS	3-(Cyclohexylamino)-1-propanesulfonic acid
CHAPS	3-((3-cholamidopropyl) dimethylammonio)-1-propanesulfonate
CHES	2-(Cyclohexylamino)ethanesulfonic acid
CMC	Critical micelle concentration
CP	Carboxypeptidation
DAAO	D-amino acid oxidase
DAP	meso-Diaminopimelic acid
DMSO	Dimethylsulfoxide
DNA	Deoxyribonucleic acid
DTT	Dithiothreitol
E_6C_{12}	Hexaethylene glycol dodecyl ether
EDTA	Ethylenediametetraacetic acid
ESI-MS	Electrospray ionisation mass spectroscopy
FAD	Flavin adenine dinucleotide
GT	Glycosyltransferation
HEPES	4-(2-Hydroxyethyl)piperazine-1-ethanesulfonic acid
HRP	Horse radish peroxidase

IC_{50}	Half maximal inhibitory concentration
IMAC	Immobilised metal affinity chromatography
IPTG	Isopropyl-β-D-thiogalactoside
kb	Kilobase
K_{cat}	Enzyme turnover number
kDa	Kilo Daltons
K_m	Michaelis constant
LB	Luria-Bertani
LCMS	Liquid chromatography-mass spectroscopy
LII	Lipid II
Lipid I	Undecaprenyl pyrophosphoryl N-acetylmuramic acid L-alanyl-γ-D-glutamyl-meso-diaminopimelyl-D-alanyl- D-alanine
Lipid II	Undecaprenyl pyrophosphoryl N-acetylmuramyl N-acetylglucosamine L-alanyl-γ-D-glutamyl-meso-diaminopimelyl-D-alanyl- D-alanine
mA	Milliamps
Moen	Moenomycin
MurNAc	N-acetylmuramic acid
N-terminus	Amino-terminus
NADP	Nicotinamide adenine dinucleotide
OD_{600}	Optical density at 600 nm
PBP	Penicillin-binding protein
PCR	Polymerase chain reaction
RFU	Relative fluorescence units
rpm	Rotations per minute
SDS	Sodium dodecyl sulfate
SDS-PAGE	Sodium dodecyl sulfate-polyacrylamide gel electrophoresis
SOC	Super optimal broth with catabolite repression
TCEP	Tris(2-carboxyethyl)phosphine hydrochloride
TEMED	Tetramethylethanediamine
TFA	Trifluoroacetic acid
TLC	Thin layer chromatography

TP	Transpeptidation
Tris	Tris(hydroxymethyl)aminomethane
U	Unit
UDP	Uridine 5'-diphosphate
UDP-GlcNAc	Uridine 5'-diphosphate-N-acetylglucosamine
UDP-MurNAc	Uridine 5'-diphosphate-N-acetylmuramic acid
V	Volts
v/v	Volume to volume ratio
w/v	Weight to volume ratio
x g	Centrifugal force

Chapter 1. Introduction

1.1 Antibiotics and antimicrobial resistance

Antibiotics have saved more lives than any other class of drugs (Blaskovich *et al.*, 2017), yet they have been overused and misused, and we are now facing a potential catastrophe of untreatable bacterial infections, driven by the rise of extensively drug-resistant bacteria.

The discovery of penicillin in 1928 by Sir Alexander Fleming initiated the 'golden age' of antibiotic development, and between the clinical introduction of penicillin in 1943 and the 1960's 10 new antibiotic classes had been introduced (Walsh and Wencewicz, 2014). Antibiotics were seen as the 'wonder drug' to treat bacterial infections, and a 'magic bullet' that selectively targeted the disease causing organism and not host cells (Aminov, 2010). The control of infectious diseases meant morbidity and mortality rates plummeted, and infectious diseases were no longer the leading cause of human death (Aminov, 2010). But the 1960's saw a decline in antibiotic research and development, and were followed by a 40 year gap in antibiotic discovery, when no new structural classes of antibiotics were introduced.

In Fleming's Nobel Prize lecture in 1945, awarded for his discovery of penicillin, he warned:
"It is not difficult to make microbes resistant to penicillin in the laboratory by exposing them to concentrations not sufficient to kill them, and the same thing has occasionally happened in the body. The time may come when penicillin can be bought by anyone in the shops. Then there is the danger that the ignorant man may easily underdose himself and by exposing his microbes to non-lethal quantities of the drug make them resistant." (Fleming, 1945).
Fleming was well aware that the emergence of resistant bacteria was inevitable, and as Fleming predicted the first penicillin resistant clinical strain was reported just 3 years after its introduction to the clinic (Palumbi, 2001). As most

antibiotics are derived from natural products produced by organisms to fight off bacteria, resistance to these compounds at some level often already exists (Aminov, 2010). Resistance to antibiotics is a natural evolutionary mechanism that all bacteria employ to survive, and antibiotic resistant genes well predate the modern 'antibiotic era'. For example bacteria found in a New Mexican cave that had been isolated for over 4 million years were reported to be highly resistant to many commercially available antibiotics, 70% of the strains were resistant to 3-4 antibiotic classes, with multiple strains being resistant to more than 10 different antibiotics (Bhullar *et al.*, 2012). However, the commercialisation and clinical use of antibiotics has rapidly accelerated the inevitable selection of resistant strains (Walsh and Wencewicz, 2014), and the clinical use of any new antibiotic is shortly followed by the emergence of resistant strains (Walsh and Wencewicz, 2014).

So, what has changed to make antibiotic resistance such a threat? We have been misusing our current antibiotics: over half of the antibiotics consumed are used on animals, with most not being used to treat infections but to prevent them, or simply as growth promoters. This use creates a reservoir of resistance and promotes resistance spread, and there is a strong body of evidence confirming the link between antibiotic use in animals and resistance in humans (O'Neill, 2016). Of the remaining human use, the majority of it is inappropriately prescribed for non-bacterial infections, as antibiotics are rarely prescribed based on definitive diagnostic tests (O'Neill, 2016). In a lot of the developing world, antibiotics are also widely available without a prescription, and self-medication most certainly results in inappropriate diagnosis, unsuitable antibiotic choice, incorrect usage and non-compliance, thus contributing to the rising resistance problem (Aminov, 2010).

Additionally, the threat posed by antibiotic resistance has been exacerbated by the lack of new antibiotics being discovered and developed. No new classes of antibiotics were produced between 1962 and 2000: all marketed antibiotics in this period were modification of existing molecules (Coates *et al.*, 2002), and since 2000 only five new classes of antibiotics have been marketed (Walsh and

Wencewicz, 2014). To make matters worse the number of scientists involved in antibiotic research has declined and large pharmaceutical companies are unwilling to invest in antibiotics which make little profit in comparison to other therapies (Blaskovich *et al.*, 2017). From an economical perspective, although antibiotic resistance increases the demand for new antibiotics, at the same time it also reduces the useful lifespan of an antibiotic, severely impairing a drugs long-term return in profits. Antibiotics cure bacterial infections in weeks, while other drugs treat life-long conditions like high-cholesterol or arthritis, and a novel antibiotic may also be held in reserve, and not used until absolutely necessary. All these reasons make antibiotic development extremely unfavourable to a profit-making company (Leeb, 2004).

Of particular worry, are the lack of new antibiotics to treat drug-resistant Gram-negative bacteria, as all five new antibiotic classes introduced since 2000 target only Gram-positive bacteria, so there are no new drugs to treat a class of organism with an additional outer membrane which is difficult to permeate, and with efflux pumps that prevent antibiotics from reaching concentrations required to inhibit intracellular targets (Blaskovich *et al.*, 2017).

1.1.1 Tackling antimicrobial resistance

Global recognition of the problem is finally apparent. In 2015 the World Health Organisation endorsed a global action plan for antimicrobial resistance (WHO, 2015), and later devised a list of priority drug-resistant pathogens on which research and development of novel antibiotics should be focused, with those of the highest priority being *Mycobacterium tuberculosis* and Gram-negative bacteria *Acinetobacter baumannii*, *Pseudomonas aeruginosa* and the *Enterobacteriaceae* family (Tacconelli *et al.*, 2018). The UK government in collaboration with the Wellcome Trust also released a review on antimicrobial resistance in 2016, analysing the current global problem and proposing actions to tackle it internationally (O'Neill, 2016).

Although solutions are still a long way from being implemented, at least there is agreement that a multi-national, interdisciplinary and coordinated approach is needed to continue treating bacterial infections: with efforts being focused on increasing awareness and understanding of antimicrobial resistance, reducing the incidence of infections through better hygiene and improved sanitation, optimising the use of antibiotics in humans and reducing the unnecessary use in animals, and increasing incentives and investments in research for rapid infection diagnostic tools, vaccines, infection prevention and new antibiotics (WHO, 2015; O'Neill, 2016).

This thesis focuses on the latter effort of developing novel antibiotics by improving our understanding of bacterial cell wall synthesis, a validated target for antibiotics, in Gram-negative bacteria. Our improved understanding of these targets and the ability to screen them, will aid the design of novel antibiotics, and along with the other interventions detailed above will help to ensure antimicrobial resistance remains a manageable health problem for future generations. Gram-negative pathogens *Escherichia coli*, *Pseudomonas aeruginosa* and *Yersinia pestis* are the focus of the work in this thesis, and the next 3 sections detail their clinical significance as pathogens, their treatments and mechanisms of resistance.

1.2 *Escherichia coli*

E. coli is both a common commensal of the human gastrointestinal tract and one of the most frequent pathogens in humans (Vila *et al.*, 2016). *E. coli* are enteric Gram-negative bacilli, and coexist as part of the human natural gastrointestinal flora, creating mutual benefit for both bacteria and host. Commensal *E. coli* inhabit the mucous layer of the human colon, and are the most abundant facultative anaerobe of the human intestinal flora. They rarely cause disease except in immunocompromised individuals or where the normal gastrointestinal barrier has been broken (Kaper *et al.*, 2004). However, if *E. coli* acquires certain virulence attributes they can inhabit new niches and confer disease. Most

virulence factors are encoded on mobile genetic elements which can be transferred between strains, with only the most successful combination of virulence factors persisting to become pathogenic 'pathotypes', that are able to cause disease in healthy individuals (Kaper *et al.*, 2004).

Pathogenic *E. coli* strains generally possess adherence and colonisation factors, like fimbriae (also called pili) which allow them to adhere to and colonise sites they do not normally inhabit, and fitness factors, like iron-acquisition systems, which contribute to their survival in the urinary tract. They also have acquired the ability to secrete toxins and effector proteins, to kill host cells and evade the host immune response, as well as forming biofilms, which provides protection from antimicrobial treatments and host defence mechanisms. The infections they cause can be split into three main categories: enteric/diarrhoeal disease, urinary tract infections and sepsis/meningitis, with *E. coli* being the leading cause of urinary tract infections, and the most frequent cause of blood stream infections among the Gram-negatives (Vila *et al.*, 2016).

E. coli has consolidated resistance mechanisms over many years, including β-lactamases and more recently extended-spectrum $\beta-$ lactamases, carbapenemases, or plasmid mediated quinolone (DNA topoisomerase inhibitors) resistance. Resistance in *E. coli* develops either through mutations, as often seen with quinolone resistance, or by acquisition of mobile genetic elements, such as those encoding β-lactam resistance (European Centre for Disease Prevention and Control, 2017). β-lactams were among those antibiotics most frequently prescribed for *E. coli* infections, however their use is being threatened by the proliferation of resistant strains (Vila *et al.*, 2016). Extended spectrum β-lactamases catalyse the hydrolysis of the β-lactam ring, and confer resistance to most β-lactams, including third-generation cephalosporins. They are often seen in combination with other resistance mechanisms, such as a decrease in the production of outer membrane proteins, which reduce the translocation of antibiotics through the outer membrane, or the expression of efflux pumps, which are multi-protein complexes that span the cell envelope and are responsible for expelling toxic compounds, such as antibiotics, out of the cell

(Zervosen *et al.*, 2012; Vila *et al.*, 2016). Carbapenems (β -lactam antibiotics) usually resist the effect of extended spectrum β -lactamases and remain one of the few treatment options for multi-drug resistance infections. However, carbapenem resistance is emerging mediated by carbapenemases, which are carbapenemase β -lactamases with additional activity against carbapenems. Worryingly, carbapenemase genes are often located on plasmids which can be exchanged between Enterobacteriaceae (European Centre for Disease Prevention and Control, 2017). Reports of resistance conferred by mutations to penicillin-binding proteins (PBPs) are extremely rare in *E. coli* (Alm *et al.*, 2015; Zhang *et al.*, 2017), as is resistance mediated by the upregulation of PBP expression (Thulin and Andersson, 2019).

In 2017 58.2% of *E. coli* isolates reported to the European Antimicrobial Resistance Surveillance Network were resistant to one or more antimicrobial group (aminopenicillins, fluoroquinolones (DNA topoisomerase inhibitors), third-generation cephalosporins, aminoglycosides (protein synthesis inhibitors) and carbapenems). Resistance to aminopenicillins was the highest (58.7%), followed by fluoroquinolones (25.7%), third-generation cephalosporins (14.9%) and aminoglycosides (11.4%), while resistance to carbapenems remained rare in *E. coli* (European Centre for Disease Prevention and Control, 2017). Owing to increasing resistance, the current recommended treatment for uncomplicated UTI's in the UK is nitrofurantoin (inhibitor of DNA and RNA synthesis), with fosfomycin (MurA inhibitor) and mecillinam (PBP2 inhibitor) as alternative treatments (Lee *et al.*, 2018; Hawkey *et al.*, 2018).

The surge in antibiotic resistant bacteria, and multidrug resistant bacterial infections led The European Centre for Disease Prevention and Control and The Infectious Diseases Society of America to term a set of difficult-to-treat pathogens, *E. faecium*, *S. aureus*, *K. pneumoniae*, *A. baumannii*, *P. aeruginosa* and *Enterobacter* species (including *E. coli*), as ESKAPE pathogens, given their propensity to develop resistance and escape from the impact of current antibiotics, leading to an increase in nosocomial infections in hospitalised patients (Rice, 2008).

1.3 *Pseudomonas aeruginosa*

P. aeruginosa is a non-fermenting bacterium that is ubiquitous in aquatic environments in nature. It is an opportunistic human pathogen capable of causing life-threatening acute and chronic infections, particularly in immunocompromised patients. It is a major cause of hospital acquired infections, and can cause pneumonia, blood stream and urinary tract infections, particularly in cystic fibrosis patients. Multi-drug resistance is a major problem in cystic fibrosis patients, with resistance increasing over time in the individual patient's lung microflora. The prevalence and persistence of *P. aeruginosa* in clinical settings is largely due to its intrinsic resistance to a wide range of antibiotics and ability to adapt and thrive in unfavourable conditions (European Centre for Disease Prevention and Control, 2017; Moradali *et al.*, 2017).

An intrinsic resistance mechanism of *P. aeruginosa* is the reduced uptake of antibiotics into the cell. This is achieved by replacing non-specific porin proteins (such as OprD porin) with specific porins or more selective transporters, that only take up the required nutrients, resulting in the outer membrane being less permeable to antibiotics. Resistance to carbapenems and cephalosporins is commonly caused by this adaption (Hancock, 1998; Moradali *et al.*, 2017). Active multidrug efflux pumps also greatly contribute to the intrinsic resistance observed in *P. aeruginosa*, where their over-expression can confer high level resistance, due to their ability to transport a wide range of substrates (Blair *et al.*, 2015; Venter *et al.*, 2015). Another player of intrinsic resistance in *P. aeruginosa* is an inducible chromosomally encoded β-lactamase (AmpC). AmpC expression is induced upon cell contact with sub-MIC levels of β-lactams and confers low level resistance to aminopenicllins and most cephalosporins (Hancock, 1998; Moradali *et al.*, 2017).

P. aeruginosa can also acquire resistance to antibiotics through mutations of intrinsic genes or acquisition of mobile elements. A common mutational feature of *P. aeruginosa* is a high level of AmpC production in the absence of antibiotics. This is mainly caused by mutational inactivation of the AmpC regulatory

repressors. Mutations to regulatory genes are also a major cause of multi-drug efflux pump over-expression, as well as mutations to porins, which increase selectivity to drugs. Plasmid encoded antibiotic resistance genes generally confer resistance to β -lactams through extended-spectrum β -lactamases and carbapenemases (Hancock, 1998; Moradali *et al.*, 2017). Mutations to PBPs which confer resistance have also been reported, these mainly occur in PBP3 (Bellido *et al.*, 1990; Gotoh *et al.*, 1990; Clark *et al.*, 2019).

In Europe 30.8% of *P. aeruginosa* isolates reported to the European Antimicrobial Resistance Surveillance Network in 2017 were resistant to one or more antimicrobial groups (piperacillin (ureidopenicillins), 3rd generation cephalosporin, fluoroquinolones, carbapenems and aminoglycosides), while 18.3% were resistant to two or more. Resistance to fluoroquinolones was the greatest (20.3%), followed by piperacillin (18.3%), carbapenems (17.4%), ceftazidime (3rd generation cephalosporin) (14.7%) and aminoglycosides (13.2%) (European Centre for Disease Prevention and Control, 2017). Owing to the resistance mechanisms of *P. aeruginosa* the current recommended treatment in the UK is a combination therapy of a β -lactam and a β -lactamase inhibitor, often ceftazidime with avibactam (β -lactamase inhibitor), or ceftolozane (5th generation cephalosporin)/ piperacillin and tazobactam (β -lactamase inhibitor), and in complicated infections also an additional aminoglycoside or fluoroquinolone (Bassetti *et al.*, 2018; Hawkey *et al.*, 2018).

1.4 *Yersinia pestis*

Y. pestis is a coccobacillus of the *Enterobacteriaceae* family and is the etiological agent of plague which has claimed over 200 million human lives in three great pandemics. Following the reappearance of plague in many parts of Africa, Asia and the Americas during the 1990s, plague has been categorised as a re-emerging disease (Stenseth *et al.*, 2008). Plague infections begin with nondescript flu-like symptoms and progresses into a fatal infection if not treated rapidly. Plague manifests itself in three disease types: most commonly bubonic plague, where

bacteria multiply in lymph nodes causing them to swell, septicaemic plague, where bacteria circulate in the blood, and pneumonic plague, where bacteria localise to the lungs (Butler, 2009).

The pathogenicity of plague is mostly owed to acquired plasmids which encode virulence factors, such as type III secretion systems and toxins that kill host cells and inhibit host immune responses (Pechous *et al.*, 2016; Yang, 2018). *Y. pestis* also encodes chromosomal virulence factors including genes for biofilm formation and iron acquisition, to colonise unfavourable habitats (Yang, 2018). Due to its rapid pathogenicity, plague requires treatment within the first 24 hours, otherwise the infection is usually fatal. Plague is most commonly treated with gentamycin or streptomycin (both protein synthesis inhibitors), or the combination of doxycycline, chloramphenicol (both protein synthesis inhibitors) and ciprofloxacin (a DNA topoisomerase inhibitor) (Stenseth *et al.*, 2008; Yang, 2018), although *in vitro* susceptibilities have shown the effectiveness of other antibiotics including β-lactams. The most effective β-lactams for varied strains of *Y. pestis* were ampicillin and 3rd generation cephalosporins (Wong *et al.*, 2000; Hernandez *et al.*, 2003), and β-lactam effectiveness in mice models has also been shown. 100% of mice treated with ceftriaxone 24 hours after exposure to *Y. pestis* survived, and 85% survived with ceftazidime, ampicillin or aztreonam treatment (Byrne *et al.*, 1998).

Multi-drug resistant *Y. pestis* strains have also been documented. A strain resistant to eight antimicrobials was first reported in Madagascar (Galimand *et al.*, 1997), and other resistant strains have been subsequently identified (Guiyoule *et al.*, 2001). The strains were resistant to many antibiotics used as recommended therapies and also alternative therapies, through plasmid encoded β -lactamases, chloramphenicol acetyltransferases, sulphonamide resistant dihydropteroate synthases, aminoglycoside adenylyltransferases and tetracycline efflux pumps which were mobile between *Yersinia* isolates (Galimand *et al.*, 2006).

There is concern that *Y. pestis* may be an attractive bioterrorism agent and because of this it has been classified as a category A bioterrorism agent by the CDC (Centre for Disease Control and Prevention, 2000). The use of *Y. pestis* as a biological weapon has occurred throughout history: infected corpses have been catapulted over city walls, infected fleas dropped from aircraft and refined modern aerosol formulations developed (Inglesby *et al.*, 2000; Koirala, 2006). The Anthrax attacks in 2001 have re-established concerns for bioterrorism and renewed interest in developing diagnostics and treatments against multi-drug resistant *Y. pestis* (Bush and Perez, 2012).

1.5 Gram-negative bacterial cell wall

1.5.1 The role of the cell wall

The bacterial cell wall is the target of many antibiotics as the cell depends on it for structure and protection. The cell wall of Gram-negative bacteria encompasses a thin layer of peptidoglycan, comprised of covalently cross-linked glycan polymers, surrounded by an outer membrane (Gram, 1884). The outer membrane is specific to Gram-negative bacteria, and it's composition is distinct from the inner membrane, comprising an asymmetrical bilayer of phospholipids in the inner leaflet, lipopolysaccharides in the outer leaflet and outer membrane proteins (Konovalova *et al.*, 2017). The outer membrane acts as a selectively permeable barrier, protecting the bacterium from harmful chemicals, like detergents and antibiotics (Konovalova *et al.*, 2017).

The peptidoglycan layer provides the bacterium with the mechanical strength to resist osmotic pressure challenges and maintain its unique shape. It also has a non-structural role acting as a scaffold to anchor lipoproteins, tethering the outer membrane to the peptidoglycan layer. These roles make the peptidoglycan layer essential for bacterial survival, and inhibition of its synthesis causes bacterial lysis (Vollmer, Blanot, *et al.*, 2008). However, recent evidence indicates that the prevailing dogma of the peptidoglycan layer being the dominant mechanical

element within the Gram-negative cell wall is not true. Instead the outer membrane can be stiffer than the peptidoglycan layer and the two structures often share the mechanical load on the cell (Rojas *et al.*, 2018).

1.5.2 Peptidoglycan structure

Peptidoglycan is a three-dimensional mesh-like structure consisting of linear glycan chains cross-linked by short peptides, and it's basic structure is conserved in most Gram-negative bacteria (Vollmer, Blanot, *et al.*, 2008). The glycan chains are comprised of alternating β1 to 4 linked *N*-acetylglucosamine (GlcNAc) and *N*-acetylmuramic acid (MurNAc) residues, and have a peptide stem attached to the lactyl group of each MurNAc. The peptide stems of adjacent glycan chains are covalently cross-linked to create a mesh-like structure, and in nascent peptidoglycan the peptide stem is most commonly L-alanyl-γ-D-glutamyl-meso-diaminopimelyl-D-alanyl-D-alanine (Vollmer and Bertsche, 2008), but a small amount of the peptides occasionally contain Gly instead of D-Ala in position 4 and 5 (Glauner *et al.*, 1988). Cross-linking of adjacent peptide stems generally occurs between the carboxyl group of D-Ala in position 4 and the amino group of DAP in position 3, creating a 3-4 cross-link. 3-3 cross-links can also occur between the DAP peptide of one stem and the DAP peptide of another stem but are a lot less frequent (Glauner *et al.*, 1988; Quintela *et al.*, 1995). In mature peptidoglycan the peptide stem rarely contains five peptides, and more commonly one or both of the D-Ala or Gly peptides at position 4 and 5 are lost, due to the action of peptidoglycan hydrolases and the cross-linking reaction (Vollmer and Bertsche, 2008). Therefore, the traits of this polymer involve unusual D-amino acids, non-protein amino acids (DAP), γ-bonded D-Glu and L-D and D-D bonds, making the peptidoglycan structure resistant to attack by most mammalian proteases (Vollmer, Blanot, *et al.*, 2008)

1.5.3 Peptidoglycan biosynthesis

Bacterial cell growth and division dictates that the peptidoglycan layer must be dynamic. It requires the synthesis of new peptidoglycan, cleavage of the existing peptidoglycan, and the insertion of newly synthesised material to be synchronised with the elongation and division of the cell (Holtje, 1998). To allow peptidoglycan synthesis to be coordinated in this way, the proteins which make up the peptidoglycan synthesis machinery are members of the divisome and elongasome protein complexes (Typas *et al.*, 2012), which coordinate peptidoglycan synthesis and remodelling during cell division and elongation respectively.

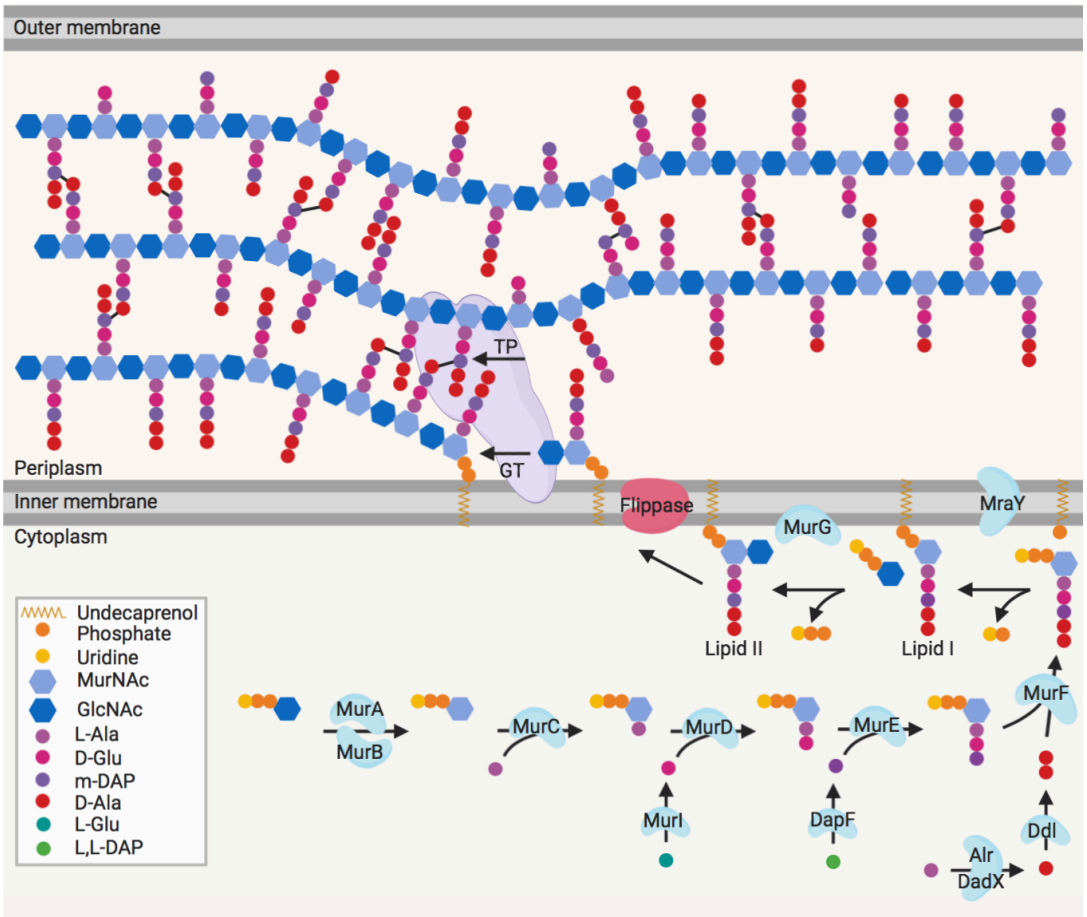

Figure 1.1: Peptidoglycan biosynthesis.
Lipid II, the peptidoglycan precursor, is synthesised in the cytoplasm by sequential enzymatic steps, and attached to undecaprenyl phosphate in the inner membrane. Lipid II is then flipped across the inner membrane by a flippase, and polymerised into glycan chains by the glycosyltransferase (GT) action of PBPs, SEDS proteins or monofunctional glycosyltransferases. The new glycan chain is attached to the existing peptidoglycan layer by the transpeptidase (TP) action of PBPs.

Peptidoglycan is synthesised from the precursor Lipid II, produced in the cytoplasm of the cell, and comprises of the two sugars GlcNAc and MurNAc and a pentapeptide stem (5P), which is attached to a lipid tail (undecaprenyl pyrophosphate) in the cell membrane to allow it to remain tethered to the membrane to facilitate incorporation into the peptidoglycan layer (Typas *et al.*, 2012) (Figure 1.1).

In the cytoplasm fructose-6-phospahte is converted in four successive enzyme activities to uridine 5'-diphosphate-*N*-acetylglucosamine (UDP-GlcNAc), catalysed by GlmS, GlmM and GlmU (bifunctional enzyme) (Barreteau *et al.*, 2008). UDP-MurNAc (uridine 5'-diphosphate-*N*-acetylmuramic acid) is then formed from UDP-GlcNAc by the two enzymes MurA and MurB. The pentapeptide stem is then appended to the D-lactoyl carboxyl group of UDP-MurNAc by sequential addition of peptides by MurC-F: these provide the addition of L-Ala (MurC), D-glutamic acid (MurD), meso-diaminopimelic acid (m-DAP) (MurE) and dipeptide D-Ala-D-Ala (MurF), with D-Glu and m-DAP being synthesised from their L or L,L stereoisomers by MurI and DapF respectively, and D-ala-D-Ala being produced from L-Ala by alanine racemases and D-Ala-D-Ala ligase (Barreteau *et al.*, 2008; Vollmer, Blanot, *et al.*, 2008). Phospho-MurNAc 5P is then transferred from UDP-MurNAc 5P to the lipid carrier in the membrane, undecaprenyl phosphate, yielding undecaprenyl diphospho MurNAc 5P (Lipid I), in a reaction catalysed by MraY. Thereafter, the transferase MurG catalyses the addition of the GlcNAc moiety from UDP-GlcNAc, to Lipid I, producing undecaprenyl diphospho MurNAc GlcNAc 5P (Lipid II) (Bouhss *et al.*, 2008), which is flipped across the membrane by a yet undetermined enzyme (candidate enzymes are MurJ, FtsW and RodA) (Mohammadi *et al.*, 2011; Sham *et al.*, 2014; Reddy Bolla *et al.*, 2018), and incorporated into peptidoglycan (Figure 1.1).

Once at the periplasmic side of the inner membrane, Lipid II is incorporated into the existing peptidoglycan layer by two successive enzyme activities. Firstly, Lipid II is polymerised into a glycan chain, creating a repeating GlcNAc MurNAc 5P oligomer, by a glycosyltransferase reaction, which releases undecaprenyl

pyrophosphate. Undecaprenyl pyrophosphate is dephosphorylated to undecaprenyl phosphate by BacA and ultimately recycled to reform Lipid I and Lipid II (Bouhss *et al.*, 2008). Secondly, cross-links are formed between the peptide stems of glycan chains, by a transpeptidation reaction, releasing the terminal D-Ala of the stem peptide. The glycosyltransferase reaction can be carried out by mono-functional glycosyltransferase MgtA (Derouaux *et al.*, 2008), shape, elongation, division and septation (SEDS) proteins RodA (Meeske *et al.*, 2016; Rohs *et al.*, 2018) and FtsW (Cho *et al.*, 2016; Taguchi *et al.*, 2019), or by bifunctional penicillin-binding proteins (PBPs), which possess glycosyltransferase activity, as well as transpeptidase activity (Bertsche *et al.*, 2005; Born *et al.*, 2006). While the transpeptidation reaction is only carried out by PBPs (Vollmer and Bertsche, 2008) (Figure 1.1).

1.5.4 Antibiotics that target the cell wall

The bacterial cell wall is an invaluable antibacterial target due to its essentiality for bacterial life, and its high conservation between species (Vollmer, Blanot, *et al.*, 2008). Penicillin and the β-lactam class of antibiotics target cell wall synthesis by covalently binding to the transpeptidase active site of PBPs due to their structural similarity to the D-Ala-D-Ala moiety of the pentapeptide stem of Lipid II. All β-lactams share the characteristic four-membered β-lactam ring, which acylates the active site serine of PBPs, preventing them from cross-linking glycan chains, weakening the peptidoglycan structure and causing cell lysis (Waxman and Strominger, 1983). Since their discovery, β-lactams have been one of the most clinically important class of antibiotics and remain the most commonly used antibiotic today (Jovetic *et al.*, 2010). No other antibiotics that target PBPs are used clinically, however non-β-lactam inhibitors do exist: lactivicin, is a transpeptidase inhibitor but is too toxic for clinical use (Nozaki *et al.*, 1989) and moenomycin inhibits glycosyltransferases but has poor pharmacokinetic properties (Ostash and Walker, 2010).

Other cell wall synthesis inhibitors include: Fosfomycin, which acts as a phospoenolpyruvate analogue to inhibit MurA, is mainly used to treat

uncomplicated urinary tract infections caused by *E. coli*, *Klebsiella pneumoniae* and *Enterobacter cloacae*, as well as Gram-positive organisms *Staphylococcus aureus*, *Enterococcus faecalis* and *Enterococcus faecium* (Castañeda-García *et al.*, 2013), and D-cycloserine, an inhibitor of D-Ala-D-Ala ligase and D-Ala racemase, which functions by starving the cell of D-Ala needed for peptidoglycan synthesis. D-cycloserine is only used as a second-line treatment for tuberculosis due to its adverse neurological side effects when administered at an effective dose (Baisa *et al.*, 2013).

All other cell wall synthesis inhibitors are only effective against Gram-positives and include: Bacitracin, which inhibits dephosphorylation of undecaprenyl pyrophosphate, thus preventing the synthesis of the lipid carrier (Pollock *et al.*, 1994). Glycopeptides, such as vancomycin (Álvarez *et al.*, 2016) and teicoplanin (Campoli-Richards *et al.*, 1990), which bind to the D-Ala-D-Ala moiety of Lipid II, which are too large to permeate the outer membrane (Sarkar *et al.*, 2017).

1.6 Penicillin-binding proteins

Although β-lactams have been studied since the 1930's (Fleming, 1929) and their targets, PBPs, since the 1960's (Tipper and Strominger, 1965), relatively little is known about the enzymatic mechanisms of PBPs, their regulation or interactions with other proteins. Progress has been hindered by complications in purifying these membrane proteins, their structurally complex natural substrates, the lack of functional assays to measure their activity *in vitro* and the essential interactions required for their activity. Recent advances in all these areas have significantly enhanced our knowledge of PBP enzymology, and these advances are discussed below.

1.6.1 PBP classification

Most Gram-negative bacteria have between 4 and 12 PBPs (Sauvage *et al.*, 2008), and the PBPs are historically numbered within organisms by molecular weight,

based on their migration by SDS-PAGE (Waxman and Strominger, 1983). Their disordered identification means some PBPs have an additional letter (e.g. PBP1a and PBP1b), and the numbering is often not comparable between organisms. PBPs can however be split into 3 main categories: Class A PBPs, bifunctional N-terminal glycosyltransferases and C-terminal D,D-transpeptidases, Class B PBPs, monofunctional D,D-transpeptidases and Class C PBPs, monofunctional carboxypeptidases, endopeptidases and L,D-transpeptidases (Ghuysen, 1991; Goffin and Ghuysen, 1998) (Figure 1.2). Class A and B PBPs also have the ability to carry out D,D-carboxypeptidation, which involves the trimming of a pentapeptide stem to a tetrapeptide, releasing D-Ala (discussed in more detail in section 1.6.4.2).

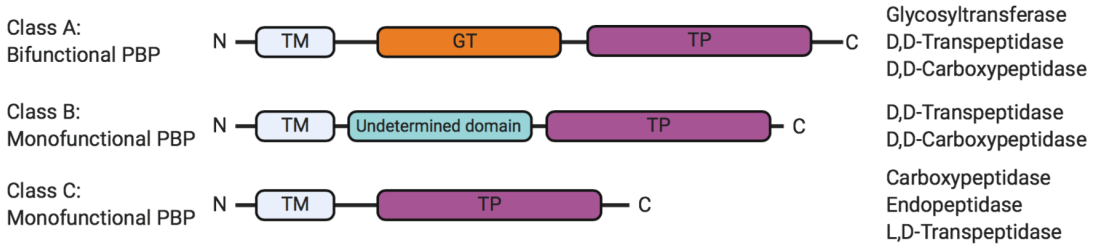

Figure 1.2: Penicillin-binding protein classification.
Classification on the left, domain topology in the middle where TM (transmembrane domain), GT (glycosyltransferase domain) and TP (transpeptidase domain), and PBP activities on the right.

This thesis focuses on PBP1b and PBP3 from Gram-negative organisms *E. coli*, *Y. pestis* and *P. aeruginosa*, and luckily the PBP nomenclature for these homologues is identical in the three organisms.

The PBP1b proteins from *E. coli* and *Y. pestis* share a high sequence homology, with 68% sequence identity and 78% sequence similarity. The sequence is conserved around the two active site domains and the UB2H domain, where the substrate and multiple interacting proteins are known to bind (Figure 1.3)

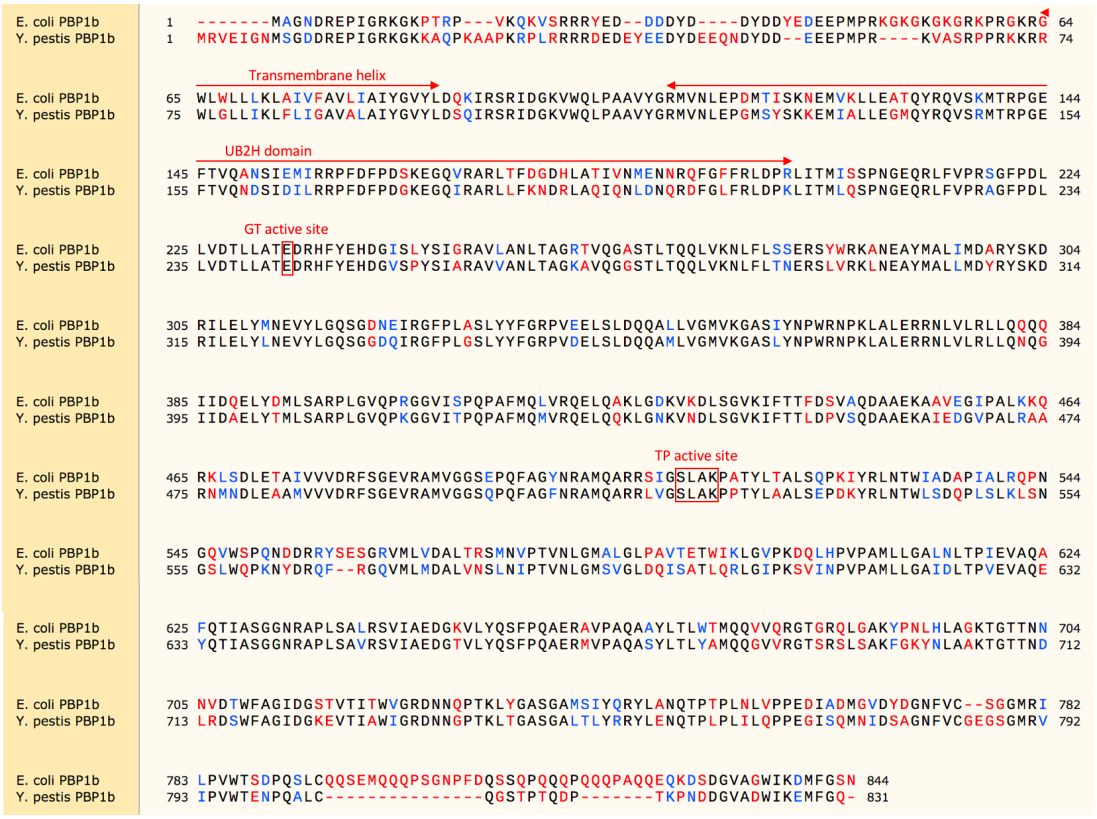

Figure 1.3: Sequence alignment of *E. coli* and *Y. pestis* PBP1b
Identical amino acids are in black, amino acids with similar properties are in blue and not similar amino acids are in red. The transmembrane and UB2H domains are highlighted with red arrows and the glycosyltransferase and transpeptidase active sites are boxed in red.

1.6.2 Bifunctional PBPs

The model Gram-negative organism *E. coli* has been the subject of most PBP investigation. *E. coli* has three bifunctional PBPs: PBP1a, PBP1b and PBP1c (Goffin and Ghuysen, 1998). PBP1a and PBP1b are partially redundant enzymes, as cell lacking both are lethal, but they are individually dispensable (Suzuki *et al.*, 1978; Yousif *et al.*, 1985), while PBP1c is not essential for cell viability and its role is not well understood (Schiffer and Höltje, 1999).

Fluorescence localisation studies found PBP1a to localise along the lateral cell periphery (Banzhaf *et al.*, 2012; Pazos *et al.*, 2018), and in the case of PBP1b also at the division site (Bertsche *et al.*, 2006; Pazos *et al.*, 2018). Cells lacking PBP1a are thinner and initiate cell division later in the cycle (Banzhaf *et al.*, 2012), supporting a role of PBP1a in cell elongation. PBP1a also directly interacts with the essential cell elongation specific transpeptidase PBP2 *in vitro* and *in vivo*

(Spratt, 1975; Banzhaf *et al.*, 2012). PBP1b on the other hand appears more specialised for cell division, and directly interacts with the essential cell division specific transpeptidase PBP3 (Spratt, 1977; Bottat *et al.*, 1981). PBP1b depends on PBP3 for localisation to the division site (Bertsche *et al.*, 2006), as well as interacting with other components of the divisome such as FtsN (Müller *et al.*, 2007) and FtsW (Leclercq *et al.*, 2017). That PBP1a and PBP1b have different localisation patterns and interacting partners supports the hypothesis of distinct roles in cell elongation and cell division respectively.

Although one of PBP1a or PBP1b is dispensable under standard growth conditions, there have been hints these enzymes are not interchangeable. Cells defective of PBP1b or LpoB (essential activator of PBP1b) are hypersensitive to many β-lactams, while mutants of PBP1a are not (Yousif *et al.*, 1985; Garcia *et al.*, 1990; Paradis-Bleau *et al.*, 2010). Inhibition of class B PBPs, PBP2 or PBP3, normally leads to the formation of spherical or filamentous cells, however similar treatment of mutants lacking PBP1b induces rapid cell lysis (Schmidt *et al.*, 1981; Garcia *et al.*, 1990). Inactivation of PBP1b in cells grown in acidic media or PBP1a in alkaline media also leads to reduced cell fitness and lysis (Mueller *et al.*, 2019), suggesting PBP1a and PBP1b may have essential roles in distinct environmental niches.

1.6.2.1 Bifunctional PBP regulation

Bacterial growth and division dictates that peptidoglycan synthesis is precisely regulated, and in Gram-negative bacteria this also involves the coordinated constriction of both the inner and outer cell membranes. This is achieved by the elongasome and divisome multi-protein complexes. In *E. coli* over 36 proteins have been identified as components of the divisome, and among these FtsN is the last essential protein recruited to the division site (Du and Lutkenhaus, 2017). The arrival of FtsN at the division site triggers cell constriction (Gerding *et al.*, 2009; Busiek and Margolin, 2014) and activates septal peptidoglycan synthesis (Du and Lutkenhaus, 2017). How exactly FtsN triggers cell constriction and peptidoglycan synthesis remains to be elucidated, however, it is thought to

involve FtsA and FtsBLQ (Busiek and Margolin, 2014; Liu *et al.*, 2015; Boes *et al.*, 2019), as well as a direct interaction with peptidoglycan synthase PBP1b (Figure 1.4) (Müller *et al.*, 2007; Pazos *et al.*, 2018; Boes *et al.*, 2019).

FtsN is a membrane protein: its N-terminus comprises a short cytoplasmic domain, followed by a transmembrane helix, which with the first 80 periplasmic amino acids is essential for its function. The C-terminal domain comprises a peptidoglycan binding domain which is dispensable (Ursinus *et al.*, 2004). The ability of FtsN to bind peptidoglycan is thought to aid its accumulation at the division site by creating a positive feedback loop, to complete divisome maturation and trigger cell envelope constriction (Gerding *et al.*, 2009).

The presence of FtsN is essential for constriction initiation and the recruitment of AmiC, a peptidoglycan hydrolase (Heidrich *et al.*, 2001; Bernhardt and De Boer, 2003), and the Tol-Pal complex, involved in outer membrane integrity, to the division site (Gerding *et al.*, 2007). Tol-Pal involvement in cell division is thought to create a link between the outer membrane and the inner membrane via the peptidoglycan layer during cell constriction (Gerding *et al.*, 2007). In *E. coli* the Tol-Pal complex consists of seven proteins: TolAQR are inner membrane bound, Pal is outer membrane bound, YbgC is cytoplasmic, and TolB and CpoB (formerly YbgF) are periplasmic proteins (Walburger *et al.*, 2002; Gerding *et al.*, 2007; Krachler, Sharma, Cauldwell, *et al.*, 2010). TolB bridges the gap between the inner membrane TolAQR complex and the outer membrane anchored Pal protein (Walburger *et al.*, 2002; Gerding *et al.*, 2007), while CpoB interacts with the complex via TolA (Walburger *et al.*, 2002). TolA and CpoB also create a link between the Tol-Pal complex and the peptidoglycan synthesis machinery by interacting with PBP1b (Figure 1.4) (Gray *et al.*, 2015; Egan *et al.*, 2018). Mutants of CpoB and PBP1b both shared increased sensitivity to β-lactams, and deletion of CpoB from a strain which solely relies on PBP1b as its bifunctional PBP (PBP1a and LpoA deletions), caused severe growth defects (Gray *et al.*, 2015), suggesting CpoB may affect PBP1b function.

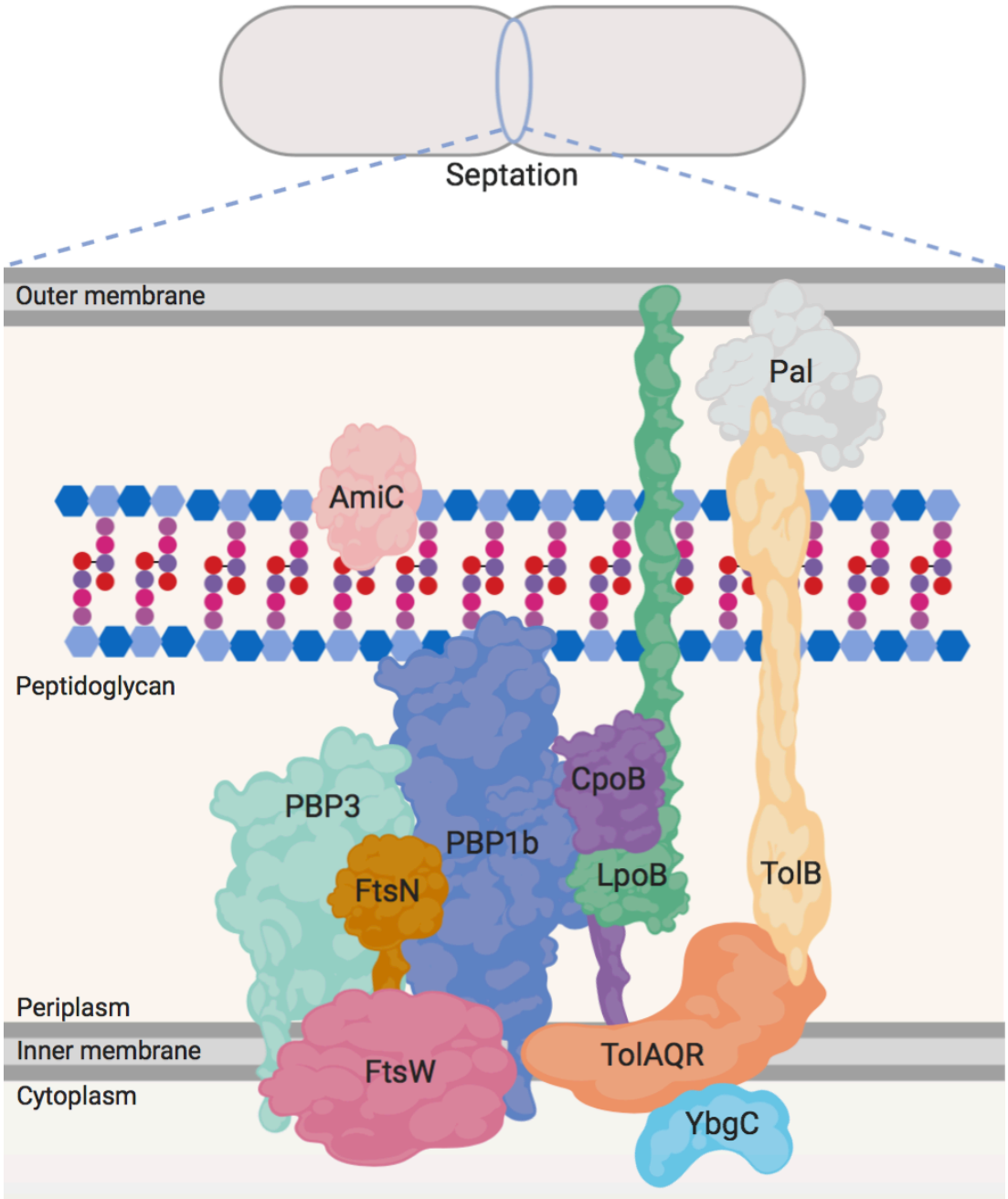

Figure 1.4: Peptidoglycan synthesis complex active during cell division.
The peptidoglycan synthesis complex during cell division involves inner membrane localised peptidoglycan synthases FtsW, PBP3 and PBP1b, with PBP1b activator, LpoB anchored to the outer membrane. Peptidoglycan synthesis is regulated by FtsN and the Tol-Pal complex (TolAQR, TolB, Pal, CpoB and YbgC) for constriction of the inner and outer membrane, and amidase enzymes (AmiC) for peptidoglycan cleavage.

The structure of CpoB is an elongated trimer composed of a N-terminal trimeric coiled coil, followed by a flexible linker and a monomeric C-terminal tetratricopeptide repeat (TPR) domain (Krachler, Sharma, Cauldwell, *et al.*, 2010), which has been shown to interact with the UB2H domain of PBP1b

(Egan *et al.*, 2018), which sits in between the glycosyltransferase and transpeptidase domains in the PBP1b structure (Sung *et al.*, 2009).

Outer membrane anchored lipoproteins were also found to control class A PBPs, and be essential for their activity *in vivo*. The Lpo proteins reach through the peptidoglycan layer and bind their cognate PBP (Figure 1.4). In *E. coli* LpoA is specifically required for PBP1a function, and LpoB for PBP1b function (Paradis-Bleau *et al.*, 2010; Typas *et al.*, 2010) (LpoP for PBP1b function in *Pseudomonas* (Greene *et al.*, 2018)). Deleting an Lpo protein mimics the *in vivo* phenotype of deleting the cognate PBP (Paradis-Bleau *et al.*, 2010; Typas *et al.*, 2010; Greene *et al.*, 2018). *E. coli* LpoB has an elongated structure with two distinct parts, an elongated disordered region near the N-terminus and a well-folded globular C-terminal domain (Egan *et al.*, 2014). The N-terminus comprises of a signal peptide which triggers the addition of a diacylglycerol moiety and an acyl group to the protein when it reaches the outer leaflet of the inner membrane before the signal peptide is cleaved. The mature triacylated lipoprotein is then translocated across the periplasm where it is anchored to the inner leaflet of the outer membrane by the localisation of lipoprotein (Lol) machinery (Nakayama *et al.*, 2012). The C-terminal domain in the periplasm is then free to bind to PBP1b, thought to be through PBP1b's UB2H domain, causing conformational changes which activate both PBP activities (Typas *et al.*, 2010; Egan *et al.*, 2014). Mutants of PBP1b which bypass the requirement for LpoB also support this model (Markovski *et al.*, 2016). The mechanism of LpoB activation is still however unclear, either LpoB stimulates PBP1b glycosyltransferase activity, which in turn provides more substrate for transpeptidation (Paradis-Bleau *et al.*, 2010; Egan *et al.*, 2014), or LpoB simultaneously stimulates both activities (Egan *et al.*, 2018). CpoB has also been reported to attenuate LpoB's activation of PBP1b by inhibiting it's activation of transpeptidation activity (Gray *et al.*, 2015; Egan *et al.*, 2018). It is however still unclear why LpoB's essentiality *in vivo* currently only reflects a modest enhancement of PBP1b activity *in vitro*.

1.6.3 Monofunctional PBPs

E. coli has two class B PBPs: PBP2 and PBP3. Both are essential for *E. coli* viability (Sauvage *et al.*, 2008), although this is not the case in all Gram-negative organisms, for example in *P. aeruginosa* PBP2 is not essential (Legaree *et al.*, 2007). PBP2 is thought to be involved in cell elongation, while PBP3 has a role in cell division. In support of this, *E. coli* thermosensitive mutants of PBP2 or cells treated with a PBP2 specific antibiotic grow as spheres, while mutants of PBP3 or cells treated with a PBP3 specific antibiotic become filamentous (Spratt, 1975)(Spratt, 1975)(Spratt, 1975)(Spratt, 1975; Bottat *et al.*, 1981; Garcia *et al.*, 1991). PBP2 has been shown to localise to the lateral wall of the cell, but also at the division site. However, it disperses before cell septation, suggesting it may play a role in cell division initiation but is not a stable member of the divisome (Den Blaauwen *et al.*, 2003). While PBP3 localises specifically to the division site and it's localisation is dependent on other divisome proteins (Weiss *et al.*, 1997). PBP3 is one of the last proteins to localise at the division site and it's localisation relies on the presence of FtsW (Pastoret *et al.*, 2004; Piette *et al.*, 2004). Both PBP3 and FtsW have been reported to directly interact *in vivo* and *in vitro* (Fraipont *et al.*, 2011).

PBP3 is a membrane protein comprising a short N-terminal cytoplasmic region, followed by a transmembrane helix, and a transpeptidase domain (Sauvage *et al.*, 2014), and is presumed to carry out peptidoglycan cross-linking during cell division, although to date this has not been confirmed *in vitro* with native substrates. FtsW, a SEDS proteins (Pastoret *et al.*, 2004; Meeske *et al.*, 2016), has recently been identified as a Lipid II polymerase (Taguchi *et al.*, 2019; Welsh *et al.*, 2019), and due to its interaction with PBP3 the two proteins have been proposed to create a two component peptidoglycan synthase during cell division (Figure 1.4). This complex would mirror the RodA-PBP2 complex which has been reported to synthesis peptidoglycan during cell elongation (Meeske *et al.*, 2016; Cho *et al.*, 2016; Rohs *et al.*, 2018). The localisation of PBP3 at the division site is also essential for PBP1b midcell localisation (Bertsche *et al.*, 2006), and FtsW, PBP3 and PBP1b have been reported to form a trimeric complex *in vitro* (Leclercq *et al.*, 2017). However, if and how these proteins function as a complex to synthesis peptidoglycan during cell division is unknown.

1.6.4 Mechanistic features of penicillin-binding protein activity

1.6.4.1 Glycosyltransferase mechanism

The glycosyltransferase reaction carried out by class A PBPs, SEDS proteins RodA and FtsW and mono-functional glycosyltransferases involves the polymerisation of Lipid II into glycan chains. A fundamental property of all of these glycosyltransferases is the direction of substrate polymerisation: Lipid II monomers are added to the reducing end of the growing glycan chain (undecaprenyl pyrophosphate end) (Figure 1.5) (Perlstein *et al.*, 2007; Welsh *et al.*, 2019). To start the catalytic cycle it is thought Lipid II binds to the glycosyltransferase donor site, which induces a conformational change to the glycosyltransferase active site facilitating Lipid II binding to the acceptor site. Catalysis occurs forming a glycosidic bond between the β1 of the MurNAc donor and β 4 of the GlcNAc acceptor, resulting in the departure of undecaprenyl pyrophosphate and translocation of the tetrasaccharide to the donor site. After initiation of glycan chain polymerisation the donor substrate becomes the growing glycan chain, and Lipid II the acceptor, and the cycle continues (Figure 1.5) (Lovering *et al.*, 2007; Bury *et al.*, 2015; King *et al.*, 2017; Punekar *et al.*, 2018). The growing glycan chain remains at the donor site until it is fully polymerised and released, suggesting that initiation of polymerisation is rate limiting and the subsequent elongation process is rapid and processive (Wang *et al.*, 2008; Punekar *et al.*, 2018).

Different glycosyltransferases differ in their processivity resulting in glycan chains of different length distributions. Glycosyltransferases have been shown to produce glycan chains with a characteristic intrinsic length distribution, which are independent of enzyme and substrate ratios (Wang *et al.*, 2008). *In vitro E. coli* PBP1b has been reported to produce glycan chains of between ~20-50 disaccharides in length depending on the assay conditions (Bertsche *et al.*, 2005; Wang *et al.*, 2008; Egan *et al.*, 2018), which are similar to the reported lengths of

~20-80 disaccharides produced *in vivo*, (Glauner *et al.*, 1988; Glauner and Holtje, 1990; Harz *et al.*, 1990).

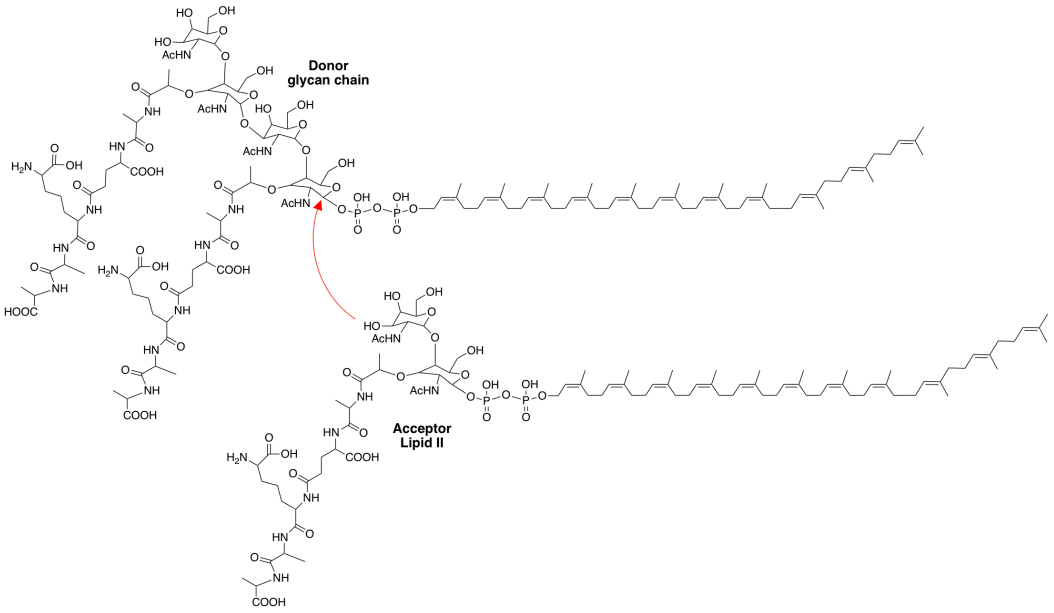

Figure 1.5: Glycosyltransferation mechanism.
Glycosyltransferases carry out the polymerisation of Lipid II into glycan chains. The active site glutamate of the glycosyltransferase deprotonates the GlcNAc 4-OH of the Lipid II acceptor. The activated nucleophile attacks the MurNAc carbon C1 of the growing glycan chain donor, leading to the formation of a β 1-4 glycosidic bond, elongation of the growing glycan chain and departure of undecaprenyl pyrophosphate.

1.6.4.2 Transpeptidase mechanism

With class A PBPs, and presumably with the SEDS proteins-class B PBP complex, the growing glycan chain is thought to be directed to the transpeptidase active site, where it acts as the donor substrate for transpeptidation. *E. coli* PBP1b has been shown to have little cross-linking activity with glycan chains not produced by itself (Terrak *et al.*, 1999). Consistent with this, a PBP1b structure-based model suggested the growing glycan chain delivered it's peptide stem to the transpeptidation active site for cross-linking (Sung *et al.*, 2009). Therefore, although glycan chain polymerisation can occur in the absence of transpeptidation, transpeptidation requires the glycan chain produced by polymerisation.

The catalysis carried out by the transpeptidase active site is initiated by the nucleophilic attack of the active site serine on the carboxyl moiety of the 4th position D-ala of the donor pentapeptide. This acylates the transpeptidase active site serine, releasing the terminal D-Ala from the donor stem peptide. The acyl-enzyme complex then either reacts with water releasing the tetrapeptide, which is termed carboxypeptidation, or with the ε-amino group of the 3rd position DAP of the acceptor stem peptide, creating a peptide bond and releasing the cross-linked product, which is termed transpeptidation (Figure 1.6) (Goffin and Ghuysen, 2002; Sauvage *et al.*, 2008). Apart from the native substrate of repeating GlcNAc MurNAc pentapeptide, the donor substrate can be a peptide with a D-Ala-D-Ala terminus or a thioester, while the acceptor substrate can be anything from a native glycan chain with a stem peptide containing DAP in the 3rd position, to a single D-amino acid (Nguyen-Disteche *et al.*, 1974; Adam *et al.*, 1991; Terrak *et al.*, 1999; Lupoli *et al.*, 2014; Boes *et al.*, 2019).

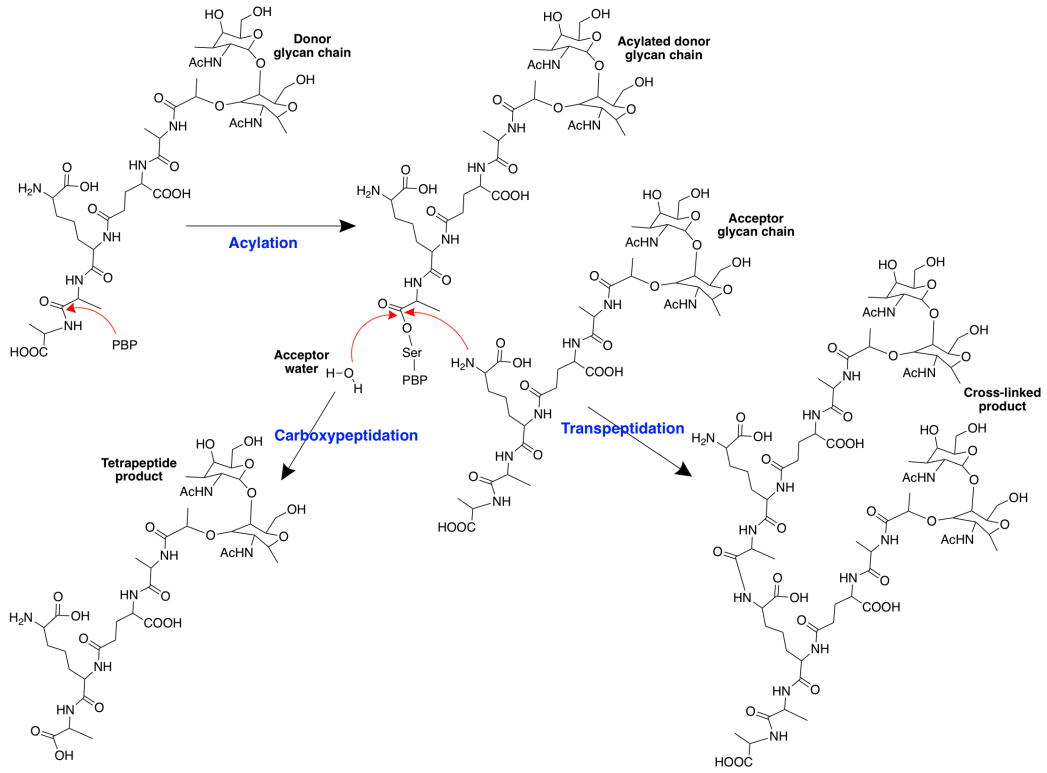

Figure 1.6: Transpeptidation and carboxypeptidation mechanisms.
Penicillin-binding proteins (PBP) cross-link the peptide stems of glycan chains to form peptidoglycan. The PBP active site serine (Ser) attacks the carboxyl moiety of the 4th position D-Ala in the donor stem peptide, releasing the 5th position D-Ala in the donor stem peptide. The acyl-enzyme complex then either reacts with water, releasing the tetrapeptide which is termed carboxypeptidation, or it reacts with the ε-amino group of the 3rd position DAP of the acceptor stem peptide, creating a peptide bond and releasing the cross-linked product which is termed transpeptidation.

In vitro different PBPs carry out transpeptidation to varying extents. *E. coli* PBP1a cross-links ~25% of stem peptides present (Born *et al.*, 2006), while PBP1b cross-links ~50% (Bertsche *et al.*, 2005; Egan *et al.*, 2018). Unlike class A PBPs there have been few reports of *in vitro* class B PBP transpeptidation activity, those that have been reported are *E. coli* PBP3 with thioester substrates (Boes *et al.*, 2019), *E. coli* PBP2 with native radioactive substrates (Banzhaf *et al.*, 2012), and *Streptococcus thermophilus* PBP2x using native substrates (Taguchi *et al.*, 2019).

1.7 Peptidoglycan hydrolases

Peptidoglycan hydrolases form a vast and highly diverse group of enzymes that cleave the covalent bonds in peptidoglycan or peptidoglycan fragments (Höltje, 1995). A hydrolytic activity has been identified for each bond linking the amino acids and sugars in peptidoglycan (Figure 1.7), and they have been shown to have roles in bacterial growth, division and shape maintenance (Vollmer, Joris, *et al.*, 2008). Assigning exact functions to hydrolases has however proved difficult, as they often have more than one function, and bacteria possess a high number of hydrolases that appear to have redundant roles (Holtje and Tuomanen, 1991; van Heijenoort, 2011). In *E. coli* at least 35 peptidoglycan hydrolases have been identified, including *N*-acetylglucosaminidase, lytic transglycosylases, carboxypeptidases, endopeptidases, LD-transpeptidases, amidases and D-Ala-D-Ala dipeptidase (van Heijenoort, 2011). They all have different cleavage sites which are often specific to a certain peptidoglycan element, fragment or modification.

There are two types of glycan chain cleavage enzymes, lytic transglycosylases, which cleave the β1-4 glycosidic bond between MurNAc and GlcNAc (Figure 1.7), creating a 1,6-anhydro bond between the C1 and C6 of MurNAc, and N-acetylglucosaminidase, which hydrolyses the β 1-4 glycosidic bond between MurNAc or 1,6-anhydro MurNAc, and GlcNAc disaccharides (Holtje *et al.*, 1975; van Heijenoort, 2011).

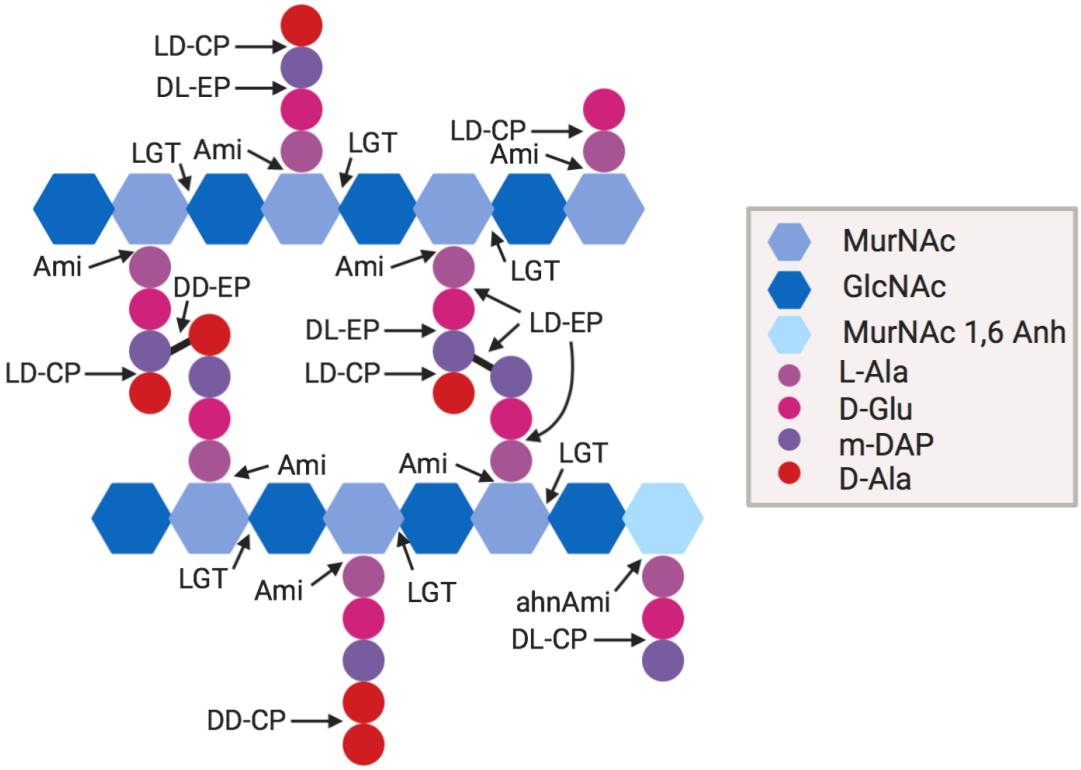

Figure 1.7: Peptidoglycan hydrolases.
Hydrolysis of amide and peptide bonds in peptidoglycan. Lytic glycosyltransferases (LGT) hydrolyse the glycosidic bond between MurNAc and GlcNAc creating 1,6-anhydroMurNAc. Amidases (Ami) hydrolyse the amide bonds between the lactyl group of MurNAc and the L-alanine of the stem peptide. Some amidases (anhAmi) specifically cleave at 1,6-anhydroMurNAc residues. Endopeptidases (D,D-EPase, L,D-EPase, D,L-EPase) cleave amide bonds in the peptide stems or the cross-links. Carboxypeptidases (D,D-CPase, L,D-CPase, D,L-CPase) hydrolyse peptide bonds to remove C-terminal D-or L-amino acids from the stem peptide.

E. coli has at least 20 peptidases which cleave the peptide bonds in peptidoglycan, muropeptides or precursors. All the class C PBPs fit into this category (van Heijenoort, 2011). The peptidases include carboxypeptidases which remove the terminal amino acid in the stem peptide, and endopeptidases which cleave within peptide stems or the cross-links, and are either D,D-peptidases which cleave between D-amino acids, or L,D- and D,L-peptidase which cleave between L- and D-amino acids (Figure 1.7) (Vollmer, Joris, *et al.*, 2008). D,D-carboxypeptidase PBP5 is thought to be the most active carboxypeptidase and its deletion gives rise to cells with altered diameters and non-uninform surfaces (Nelson and Young, 2000). L,D-transpeptidases are also classed as hydrolases, and they are responsible for the formation of m-DAP-m-DAP cross-links, which also cause L,D-carboxypeptidation (release of D-Ala) (Figure 1.7) (Magnet *et al.*, 2008).

Amidases hydrolyse the amide bond between the L-Ala in the stem peptide and the D-lactoyl moiety of MurNAc (Figure 1.7) (Vollmer, Joris, *et al.*, 2008), and they have been found to be important in cell septation, as double and triple mutants of AmiA, AmiB and AmiC grow as filaments and were unable to cleave peptidoglycan at the septum to permit cell division (Heidrich *et al.*, 2001). Finally the D-Ala-D-Ala dipeptidase which is responsible for the hydrolysis of the peptide bonds between D-Ala-D-Ala dipeptides (Lessard *et al.*, 1998; Lessard and Walsh, 1999).

1.8 Thesis aims

Antimicrobial resistance poses an already growing problem for modern day medicine. A world-wide coordinated effort is required to prolong the life of our current antibiotics, in addition to the development of novel antibiotics. A better understanding of existing valuable drug targets is required and this thesis aims to contribute to this by extending our current understanding of the function and enzymatic mechanisms of PBPs in Gram-negative bacteria by:

- Development of existing glycosyltransferase and transpeptidase assays to measure *Y. pestis* PBP1b *in vitro* activity to investigate its substrate specificity.

- Reconstitute the cell wall synthesis complex *in vitro* to investigate the interactions between *Y. pestis* and *E. coli* PBP1b and divisome proteins LpoB, CpoB and FtsN.

- Development of an *in vitro* assay to measure *P. aeruginosa* PBP3 activity to investigate its enzymology.

Chapter 2. Materials and methods

2.1 Materials

2.1.1 Chemicals, buffers and solutions

All chemicals used were of analytical grade and from Sigma Aldrich, Fischer Scientific or Melford, unless otherwise stated. All buffers were prepared using MilliQ purified water and adjusted to the correct pH using a SevenEasy pH meter (Mettler Toledo), calibrated at ambient temperature with pH 4.0, 7.0 and 10.0 buffer standards. For molecular biology techniques and chromatography, buffers were filtered using 0.22 μm MF-Millipore membrane filter (Merck) and stored at 4 °C.

2.1.2 *E. coli* strains

E. coli NEB5-α was used for molecular cloning, and BL21 (DE3), BL21 (DE3)*pRosetta or C43 (DE3) were used for recombinant protein expression (detailed in table 2.2).

2.1.3 Growth media

E. coli strains were grown in Luria-Bertani (LB) media, super optimal broth with catabolite repression (SOC) media, or on Luria-Bertani agar plates. For selective media, kanamycin was used at 100 μg mL^{-1} and chloramphenicol at 35 μg mL^{-1}.

LB media consisted of 1 % (w/v) tryptone, 0.5 % (w/v) NaCl and 0.5 % (w/v) yeast extract. LB agar plates were made with LB media supplemented with 1.5 (w/v) bacto-agar. SOC media consisted of 2 % (v/v) peptone, 0.5 % (w/v) yeast extract, 10 mM NaCl, 2.5 mM KCl, 10 mM $MgCl_2$, 10 mM $MgSO_4$ and 20 mM glucose.

2.1.4 Vectors and oligonucleotides

Vectors and oligonucleotides were purchased from Integrated DNA Technologies. Oligonucleotides were designed against the appropriate gene or plasmid of interest with the relevant restriction enzyme or mutation sites. Oligonucleotides for Gibson assembly were designed using the online NEBuilder Assembly Tool (New England BioLabs). The oligonucleotides used are detailed in table 2.1.

2.2 Molecular biology

2.2.1 Preparation of chemically competent *E. coli* cells

An overnight culture was prepared by inoculating 10 mL of LB media, supplemented with the appropriate antibiotics, with an *E. coli* colony of the required strain. The culture was incubated overnight at 37 °C with shaking at 180 rpm. 1 mL of the overnight culture was used to inoculate 100 mL of LB media supplemented with the appropriate antibiotics and 20 mM $MgSO_4$, and incubated at 37 °C with shaking at 180 rpm until the optical density (absorbance at 600 nm, OD_{600}) was in the range of 0.5-0.6. The cells were harvested at 3000 rpm for 10 minutes at 4 °C and then resuspended in 40 mL of ice cold TBF1 buffer (30 mM potassium acetate, 100 mM $RbCl_2$, 50 mM $MnCl_2$, 10 mM $CaCl_2$ and 15% (v/v) glycerol pH 5.8) and incubated on ice for 5 minutes. The cells were harvested again as before, and resuspended in 2 mL of ice cold TBF2 buffer (10 mM MOPS, 10 mM $RbCl_2$, 75 mM $CaCl_2$ and 15% (v/v) glycerol pH 6.5) and incubated on ice for 1 hour. The competent cells were aliquoted in 50 μL aliquots, flash frozen in liquid nitrogen and stored at -80 °C.

Table 2.1 Constructs used for recombinant protein expression in *E. coli.*

Kan_R: kanamycin resistant vector, T7: T7 expression system using the bacteriophage T7 promoter, His tag: hexa-histidine tag, DAAO: D-amino acid oxidase, F: forward oligonucleotide, and R: reverse oligonucleotide. Oligonucleotide restriction sites are in bold and mutated residues in red.

Construct	Vector	Vector features	Cloning (type and features)	Gene encoding	Source (if this study oligonucleotides (5'-3'))
pET47b_Yp1b	pET-47b	T7, N-terminal His tag cleavable by 3C protease, Kan_R	Restriction enzyme, KpnI and SacI	*Y. pestis* PBP1b (61-803)	F:TCCCA**GGTACC**AGCCACCTCGCAAGAAACGCC, R:ATAGT**GAGCTC**TCAAGTGGGTGTTGATCCCTGAC
pET47b_Yp1bI205F	pET-47b	T7, N-terminal His tag cleavable by 3C protease, Kan_R	Site directed mutagenesis	*Y. pestis* PBP1b (61-803) I205F	F:GCCTCGATCCCAAGTTGTTTACCATGCTGCAATCACCTAACG, R:CGTTAGGTGATTGCAGCATGGTAAACAACTTGG GATCGAGGC
pET47b_Yp3	pET-47b	T7, N-terminal His tag cleavable by 3C protease, Kan_R	Restriction enzyme, BamHI and HindIII	*Y. pestis* PBP3 (59-587)	F:TTCCCA**GGATCC**GCGCTCGCTGCGAGTACAAGAG, R:ATAGT**AAGCTT**TTACGATCTGCCACCTGAACCC
pET47b_YpLpoB	pET-47b	T7, N-terminal His tag cleavable by 3C protease, Kan_R	Restriction enzyme BamHI and SacI	*Y. pestis* LpoB (57-191)	F:TTCCCA**GGATCC**GATTGACTGGGCTGTCAGTGTTG, R:ATAGT**GAGCTC**TCAATATTGGACAGGCGCATTACC
pET47b_YpCpoB	pET-47b	T7, N-terminal His tag cleavable by 3C protease, Kan_R	Gibson assembly	*Y. pestis* CpoB (24-269)	F:TCCTCTTTCAGGGACCCGGGGCTACTGCCCAAGCGCCA, R:TTTCT TTACTACCGCGTGGCCTAAAGAGCAGATAAACGTTTCTGTGCC
pET47b_YpFtsN	pET-47b	T7, N-terminal His tag cleavable by 3C protease, Kan_R	Restriction enzyme, BamHI and HindIII	*Y. pestis* FtsN (1-281)	F:TTCCCA**GGATCC**GGCACAAAGAGATTATGTAAGCCGA, R:ATAGT**AAGCTT**TCAACCCCCAACAGAGAGGG
pDB_Ec1b	pET-47b	T7, N-terminal His tag cleavable by 3C protease, Kan_R	N/A	*E. coli* PBP1b (58-804	Bellini D., (unpublished)
pET47b_EcLpoB	pET-47b	T7, N-terminal His tag cleavable by 3C protease, Kan_R	Gibson assembly	*E. coli* LpoB (78-213)	F:CAGGGACCCGGGTATGACTGGAATGGCGCAATG, R:CTACCGCGTGGCTTATTGCTGCGAAACGGCAC
pET47b_EcCpoB	pET-47b	T7, N-terminal His tag cleavable by 3C protease, Kan_R	Gibson assembly	*E. coli* CpoB (27-263)	F:TCCTCTTTCAGGGACCCGGGCAGGCACCAATCAGTAGTG, R:TTTCTTTACTACCGCGTGGCTTACATCGCGTTCAGACG
pDB_EcFtsN	pET-47b	T7, N-terminal His tag cleavable by 3C protease, Kan_R	N/A	*E. coli* FtsN (1-319)	Bellini D., (unpublished)
pET28b_EcMepA	pET-28b	T7, C-terminal His tag, Kan_R	Gibson assembly	*E. coli* MepA (1-274)	F:CAGTGGTGGTGGTGGTGGTGGATCACGTGCTCATCCAG, R:CTTTAAGAAGGAGATATACCATGAATAAAACCGCGATTGC
pET47b_Pa1b	pET-47b	T7, N-terminal His tag cleavable by 3C protease, Kan_R	Gibson assembly	*P. aeruginosa* PBP1b (16-740)	F:TTTCTTTACTACCGCGTGGCTCATACGGCATTCGGGCAATCCG, R:TCCTCTTTCAGGGACCCGGGCCGGCACCCGGCCT GAAC
pET47b_PaLpoB	pET-47b	T7, N-terminal His tag cleavable by 3C protease, Kan_R	Gibson assembly	*P. aeruginosa* LpoP (123-259)	F:TTTCTTTACTACCGCGTGGCTCAGGAGCTGACCTTGGC, R:TCCTCTTTCAGGGACCCGGGTACAACATGCCGCCCAGC
pDB_3C	pET-28a	T7, N-terminal His tag, Kan_R	N/A	Human Rhinovirus 3C protease	Bellini D., (unpublished)
pET28a_RgDAAO	pET-28a	T7, His tag, Kan_R	N/A	*Rhodotorula gracilis* DAAO	Bibi S., (2010)
Gibson assembly linear vector	pET-47b	T7, N-terminal His tag cleavable by 3C protease, Kan_R	Gibson assembly	N/A	F:CCCGGGTCCCTGAAAGAGG, R:GGTTTCTTTACTACCGCGTGGC
Gibson assembly linear vector	pET-28b	T7, C-terminal His tag, Kan_R	Gibson assembly	N/A	F:GGTATATCTCCTTCTTAAAGTTAAACAAAATTATTTCTAGAGGGG AATTGTTATC, R:CACCACCACCACCACCACTG

2.2.2 Transformation of chemically competent *E. coli* cells

Plasmid DNA (1-2 μL of 50-100 ng μL^{-1}) was incubated with 50 μL of thawed competent cells on ice for 30 minutes. Cells were heat shocked at 42 °C for 30 seconds and returned to ice for 10 minutes. Outgrowth was performed by the addition of 950 μL SOC media and incubation at 37 °C for 1 hour with shaking at 180 rpm. 100 μL of the culture was spread on a LB agar plate, supplemented with the appropriate antibiotics, and incubated overnight at 37 °C to allow for selection of positive transformants.

2.2.3 Polymerase chain reaction

Polymerase chain reaction (PCR) was carried out with Phusion High-Fidelity DNA polymerase (New England BioLabs) according to the manufacturer's instructions, with a SureCycler 8800 thermocycler (Agilent Technologies). *E. coli* K12 genomic DNA, and *Y. pestis* strain C092 genomic DNA kindly gifted by H. Atkins (DSTL), were used as templates to amplify the genes of interest with the oligonucleotides detailed in table 2.1. Oligonucleotide annealing temperatures were determined using the online NEB Tm Calculator (New England BioLabs), and PCR reactions were run with annealing temperatures over a gradient of 3 °C either side of the calculated annealing temperature.

2.2.4 Agarose gel electrophoresis

1% (w/v) agarose gels were prepared in TAE buffer (40 mM Tris-acetate pH 8.3, 20 mM acetic acid and 1 mM EDTA) using GelRed Nucleic Acid Gel Stain (Biotum) (1 μL to 100 mL 1% (w/v) agarose). 5 μL of PCR product was mixed with 6x Gel loading dye (New England BioLabs) and loaded onto the gel submerged in TAE buffer in a MultiSUB Midi Horizontal Gel System (Cleaver Scientific). 100 bp or 1 kb DNA ladder (New England BioLabs) were loaded as a size reference for the sample lanes. Electrophoresis was carried out at 120 V, 400 mA for 1 hour and DNA was visualised under ultraviolet light using an E-box illuminator (Vilber).

2.2.5 Purification and gel extraction of PCR products

If the PCR product was free of any contaminating bands of the incorrect size the DNA was purified using a Monarch PCR and DNA clean-up kit (New England BioLabs) according to the manufacturer's instructions. If the PCR product contained contaminating bands, the entire PCR product was run on an agarose gel as in section 2.2.4, and the band of interest was excised from the gel. The DNA was then extracted from the gel slice using a Monarch DNA Gel Extraction kit (New England BioLabs), following the manufacturer's instructions.

2.2.6 Restriction enzyme digestion

For restriction enzyme cloning, restriction digestion of the purified PCR products or vector were performed with the appropriate restriction enzymes (New England BioLabs) (detailed in table 2.1), according to the manufacturer's protocol. Digested plasmid was subsequently treated with shrimp alkaline phosphatase (New England BioLabs) according to the manufacturer's instructions to prevent plasmid self-ligation.

For Gibson cloning, the linearised vector PCR product was treated with DpnI (New England BioLabs) according to the manufacturer's instructions, to cleave any template plasmid and prevent false positive transformants.

2.2.7 Restriction enzyme cloning ligation

Ligation reactions were carried out using T4 DNA ligase (New England BioLabs) according to the manufacturer's instructions. Approximately 50 ng of linearised vector was used in a 3:1 ratio (insert:vector), with the insert mass calculated using the online NEBio Calculator (New England BioLabs). 2 μL of the ligation reaction was then transformed into chemically competent NEB5-α cells as described in 2.2.2.

2.2.8 Gibson assembly

Gibson assembly reactions were carried out using a NEBuilder HiFi DNA assembly cloning kit (New England BioLabs) according to the manufacturer's instructions for a 2-3 fragment assembly. 50 ng of vector DNA was used in a 2:1 ratio (insert:vector), with the insert mass calculated using the online NEBio Calculator (New England BioLabs). 2 μL of the ligated construct was then transformed into chemically competent NEB5-α cells as described in 2.2.2.

2.2.9 Plasmid purification

An overnight culture was prepared by inoculating 10 mL of LB media, supplemented with the appropriate antibiotics, with a transformed colony. The culture was incubated overnight at 37 °C with shaking at 180 rpm. The plasmid was purified using a Monarch Plasmid miniprep kit (New England BioLabs) according to the manufacturer's instructions.

2.2.10 DNA quantification and sequencing

DNA was quantified using a NanoDrop ND60 spectrophotometer (Agilent) and sequenced by GATC Biotech (Germany) with T7 promoter and terminator oligonucleotides (T7 promoter- 5' TAATACGACTCACTATAGGG, T7 terminator- 5' GCTAGTTATTGCTCAGCGG).

2.2.11 Plasmid mutagenesis

Plasmid mutagenesis was carried out with a Q5 Site-Directed Mutagenesis kit (New England BioLabs) according to the manufacturer's instructions using the oligonucleotides detailed in table 2.1. 2 μL of the multi-enzyme treated ligation mix was then transformed into chemically competent NEB5-α cells, the plasmid purified, quantified and sequenced as in sections 2.2.2, 2.2.9 and 2.2.10.

2.3 Protein expression and purification

2.3.1 Recombinant protein expression in *E. coli*

An overnight culture was prepared by inoculating 10 mL of LB media with a single colony of transformed construct in the appropriate *E. coli* expression strain (detailed in table 2.2), which was grown over night at 37 °C with shaking at 180 rpm. The protein of interest was expressed in 3 L of LB media. 5 mL of the starter culture was used to inoculate 1L of LB media, supplemented with the appropriate antibiotics, and grown at 37 °C with shaking at 180 rpm until an OD_{600} of 0.5-0.6 was achieved. Depending on the protein being expressed, the cultures may have been cold-shocked before protein expression was induced by placing the cultures at 4 °C , detailed in table 2.2. Protein expression was induced with the concentration of IPTG detailed in table 2.2 and the cultures incubated for the length of time and at the temperature specified in table 2.2, with shaking at 180 rpm. Cells were pelleted at 5000 rpm for 15 minutes at 4 °C in a Beckman JLA 8.1000 rotor, and stored at -20 °C if not being purified the same day.

2.3.2 Protein purification and quantification

Membrane proteins (detailed in table 2.3) were purified from cell pellets using the method in section 2.3.2.1, while soluble proteins (detailed in table 2.3) were purified using the method in section 2.3.2.2, with the exception of *Rhodotroula gracilis* D-amino acid oxidase (DAAO) which was purified as in section 2.3.2.3.

E. coli PBP1b (residues in parenthesis) (58-804) I202F, *E. coli* PBP1b (58-804) S510A, *E. coli* PBP3 (60-588), *P. aeruginosa* PBP3 (64-579), *A. baumanni* PBP3 (64-579) and *B. pseudomallei* PBP3 (63-614) proteins were kindly gifted by D. Bellini (Warwick) and *E. coli* DacB (21-477) by A. Lloyd (Warwick).

Table 2.2 Conditions for recombinant protein expression in *E. coli*.
Cold shock at 4 °C and expression conditions also involve shaking at 180 rpm.

Protein	Construct	*E. coli* expression strain	Protein expression details		
			Cold shock	IPTG concentration	Expression condition
***Y. pestis* PBP1b (61-803)/ I205F**	pET47b_Yp1b/ I205F	C43 (DE3)	30 minutes	0.65 mM	20 °C for 17 hours
***Y. pestis* FtsN (1-281)**	pET47b_YpFtsN	BL21 (DE3)	30 minutes	0.65 mM	20 °C for 17 hours
***E. coli* PBP1b (58-804)**	pDB_Ec1b	C43 (DE3)	30 minutes	0.65 mM	20 °C for 17 hours
***E. coli* FtsN (1-319)**	pDB_EcFtsN	BL21 (DE3)*pRosetta	30 minutes	0.65 mM	20 °C for 17 hours
***Y. pestis* LpoB (57-191)**	pET47b_YpLpoB	BL21 (DE3)	20 minutes	1 mM	37 °C for 4 hours
***Y. pestis* CpoB (24-269)**	pET47b_YpCpoB	BL21 (DE3)	-	1 mM	25 °C for 17 hours
***E. coli* LpoB (78-213)**	pET47b_EcLpoB	BL21 (DE3)	20 minutes	1 mM	20/25 °C for 17 hours
***E. coli* CpoB (27-263)**	pET47b_EcCpoB	BL21 (DE3)	-	1 mM	25 °C for 17 hours
***Y. pestis* PBP3 (59-587)**	pET47b_Yp3	BL21 (DE3)	1 hour	0.25 mM	20/25 °C for 17 hours
***E. coli* MepA (1-274)**	pET28b_EcMepA	BL21 (DE3)	15 minutes	0.5 mM	25 °C for 17 hours
Human Rhinovirus 3C protease	pDB_3C	BL21 (DE3)	30 minutes	0.65 mM	25 °C for 17 hours
***Rhodotorula gracilis* DAAO**	pET28a_RgDAAO	BL21 (DE3) *pRosetta	-	1 mM	20 °C for 17 hours

Table 2.3 Recombinant protein purification methods and buffers.

Protein	Purification type	Pellet resuspension buffer	Buffer A	Buffer B	Storage buffer
Y. pestis **PBP1b (61-803)/ I205F** ***Y. pestis*** **FtsN (1-281)** ***E. coli*** **PBP1b (58-804)** ***E. coli*** **FtsN (1-319)**	Membrane protein	100 mM Tris, 500 mM NaCl, 20 mM Imidazole, 2 % (v/v) glycerol pH 8.0	100 mM Tris, 500 mM NaCl, 20 mM Imidazole, 2 % (v/v) glycerol, 0.86% (w/v) CHAPS pH 8.0	100 mM Tris, 500 mM NaCl, 500 mM Imidazole, 2 % (v/v) glycerol, 0.86% (w/v) CHAPS pH 8.0	10 mM Tris, 500 mM NaCl, 2% (v/v) glycerol, 0.86% (w/v) CHAPS pH 8.0
Y. pestis **LpoB (57-191)** ***Y. pestis*** **CpoB (24-269)** ***E. coli*** **LpoB (78-213)** ***E. coli*** **CpoB (27-263)** ***Y. pestis*** **PBP3 (59-587)**	Soluble protein	100 mM Tris, 500 mM NaCl, 20 mM Imidazole, 2 % (v/v) glycerol pH 8.0		100 mM Tris, 500 mM NaCl, 500 mM Imidazole, 2 % (v/v) glycerol pH 8.0	10 mM Tris, 500 mM NaCl, 2% (v/v) glycerol pH 8.0
E. coli **MepA (1-274)**	Soluble protein	50 mM Tris, 200 mM NaCl, 20 mM Imidazole pH 7.5		50 mM Tris, 200 mM NaCl, 500 mM Imidazole pH 7.5	10 mM Tris pH 7.5
Human Rhinovirus 3C protease	Soluble protein	100 mM Tris, 500 mM NaCl, 20 mM Imidazole, 10 % (v/v) glycerol pH 8.0		100 mM Tris, 500 mM NaCl, 500 mM Imidazole, 10 % (v/v) glycerol pH 8.0	10 mM Tris, 500 mM NaCl, 10% (v/v) glycerol pH 8.0
Rhodotorula gracilis **DAAO**	Soluble protein	50 mM Tris, 2 μM pepstatin, 0.2 mM PMSF, 5% (v/v) glycerol pH 8.0	50 mM Tris, 300 mM NaCl, 250 μM FAD, 5% (v/v) glycerol pH 8.0	50 mM Tris, 300 mM NaCl, 500 mM Imidazole, 250 μM FAD, 5% (v/v) glycerol pH 8.0	50 mM Tris, 50 mM Lactitol, 5 mM EDTA, 25 μM FAD, 10% (v/v) glycerol pH 7.5

2.3.2.1 Membrane protein purification and quantification

Combined cell pellets from 3 L of culture was resuspended in 135 mL of cold pellet resuspension buffer (detailed in table 2.3 for membrane protein purifications), supplemented with 10 mM $MgCl_2$, 20 μg mL^{-1} deoxyribonuclease I from bovine pancreas (Sigma Aldrich) and 1 mg mL^{-1} lysozyme from chicken egg white (Sigma Aldrich) at 4 °C. The cells were lysed by passing through a continuous cell disrupter (Constant systems) twice at 30 000 psi. The lysed cells were then incubated with 3.25% (w/v) CHAPS to solubilise the membranes (addition of 15 mL 32.5% (w/v) CHAPS) for 4 hours at 4 °C. The cell debris was then pelleted at 16 000 rpm for 30 mins at 4 °C in a Beckman JA 25.50 rotor. The supernatant was loaded onto a 5 mL HisTrap HP column (GE Healthcare) equilibrated in Buffer A (detailed in table 2.3) at 4 °C. Using an AKTA 10/100 system (GE Healthcare) in a cold cabinet at 4 °C, unbound proteins were washed off the column with 30 mL of buffer A, and then weakly bound proteins were washed off the column with 30 mL of 10% (v/v) Buffer B in Buffer A (detailed in table 2.3). The target protein was eluted with a gradient of 10-100% (v/v) Buffer B in Buffer A (detailed in table 2.3) over 30 mL, where 2 mL fractions were collected.

The protein-containing fractions were pooled, and their concentration was measured by a NanoDrop ND60 spectrophotometer (Agilent) using the extinction coefficient calculated by the online ExPASy ProtParam tool at 280 nm. The His-tag was cleaved with human rhinovirus 3C protease (1:30, 3C:Protein) overnight at 4 °C, while dialysing (dialysis tubing: 15.9 mm diameter, 12-14 kDa MWCO (Medicell International)) into storage buffer (detailed in table 2.3).

The untagged protein was separated from the His-tag by reverse IMAC using a 5 mL HisTrap HP column (GE Healthcare) equilibrated in the dialysis buffer on an AKTA 10/100 system (GE Healthcare) in a cold cabinet at 4 °C. The flow through containing the untagged protein of interest was then concentrated to the required concentration using a vivaspin (GE Healthcare) and stored at -20 °C.

2.3.2.2 Soluble protein purification and quantification

Combined cell pellets from 3 L of culture was resuspended in 150 mL of cold pellet resuspension buffer (detailed in table 2.3 for soluble protein purifications), supplemented with 10 mM $MgCl_2$, 20 μg mL^{-1} deoxyribonuclease I from bovine pancreas (Sigma Aldrich) and 1 mg mL^{-1} lysozyme from chicken egg white (Sigma Aldrich) at 4 °C. The cells were lysed by sonication on ice 10 times for 20 seconds, interspaced with 40 seconds of cooling on ice, at 70% power (Bandelin Sonoplus) and the cell debris was then pelleted at 16 000 rpm for 30 mins at 4 °C in a Beckman JA 25.50 rotor. The supernatant was loaded onto a 5 mL HisTrap HP column (GE Healthcare) equilibrated in Buffer A (detailed in table 2.3) at 4 °C. Using an AKTA 10/100 system (GE Healthcare) in a cold cabinet at 4 °C, unbound proteins were washed off the column with 30 mL of buffer A, and then weakly bound proteins were washed off the column with 30 mL of 10% (v/v) Buffer B in Buffer A (detailed in table 2.3). The target protein was eluted with a gradient of 10-100% (v/v) Buffer B in Buffer A (detailed in table 2.3) over 30 mL, where 2 mL fractions were collected.

The protein-containing fractions were pooled, and their concentration was measured by a NanoDrop ND60 spectrophotometer (Agilent) using the extinction coefficient calculated by the online ExPASy ProtParam tool at 280 nm. Excluding purifications for human rhinovirus 3C protease and *E. coli* MepA, the His-tag was cleaved from the protein with human rhinovirus 3C protease (1:30, 3C:Protein) overnight at 4 °C, while dialysing (dialysis tubing: 15.9 mm diameter, 12-14 kDa MWCO (Medicell International), or for LpoB: 32 mm benzoylated 2000 MWCO (Sigma Aldrich)) into storage buffer (detailed in table 2.3).

The untagged protein was separated from the His-tag by reverse IMAC using a 5 mL HisTrap HP column (GE Healthcare) equilibrated in the dialysis buffer on an AKTA 10/100 system (GE Healthcare) in a cold cabinet at 4 °C. The flow through containing the untagged protein of interest was then concentrated to the required concentration using a vivaspin (GE Healthcare) and stored at -20 °C.

For human rhinovirus 3C protease and *E. coli* MepA purifications, the pooled fractions were dialysed (dialysis tubing: 15.9 mm diameter, 12-14 kDa MWCO (Medicell International) overnight at 4 °C into storage buffer (detailed in table 2.3). The dialysed protein was then concentrated to the required concentration using a vivaspin (GE Healthcare) and stored at -20 °C.

2.3.2.3 *Rhodotroula gracilis* D-amino acid oxidase purification, quantification and activity determination

R. gracilis DAAO was purified, quantified and assayed for activity as previously described by Catherwood *et al.* (2019). In brief, combined cell pellets from 3 L of culture was resuspended in 100 mL of cold pellet resuspension buffer (detailed in table 2.3) with 20 μg mL^{-1} deoxyribonuclease I from bovine pancreas (Sigma Aldrich), 2.5 mg mL^{-1} lysozyme from chicken egg white (Sigma Aldrich) and 3 mM flavin adenine dinucleotide (FAD) at 4 °C. The cells were lysed by sonication on ice 10 times for 15 seconds, interspaced with 45 seconds of cooling on ice, at 70% power (Bandelin Sonoplus) and the cell debris was then pelleted at 50 000 x g for 45 mins at 4 °C in a Beckman JA 25.50 rotor. The supernatant was loaded onto a 5 mL HisTrap HP column (GE Healthcare) at 4 °C, equilibrated in Buffer A (detailed in table 2.3). Using an AKTA 10/100 system (GE Healthcare) in a cold cabinet at 4 °C, unbound proteins were washed off the column with 30 mL of Buffer A, and the target protein was eluted with a gradient of 0-100% (v/v) Buffer B in Buffer A (detailed in table 2.3) over 50 mL, where 2 mL fractions were collected.

The protein containing fractions were pooled, and subjected to cycles of concentration and dilution with 50 mM Tris, 300 mM NaCl, 0.25 mM FAD and 5% (v/v) glycerol pH 8.0 in a vivaspin (GE Healthcare) at 4000 rpm at 4 °C until the estimated imidazole concentration was ~37.5 μM. The protein was diluted into storage buffer (table 2.3) and concentrated to a protein concentration of >60 mg mL^{-1}, determined using a Bradford protein assay at A_{595} (Bio-Rad protein assay dye reagent concentrate, Bio-Rad). The FAD concentration of the sample was estimated in 50 mM sodium phosphate pH 7.0 at A_{450} (molar extinction

coefficient of FAD at A_{450} = 11 300 $M^{-1}cm^{-1}$ (Dawson *et al.*, 1986)), and the FAD concentration was then corrected to be 1.1 times the molar concentration of DAAO in the sample.

The activity of *R. gracilis* DAAO was then determined by diluting DAAO 1 in 10000 in storage buffer (table 2.3). Activity assays contained 50 mM Bis-Tris propane pH 8.5, 20 mM $MgCl_2$, 0.1% (v/v) Triton X-100, 22.5-35 U ml^{-1} rabbit muscle L-lactate dehydrogenase, 0.3 mM NADH and ~1.25 nM DAAO. Auto-oxidation of NADH was followed for 5 minutes at A_{340}, after which time, DAAO activity was initiated by the addition of 1 mM D-alanine. The unit concentration of DAAO was derived from its initial rate calculated by the difference between rates in the presence and absence of 1 mM D-alanine (molar extinction coefficient of NADH at A_{340}= 6220 M^{-1} cm^{-1} (Dawson *et al.*, 1986)). DAAO activity was adjusted to 2891 μmol^{-1} min^{-1} mL^{-1} in storage buffer and stored at -80 °C.

2.3.2.4 Protein visualisation by SDS-PAGE gel electrophoresis

Protein samples were visualised under denaturing conditions by SDS-PAGE gel electrophoresis in a discontinuous Tris-glycine buffer system. 5 μg of purified protein was mixed with loading dye (5x stock: 312 mM Tris, 10% (w/v) SDS, 50% (v/v) glycerol, 0.05% (w/v) bromophenol blue, 50 mM DTT pH 6.8). 12 % (v/v) acrylamide:bis-acrylamide (29:1) gels were cast using a Mini- Protean Tetra System gel kit (Bio-Rad). 5 mL resolving gel consisting of 375 mM Tris pH 8.8, 12% (v/v) acrylamide:bis-acrylamide (29:1) and 0.1 % (w/v) SDS, was polymerised with 37.5 µL of 10 % (w/v) ammonium persulfate (APS), and 7.5 µL tetramethylethanediamine (TEMED). 1.5 mL stacking gel consisted of 125 mM Tris pH 6.8, 5 % (v/v) acrylamide:bis-acrylamide (29:1) and 0.1 % (w/v) SDS, was polymerised with 7.5 µL of 10 % (w/v) APS and 1.5 µL TEMED. The samples were loaded onto the gel along with a protein molecular weight marker (colour prestained protein standard, New England BioLabs) for size reference and gel electrophoresis was carried out in 25 mM Tris, 190 mM glycine and 0.1% (w/v) SDS pH 8.3 at 200 V and 400 mA for ~50 minutes. The gel was stained with InstantBlue (Exedeon) and imaged with an E-box illuminator (Vilber).

2.4 PBP substrate synthesis

2.4.1 UDP-MurNAc pentapeptide synthesis and quantification

All PBP substrates were prepared via enzymatic synthesis of their UDP-MurNAc 5P (DAP) precursor as described by Lloyd *et al.* (2008). Briefly a 2 mL reaction contained 50 mM HEPES pH 7.6, 10 mM $MgCl_2$, 200 mM phosphoenolpyruvate, 1 mM dithiothreitol (DTT), 50 mM KCl, 8.22 mM UDP-GlcNAc, 1.2 μM MurA, 57.3 μM MurB, 0.2 mM NADP, 1.48 U mL^{-1} isocitrate dehydrogenase (Sigma-Aldrich), 26 mM D,L- isocitrate, 6 mM ATP, 5.53 U mL^{-1} pyruvate kinase (Sigma-Aldrich), 4.3 μM MurC, 35 mM L-Ala, 1.1 μM MurD, 105 mM D-isoGln, 4.0 μM MurE, 80 mM D,L-DAP, 8.5 μM MurF and 35 mM D-alanyl-D-alanine. All Mur ligases were from *P. aeruginosa* and kindly supplied by A. Catherwood and J. Tod (Warwick). Syntheses were incubated at 37 °C overnight, and then diluted with 5 mL of sterile water prior to filtration using a 10 000 MWCO vivaspin (GE Healthcare) at 4000 rpm and 4 °C, to separate the reaction products from the proteins. The filtered sample was further diluted into 100 mL sterile water.

UDP-MurNAc 5P was purified by anion exchange on an AKTA Pure system (GE Healthcare). The filtrate was loaded onto a 75 mL Source30Q resin column (GE Healthcare) equilibrated in 10 mM ammonium acetate pH 7.6, and the products were eluted at 10 mL min^{-1} using a gradient of 10 mM to 1 M ammonium acetate pH 7.6 over 90 minutes, where 5 mL fractions were collected. The product containing fractions were pooled and lyophilised 5-10 times from water in a round-bottom flask to remove ammonium acetate. The product was resuspended in 1 mL of sterile water, quantified and stored at -20 °C. UDP-MurNAc 5P was quantified by A_{260} (molar extinction coefficient of uracil at A_{260}= 10 000 M^{-1} cm^{-1}(Dawson *et al.*, 1986))

2.4.2 Acetylation of UDP-MurNAc pentapeptide

The DAP moiety of UDP-MurNAc 5P was acetylated as described by Catherwood *et al.* (2019). UDP-MurNAc 5P was buffer exchanged by diluting it in 100 mL sterile water and loading it onto a 30 mL Q Sepharose resin column (GE Healthcare) equilibrated in 10 mM $NaHCO_3$ pH 9.0. UDP-MurNAc 5P was eluted at 4 mL min^{-1} in 250 mM $NaHCO_3$ pH 9.0 over 100 mL, collecting 5 mL fractions, and the product containing fractions were pooled. UDP-MurNAc 5P was confirmed free of residual ammonium acetate with Nessler's Reagent (Sigma Aldrich) at A_{425} and quantified at A_{260} as in section 2.4.1.

A fifty-fold molar excess of acetic anhydride was added to UDP-MurNAc 5P which was stirred overnight at room temperature in the dark. The reaction was diluted to 100 mL in sterile water and purified using a 75 mL Source30Q resin column (GE Healthcare) as in section 2.4.1. The product containing fractions were pooled and lyophilised 5-10 times with water in a round-bottom flask to remove ammonium acetate. The product was resuspended in 1 mL sterile water, quantified by A_{260} as in section 2.4.1 and stored at -20 °C. Confirmation of the synthesis of UDP-MurNAc 5P (acetylated DAP) was established by nanospray mass spectroscopy using a Waters Synapt G2Si Q-Tof mass spectrometer as detailed in section 2.4.5.

2.4.3 Acid hydrolysis of UDP-MurNAc pentapeptide

For the synthesis of MurNAc 5P, 10 mg of UDP-MurNAc 5P (DAP) was resuspended in HCl to a final concentration of 0.1 M and pH 1.0, and heated at 99 °C for 30 minutes. The solution was then neutralised to pH 7.5 with NaOH, diluted to 100 mL in water and purified using a 75 mL Source30Q resin column (GE Healthcare) as in section 2.4.1. Eluate was monitored at 218, 254 and 280 nm. Fractions with high 218 nm absorbance but negligible absorbance at the higher wavelengths due to the removal of the uracil ring, contained the muropeptides of interest. The product containing fractions were pooled and lyophilised 5-10 times with water in a round-bottom flask to remove ammonium

acetate. The product was finally resuspended in 1 mL sterile water, quantified and stored at -80 °C.

MurNAc 5P was quantified using the D-Ala release assay (described in section 2.7.4) coupled to *E. coli* DacB/PBP4 (21-477), a D,D-carboxypeptidase., kindly gifted by A. Catherwood (Warwick). A 200 μL assay consisted of 50 mM HEPES pH 7.6, 10 mM $MgCl_2$, 2.72 μM *E. coli* DacB, 50 μM amplex red, 14.3 U mL^{-1} HRP and 36.1 U mL^{-1} DAAO. D-Ala release was followed at A_{555} on a Varian Cary 100 spectrophotometer at 30 °C . 2-5 μL MurNAc 5P was added to initiate the reaction and D-Ala release was followed to completion. The concentration of D-Ala was derived from the difference in A_{555} between the presence and absence of MurNAc 5P (molar extinction coefficient of resorufin at A_{555}= 54 000 M^{-1} cm^{-1}(Zhou *et al.*, 1997)).

Confirmation of the synthesis of MurNAc 5P (DAP) was established by nanospray mass spectroscopy (Waters Synapt G2Si Q-Tof mass spectrometer) detailed in section 2.4.5.

2.4.4 Lipid II synthesis from UDP-MurNAc pentapeptides and quantification

Lipid II was synthesised from its UDP-MurNAc 5P precursor as described by Lloyd *et al.* (2008). A 3.5 mL Lipid II synthesis reaction (for Lipid II (acetylated DAP) or Lipid II (dansylated DAP)) contained 0.1 M Tris pH 8.0, 5 mM $MgCl_2$, 1 % (w/v) Triton X-100, 6 mM UDP-GlcNAc, 2 mM UDP-MurNAc 5P (acetylated DAP) or UDP-MurNAc 5P (dansylated DAP), 1.35 mM undecaprenyl phosphate (Larodan AB, Sweden) and 15 μM *E. coli* MurG, with the remaining volume being made up with *Micrococcus flavus* cell membranes (~20 mg). The mixture was incubated overnight at 37 °C. UDP-MurNAc 5P (dansylated DAP (dansylated by click chemistry)) was kindly gifted by R. Cain (Warwick), and *E. coli* MurG and *M. flavus* cell membranes by A. Catherwood and J. Tod (Warwick). The sample was then partially purified by the addition of 1 volume of 6 M pyridium acetate pH 4.5 and 2 volumes of n-butanol, and centrifuged for 10 minutes at 3000 rpm. The

lipid upper phase was extracted and diluted in 1 volume of sterile water and centrifuged again at 3000 rpm for 10 minutes. The lipid upper phase was extracted, the solvents removed from it by rotary evaporation (Buchi R-210 Rotavapor), and the dried mixture resuspended in 6 mL of solvent A (2:3:1, chloroform:methanol:water).

Lipid II was purified using a 4 mL diethylaminoethyl sephacel resin column (GE Healthcare), which had been washed in 1 M ammonium acetate followed by water and then equilibrated in solvent A. The sample was loaded onto the column and weakly bound molecules were washed off with 12 mL of solvent A. Bound molecules were washed off the column with stepwise 12 mL washes of increasing ammonium bicarbonate concentrations in solvent A (8, 16, 25, 33, 42, 50, 83, 167 mM ammonium bicarbonate). 400 μL of each wash was desiccated and resuspended in 25 μL of solvent A. The samples were analysed by thin-layer chromatography (TLC) using silica 60-coated ALUGRAM Xtra SIL G plates (Macherey-Nagel) run in 88:48:10:1 chloroform:methanol:water:ammonia mobile phase. The TLC plate was stained in iodine vapour and imaged using a scanner. Washes containing the desired Lipid II product were pooled and dried by rotary evaporation (Buchi R-210 Rotavapor), followed by 5-10 rounds of lyophilisation with water to remove the ammonium bicarbonate. Lipid II was then resuspended in 1.5 mL of solvent A, quantified and stored at -80 °C.

Lipid II was quantified using a phosphate release assay. Two 50 μL Lipid II samples and a solvent A sample as a control were dried down under nitrogen gas and resuspended in 50 μL 50 mM HEPES, 10 mM $MgCl_2$, 30 mM KCl and 1.5 % (w/v) CHAPS pH 7.6. To one Lipid II sample and the solvent A sample 50 μL 1M HCl was added and the samples were boiled at 100 °C for 30 minutes. 1M NaOH was then used to adjust the samples to pH 7.6. The phosphate released from the undecaprenyl pyrophosphate moiety of Lipid II by acid hydrolysis was then quantified. A 200 μL activity assay contained 50 mM HEPES, 10 mM $MgCl_2$, 5 U mL^{-1} purine nucleoside phosphorylase, 5 U mL^{-1} inorganic pyrophosphatase and 200 μ M 7-methyl-6-thioguanosine (Berry and Associates). Any residual phosphate was followed for 5 minutes at A_{360}, after which time 10 μL of the Lipid

II/solvent A sample was added and phosphate release was followed to completion. The unit concentration of phosphate was derived from the difference in A_{360} between the presence and absence of the Lipid II/solvent A samples (molar extinction coefficient of 7-methyl-6-thioguanine at A_{360}= 10 000 M^{-1} cm^{-1} (Lloyd *et al.*, 1995)).

Confirmation of the synthesis of Lipid II substrates was established by nanospray mass spectroscopy using a Waters Synapt G2Si Q-Tof mass spectrometer as detailed in section 2.4.5.

2.4.5 Mass spectroscopy of PBP substrates

All PBP substrates and intermediates were analysed by negative ion nano-spray time of flight mass spectrometry using a Waters Synapt G2Si Q-Tof mass spectrometer. 1-5 μM of sample was diluted in 50 % (v/v) acetonitrile for UDP-MurNAc 5P and MurNAc 5P intermediates, and 30 % (v/v) 25 mM ammonium acetate in 70 % (v/v) methanol for lipid-linked substrates and injected via a Waters thin wall nanoflow capillary at a capillary voltage of 2.0 kV, cone voltage of 100 V and a source offset of 41 V. Data was collected by A. Lloyd, J. Tod or A. Catherwood (Warwick) and analysed using Waters Mass Lynx software.

2.5 Analytical ultracentrifugation

All proteins for analytical ultracentrifugation (AUC) analysis were purified fresh for the experiment and stored at 4 °C until needed. The proteins were expressed and purified as in sections 2.3, with the storage buffer being changed to 10 mM Tris, 500 mM NaCl, 0.6% (w/v) CHAPS pH 8.0 for all proteins, including soluble proteins. The proteins were concentrated to 25 times the desired concentration for AUC with a vivaspin (GE Healthcare) and diluted into 10 mM Tris, 500 mM NaCl and 0.35% (v/v) C_8E_5 pH 8.0.

Analytical ultracentrifugation experiments were carried out at Research Complex at Harwell. *E. coli* and *Y. pestis* PBP1b, LpoB, CpoB and FtsN were analysed separately and in complexes of PBP1b with either LpoB, CpoB or FtsN. Samples were loaded into the sample sector of two-channel Ti centrepiece cells (400 μL), and control buffer (10 mM Tris, 500 mM NaCl, 0.35% (v/v) C_8E_5, 0.025% (w/v) CHAPS pH 8.0) into the refence sector. Sedimentation velocity experiments were performed using an Optima AUC and An-50 Ti analytical rotor (both Beckman Coulter) at 50 000 rpm and 20 °C with absorbance monitoring at 280 nm.

Buffer density and viscosity was measured using a Density meter DMA 5000 M equipped with a Lovis 200 M viscometer module (Anton Paar). The partial specific volumes were calculated from the amino acid sequences using Sednterp. Data was processed with SEDFIT (Schuck, 2000) using the continuous size distribution c(s) method to determine values of the sedimentation coefficients with help from G. Harris (RCaH, Harwell).

2.6 Protein LCMS

10 μg of protein was resuspended in 50 mM ammonium bicarbonate, 10 mM Tris(2-carboxyethyl)phosphine hydrochloride (TCEP), 40 mM chloroacetamide (CAA) and 0.1 μg trypsin (from porcine pancreas, Sigma Aldrich) and incubated overnight at 37 °C. Trifluoroacetic acid (TFA) was added to a concentration of 1% (v/v) to yield a pH of 3.0-4.0. The sample was purified from detergents using a C18 membrane equilibrated with sequential steps of 50 μL methanol, acetonitrile and 0.1% (v/v) TFA in 2% (v/v) acetonitrile. The peptides were loaded onto the equilibrated membrane and washed with 50 μL 1% (v/v) TFA in ethyl acetate and then 0.1% (v/v) TFA in 2% (v/v) acetonitrile. The peptides were eluted using 20 μL of 0.1% (v/v) TFA in 80% (v/v) acetonitrile, the solvent was removed by a speed vacuum concentrator and resuspended in 0.1% (v/v) TFA in 2% (v/v) acetonitrile.

The samples were run by the Proteomics Research Technology Platform, University of Warwick, by nanoLC-ESI-MS/MS using an Ultimate 3000/Orbitrap Fusion instrumentation (Thermo Scientific) with a 60 min LC separation on a 50 cm column. Results were compared to the Uniprot *E. coli* database and the common contaminant database using the MaxQuant software. Scaffold software was then used to analyse and visualise the results.

2.7 PBP activity assays and LCMS of PBP reaction products

2.7.1 Continuous glycosyltransferase assay

Continuous glycosyltransferase activity was monitored using a fluorescence based assay adapted from Schwartz *et al.* (2002) and Walkowiak (2017). Assay components varied between experiments and are described in the figure legends. Generally, 20 μL reactions consisted of 50 mM HEPES pH 7.5, 115 mM NaCl, 10 mM $MgCl_2$, 10% (v/v) DMSO, 1% (v/v) glycerol, 0.155% (v/v) Triton X-100, 0.1 mg mL^{-1} lysozyme from chicken egg white (Sigma Aldrich), 50 nM PBP1b and 2 μM LpoB. Moenomycin (Santa Cruz Biotechnology) was used as a control at 5 μM and additional PBP regulators were added at 3 or 10 μM. If Lipid II or protein was omitted from a reaction it was replaced with its buffer, 0.1% Triton X-100 or protein storage buffer, respectively. Reactions were assembled into 384 well black F-bottom microplates (Greiner bio-one) and the reaction was initiated with 5 μM Lipid II (dansylated DAP). Dansyl group fluorescence was followed at excitation 340 nm and emission 521 nm using a CLARIOstar plate reader (BMG Labtech) at 30 °C. The initial rate was calculated by the difference in rate between the presence and absence of PBP1b in the reaction.

2.7.2 SDS-PAGE glycosyltransferase assay

The length of glycan chains produced by PBP1b was measured by a SDS-PAGE glycosyltransferase assay adapted from Helassa *et al.* (2012). Assay components

and reaction length varied between experiments and are described in the figures but generally a 15 μL reaction consisted of 50 mM Bis-Tris propane pH 8.5, 15 mM NaCl, varied $MgCl_2$, 10% (v/v) DMSO, 1% (v/v) glycerol, 0.130% (v/v) Triton X-100, 50 nM PBP1b and 2 μ M LpoB. 5 μM moenomycin (Santa Cruz Biotechnology) was used as a control and additional PBP regulators were added at 3 or 10 μM. If protein was omitted from a reaction it was replaced with its buffer. 10 μM Lipid II (dansylated DAP) was used to initiate the reaction which was incubated at 30 °C.

The reaction was stopped by the addition of loading dye (6x stock: 100 mM Tris, 4 % (w/v) SDS, 40% (v/v) glycerol and 0.05% (w/v) bromophenol blue pH 8.8), and the samples were loaded onto a 16.5% Criterion Tris-Tricine gel (Bio-Rad). Gel electrophoresis was carried out with 100 mM Tris pH 8.8 anode buffer and 100 mM Tris, 100 mM Tricine and 0.1% (w/v) SDS pH 8.25 cathode buffer at 100 V and 100 mA for 3 hours. The gel was imaged using an ImageQuant LAS 4000 instrument (GE Healthcare) using the Ethidium bromide fluorescence setting (transmitted light at 312 nm, and the 605DF40 emission filter) to allow imaging of glycan strands based on dansyl group fluorescence.

2.7.3 LCMS of glycan chain products

Glycan chains for LCMS analysis were polymerised in 15 μL reaction consisting of 50 mM Bis-Tris propane pH 8.5, 15 mM NaCl, 1% (v/v) glycerol, 0.0468% (v/v) E_6C_{12}, 50 nM PBP1b and 2 μ M LpoB. 5 μ M moenomycin (Santa Cruz Biotechnology) or 30 mM EDTA were used as controls. Reaction were initiated with 10 μM Lipid II (DAP/ dansylated DAP) (specified in figures) and reaction lengths varied (specified in figures). The polymerised glycan chains were prepared for LCMS analysis by dilution to 150 μL in 50 mM Bis-Tris propane pH 8.5. The sample was loaded onto a Bond Elut-CN-E 1 mL/100 mg reverse phase column (Chrom Tech) equilibrated with 5 mL 2:1 isopropanol:methanol followed by water. The glycan chains were eluted with a 0.5 mL water wash and followed by a 1 mL wash of 6.6% (v/v) isopropanol in 3.3% (v/v) methanol. The washes were dried down in a desiccator and resuspended in 0.1% (v/v) formic acid.

Positive mode LCMS analysis was performed where samples were delivered from a Waters M-class sample manager through a Waters Acuity UPLC BEH 300 Å 1.7 μm C18 column (2.1 x 50 mm) that had been equilibrated in 0.1% (v/v) formic acid at a flow rate of 50 μL min^{-1} through an electrospray source into a Waters Synapt G2Si quadrupole-time of flight instrument. The column was developed at the same flow rate at 20 °C with a 0-63% gradient into 0.1% (v/v) formic acid in acetonitrile over 30 minutes. Total ion chromatographs were collected at a capillary voltage of 2.0 kV, sampling cone voltage of 99 V, source offset of 0 V. Scans were converted to centred mass spectra and analysed by Waters Mass Lynx software. m/z and peak intensity values were determined by summing the spectrums of the region containing the product of interest.

2.7.4 Continuous transpeptidase assay

Transpeptidase and carboxypeptidase activity was monitored by the release of D-Ala, which was converted into a measurable product that has an absorbance at A_{555} as detailed by Catherwood *et al.* (2019). Briefly D-Ala was oxidised by DAAO producing H_2O_2, which was consumed by horse radish peroxidase (HRP), which with the chromogen amplex red forms the dye resorufin. Assay components varied between experiments and are described in the figures, but a 200 μL assay generally consisted of 50 mM Bis-Tris propane pH 8.5, 6 mM NaCl, 20 mM $MgCl_2$, 1% (v/v) glycerol, 0.130% (v/v) Triton X-100, 50 μM amplex red, 14.3 U mL^{-1} HRP, 36.1 U mL^{-1} DAAO, 20 μM Lipid II (DAP/ acetylated DAP) and 2 μM LpoB. Amplex red, HRP and Lipid II (DAP) was kindly gifted by A. Lloyd (Warwick). 5 μM Moenomycin (Santa Cruz Biotechnology) and 3 mM Ampicillin (Formedium) were used as controls and additional PBP interactors were added at 3 or 10 μM. If Lipid II or protein was omitted from a reaction it was replaced with its buffer, 0.1% Triton X-100 or protein storage buffer, respectively. D-Ala release was followed at 555 nm on a Varian Cary 100 spectrophotometer at 30 °C. 50 nM PBP1b was added to initiate the reaction, and the D-Ala release from carboxypeptidation was monitored before the addition of 20 μM MurNAc 5P (DAP) acceptor to initiate transpeptidation. The rate of D-Ala release was derived

from its initial rate calculated by the difference between rates in the presence and absence of the donor substrate (molar extinction coefficient of resorufin at A_{555}= 54 000 M^{-1} cm^{-1}(Zhou *et al.*, 1997)).

2.7.5 LCMS of transpeptidase and carboxypeptidase products

LCMS was used to analyse the transpeptidase and carboxypeptidase reaction products produced in the D-Ala release assay as described by Catherwood *et al.* (2019). The assay components followed those detailed in section 2.7.4 with 0.130% and 0.100% (v/v) Triton X-100 being swapped to 0.0468% and 0.0360% (v/v) E_6C_{12}, respectively. The 200 μL assay products were treated with 20 μL 2.2 M Bis-Tris propane pH 6.2 and 20 μL 10 mg mL^{-1} *Streptomyces globisporus* mutanolysin (Sigma Aldrich, prepared in 10 mM HEPES and 2.5 mM $MgCl_2$ pH 7.6). The sample was incubated for 2 hours at 37 °C, supplemented with a further 20 μL 10 mg mL^{-1} *S. globisporus* mutanolysin and incubated for a further 2 hours at 37 °C. The sample was boiled at 100 °C for 10 minutes and the proteins pelleted at 13 000 rpm for 10 minutes. The supernatant containing the muropeptides was treated with 150 μL 10 mg mL^{-1} $NaBH_4$ and incubated at room temperature for 30 minutes, followed by the addition of 17.5 μL 20 % (v/v) phosphoric acid.

Positive mode LCMS analysis was performed where samples were delivered from a Waters M-class sample manager through a Waters Acuity UPLC BEH 300 Å 1.7 μm C18 column (2.1 x 50 mm) that had been equilibrated in 0.1% (v/v) formic acid in 1% (v/v) acetonitrile at a flow rate of 50 μL min^{-1} through an electrospray source into a Waters Synapt G2Si quadrupole-time of flight instrument. The column was developed at the same flow rate at 20 °C with a 0-37% gradient into 0.1% (v/v) formic acid in acetonitrile over 30 minutes. Total ion chromatographs were collected at a capillary voltage of 2.5-3.0 kV, sampling cone voltage of 25 V, source offset of 80 V. Scans were converted to centred mass spectra and analysed by Waters Mass Lynx software. The spectra in the figures were generated by summing the spectrums of the region containing the muropeptide of interest.

Chapter 3. *E. coli* and *Y. pestis* PBP1b assay development

3.1 Introduction

The bacterial cell wall is composed of a layer of peptidoglycan that surrounds the cell membrane, allowing bacteria to resist osmotic stresses and maintain their unique shape (Weidel and Pelzer, 1964). Peptidoglycan is made up of glycan chains, cross-linked to one another by peptide side chains and is synthesised by PBPs. Bacterial growth and division dictates that peptidoglycan synthesis be a dynamic process, requiring the hydrolysis of existing peptidoglycan to allow the insertion of newly synthesised peptidoglycan (Höltje and Holtje, 1998). The essentiality and uniqueness of the bacterial peptidoglycan layer makes it an important therapeutic target, with many of the currently most clinically important antibiotics targeting peptidoglycan synthesis. As their name suggests PBPs are the target of penicillin and other β-lactam antibiotics (Typas *et al.*, 2012). PBPs fall into three main categories on the basis of their enzymatic activity: Bifunctional PBPs (class A PBPs) that possess both glycosyltransferase activity to polymerise Lipid II into glycan chains and transpeptidase activity to generate the cross-links between them, monofunctional transpeptidases (class B PBPs) (Ghuysen, 1991; Goffin and Ghuysen, 1998) and monofunctional carboxypeptidases and endopeptidases (Class C) (Sauvage *et al.*, 2008).

3.1.1 *E. coli* PBP1b

E. coli has three bifunctional PBPs (PBP1a, PBP1b and PBP1c) (Goffin and Ghuysen, 1998): PBP1a and PBP1b are partially redundant enzymes, as mutations depriving *E. coli* of both their activities are lethal. However the activity of either PBP1a or PBP1b is individually dispensable (Suzuki *et al.*, 1978; Yousif *et al.*, 1985), suggesting they have similar and essential functions that cannot be replicated by another PBP. In *E. coli*, localisation and protein-protein interaction studies suggest PBP1a primarily participates in cell elongation and PBP1b in cell division (Bertsche *et al.*, 2006; Müller *et al.*, 2007; Banzhaf *et al.*, 2012). Whereas

PBP1c is non-essential and is thought to be involved in peptidoglycan repair (Budd *et al.*, 2004).

The glycosyltransferase and transpeptidase activities of PBPs have been reconstituted *in vitro* with the availability of their Lipid II substrates (Lupoli *et al.*, 2014; Egan *et al.*, 2015; King *et al.*, 2017). Lipid II can be accumulated and extracted from bacteria after treatment with antibiotics or protein blocking agents (Qiao *et al.*, 2017), however, producing adequate quantities of pure Lipid II substrate by this approach is difficult. Instead Lipid II can be biochemically synthesised, by purifying the enzymes that carry out Lipid II synthesis *in vivo* and reconstituting the reactions *in vitro* (Lloyd *et al.*, 2008). This method also allows modifications of the pentapeptide stem to be carried out before it's conversion to Lipid II, which produces higher yields.

Genetic studies have revealed that *E. coli* PBP1a and PBP1b require activation from a lipoprotein for function *in vivo* (Paradis-Bleau *et al.*, 2010; Typas *et al.*, 2010). LpoA is specifically required for PBP1a function, and LpoB for PBP1b function. LpoA and LpoB are outer membrane anchored proteins that span the periplasm to interact directly with their cognate PBP, and when added to *in vitro* assays increase the activity of their target PBP (Paradis-Bleau *et al.*, 2010; Typas *et al.*, 2010). *E. coli* PBP1b alone has been shown to produce glycan chains of varied length, and cross-link ~50% of their peptide stems, however in the presence of LpoB shorter glycan chains are produced and cross-linking increases to ~70% (Paradis-Bleau *et al.*, 2010; Typas *et al.*, 2010; Egan *et al.*, 2018).

3.1.2 *Y. pestis* PBP1b

Y. pestis possesses PBP1b and LpoB homologues, and similar to *E. coli* it's PBP1b is predicted to be a bifunctional PBP and LpoB an outer membrane anchored protein (Parkhill *et al.*, 2001). The *E. coli* and *Y. pestis* PBP1b protein sequences are 69% identical, while LpoB is only 45% identical between the two species. *Y. pestis* PBPs have not been extensively investigated, with the last published data

being a study on *Y. pestis* PBPs affinity and sensitivity to β-lactams using radiolabelled penicillin (Ferreira *et al.*, 1994; Ferreira *et al.*, 1995).

Due to the similarities between *Y. pestis* and *E. coli* PBPs, this study aimed to use the current knowledge and understanding of how *E. coli* PBP1b functions *in vitro* to establish *Y. pestis* PBP1b activity *in vitro*. This approach allowed us to demonstrate the first example of *in vitro Y. pestis* PBP1b activity. Preliminary data from our laboratory gained prior to the commencement of the work reported in this thesis had shown that *Y. pestis* PBP1b transpeptidase and/or carboxypeptidase activity was specific for DAP containing substrates (Table 3.1) (Smart K. and Lloyd A., unpublished), suggesting *Y. pestis* PBP1b, unlike *E. coli* PBP1b (Catherwood *et al.*, 2019), is only able to utilise its native DAP peptide containing substrate (Khomenko *et al.*, 1980) for crosslinking.

Substrate		**Transpeptidase/ carboxypeptidase activity**
Donor	**Acceptor**	***Y. pestis* PBP1b**
Lipid II (Lys)	MurNAc 5P (DAP)	✗
Lipid II (Lys)	Lipid II (DAP 4P)	✗
Lipid II (DAP)	Lipid II (DAP)	✓

Table 3.1. Initial observations of *Y. pestis* PBP1b substrate utilisation *in vitro*. D-Ala release was assayed using the amplex red assay for D-Ala release by *Y. pestis* PBP1b *in vitro*. Reactions consisted of 50 mM Bis-Tris propane pH 8.5, 6 mM NaCl, 20 mM $MgCl_2$, 1% (v/v) glycerol, 0.130% (v/v) Triton X-100, amplex red coupling reagents, 20 μM donor and acceptor substrates, 50 nM *Y. pestis* PBP1b, and 2 μM LpoB.

3.1.3 Glycosyltransferase assays

Two complementary glycosyltransferase assays were selected for this project. The first was a continuous fluorescence based assay using a dansylated Lipid II substrate (Schwartz *et al.*, 2002; Offant *et al.*, 2010). In this assay glycan chains polymerised from Lipid II (dansylated-DAP) are digested by lysozyme as they are formed, resulting in the formation of dansylated muropeptides that have a lower fluorescence intensity than the original Lipid II substrate, due to the removal of

the lipid tail (Figure 3.1). The advantage of this continuous assay is that it allows the measurement of initial glycosyltransferase rates in isolation from transpeptidation, as the location of the dansyl fluorescent group, on the 3rd position DAP on the stem peptide, prevents transpeptidation from occurring. Previous studies have confirmed that *E. coli* PBP1b glycosyltransferase kinetics are similar for fluorescently labelled and unlabelled substrates (Schwartz *et al.*, 2002). However, the disadvantage to this assay system is no direct measurement of substrate loss or product formation is made.

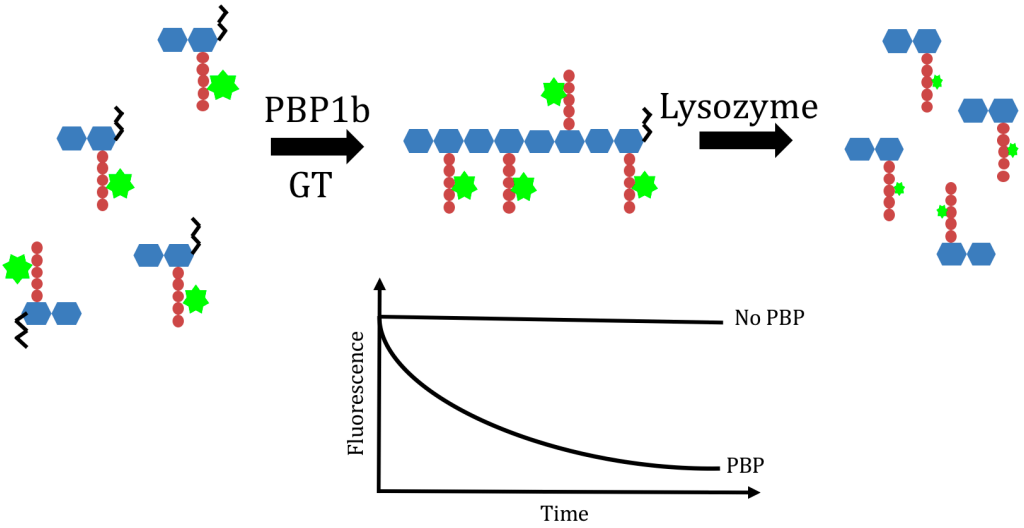

Figure 3.1. *In vitro* continuous glycosyltransferase assay principle.
Lipid II (dansylated DAP) is polymerised into glycan chains by PBP1b, followed by their digestion by lysozyme, resulting in a reduction in fluorescence due to the formation of muropeptides.

The second complementary glycosyltransferase assay allows the visualisation of fluorescently labelled glycosyltransferase reaction products, providing qualitative data on the length of glycan chains produced, and is discussed in detail in chapter 4.

3.1.4 Transpeptidase assay

Most existing assays to measure transpeptidation use radiolabelled substrates and do not distinguish between transpeptidation and carboxypeptidation, and of those that do, none are continuous assays (Bertsche *et al.*, 2005; Lupoli *et al.*, 2014). Chromogenic assays are available to follow the release of D-Ala (Clarke *et*

al., 2009) and Catherwood *et al.* has recently developed an assay to continuously monitor and distinguish between *E. coli* PBP1b transpeptidase and carboxypeptidase D-Ala release (2019). In this project the spectrophotometric D-Ala release assay was used to continuously measure D-Ala release from carboxypeptidation and transpeptidation with non-labelled substrates, that could act exclusively as transpeptidation donor and acceptors (Figure 3.2).

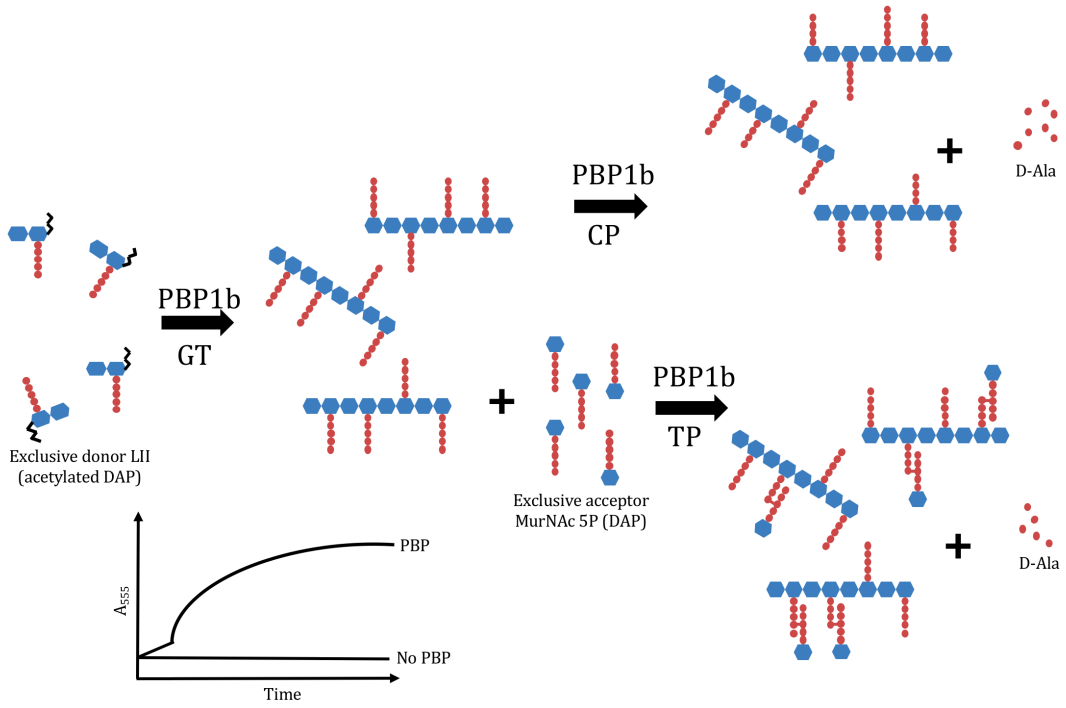

Figure 3.2. *In vitro* continuous D-Ala release assay principle.
Lipid II (acetylated DAP) (rendered donor only substrate by acetylating the ε-amino group of the third DAP residue in the stem peptide) is polymerised into glycan chains (GT) and acylated to the transpeptidase active site serine of PBP1b releasing D-Ala. Upon addition of MurNAc 5P (DAP) (an exclusive acceptor substrate) transpeptidation (TP) occurs releasing the transpeptidation product. If water is used in the place of acceptor substrate carboxypeptidation (CP) occurs releasing the stem tetrapeptide. The release of D-Ala is monitored via a coupled enzyme detection system.

3.2 Experimental Aims

- To synthesise Lipid II (acetylated DAP), MurNAc pentapeptide (DAP) and Lipid II (dansylated DAP).
- To clone, express and purify *Y. pestis* PBP1b, PBP3, LpoB, CpoB and FtsN and *E. coli* PBP1b, LpoB, CpoB and FtsN.
- To test substrate usage of *Y. pestis* PBP1b.

- To optimise conditions for *Y. pestis* PBP1b activity in the *in vitro* continuous glycosyltransferase and transpeptidase assays.
- To establish kinetic parameters for *Y. pestis* PBP1b activity.
- To validate assays for inhibitor testing.

3.3 Results

3.3.1 Enzymatic biosynthesis of Lipid II (acetylated DAP)

3.3.1.1 Substrate choice rationale

Preliminary *in vitro* studies on *Y. pestis* PBP1b activity suggested it was able to utilise Lipid II substrates with stem peptides containing DAP but not Lys at the third position for transpeptidation or carboxypeptidation (Section 3.1.2). The substrate used for these preliminary studies was Lipid II (DAP), which could act as both a transpeptidase donor and acceptor substrate, hence the D-Ala release measured in the assay could be either carboxypeptidase and/or transpeptidase activity (Section 3.1.4). To distinguish between the two activities, modifications were made to the substrates to create donor and acceptor only substrates, allowing carboxypeptidase activity to be measured independently in the assay. Acetylating the ε-amino group of the third position DAP residue (addition of a CH_3CO group, Figure 3.3) would create a donor only substrate, and this modification was hypothesised to have little effect on PBP1b activity. *E. coli* PBP1b has previously been shown to be able to utilise Lipid II (acetylated DAP) as a substrate (Zhang *et al.*, 2007; Catherwood *et al.*, 2019). Use of this substrate would allow a carboxypeptidase only rate to be measured, before the addition of a transpeptidase acceptor only substrate that initiated transpeptidation.

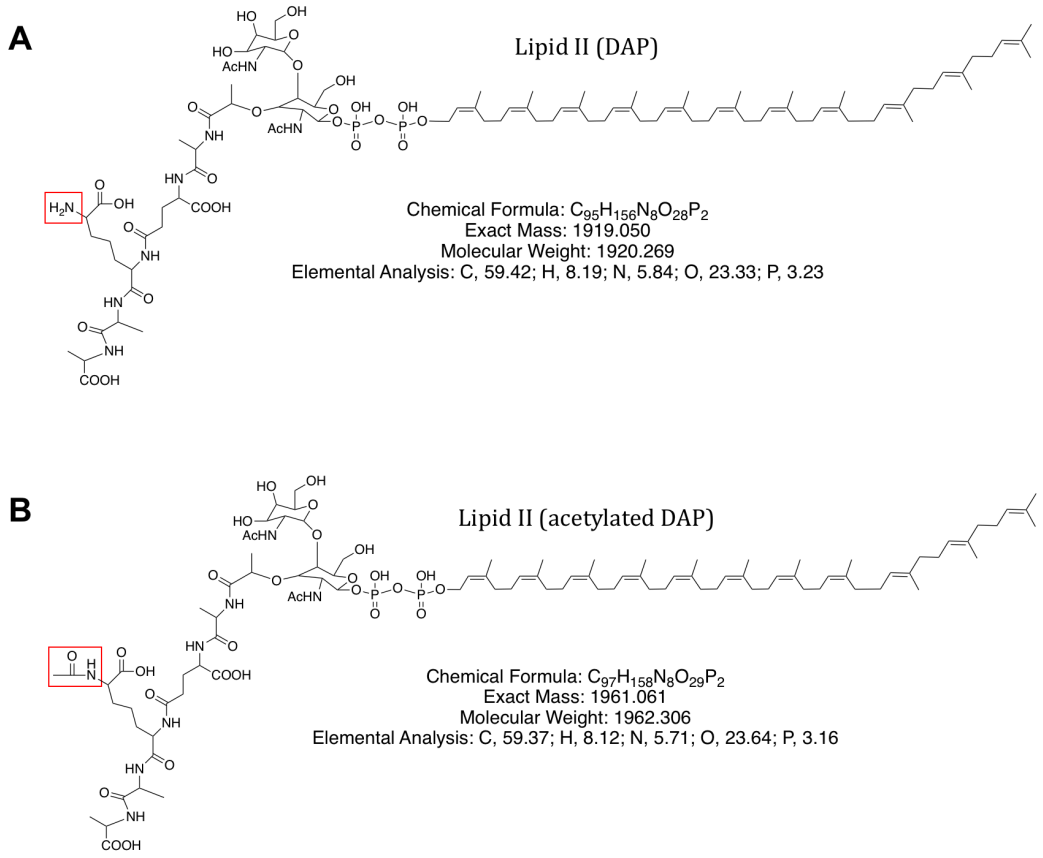

Figure 3.3. Lipid II (DAP) and Lipid II (acetylated DAP) structures.
(A) Lipid II (DAP) and **(B)** Lipid II (acetylated DAP). Red box highlights the differences between the structures.

3.3.1.2 Enzymatic biosynthesis of UDP-MurNAc pentapeptide (DAP)

Lipid II is synthesised by the production of UDP-MurNAc 5P, followed by any necessary modification to the pentapeptide stem, before conversion to Lipid II. UDP-MurNAc 5P (DAP) can be synthesised *in vitro* as *in vivo* by enzymes MurA-MurF which construct the stem peptide as part of a UDP-nucleotide. UDP-MurNAc 5P (DAP) was synthesised in one-step, by purified enzymes MurA-MurF and their substrates, and the product purified according to Lloyd *et al.* (2008). The product was quantified by uracil A_{260}.

3.3.1.3 Acetylation of UDP-MurNAc pentapeptide (DAP)

UDP-MurNAc 5P (DAP) was buffer exchanged into 250 mM $NaHCO_3$ and acetylated by the addition of 50x excess acetic anhydride and purified as

previously described (Catherwood *et al.*, 2019). The product was quantified by uracil A_{260} and confirmed by negative ion mass spectroscopy.

3.3.1.4 Conversion of UDP-MurNAc pentapeptide (acetylated DAP) into Lipid II

UDP-MurNAc 5P (acetylated DAP) was converted into Lipid II *in vitro* as *in vivo* by enzymes MraY and MurG, which append phosphoMurNAc 5P (acetylated DAP) (from UDP-MurNAc 5P (acetylated DAP)) to undecaprenyl phosphate to form Lipid I, which is then glycosaminylated with UDP-GlcNAc to form Lipid II (acetylated DAP). This one-step reaction was carried out with purified enzyme MurG and bacterial cell membranes (to supply MraY) and the Lipid II product purified according to Breukink *et al.* and Lloyd *et al.* (2003; 2008). Washes from the purification of Lipid II (acetylated DAP) were analysed by thin-layer chromatography and are shown in Figure 3.4.

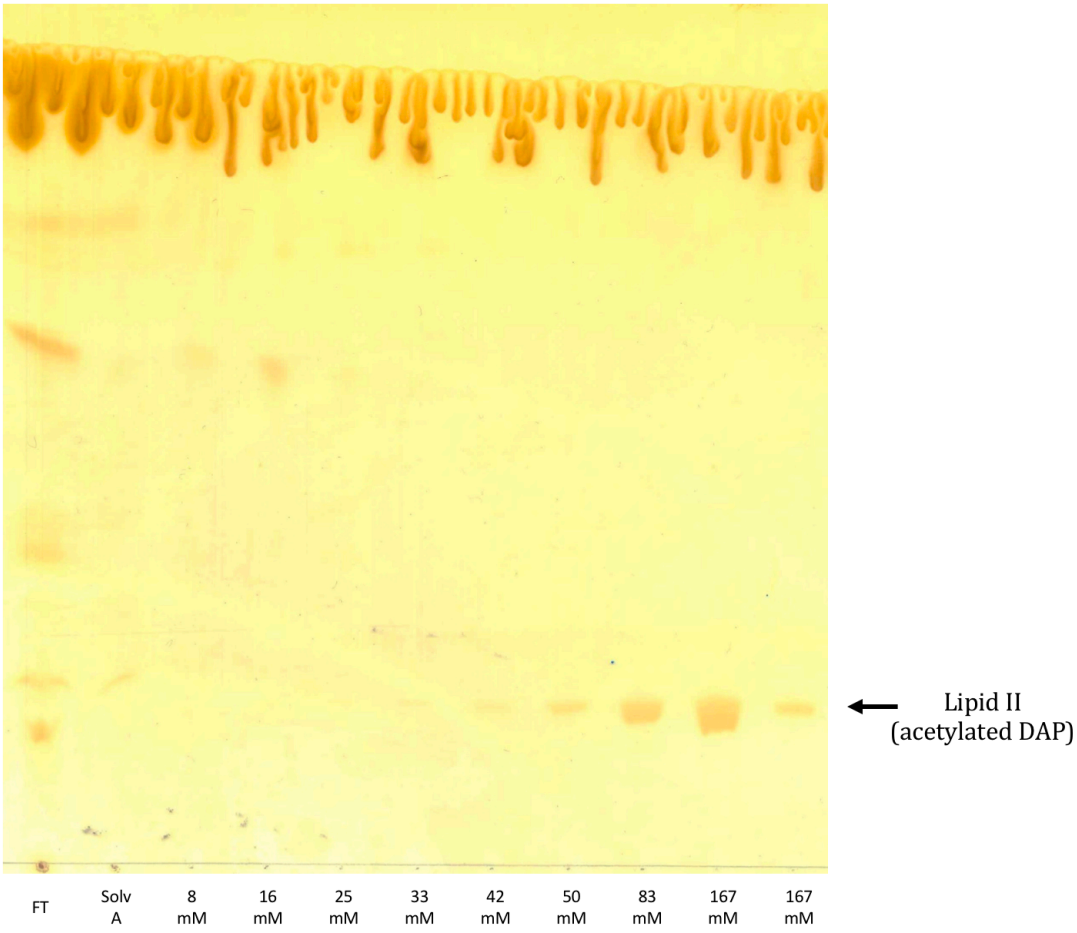

Figure 3.4 Thin-layer chromatography of washes collected from anion exchange purification of Lipid II (acetylated DAP).
Washes from anion exchange chromatography run by TLC on silica with Chloroform:methanol:water:ammonia (88:48:10:1) mobile phase. FT: Flow through from anion exchange column loading, Solv A: Solvent A, chloroform:methanol:water (2:3:1), 8-167 mM: concentration of ammonium bicarbonate in solvent A column washes. TLC plate stained with iodine vapour.

The washes containing the product was quantified by inorganic phosphate detection at A_{360}, and confirmed by negative ion mass spectroscopy (Figure 3.5).

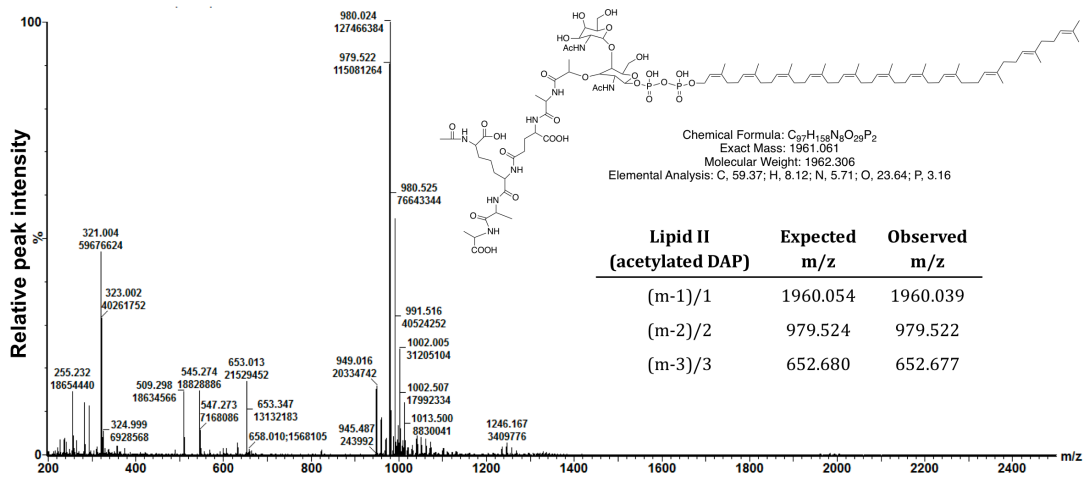

Lipid II (acetylated DAP)	Expected m/z	Observed m/z
(m-1)/1	1960.054	1960.039
(m-2)/2	979.524	979.522
(m-3)/3	652.680	652.677

Figure 3.5 Negative ion mass spectrum of Lipid II (acetylated DAP).
Negative ion mass spectra of Lipid II (acetylated DAP) with observed charged states for singly, doubly and triply ionised molecules as expected. Major peaks are annotated as m/z and ion count.

3.3.2 Enzymatic biosynthesis of MurNAc pentapeptide (DAP)

3.3.2.1 Substrate choice rationale

Previous studies have shown that bifunctional PBP's and mono-functional transpeptidases require a polymeric transpeptidase donor substrate for transpeptidation and carboxypeptidation (Lupoli *et al.*, 2011; Taguchi *et al.*, 2019), whereas the transpeptidase acceptor substrate can be monomeric, as small as a single amino acid (Adam *et al.*, 1991; Lupoli *et al.*, 2011; Catherwood *et al.*, 2019). A monomeric transpeptidase acceptor substrate would be favourable for D-Ala release as it is non polymerisable by PBP1b, therefore would not fulfil the role of a transpeptidase donor substrate, and consequently would not be able to be carboxypeptidated. Hence, its addition to the assay would only affect the rate of D-Ala release from transpeptidation.

MurNAc-5P DAP is a known monomeric transpeptidase acceptor substrate of *E. coli* PBP1b (Catherwood *et al.*, 2019), and using the D-Ala release assay we determined that it was also a suitable substrate for *Y. pestis* PBP1b (MurNAc 5P (DAP) was kindly supplied by J. Todd and A. Catherwood (Warwick)). It was decided to use MurNAc 5P (DAP) as the transpeptidase acceptor only substrate

due to it being a substrate for both *Y. pestis* and *E. coli* PBP1b (Catherwood *et al.*, 2019), as well as the advantages discussed above.

3.3.2.2 Biochemical synthesis of MurNAc pentapeptide (DAP)

UDP-MurNAc 5P (DAP) was synthesised and subjected to hydrolysis with HCl to hydrolyse off UDP, according to Catherwood *et al.* (2019). The product was purified by anion exchange chromatography, quantified by the DacB D-Ala release assay and confirmed by negative ion mass spectroscopy. Mass spectroscopy determined the sample to contain the masses of MurNAc 5P (DAP), as well as Lactyl 5P (DAP) (Figure 3.6). However, work done previously by Lloyd A. (unpublished) has found that the presence of a mass corresponding to Lactyl 5P (DAP) is unlikely due to sample contamination, but due to in source fragmentation of MurNAc 5P (DAP), as LC-MS experiments found Lactyl 5P (DAP) to elute identically with MurNac-5P DAP.

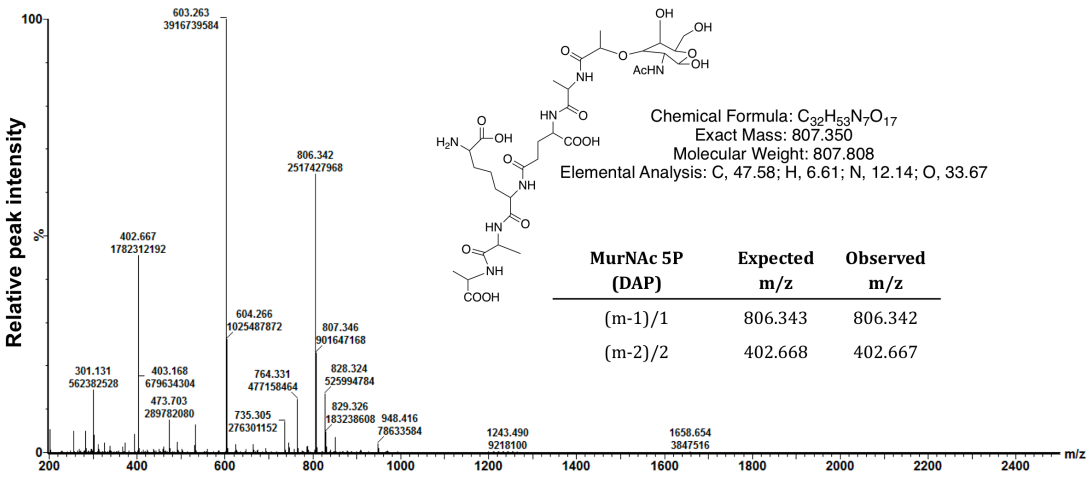

Figure 3.6 Negative ion mass of MurNAc 5P (DAP).
Negative ion mass spectra of MurNAc 5P (DAP) with observed charged states for singly and doubly ionised molecules as expected. MurNAc 5P (DAP) experienced in source fragmentation yielding the associated mass of Lactyl 5P (DAP), (m-1)/1 expected: 603.262 and observed: 603.263, (m-2)/2 expected: 301.127, observed: 301.131. Major peaks are annotated as m/z and ion count.

3.3.3 Enzymatic biosynthesis of Lipid II (dansylated DAP)

UDP-MurNAc 5P (dansylated DAP (dansylated by click chemistry)) was kindly supplied by R. Cain (Warwick), synthesised into Lipid II and purified. Washes from the purification of Lipid II (dansylated DAP) were analysed by thin-layer chromatography and are shown in Figure 3.7.

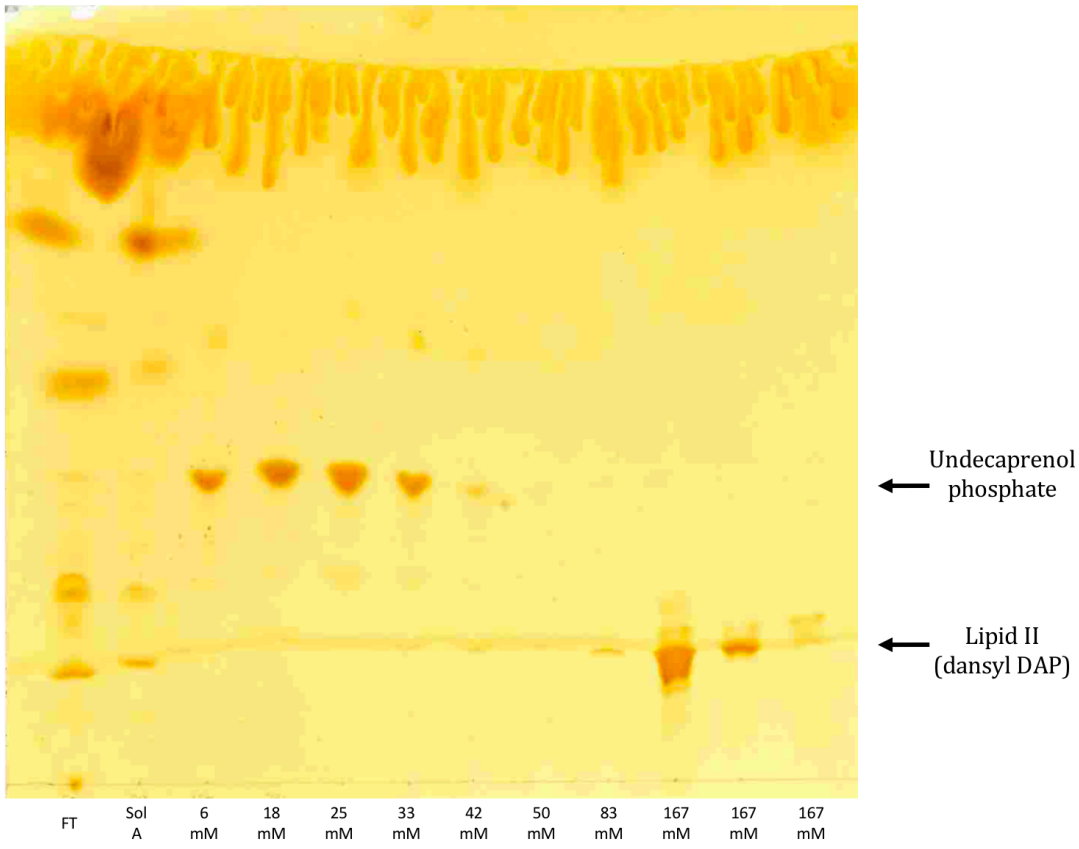

Figure 3.7 Thin-layer chromatography of washes collected from anion exchange purification of Lipid II (dansylated DAP).
Washes from anion exchange chromatography run by TLC on silica with Chloroform:methanol:water:ammonia (88:48:10:1) mobile phase. FT: Flow through from anion exchange column loading, Sol A: Solvent A, chloroform:methanol:water (2:3:1), 6-167 mM: concentration of ammonium bicarbonate in solvent A column washes. TLC plate stained with iodine vapour.

The washes containing the product was quantified by inorganic phosphate detection at A_{360}, and confirmed by negative ion mass spectroscopy (Figure 3.8).

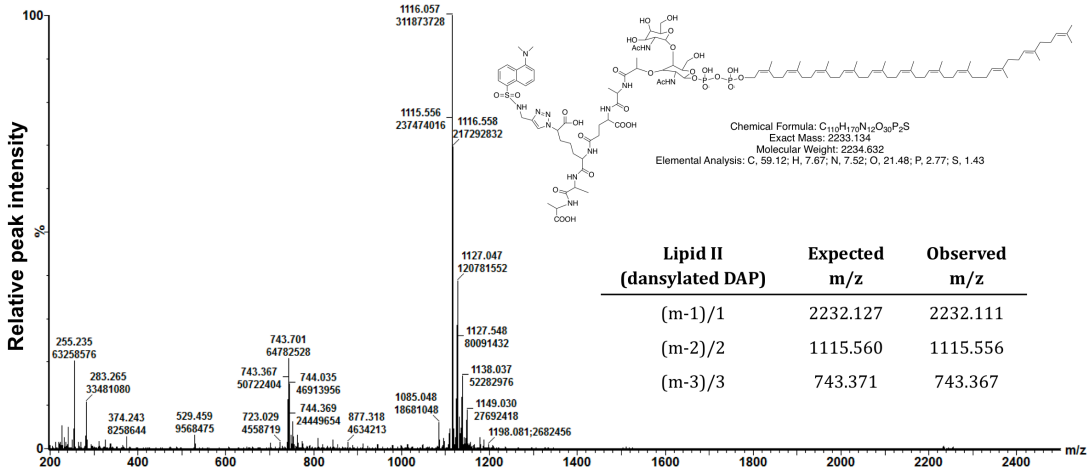

Lipid II (dansylated DAP)	Expected m/z	Observed m/z
(m-1)/1	2232.127	2232.111
(m-2)/2	1115.560	1115.556
(m-3)/3	743.371	743.367

Figure 3.8 Negative ion mass spectrum of Lipid II (dansylated DAP).
Negative ion mass spectra of Lipid II (dansylated DAP) with observed charged states for singly, doubly and triply ionised molecules as expected. Major peaks are annotated as m/z and ion count.

3.3.4 Recombinant protein cloning, expression and purification

Restriction enzyme or Gibson assembly cloning was used to construct the gene of interest into the vector, and the construct was expressed, purified by immobilised metal affinity chromatography, the His-tag cleaved and the protein separated from the tag by reverse immobilised metal affinity chromatography. Final protein purity for *Y. pestis* PBP1b (61-803), *Y. pestis* PBP1b (61-803) I205F, *Y. pestis* PBP3 (59-587), *Y. pestis* LpoB (57-191), *Y. pestis* CpoB (24-269), *Y. pestis* FtsN (1-281), *E. coli* PBP1b (58-804), *E. coli* LpoB (78-213), *E. coli* CpoB (27-263), *E. coli* FtsN (1-319) are shown in Figure 3.9.

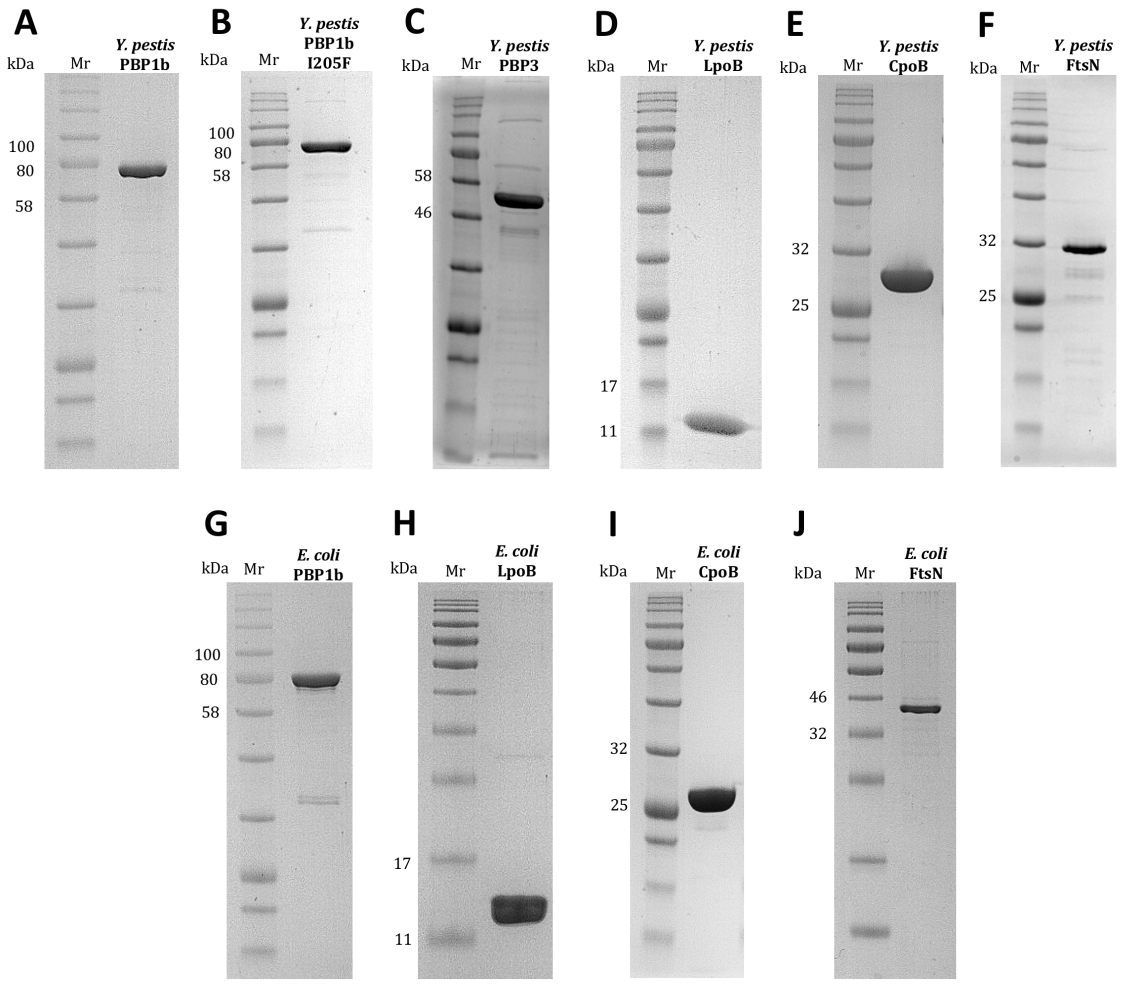

Figure 3.9 Final purity of purified recombinant proteins.
12% SDS-PAGE coomassie stained gels loaded with 2-10 μg of purified proteins. Molecular weight marker (Mr) in kDa (NEB colour prestained protein standard). **(A)** *Y. pestis* PBP1b (61-803) 82.7 kDa, **(B)** *Y. pestis* PBP1b I205F (61-803) 82.7 kDa, **(C)** *Y. pestis* PBP3 (59-587) 57.6 kDa, **(D)** *Y. pestis* LpoB (57-191) 14.9 kDa, **(E)** *Y. pestis* CpoB (24-269) 26.8 kDa, **(F)** *Y. pestis* FtsN (1-281) 30.9 kDa, **(G)** *E. coli* PBP1b (58-804) 83.7 kDa, **(H)** *E. coli* LpoB (78-213) 14.4 kDa, **(I)** *E. coli* CpoB (27-263) 25.7 kDa, **(J)** *E. coli* FtsN (1-319) 36.2 kDa.

3.3.5 Development of assay conditions for *E. coli* and *Y. pestis* PBP1b glycosyltransferase activity

3.3.5.1 Initial observations of *E. coli* and *Y. pestis* PBP1b glycosyltransferase activity

E. coli PBP1b glycosyltransferase activity is well documented, and it is understood that it's activity is greatly enhanced by the binding of outer membrane lipoprotein LpoB (Schwartz *et al.*, 2002; Paradis-Bleau *et al.*, 2010;

Egan *et al.*, 2014; Lupoli *et al.*, 2014). These findings were replicated using the *in vitro* continuous glycosyltransferase assay (Figure 3.10A). However, no previous *Y. pestis* PBP1b *in vitro* activity has been published. To establish if *Y. pestis* PBP1b glycosyltransferase can utilise Lipid II (dansylated DAP) as a substrate, its activity was investigated in the *in vitro* continuous glycosyltransferase assay in the absence and presence of LpoB. *Y. pestis* PBP1b activity was seen in the absence of LpoB, but greatly enhanced in the presence of LpoB, confirming that *Y. pestis* PBP1b could utilise Lipid II (dansylated DAP) as a substrate, and its activity was also increased by the presence of LpoB (Figure 3.10B). As expected the addition of moenomycin, a potent PBP glycosyltransferase inhibitor, completely abolished *E. coli* and *Y. pestis* PBP1b activity (Figure 3.10).

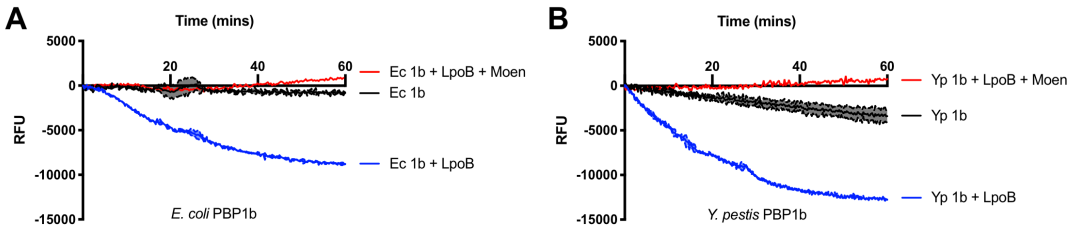

Figure 3.10 Initial observations of *E. coli* and *Y. pestis* PBP1b glycosyltransferase activity.
Glycosyltransferase rate was assayed by the consumption of fluorescently labelled Lipid II by **(A)** *E. coli* PBP1b (Ec 1b) and **(B)** *Y. pestis* PBP1b (Yp 1b) *in vitro.* Reactions consisted of 50 mM HEPES pH 7.5, 115 mM NaCl, 10 mM $MgCl_2$, 10% (v/v) DMSO, 1% (v/v) glycerol, 0.155% (v/v) Triton X-100, 0.1 mg ml^{-1} lysozyme, 5 μM Lipid II (dansyl DAP), 50 nM PBP1b $\pm$ 2 μM LpoB and 5 μM Moenomycin (Moen). Data is shown as mean $\pm$ SD (n=3).

3.3.5.2 Optimisation of assay conditions for *Y. pestis* PBP1b glycosyltransferase activity

In vitro glycosyltransferase activity has been shown to be severely affected by buffer conditions including pH, divalent cations, detergent and DMSO concentration (Schwartz *et al.*, 2002; Offant *et al.*, 2010; Helassa *et al.*, 2012). Buffer conditions had previously been optimised for *E. coli* PBP1b glycosyltransferase activity (Schwartz *et al.*, 2002; Walkowiak, 2017) and these were used as a starting point for *Y. pestis* PBP1b glycosyltransferase activity optimisation.

Previous studies have identified buffer pH and divalent cation concentration to significantly affect the catalysis of transglycosylation: pH aiding deprotonation of the hydroxyl nucleophile of the Lipid II acceptor and a divalent metal stabilising and assisting departure of the leaving undecaprenyl pyrophosphate (Schwartz *et al.*, 2002). The effect of pH on *Y. pestis* PBP1b glycosyltransferase activity was investigated using the *in vitro* continuous glycosyltransferase assay, and as seen with *E. coli* PBP1b (Schwartz *et al.*, 2002) there was no significant difference in glycosyltransferase activity between pH 7.5-8.5 (Figure 3.11A). The fluorescence of Lipid II (dansylated DAP) was not found to change with pH.

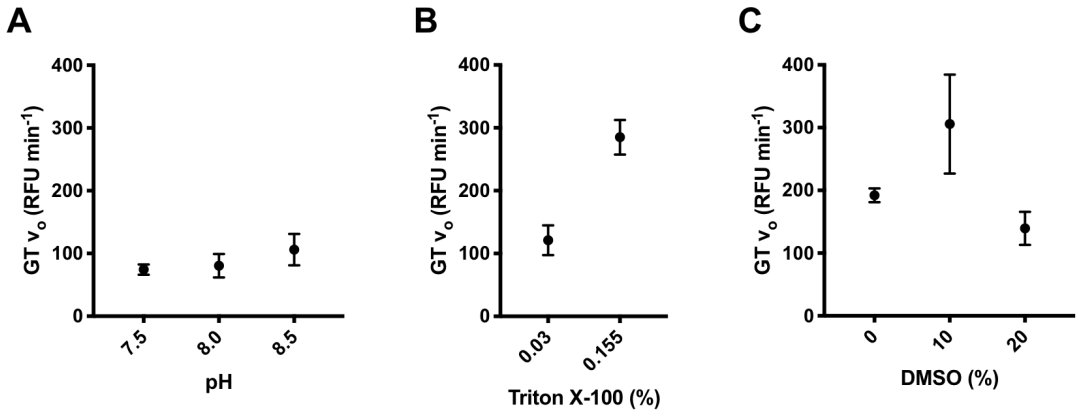

Figure 3.11 Effect of pH, detergent and DMSO concentration on *Y. pestis* PBP1b glycosyltransferase activity.
Glycosyltransferase rate was assayed by the consumption of fluorescently labelled Lipid II by *Y. pestis* PBP1b *in vitro,* **(A)** at different pH's, **(B)** detergent concentrations and **(C)** DMSO concentrations, shown as initial rates. Reactions consisted of 50 mM HEPES pH 7.5, 115 mM NaCl, 10 mM $MgCl_2$, 20% (v/v) DMSO, 1% (v/v) glycerol, 0.03% (v/v) Triton X-100, 0.1 mg ml^{-1} lysozyme, 5 μM Lipid II (dansyl DAP), 50 nM PBP1b and 2 μM LpoB, unless otherwise stated. Buffers used were HEPES pH 8.0 and 8.5. Data is shown as mean $\pm$ SD (n=3).

The presence of detergent, Triton X-100 in this case, is important for solubility of the Lipid II substrate and PBP1b due to its possession of a transmembrane helix. Previous studies have shown that high detergent concentrations can have an inhibitory effect on PBP glycosyltransferase activity, however these effects can be counteracted by the addition of DMSO (Schwartz *et al.*, 2002; Offant *et al.*, 2010; Helassa *et al.*, 2012; Egan and Vollmer, 2016). This effect has been hypothesised to be due to DMSO increasing the solubility of Lipid II, and aiding more rapid exchange between micelles (Schwartz *et al.*, 2002). However, DMSO has also previously been shown to impair the interaction between PBP1b and

LpoB, reducing its glycosyltransferase activity (Egan and Vollmer, 2016). The effect of Triton X-100 and DMSO concentration on *Y. pestis* PBP1b glycosyltransferase activity was investigated (Figure 3.11B & C). *Y. pestis* PBP1b exhibited greater activity at 0.155% than 0.03% (v/v) Triton X-100 (10x and 2x CMC respectively), when 20% (v/v) DMSO was present. At the lower detergent concentrations (0.030% (v/v), 2x cmc) *Y. pestis* PBP1b had the greatest activity at a DMSO concentration of 10% (v/v) compared to 0% or 20% (v/v) (Figure 3.11). Final reaction buffers used for all *in vitro* continuous glycosyltransferase assays from now on were HEPES pH 7.5, 0.155% (v/v) Triton X-100 and 10% (v/v) DMSO.

3.3.6 Development of assay conditions for *E. coli* and *Y. pestis* PBP1b transpeptidase activity

3.3.6.1 Initial observation of *E. coli* and *Y. pestis* PBP1b transpeptidase activity

Like *E. coli* PBP1b glycosyltransferase activity, the transpeptidase activity is well documented (Bertsche *et al.*, 2005; Catherwood *et al.*, 2019), and it is known that it can utilise Lipid II (acetylated DAP) and MurNAc 5P (DAP). To establish if *Y. pestis* PBP1b could utilise the same substrates, the carboxypeptidase and transpeptidase activity of *Y. pestis* PBP1b was measured in the continuous *in vitro* D-Ala release assay (details in 3.1.4). The D-Ala release assay was initiated (at ~3mins) with the addition of *Y. pestis* PBP1b, which was able to transglycosylate and subsequently carboxypeptidate the donor only substrate present in the reaction (Lipid II (acetylated DAP)). Once a carboxypeptidase rate was determined, the transpeptidase acceptor only substrate (MurNAc 5P (DAP)) was added (at ~8 mins) to initiate transpeptidation. As hoped *Y. pestis* PBP1b, like *E. coli*, could utilise Lipid II (acetylated DAP) and MurNAc 5P (DAP) as transpeptidation substrates (Figure 3.12), and as expected their activity was inhibited by moenomycin and ampicillin (PBP glycosyltransferase and transpeptidase inhibitors respectively) (Figure 3.12). The concentration of

control inhibitors used is known not to affect the assay converting enzyme system (Lloyd A., unpublished).

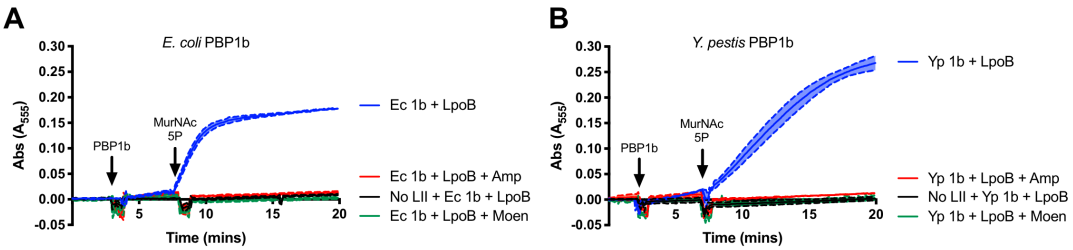

Figure 3.12 Initial observations of *E. coli* and *Y. pestis* PBP1b transpeptidase activity.
Transpeptidase rate was assayed using the amplex red assay for D-Ala release by **(A)** *E. coli* PBP1b (Ec 1b) and **(B)** *Y. pestis* PBP1b (Yp 1b) *in vitro*. Reactions consisted of 50 mM Bis-Tris propane pH 8.5, 6 mM NaCl, 20 mM $MgCl_2$, 1% (v/v) glycerol, 0.130% (v/v) Triton X-100, amplex red coupling reagents, 20 μM Lipid II (acetylated DAP), 50 nM PBP1b, 20 μM MurNac 5P (DAP), 2 μM LpoB, 5 μM Moenomycin (Moen) and 3 mM Ampicillin (Amp) as controls. Data is shown as mean $\pm$ SD (n=3), or minimum and maximum values (n=2).

3.3.6.2 Optimisation of buffer conditions for *Y. pestis* PBP1b transpeptidase activity

The initial *Y. pestis* PBP1b D-Ala release assay experiments highlighted that *Y. pestis* had a higher carboxypeptidation rate (3-8 mins in Figure 3.12B), and lower transpeptidation rate (8-20 mins in Figure 3.12B) than *E. coli* (Figure 3.12A), reducing the transpeptidation:carboxypeptidation activity ratios. In an attempt to increase the transpeptidation:carboxypeptidation activity ratios the pH of the assay buffer was varied, along with the temperature. It was hypothesised that increasing the pH would improve deprotonation of the acceptor nucleophile promoting transpeptidation catalysis (Lloyd A., personal communication), and varying the temperature would replicate different stages in the *Y. pestis* life cycle (Easterday *et al.*, 2012; Pechous *et al.*, 2016) which may affect rates of transpeptidation and carboxypeptidation.

In order to confirm that any changes in D-Ala release seen were due to changes in PBP1b activity, the effect of varying the pH and temperature on the converting enzyme system was first investigated. The extinction coefficients of resorufin, the product of the enzyme converting system, was determined for pH's 7.5-11.0

(Appendix 9.1), and were used in future analysis. This allowed the specific activity of DAAO, which coverts D-Ala to hydrogen peroxide in the co verting enzyme system, to be calculated. The specific activity of DAAO was optimum at pH 8.5-9.0 and 30 °C (Figure 3.13A), but was sufficiently active pH 8.0-10.5 and 20-37 °C (Figure 3.13B). Consequently, PBP1b transpeptidase activity was measured between pH 8.5-10.5 and 20-37 °C, as at these conditions the converting enzyme system was sufficiently active to monitor D-Ala release in the assay.

The results of this optimisation revealed that *Y. pestis* PBP1b transpeptidase activity decreased with increasing pH (Figure 3.14A), and generally the carboxypeptidase rate mirrored this decrease, shown by no change in the transpeptidation:carboxypeptidation activity ratio (Figure 3.14C), suggesting both activities are similarly affected by pH. The exception was pH 9.5, which exhibited a rise in transpeptidation:carboxypeptidation activity ratio (Figure 3.14C), however it was decided not to carry out the assay at pH 9.5 due to it not being a physiologically relevant pH. Temperature also affected the transpeptidase activity of *Y. pestis* PBP1b, increasing with increasing temperature (Figure 3.14B), but again this rise in transpeptidase activity was mirrored by a rise in carboxypeptidation activity (Figure 3.14D). Although 37 °C showed the highest transpeptidase activity, the transpeptidation:carboxypeptidation activity ratio was lower than that of 30 °C (Figure 3.14D). Therefore, it was decided to maintain the assay conditions at pH 8.5 and 30 °C as these gave the optimal, as well as the most repeatable transpeptidase rate and transpeptidation:carboxypeptidation activity ratio, and importantly, were also the optimal conditions for *E. coli* PBP1b transpeptidase activity (Catherwood *et al.*, 2019).

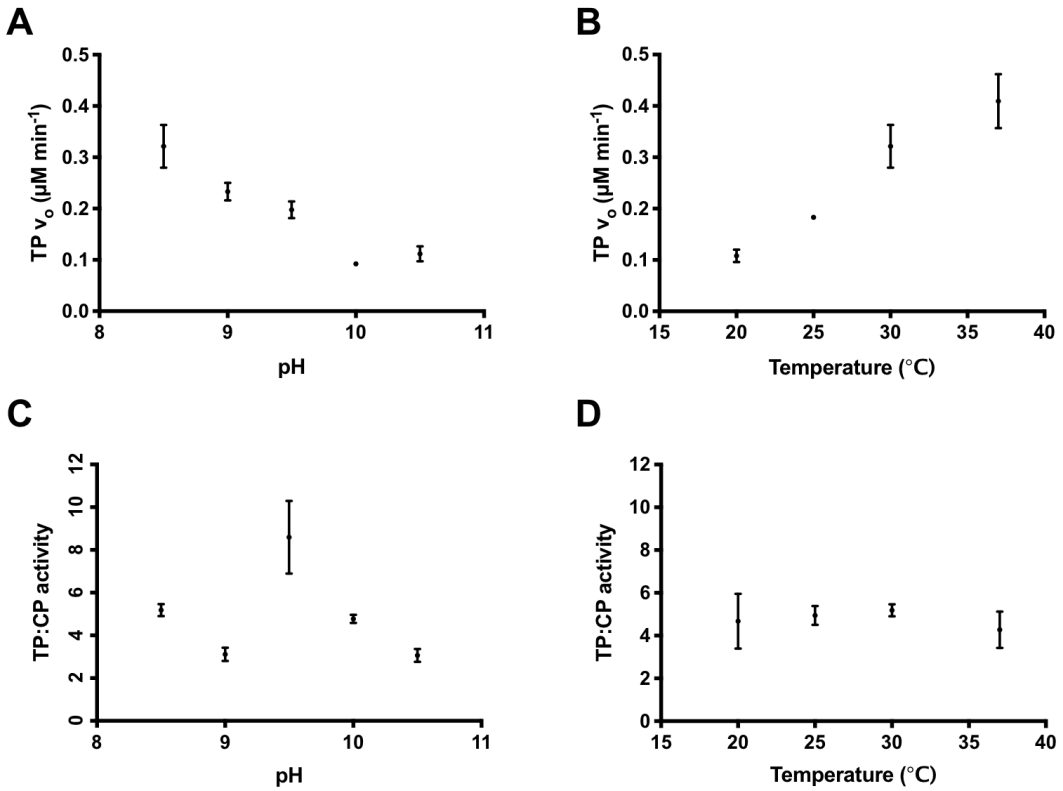

Figure 3.14 Effect of pH and temperature on *Y. pestis* PBP1b transpeptidase and carboxypeptidase activity.
Initial transpeptidase (TP) and carboxypeptidase (CP) rates were assayed using the amplex red assay for D-Ala release by *Y. pestis* PBP1b *in vitro*, at various **(A** and **C)** pH's and **(B** and **D)** temperatures, shown as initial rates and TP:CP activity ratio. Reactions consisted of 50 mM Bis-Tris propane pH 8.5, 6 mM NaCl, 20 mM $MgCl_2$, 1% (v/v) glycerol, 0.130% (v/v) Triton X-100, amplex red coupling reagents, 20 μM Lipid II (acetylated DAP), 50 nM PBP1b, 2 μM LpoB and 20 μM MurNac 5P. Buffers used were Bis-Tris propane pH 8.5, CHES pH 9.0-9.5, CAPS pH 10.0-10.5. Data is shown as mean, maximum and minimum values (n=2).

3.3.6.3 Optimisation of protein concentration for *Y. pestis* PBP1b transpeptidase activity

To confirm the activity observed was dependent on *Y. pestis* PBP1b concentration, the effect of *Y. pestis* PBP1b concentration on the transpeptidation and carboxypeptidation rate was investigated. As predicted there was a linear relationship between enzyme concentration and initial transpeptidase and carboxypeptidase rates (Figure 3.15A). Also showing that the transpeptidation:carboxypeptidation activity ratio is not dependent on enzyme concentration.

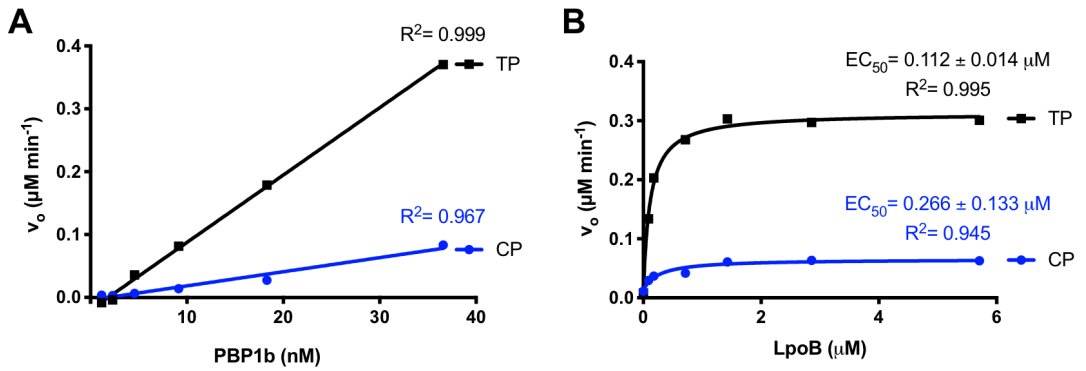

Figure 3.15 Effect of protein concentration on *Y. pestis* PBP1b activity. Transpeptidase (TP) and carboxypeptidase (CP) rate was assayed using the amplex red assay for D-Ala release by *Y. pestis* PBP1b *in vitro*, shown as initial rates. **(A)** Varied PBP1b concentration data was fitted to a straight-line model, while **(B)** varied LpoB concentration data was fitted to a three-parameter dose-response curve. Reactions consisted of 50 mM Bis-Tris propane pH 8.5, 6 mM NaCl, 20 mM $MgCl_2$, 1% (v/v) glycerol, 0.130% (v/v) Triton X-100, amplex red coupling reagents, 20 μM Lipid II (acetylated DAP), 50 nM PBP1b, 2 μM LpoB and 20 μM MurNac 5P, unless otherwise stated (n=1).

E. coli PBP1b glycosyltransferase and transpeptidase activity is known to be enhanced by outer membrane lipoprotein LpoB (Paradis-Bleau *et al.*, 2010; Typas *et al.*, 2010). Initial observations of *Y. pestis* PBP1b glycosyltransferase activity suggest LpoB has a similar effect on *Y. pestis* PBP1b (Figure 3.10). To investigate the response of *Y. pestis* PBP1b to LpoB, the relationship between *Y. pestis* PBP1b activity and LpoB concentration was measured (Figure 3.15B). LpoB had a positive concentration-dependent effect on *Y. pestis* PBP1b transpeptidase and carboxypeptidase activity until a concentration of ~1.5 μM LpoB, after which its enhancement effect plateaued, where the LpoB

concentration eliciting a half-maximal response was 0.112 ± 0.014 μM when fitted to a three-parameter dose response model based on equation Y=Bottom+X*(Top-Bottom)/(EC_{50}+X) (Figure 3.15B). This data confirmed that the concentration of LpoB currently used in the D-Ala release assay, 2 μM, also used by Catherwood *et al*. (2019), is sufficient to allow maximum enhancement of *Y. pestis* PBP1b activity at 50 nM.

3.3.6.4 Inhibition of *Y. pestis* PBP1b transpeptidase activity by ampicillin

To validate the *Y. pestis* PBP1b transpeptidase assay for the detection of inhibitors, the specific PBP transpeptidase inhibitor ampicillin was used a control. Initial rates were used to compute the percentage activity in relation to the no inhibitor control and fitted to a four-parameter dose-response curve model based on equation $Y= 100/1+[S]^{hs}/IC_{50}^{hs}$. The IC_{50} of ampicillin for *Y. pestis* PBP1b transpeptidase activity was determined to be 25.8 ± 3.6 μM and 77.8 ± 7.6 μM for carboxypeptidase activity at 50 nM enzyme (Figure 3.16).

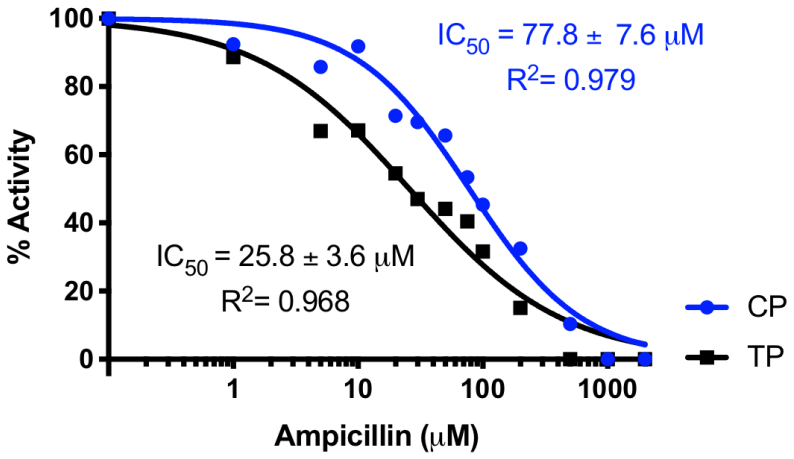

Figure 3.16 Inhibition of *Y. pestis* PBP1b transpeptidase and carboxypeptidase activity by ampicillin.
Transpeptidase (TP) and carboxypeptidase (CP) initial rates were assayed using the amplex red assay for D-Ala release by *Y. pestis* PBP1b *in vitro*, shown as percentage activity in relation to the no inhibitor control and fitted to a four-parameter dose-response curve model. Reactions consisted of 50 mM Bis-Tris propane pH 8.5, 6 mM NaCl, 20 mM $MgCl_2$, 1% (v/v) glycerol, 0.130% (v/v) Triton X-100, amplex red coupling reagents, 20 μM Lipid II (acetylated DAP), 50 nM PBP1b, 2 μM LpoB, 20 μM MurNac 5P and varied ampicillin concentration (n=1).

3.3.7 Establishing kinetic parameters for *E. coli* and *Y. pestis* PBP1b activity with varied substrates

To establish kinetic parameters for *Y. pestis* PBP1b, the impact of substrate concentration on glycosyltransferase and transpeptidase activity was investigated. The dependence of *E. coli* PBP1b glycosyltransferase rate on Lipid II (dansylated DAP) was sigmoidal (Figure 13.7A), suggesting positive cooperative binding; binding of one substrate affects the affinity of a second binding site for its substrate. Therefore, the data was fitted to the Michaelis Menten equation (Equation 1), as well a variation of the Michaelis Menten equation considering cooperativity in activity (Equation 2). Using the R^2 value to determine the best fit, *E. coli* and *Y. pestis* PBP1b utilisation of Lipid II (dansylated DAP) best fitted equation 2, producing K_m of $6.96 \pm 0.48\ \mu$M and $11.19 \pm 3.01\ \mu$M for *E. coli* and *Y. pestis* respectively (Figure 3.17C). Unfortunately, K_{cat} values could not be calculated for Lipid II (dansylated DAP) as the continuous glycosyltransferase assay does not permit the change in fluorescence to be equated to a quantifiable change in substrate or product.

$$\text{Equation 1: } Vo = \frac{V_{max}[S]}{K_m + [S]}$$

$$\text{Equation 2: } Vo = \frac{V_{max}[S]^h}{{K_{0.5}}^h + [S]^h}$$

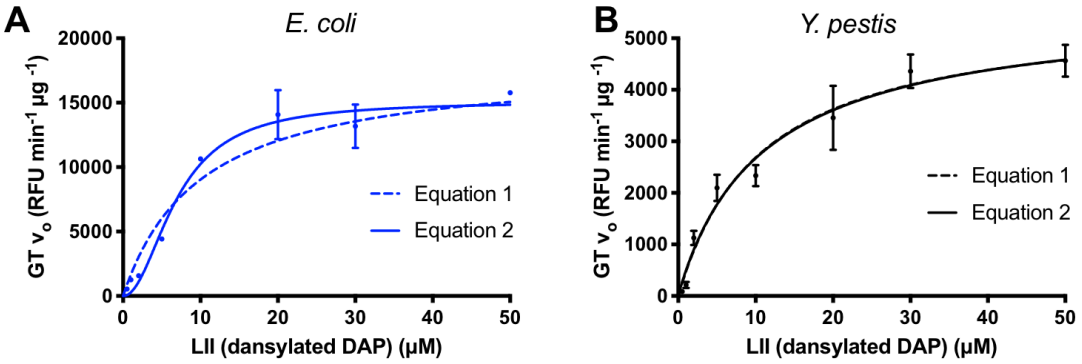

C

PBP1b	Substrate	Equation	V_{max} (RFU min^{-1} μg^{-1})	$K_{m/0.5}$ (μM)	$V_{max}/K_{m/0.5}$	Hill coefficient	R^2 of fit
E. coli	LII (dansyl DAP)	1	18081 ± 1796	10.02 ± 2.83	1806 ± 146	1.0	0.946
		2	15101 ± 448	6.96 ± 0.48	2153 ± 43	2.047	0.977
Y. pestis	LII (dansyl DAP)	1	5556 ± 520	10.70 ± 2.86	512 ± 100	1.0	0.962
		2	5655 ± 562	11.19 ± 3.01	490 ± 142	0.971	0.962

Figure 3.17 Effect of substrate concentration on *E. coli* and *Y. pestis* PBP1b glycosyltransferase activity.
(A) *E. coli* PBP1b **(B)** and *Y. pestis* PBP1b *in vitro* activity, shown as initial glycosyltransferase rates (GT) fitted to two Michaelis-Menten models. **(C)** Table of resulting kinetic parameters. Glycosyltransferase rate was assayed by the consumption of fluorescently labelled Lipid II. Reactions consisted of 50 mM HEPES pH 7.5, 115 mM NaCl, 10 mM $MgCl_2$, 10% (v/v) DMSO, 1% (v/v) glycerol, 0.155% (v/v) Triton X-100, 0.1 mg ml^{-1} lysozyme, varied concentrations of Lipid II (dansyl DAP), 50 nM PBP1b and 2 μM LpoB. Data is shown as mean ± SD (n=3).

To explore the dependence of *Y. pestis* PBP1b transpeptidase rate on its substrate, exclusive donor and acceptor only substrates were utilised. Using Lipid II (acetylated DAP) as a donor, with 20 μM MurNAc 5P (DAP) as acceptor, *Y. pestis* PBP1b was hyperbolically dependent on Lipid II (acetylated DAP) (Figure 3.18A) and fitted the Michaelis Menten equation (Equation 1). This now suggested one donor substrate: PBP interaction was required for transpeptidation as expected, and produced a K_m of 3.44 ± 0.71 μM and K_{cat} of 0.231 ± 0.009 s^{-1} (Figure 13.8C). Using 20 μM Lipid II (acetylated DAP) as a donor, with MurNAc 5P (DAP) as acceptor, *Y. pestis* PBP1b transpeptidation was dependent on MurNAc 5P (DAP) (Figure 3.18B) and fitted the Michaelis Menten equation (Equation 1). Although a full data set could not be attained for MurNAc 5P (DAP), as insufficient substrate concentrations were available to see a plateau

in *Y. pestis* PBP1b transpeptidation, the data yielded a K_m of 166.80 ± 32.53 μM and K_{cat} of 1.703 ± 0.238 s^{-1} (Figure 13.8C).

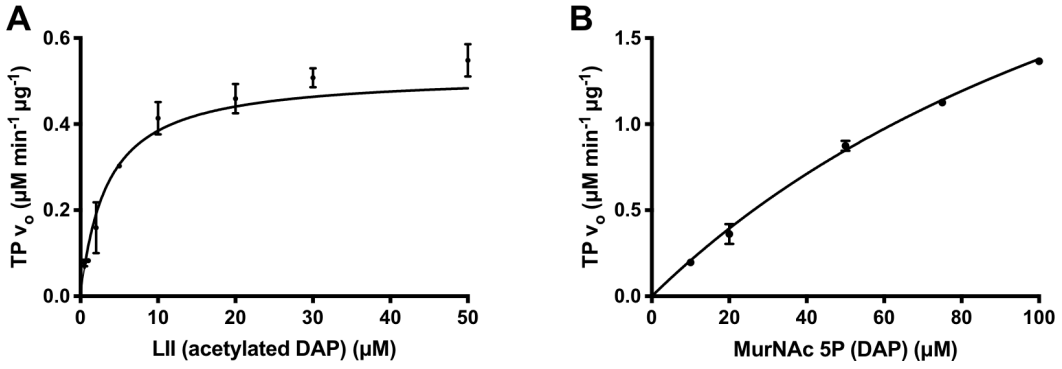

C

PBP1b	Substrate	V_{max} (μM min^{-1} μg^{-1})	K_m (μM)	V_{max}/K_m	K_{cat} (s^{-1})	K_{cat}/K_m (M^{-1} s^{-1})	R^2 of fit
Y. pestis	LII (acetyl DAP)	0.52 ± 0.02	3.44 ± 0.71	0.1509 ± 0.0283	0.239 ± 0.009	1011.0 ± 29.7	0.906
	MurNAc 5P (DAP)	3.68 ± 0.52	166.80 ± 32.53	0.0218 ± 0.0006	1.703 ± 0.238	6985.2 ± 1310.2	0.993

Figure 3.18 Effect of substrate concentration on *Y. pestis* PBP1b transpeptidase activity.
Y. pestis PBP1b *in vitro* activity, shown as initial transpeptidase rates (TP) utilising **(A)** Lipid II (acetylated DAP) and **(B)** MurNAc 5P (DAP), fitted to a Michaelis-Menten model (equation 1). **(C)** Table of resulting kinetic parameters. Transpeptidase rate was assayed using the amplex red assay for D-Ala release. Reactions consisted of 50 mM Bis-Tris propane pH 8.5, 6 mM NaCl, 20 mM $MgCl_2$, 1% (v/v) glycerol, 0.130% (v/v) Triton X-100, amplex red coupling reagents, 20 μM Lipid II- 5P (acetylated DAP), 50 nM PBP1b, 2 μM LpoB, 20 μM MurNac- 5P, unless otherwise stated. Data is shown as mean ± SD (n=3).

3.4 Discussion and future work

3.4.1 Substrate synthesis

Lipid II (dansylated DAP), Lipid II (acetylated DAP) and MurNAc 5P (DAP) were successfully synthesised enzymatically, purified, and identified by negative ion mass spectroscopy. TLC purity analysis coupled with negative ion mass spectroscopy confirmed the substrates were of high purity due to the absence of any other significant bands or peaks, and the purifications produced high yields of substrates. The enzymatic biosynthesis method used to synthesise these substrates was successful in producing high yields of pure substrates, which

would have been difficult to produce in such quantities and purity by extraction from bacteria and post extraction modification (Van Heijenoort *et al.*, 1992).

3.4.2 Limitations of the continuous glycosyltransferase and D-Ala release assays

Before the results of the assay optimisations are discussed it is important to consider the limitations of using non-native Lipid II as substrates for PBP1b. It has previously been established that the use of substrates with modifications to the third position stem peptide does not significantly affect the glycosyltransferase kinetics of *E. coli* PBP1b, in the case of dansylation (Schwartz *et al.*, 2002) and acetylation (Zhang *et al.*, 2007), however no such studies have tested their effect on *Y. pestis* PBP1b, hence their comparability to native substrate is unknown. To minimise any effect substrate modifications may have on the kinetics, modifications which were thought to cause the least steric hindrance were chosen.

3.4.2.1 Limitations of the continuous glycosyltransferase assay

The continuous glycosyltransferase assay follows the decrease in fluorescence of the dansyl group (attached to the third position DAP of Lipid II), due to a change in its micelle environment. As Lipid II is polymerised into glycan chains by PBP1b the dansyl group is in a hydrophobic micellar environment, subsequent digestion of the glycan chains by lysozyme then transfers the dansyl group into an aqueous environment due to the muropeptide produced being soluble (Pompliano *et al.*, 1992; Schwartz *et al.*, 2002). It is known that lysozyme recognises heptasaccharide units as it's preferential substrate and cleaves off tetrasaccharides from heptasaccharides (Vocadlo *et al.*, 2001), however it is not known how lysozyme interacts with a growing glycan chain. The major limitation to this assay is that it is not quantifiable in terms of the fluorescence change directly measuring substrate loss or product production. Schwartz et al. have shown that Lipid II was fully converted into muropeptides by *E. coli* PBP1b and

lysozyme, by accompanying this assay with a parallel HPLC analysis (2002), however this should not be assumed for different enzymes or buffer conditions. No parallel analysis to confirm full conversion of Lipid II to muropeptides was performed in this project, hence full conversion was not assumed and therefore K_{cat} measurements could not be extracted from the data.

To overcome this limitation another method for measuring glycosyltransferase activity was tested. This method quantitatively measures the production of pyrophosphate with an antibody sensor, and has previously been used to continuously follow *E. coli* PBP1b glycosyltransferase activity (King *et al.*, 2017). However, when tested the pyrophosphate antibody sensor was found not to be specific for free pyrophosphate, but also bound the pyrophosphate moiety of Lipid II, rending the assay ineffective, as the sensor could bind both the substrate and product causing no overall fluorescence change.

Due to the failure of the pyrophosphate assay to measure glycosyltransferase activity quantitatively, the continuous fluorescence glycosyltransferase assay should be made quantitative. This could be achieved by separating the assay products by anion-exchange HPLC to investigate if all Lipid II was converted into muropeptides (Schwartz *et al.*, 2002), or extracting the undecaprenyl phosphate produced by TLC and quantifying it by the phosphate release assay or mass spectroscopy (Mesleh *et al.*, 2016). If this is the case, the fluorescence change could be converted to a known concentration of substrate lost.

3.4.2.2 Limitations of the continuous D-Ala release assay

The continuous D-Ala release assay follows the release of D-Ala, firstly with the transpeptidase donor only substrate present, allowing the rate of D-Ala release from carboxypeptidation to be monitored, then with the addition of an acceptor only transpeptidase substrate the rate of D-Ala release due to transpeptidation and carboxypeptidation can be monitored. In order to calculate the rate of transpeptidase activity only, the rate of D-ala release from carboxypeptidation is subtracted from the rate of D-ala release from carboxypeptidation and

transpeptidation combined (TP rate= (TP+CP rate)- CP rate). However, this assumes that the rate of carboxypeptidation stays constant even though transpeptidation is now also occurring. Although this is an assumption, the assumed carboxypeptidation rate in the presence of a transpeptidase acceptor only substrate is likely accurate or an overestimation, as the carboxypeptidation rate is unlikely to increase in the presence of a transpeptidase acceptor only substrate, as there is now competition for the donor peptide. Therefore, the calculated transpeptidation only rate is most likely an underestimation.

To investigate if this assumption is correct LCMS could be carried out to quantify the amount of carboxypeptidation product in the absence and presence of MurNAc 5P (DAP). Alternatively, the assay products could be separated and the carboxypeptidation product quantified by reverse-phase HPLC in the absence and presence of MurNAc 5P (DAP) (Glauner and Entwi, 1988; Ropy *et al.*, 2015; Peters *et al.*, 2018).

3.4.3 Lipid II (dansylated DAP), Lipid II (acetylated DAP) and MurNAc 5P (DAP) as substrates for *Y. pestis* PBP1b

Y. pestis PBP1b was successfully able to utilise Lipid II (dansylated DAP) and Lipid II (acetylated DAP) as glycosyltransferase substrates, and MurNAc 5P DAP as a transpeptidase acceptor only substrate.

The $K_{0.5}$ values of 6.96 ± 0.48 μM calculated for *E. coli* PBP1b transglycosylation and 11.19 ± 3.01 μM for *Y. pestis* PBP1b transglycosylation using fluorescently labelled (dansylated) Lipid II are consistent with previous studies determining *E. coli* PBP1b to have a K_m of 2.5 μM (Schwartz *et al.*, 2002) and 18.3 ± 4.05 μM (Sung *et al.*, 2009) with fluorescently labelled substrate, which indicate that *Y. pestis* PBP1b has comparable affinity for the substrate as *E. coli*. The K_m for *Y. pestis* PBP1b donor transpeptidation using unlabelled Lipid II (acetylated DAP) was 3.44 ± 0.71 μM, and the K_{cat} 0.239 ± 0.009 s^{-1}, which is also consistent with previous findings determining the K_m of *E. coli* PBP1b with unlabelled or radio-labelled Lipid II to be between 2.0 and 14.42 μM, and K_{cat} to be between 0.07 and

0.238 s^{-1} (Terrak *et al.*, 1999; Chen *et al.*, 2003; King *et al.*, 2017; Catherwood *et al.*, 2019).

The data obtained for the response to varied MurNAc 5P (DAP) concentrations should not be assumed as accurate, as inadequate substrate concentrations were tested to reach a plateau in activity. However, the data collected accurately fitted a Michaelis-menten model and produced a K_m of 166.80 ± 32.53 μM which is significantly higher than any other substrate tested, suggesting *Y. pestis* PBP1b has the lowest affinity for this substrate. This agrees with Catherwood *et al*. who also found *E. coli* PBP1b to have the lowest affinity for MurNAc 5P (DAP) (K_m= 42.97 ± 8.19 μM) out of all the acceptor only substrates tested (2019). The K_{cat} value extracted for MurNAc 5P (DAP) was 1.703 ± 0.238 s^{-1} which is also in agreement with Catherwood *et al.* who found *E. coli* PBP1b to have a K_{cat} of 1.863 ± 0.210 s^{-1} (2019), suggesting *Y. pestis* is able to turnover this substrate as quickly as *E. coli*. In order to confirm these results are accurate further concentrations of MurNAc 5P (DAP) should be tested until a plateau in activity is seen.

Previous studies have compared the calculated *in vitro* affinity of PBPs to their substrate and compared them to *in vivo* concentrations of substrates. Van Heijenoort *et al.* calculated the number of Lipid II molecules per *E. coli* cell to be 1000-2000 (1992), which equate to a cellular concentration significantly lower than the calculated K_m for *E. coli* or *Y. pestis* PBP1b. It is however important to consider that Lipid II is likely to be sequestered to specific membrane locations, therefore the local concentration seen by PBP1b is likely very high. There is also a large discrepancy between the K_{cat} values extracted from *in vitro* experiments compared to calculated number of reactions/second/PBP required to support the growth and division of *E. coli*. For example it is estimated that 5 glycosyltransferase and 2 transpeptidase reactions must occur per second per PBP1b (Galley *et al.*, 2014), whereas the K_{cat} values calculated for *Y. pestis* PBP1b and previous work are significantly less. This is unsurprising given the removal of the enzyme from its native environment and interacting partners, however more biologically relevant assay systems are not currently available.

3.4.4 Effect of buffer conditions on *Y. pestis* PBP1b activity

Y. pestis PBP1b was most active between pH 7.5-9.5, with activity rapidly decreasing after this, agreeing with previous data of *E. coli* PBP1b activity (Schwartz *et al.*, 2002). The *E. coli* periplasm has been shown to have a native pH of 7.5-7.6, however the pH was shown to have a slow recovery when the external environmental pH changed (Wilks and Slonczewski, 2007). *Y. pestis* over its life cycle will encounter a wide range of external pH values, including the human intestinal tract pH 4.5-9.0 (Jonge *et al.*, 2003), human macrophage pH 5.0-7.5 (Canton *et al.*, 2014) and decaying corpse ~pH 4.0 (Easterday *et al.*, 2012), hence it would be advantageous for *Y. pestis* PBP1b to be active over a wide pH range as seen.

Previous studies have published contradictory results regarding the effect of detergent and DMSO concentration on *E. coli* PBP1b activity. The most consistent findings suggest DMSO aids rapid exchange of Lipid II between micelles at otherwise inhibitory high detergent concentrations (Schwartz *et al.*, 2002; Offant *et al.*, 2010; Helassa *et al.*, 2012; Egan and Vollmer, 2016), however DMSO has a negative impact on the ability of LpoB to activate PBP1b (Egan and Vollmer, 2016). Optimum *Y. pestis* PBP1b activity conditions clarify these findings by indicating that high DMSO concentrations, weakening the LpoB-PBP1b interaction, has a greater inhibitory effect on PBP1b activity than the high detergent concentration needed in the absence of DMSO. Unfortunately, DMSO could not be fully excluded from the continuous glycosyltransferase assay as previous work (Galley N & Rowland C, personal communication), along with this study, found DMSO was needed to visualise the dansyl group fluorescence, hence a low DMSO concentration (10%) was used to aid fluorescence visualisation while minimising its inhibitory effect on PBP1b transglycosylase activity.

This study highlighted the detrimental effect of NaCl on PBP1b transpeptidase activity (detailed in 5.3.5.1), and it is still unknown whether NaCl effects PBP1b activity directly or it's activation by LpoB. To investigate this a mutation to the UB2H domain of PBP1b could be made to simulate LpoB activation (detailed in

5.3.2.1) and its activity measured in low and high salt concentrations, in order to establish if the inhibitory effect of NaCl is on the PBP1b-LpoB interaction.

3.4.5 Effect of protein and inhibitor concentration on *Y. pestis* PBP1b activity

Once optimal buffer conditions for *Y. pestis* PBP1b activity were established, the assays were validated. As expected there was a linear relation between PBP1b concentration and activity and the concentration of LpoB needed to gain maximum PBP1b activity was also determined to be 1.5 μM, 30x greater than the PBP1b concentration. Data suggests *E. coli* PBP1b-LpoB bind in a 1:1 stoichiometry *in vitro*, and there *in vivo* copy numbers have also been found to be very similar, PBP1b 1000 and LpoB 2300 molecules per cell (Typas *et al.*, 2010). To ensure full PBP1b activation by LpoB *in vivo* the proximity of the two proteins at the surface of the extracellular face of the membrane will be key. Indeed, *in vivo* it is known that peptidoglycan synthesis occurs in "hotspots" where all the necessary proteins localise to create a multi-protein complex, hence the proximity of the two proteins is likely a lot closer than *in vitro*.

To validate the assay setup for inhibitors, ampicillin was tested as a transpeptidase inhibitor. An IC_{50} value of 25.77 ± 3.64 μM was established for *Y. pestis* PBP1b which is comparable to that obtained for *E. coli* PBP1b inhibition, 22.0 ± 1.8 μM (King *et al.*, 2017), suggesting *Y. pestis* PBP1b is just as susceptible to ampicillin as *E. coli*.

3.4.6 Future work

In addition to the further work that has been generated from the results in this chapter discussed above, the development of a functional assay for *Y. pestis* PBP1b enables further investigation into its function and protein-protein interactions.

The evidence from this chapter suggests *Y. pestis* PBP1b is more sensitive to substrate variations than *E. coli* PBP1b, even though most other aspects of their enzymology are very similar. Modelling the structure of *Y. pestis* PBP1b on the crystal structure of *E. coli* PBP1b may reveal structural differences which rationalise these substrate and kinetic differences, as their sequences differ by only 30%. Although the exact residues which interact with the two substrates are unknown, the binding of β-lactams to PBPs have identified three motifs thought to be important in binding. The first motif containing the active site serine, SXXK is conserved in *E. coli* and *Y. pestis* PBP1b, along with the second and third motifs, SXN (S572 in *E. coli*) and KTGT (K698 in *E. coli*) respectively (Sauvage *et al.*, 2008), suggesting other non-conserved residues are involved in the differential substrate recognition. Investigating the affinity of *Y. pestis* PBP1b for other donor and acceptor only substrates using the assays developed in this chapter will also increase our understanding on why *Y. pestis* PBP1b is more sensitive to substrate modifications. Crystallography of *Y. pestis* PBP1b protein was attempted with no success.

It is also unknown for all bifunctional PBP's if the rate of glycosyltransferase activity governs the rate of transpeptidase activity, as it is hypothesised that the growing glycan chain may be directed from the glycosyltransferase site into the transpeptidation active site. This question highlights the need for a continuous glycosyltransferase assay which utilises native Lipid II substrates. However, in the absence of such assay the glycosyltransferase rate could be measured in continuous fluorescence assay in the presence of MurNAc 5P. If the growing glycan chain does get directed from the glycosyltransferase site to the

transpeptidase site the presence of MurNAc 5P in the transpeptidase active site would likely slow glycosyltransferase activity.

PBPs are known to interact with other PBPs, as well as regulatory proteins in the elongasome and divisome complexes formed during peptidoglycan synthesis (Typas *et al.*, 2012). The ultimate aim of the assay systems developed in this chapter is to reconstitute the cell wall synthesis complex *in vitro*. Hence, these assays are an excellent tool to enable the effect of interacting proteins on PBP1b function to be defined, ultimately increasing our understanding of how peptidoglycan synthesis is controlled and coordinated (discussed in chapter 4).

Most importantly the assays developed in this chapter are an excellent platform to test and screen novel inhibitors, with the assays already being validated for high-throughput use. The continuous glycosyltransferase assay was optimised for a 384-well format in this study and the D-Ala release assay has previously been optimised for a 1536-well format (Walkowiak, 2017).

3.5 Conclusions

This study has seen the first observations of *Y. pestis* PBP1b activity *in vitro*, enabled by the successful biosynthesis of *Y. pestis* PBP1b substrates, as well as the cloning, expression and purification of all the necessary proteins. This allowed the optimal conditions for *Y. pestis* PBP1b activity to be developed in continuous glycosyltransferase and transpeptidase assays. The kinetic parameters of *Y. pestis* PBP1b were determined and the assays were validated for inhibitor testing. The results in this chapter confirm *Y. pestis* PBP1b is more sensitive to substrate modifications than *E. coli* PBP1b, although other aspects of its enzymology, including optimal buffer conditions for activity, are extremely similar.

Chapter 4. Investigation of glycan chain cleavage

4.1 Introduction

4.1.1 Glycosyltransferase activity

In vitro glycosyltransferase activity is well reported in the literature for bifunctional PBPs (Barrett *et al.*, 2005; Born *et al.*, 2006; Offant *et al.*, 2010; Helassa *et al.*, 2012; Egan *et al.*, 2018), mono-functional glycosyltransferases (Terrak and Nguyen-Distèche, 2006) and SEDS proteins (Taguchi *et al.*, 2019; Welsh *et al.*, 2019) from multiple Gram-positive and -negative bacteria. The most commonly used *in vitro* methods to measure glycosyltransferase activity are a continuous fluorescence assay, using dansylated Lipid II (Schwartz *et al.*, 2002) (discussed in chapter 3), the separation of dansylated or radioactive glycan chains by Tris-tricine SDS-PAGE analysis (Schägger and von Jagow, 1987; Barrett *et al.*, 2007; Helassa *et al.*, 2012) (discussed in this chapter), and two quantitative undecaprenyl pyrophosphate detection assays, one using high-throughput "rapid fire" MSMS (Mesleh *et al.*, 2016) and the other an antibody sensor (King *et al.*, 2017). These methods have established that the general catalytic mechanism of peptidoglycan synthesising glycosyltransferases is to add Lipid II monomers to the reducing end of the growing glycan chain (Perlstein *et al.*, 2007; Welsh *et al.*, 2019), and each glycosyltransferase polymerises a characteristic intrinsic length of glycan chain, which is independent of enzyme:substrate ratios (Wang *et al.*, 2008). The requirement of metal ions for functionality is also a feature of many glycosyltransferases (Schwartz *et al.*, 2002; Terrak and Nguyen-Distèche, 2006).

4.1.2 SDS-PAGE glycosyltransferase assay

To complement the continuous fluorescent glycosyltransferase assay optimised in chapter 3, this project also used an SDS-PAGE analysis method to visualise fluorescently labelled glycosyltransferase reaction products, providing

qualitative data on the length of glycan chains produced. Like the continuous fluorescence-based assay, the SDS-PAGE assay uses dansylated Lipid II which is polymerised into glycan chains by PBP1b. These glycan chains have a net negative charge and can be separated by size via SDS-PAGE before visualisation (Schägger and von Jagow, 1987; Helassa *et al.*, 2012) (Figure 4.1). However, the disadvantage of this technique is the lack of suitable standards of glycan chain length for comparison.

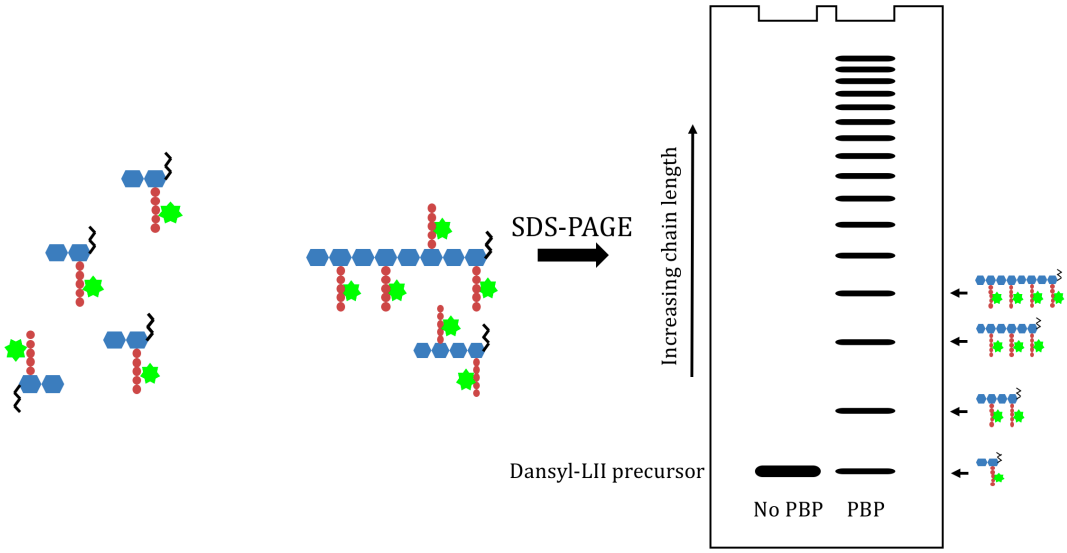

Figure 4.1. *In vitro* SDS-PAGE glycosyltransferase assay principle.
Lipid II (dansylated DAP) is polymerised into glycan chains by PBP1b. The glycan chains are then separated by SDS-PAGE.

4.2 Experimental aims

- To characterise *E. coli* PBP1b glycan chain polymerisation.
- To analyse the stability of glycan chains.
- To determine the impact of environmental factors, such as metal ions, on glycan chain stability.
- To determine the impact of cross-linking on glycan chain stability and structure.

4.3 Results

4.3.1 Initial observations of glycan chain polymerisation by *E. coli* PBP1b

In chapter 3, optimal PBP1b glycosyltransferase conditions in terms of pH, detergent and DMSO concentration, were established, and these were used to visualise glycan chains polymerised by *E. coli* PBP1b in this chapter. A transpeptidase inactive mutant of *E. coli* PBP1b S510A was used for some of this work (kindly gifted by D. Bellini (Warwick)), made by mutating the transpeptidase active site serine to an alanine.

As expected from the initial results of the continuous glycosyltransferase assay (section 3.3.5), glycan chains accumulated over time when visualised by SDS-PAGE analysis, seen by the disappearance of the Lipid II band (Figure 4.2). PBP1b glycosyltransferase rate is known to be affected by metal ion concentration (Schwartz *et al.*, 2002; Barrett *et al.*, 2004), and we also found this observation to be true. Not only did the $MgCl_2$ concentration affect the rate of Lipid II polymerisation, it also affected the length of glycan chains produced by *E. coli* PBP1b, seen by the longer glycan chains being polymerised with increasing $MgCl_2$ concentration (Figure 4.2). This increase in glycan chain length was also seen with $MnCl_2$ and $NiCl_2$, while increasing $CuCl_2$ and $ZnCl_2$ concentration inhibited PBP1b activity (Appendix 9.2).

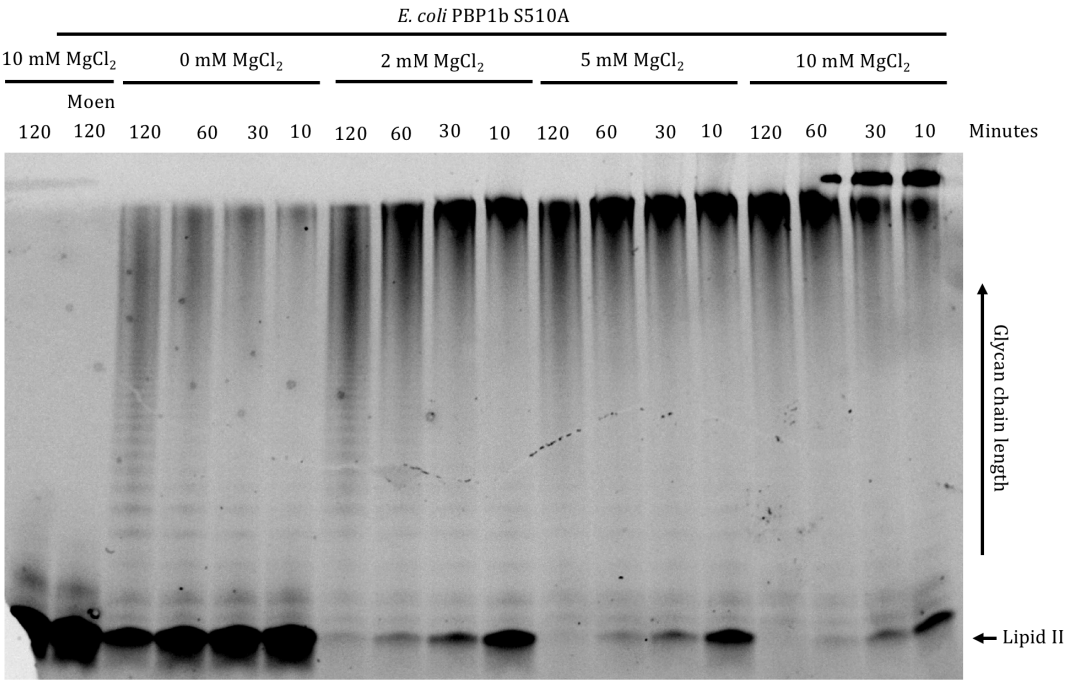

Figure 4.2 *E. coli* PBP1b glycan chain accumulation over 2 hours.
E. coli PBP1b glycosyltransferase activity was assayed by the polymerisation of fluorescently labelled Lipid II *in vitro,* where the glycan chain products were separated by SDS-PAGE and visualised using the fluorescence of the dansyl group labelling the stem peptide. Reactions consisted of 50 mM Bis-Tris propane pH 8.5, 15 mM NaCl, varied $MgCl_2$, 10% (v/v) DMSO, 1% (v/v) glycerol, 0.130% (v/v) Triton X-100, 10 μM Lipid II (dansyl DAP), 50 nM *E. coli* PBP1b S510A, 2 μM LpoB and 5 μM moenomycin (Moen) as a control. Representative gel of two independent experiments.

Interestingly, the length of polymerised glycan chains decreased with time. This observation was more evident in the lower $MgCl_2$ conditions, due to the enhanced separation of the shorter glycan chains. This observation was surprising and prompted the work carried out in this chapter.

4.3.2 Establishing if the decrease in glycan chain length is enzymatic

4.3.2.1 Establishing if the length of glycan chains polymerised by *E. coli* PBP1b decrease with Lipid II abundance

It was possible that *E. coli* PBP1b may polymerise shorter glycan chains as the availability of Lipid II decreases. To investigate this a longer time course of glycan

chain polymerisation was carried out, to observe if the length of glycan chains continued to decrease after all the Lipid II had been polymerised. Indeed, this was the case (Figure 4.3), suggesting the decrease in glycan chain length is not due to a reduction in the transglycosylase processivity of *E. coli* PBP1b S510A, and therefore glycan chain length diminution was due to glycan chain cleavage.

Moenomycin was also observed to distort the Lipid II band. On further investigation this effect was found to be protein independent (Appendix 9.3), suggesting moenomycin may be able to bind Lipid II and affect its migration by SDS-PAGE analysis. As moenomycin was only being used as a control to inhibit polymerisation of Lipid II the band distortion was ignored.

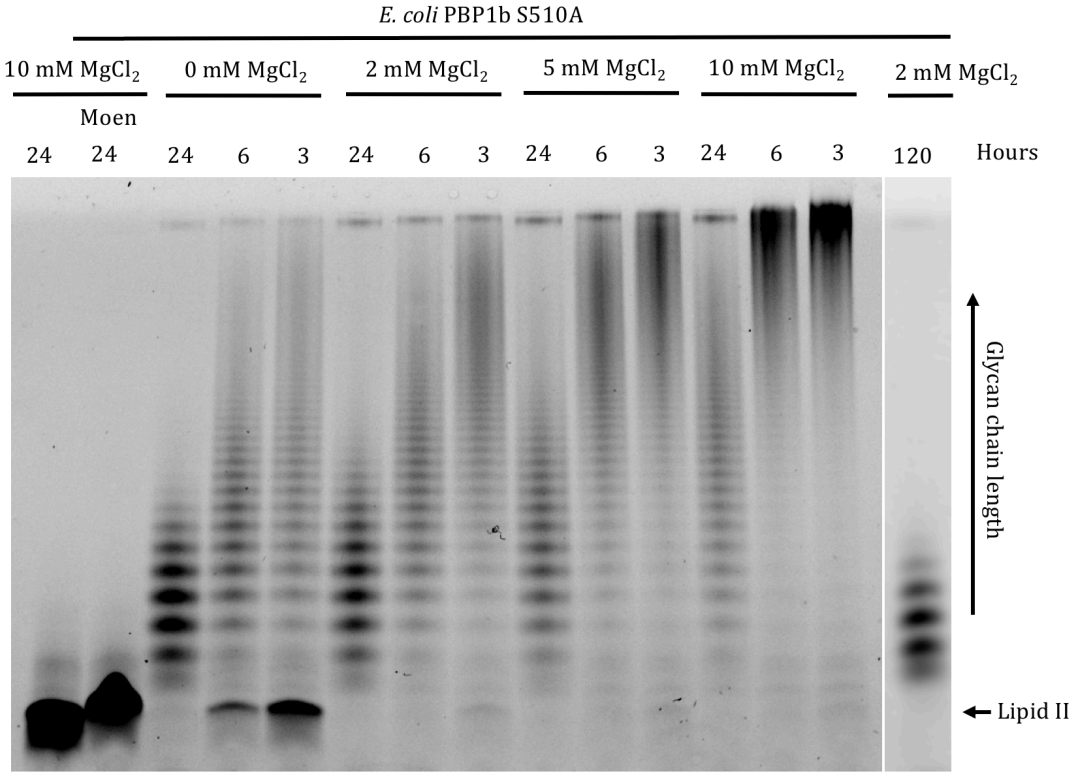

Figure 4.3 *E. coli* PBP1b glycan chain accumulation over 120 hours.
E. coli PBP1b glycosyltransferase activity was assayed by the polymerisation of fluorescently labelled Lipid II *in vitro*, where the glycan chain products were separated by SDS-PAGE and visualised using the fluorescence of the dansyl group labelling the stem peptide. Reactions consisted of 50 mM Bis-Tris propane pH 8.5, 15 mM NaCl, varied $MgCl_2$, 10% (v/v) DMSO, 1% (v/v) glycerol, 0.130% (v/v) Triton X-100, 10 μM Lipid II (dansyl DAP), 50 nM *E. coli* PBP1b S510A, 2 μM LpoB and 5 μM moenomycin (Moen) as a control. Representative gel of two independent experiments.

4.3.2.2 Establishing if glycan chain cleavage occurs with wild type PBP1b

Next, we investigated if the glycan chain cleavage also occurred with wild type PBP1b. Wild type *E. coli* PBP1b (46-844) (a longer version than the *E. coli* PBP1b S510A (58-804) mutant used in this work so far) was kindly gifted by A. Lloyd (Warwick), to eliminate any effects the transpeptidase inactive mutation may have, but also the truncation to the protein length. Glycan chains produced by both wild type *E. coli* PBP1b (46-844) (Figure 4.4) and *Y. pestis* PBP1b (61-803) (data not shown) were cleaved, confirming that the cleavage is not due to the transpeptidation inactivating mutation or specific to *E. coli* PBP1b.

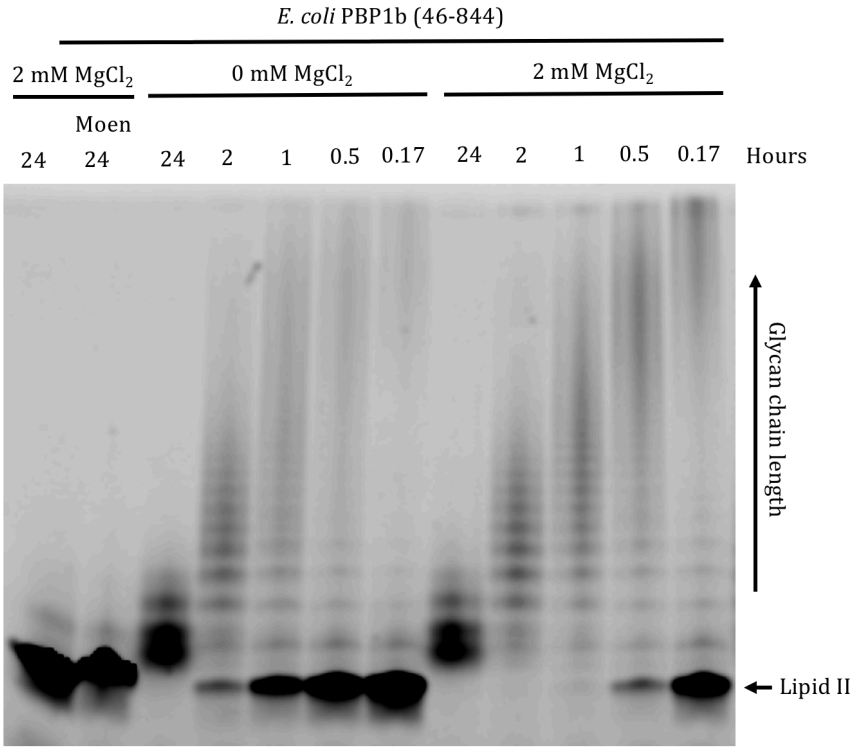

Figure 4.4 *E. coli* PBP1b glycan chain cleavage occurs with wild type *E. coli* PBP1b. *E. coli* PBP1b glycosyltransferase activity was assayed by the polymerisation of fluorescently labelled Lipid II *in vitro,* where the glycan chain products were separated by SDS-PAGE and visualised using the fluorescence of the dansyl group labelling the stem peptide. Reactions consisted of 50 mM Bis-Tris propane pH 8.5, 15 mM NaCl, varied $MgCl_2$, 10% (v/v) DMSO, 1% (v/v) glycerol, 0.130% (v/v) Triton X-100, 10 μM Lipid II (dansyl DAP), 50 nM *E. coli* PBP1b (46-844), 2 μM LpoB and 5 μM moenomycin (Moen) as a control. Representative gel of two independent experiments.

4.3.2.3 Establishing if glycan chain cleavage is inhibited by protein denaturation

Our next hypothesis was that the protein samples could be contaminated with a muramidase, potentially lysozyme (which was used in the first step of the protein purification protocol) or another peptidoglycan cleaving enzyme, such as a lytic transglycosylase. To test this hypothesis polymerisation was allowed to proceed for 2 hours, the reaction was then heated at 95 °C for 10 or 30 minutes, denaturing any proteins which may be causing the glycan chain cleavage, and left for a further 2 hours to see if cleavage occurred. Intriguingly, we found the glycan chains were still subject to cleavage after heat treatment, and the further addition of more PBP1b or LpoB to the reaction had no effect (Figure 4.5B). To confirm the denaturation of proteins at 95 °C, polymerisation did not occur in the samples heated at 95 °C before polymerisation was initiated with Lipid II. These results suggest that the cleavage is independent of active proteins in the reaction and therefore it is unlikely to be enzymatic cleavage of the glycan chains.

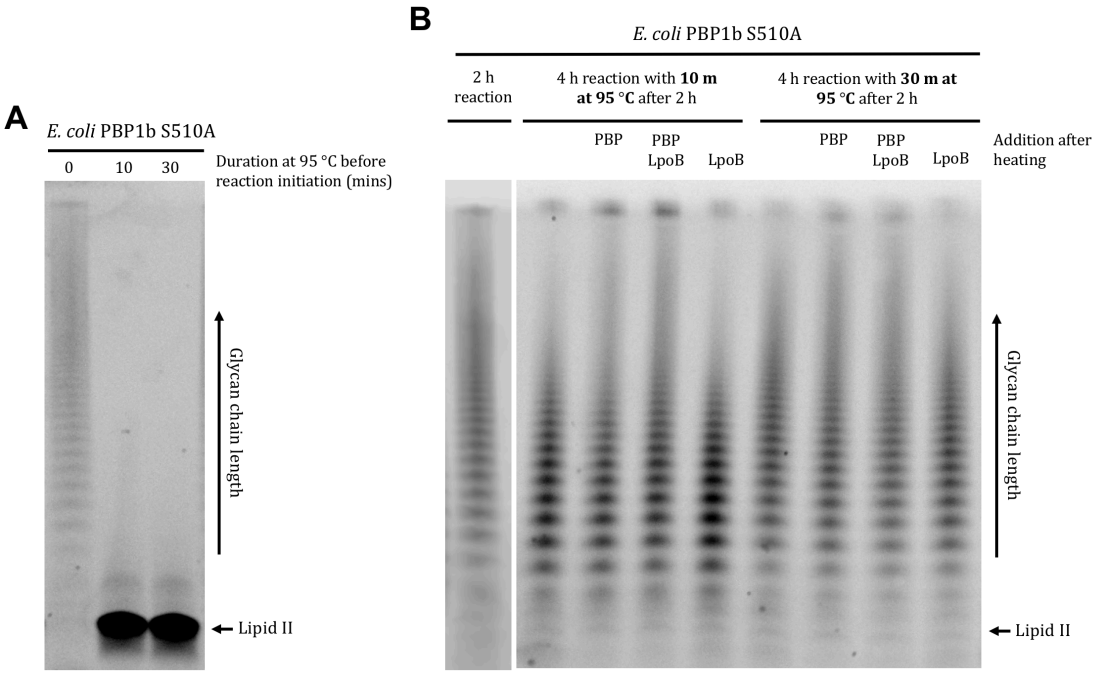

Figure 4.5 Glycan chain cleavage after thermal denaturation of the polymerisation reaction.
E. coli PBP1b glycosyltransferase activity was assayed by the polymerisation of fluorescently labelled Lipid II *in vitro,* where the glycan chain products were separated by SDS-PAGE and visualised using the fluorescence of the dansyl group labelling the stem peptide. **(A)** Reaction was heated before polymerisation was initiated with Lipid II for 2 hours, **(B)** Reaction was heated after 2 hours of polymerisation. Reactions consisted of 50 mM Bis-Tris propane pH 8.5, 15 mM NaCl, 2 mM $MgCl_2$, 10% (v/v) DMSO, 1% (v/v) glycerol, 0.130% (v/v) Triton X-100, 10 μM Lipid II (dansyl DAP), 50 nM *E. coli* PBP1b S510A and 2 μM LpoB. With the addition of 250 nM *E. coli* PBP1b S510A and 2 μM LpoB where stated. Heated at 95 °C. Representative gel of two independent experiments.

4.3.2.4 Establishing if glycan chain cleavage is inhibited by protein digestion

To support the finding that the glycan chain cleavage observed was not due to protein sample contamination with a muramidase, the polymerisation reaction was also treated with Pronase E, a mixture of proteases that hydrolyse glyco protein peptide linkages, 30 minutes before polymerisation initiation, or an hour after initiation, and left for a further 24 hours to allow cleavage to occur. The Pronase E treated glycan chains were cleaved to the same extent as the non-treated glycan chains, whereas the sample treated with Pronase E 30 minutes prior to polymerisation initiation failed to exhibit any transglycosylase activity

(Figure 4.6), confirming that Pronase E successfully cleaved the proteins in the reaction and that cleavage is not dependent on intact proteins.

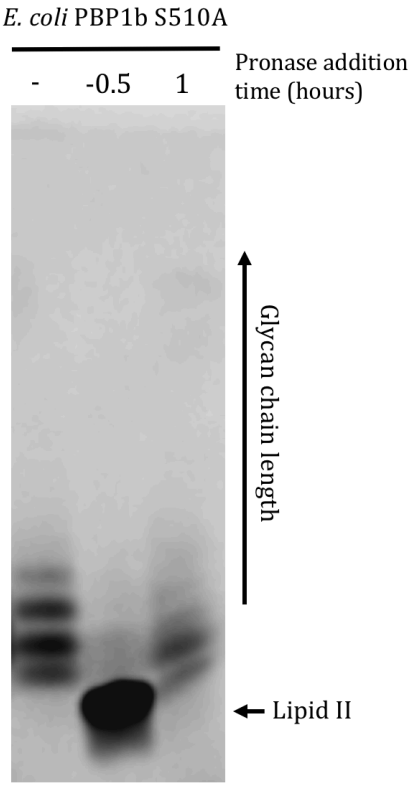

Figure 4.6 *E. coli* PBP1b glycan chain cleavage after proteolytic cleavage.
E. coli PBP1b glycosyltransferase activity was assayed by the polymerisation of fluorescently labelled Lipid II *in vitro,* where the glycan chain products were separated by SDS-PAGE and visualised using the fluorescence of the dansyl group labelling the stem peptide. 24 hour reactions consisted of 50 mM Bis-Tris propane pH 8.5, 15 mM NaCl, 2 mM $MgCl_2$, 10% (v/v) DMSO, 1% (v/v) glycerol, 0.130% (v/v) Triton X-100, 10 μM Lipid II (dansyl DAP), 50 nM *E. coli* PBP1b S510A, 2 μM LpoB and 1 mg/mL Pronase E (Sigma) where stated (n=1).

4.3.2.5 LCMS of *E. coli* PBP1b and LpoB samples for the presence of contaminating hydrolases

To discount the possibility that the observed glycan chain cleavage was a consequence of a yet unidentified lytic hydrolase enzyme, the protein samples used in the assays were analysed by mass spectroscopy. The most abundant protein in the samples were *E. coli* PBP1b and LpoB, and no muramidases or other peptidoglycan cleaving enzymes were identified (Appendix 9.4 and 9.5), suggesting that the glycan chain cleavage observed was most likely chemical, and not enzymatic cleavage.

4.3.3 Establishing if glycan chain cleavage is due to the dansyl group

4.3.3.1 Establishing if glycan chain cleavage is due to the clickable dansyl group

We considered the possibility that the dansyl fluorescent group could have caused the glycan chains to undergo cleavage. We first assessed if the click chemistry dansylation method used to synthesise the Lipid II (dansylated DAP) used in this work, had an effect on the cleavage, where Lipid II synthesised via the normal dansylation method would not be subject to such instability (Schwartz *et al.*, 2002). However, glycan chains produced from Lipid II (dansylated Lys) (kindly gifted by R. Cain (Warwick), dansylated in the traditional method) were also cleaved (Figure 4.7).

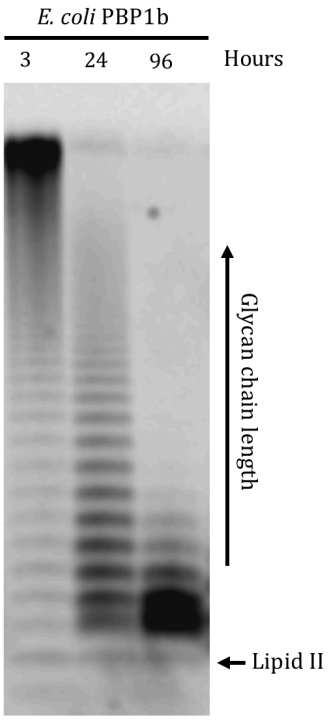

Figure 4.7 *E. coli* PBP1b glycan chain cleavage is not due to the clickable dansyl group.
E. coli PBP1b glycosyltransferase activity was assayed by the polymerisation of fluorescently labelled Lipid II *in vitro,* where the glycan chain products were separated by SDS-PAGE and visualised using the fluorescence of the dansyl group labelling the stem peptide. Reactions consisted of 50 mM Bis-Tris propane pH 8.5, 15 mM NaCl, 2 mM $MgCl_2$, 10% (v/v) DMSO, 1% (v/v) glycerol, 0.130% (v/v) Triton X-100, 10 μM Lipid II (dansyl Lys), 50 nM *E. coli* PBP1b and 2 μM LpoB (n=1).

4.3.3.2 LCMS of dansylated and non-dansylated cleaved glycan chains

To investigate if the glycan chains produced from non-dansylated Lipid II (DAP) were also sensitive to cleavage we employed LCMS analysis, as in the absence of the fluorescent group the glycan chains could not be visualised by SDS-PAGE analysis.

To confirm the cleaved glycan chains could be seen by LCMS, we first analysed dansylated cleaved glycan chains. LCMS detected m/z values for GlcNAc MurNAc 5P (dansylated DAP), GlcNAc 1,6-anhydro MurNAc 5P (dansylated DAP), and the glycan chain products (GlcNAc MurNAc 5P (dansylated DAP))$_2$, GlcNAc MurNAc 5P (dansylated DAP), GlcNAc 1,6-anhydro MurNAc 5P (dansylated DAP) and

(GlcNAc MurNAc 5P (dansylated DAP))$_3$ (Table 4.1), which are consistent with the cleaved glycan chains lengths seen by SDS-PAGE analysis (Figure 4.3).

Table 4.1 LCMS analysis of cleaved dansylated glycan chains.
Positive ion LCMS analysis of cleaved glycan chain products, produced from glycan chains polymerised from Lipid II (dansylated DAP) by *E. coli* PBP1b S510A. 120 hour reactions consisted of 50 mM Bis-Tris propane pH 8.5, 15 mM NaCl, 0 mM $MgCl_2$, 1% (v/v) glycerol, 0.0468% (v/v) E_6C_{12}, 10 μM Lipid II (dansyl DAP), 50 nM *E. coli* PBP1b S510A and 2 μM LpoB. Prepared for LCMS by silica solid phase purification. m/z and peak intensity values determined by combining the spectrums of the peak relating to the ion of interest.

				120h
Glycan chain size	**Exact mass**	**Charge state**	**Expected mass (m/z)**	**Observed mass (m/z) (Peak intensity)**
GlcNac MurNac 5P (dansyl DAP)	1324.513	(m+1)/1	1325.521	135.524 (3510)
		(m+2)/2	663.265	663.264 (176761)
GlcNac 1,6-anhydro MurNac 5P (dansyl DAP)	1306.502	(m+1)/1	1307.510	-
		(m+2)/2	654.259	654.258 (181329)
(GlcNac MurNac 5P(dansyl DAP))$_2$	2631.015	(m+1)/1	2632.023	-
		(m+2)/2	1316.516	1316.519 (12118)
		(m+3)/3	878.013	878.011 (322315)
GlcNac MurNac 5P (dansyl DAP), GlcNAc 1,6-anhydro MurNAc 5P (dansyl DAP)	2613.005	(m+1)/1	2614.013	-
		(m+2)/2	1307.511	-
		(m+3)/3	872.010	872.008 (15316)
(GlcNac MurNac 5P(dansyl DAP))$_3$	3937.518	(m+1)/1	3938.526	-
		(m+2)/2	1969.767	-
		(m+3)/3	1313.514	1313.512 (10104)
		(m+4)/4	985.388	985.386 (71994)

As LCMS successfully identified the cleaved dansylated glycan chains, the same experiment was carried out with non-dansylated glycan chains. LCMS detected glycan chains from native Lipid II, with m/z values for GlcNAc MurNAc 5P (DAP), GlcNAc 1,6-anhydro MurNAc 5P (DAP), (GlcNAc MurNAc 5P (DAP))$_2$, GlcNAc MurNAc 5P (DAP) GlcNAc 1,6-anhydro MurNAc 5P (DAP), (GlcNAc MurNAc 5P (DAP))$_3$, (GlcNAc MurNAc 5P (DAP))$_2$ GlcNAc 1,6-anhydro MurNAc 5P (DAP), (GlcNAc MurNAc 5P (DAP))$_4$ and (GlcNAc MurNAc 5P (DAP))$_5$. The abundance of the products also increased as cleavage was allowed to proceed for longer, seen by the increase in peak intensity (Table 4.2). No m/z values for the cleaved products were seen when PBP1b or Lipid II was omitted from the reaction, or when glycan chain polymerisation was inhibited by moenomycin (Table 4.2). This data is consistent with the hypothesis that native glycan chains are vulnerable to spontaneous cleavage *in vitro*, and cleave via hydrolysis of the glycosidic bond between the sugars. This data raised the possibility that cross-linking may protect the glycan chains from cleavage.

Table 4.2 LCMS analysis of cleaved native glycan chains.
Positive ion LCMS analysis of cleaved glycan chain products, produced from glycan chains polymerised from Lipid II (DAP) by *E. coli* PBP1b S510A. Reactions consisted of 50 mM Bis-Tris propane pH 8.5, 15 mM NaCl, 0 mM $MgCl_2$, 1% (v/v) glycerol, 0.0468% (v/v) E_6C_{12}, 10 μM Lipid II (DAP), 50 nM *E. coli* PBP1b S510A and 2 μM LpoB. Moenomycin (Moen) at 5 μM and EDTA at 30 mM. Prepared for LCMS by silica solid phase purification. m/z and peak intensity values determined by combining the spectrums of the peak relating to the ion of interest.

				6 h, PBP1b	40 h, PBP1b	24 h, -PBP1b	24 h, PBP1b + Moen	24 h, PBP1b + EDTA	24 h, PBP1b -LII
Glycan chain size	Exact mass	Charge state	Expected mass (m/z)	Observed mass (m/z) (Peak intensity)					
GlcNAc MurNAc 5P (DAP)	1010.429	(m+1)/1	1011.437	1011.431 (590407)	1011.431 (766504)	1011.429 (1055464)	1011.438 (199980)	1011.425 (962370)	-
		(m+2)/2	506.223	-	506.222, (23755)	-	-	-	-
GlcNAc 1,6-anhydro MurNAc 5P (DAP)	992.418	(m+1)/1	993.426	993.441 (69381)	993.431 (46186)	-	-	-	-
		(m+2)/2	497.217	497.216 (10447)	497.217 (65003)	-	-	-	-
$(GlcNAc\ MurNAc\ 5P(DAP))_2$	2002.848	(m+1)/1	2003.856	-	-	-	-	-	-
		(m+2)/2	1002.432	1002.411 (7523)	1002.430 (109289)	-	-	-	-
		(m+3)/3	668.624	668.621 (10039)	668.626, (111723)	-	-	-	-
GlcNAc MurNAc 5P (DAP), GlcNAc 1,6-anhydro MurNAc 5P (DAP)	1984.837	(m+1)/1	1985.845	-	-	-	-	-	-
		(m+2)/2	993.427	-	-	-	-	-	-
		(m+3)/3	662.620	-	662.620 (33004)	-	-	-	-
$(GlcNAc\ MurNAc\ 5P(DAP))_3$	2995.266	(m+1)/1	2996.274	-	-	-	-	-	-
		(m+2)/2	1498.641	-	1498.640 (5541)	-	-	-	-
		(m+3)/3	999.430	999.435 (7935)	999.431 (165181)	-	-	-	-
		(m+4)/4	749.825	749.839 (2526)	749.823 (31112)	-	-	-	-
$(GlcNAc\ MurNAc\ 5P\ (DAP))_2$, GlcNAc 1,6-anhydro MurNAc 5P (DAP)	2977.255	(m+1)/1	2978.263	-	-	-	-	-	-
		(m+2)/2	1489.636	-	-	-	-	-	-
		(m+3)/3	993.426	-	-	-	-	-	-
		(m+4)/4	745.322	-	745.320 (6634)	-	-	-	-
$(GlcNAc\ MurNAc\ 5P(DAP))_4$	3987.685	(m+1)/1	3988.693	-	-	-	-	-	-
		(m+2)/2	1994.851	-	-	-	-	-	-
		(m+3)/3	1330.236	-	1330.236 (7530)	-	-	-	-
		(m+4)/4	997.929	997.933 (3773)	997.930 (54013)	-	-	-	-
$(GlcNAc\ MurNAc\ 5P(DAP))_5$	4980.104	(m+1)/1	4981.112	-	-	-	-	-	-
		(m+2)/2	2491.060	-	-	-	-	-	-
		(m+3)/3	1661.043	-	-	-	-	-	-
		(m+4)/4	1246.034	-	1246.050 (4595)	-	-	-	-
		(m+5)/5	997.029	-	997.036 (10917)	-	-	-	-

4.3.4 Establishing if cross-linking affects glycan chains cleavage

In peptidoglycan the glycan chains are cross-linked together to create a mesh-like structure. This suggests that these cross-links may be present to prevent peptidoglycan from falling apart. This was investigated by visualising peptidoglycan produced by *E. coli* PBP1b, from Lipid II (DAP) mixed with Lipid II (dansylated DAP), over increasing incubation times, to establish if the cross-linked structure also undergoes cleavage.

The presence of peptidoglycan was detected as the appearance of dark bands at the top of the gel, only when Lipid II DAP was present (Figure 4.8). After 24 or 96 hours in conditions where cross-linking could have occurred, some cleavage of the cross-linked products was apparent, however the reaction products appeared as a smear, rather than resolved bands on the gel. A possible interpretation of this observation was that cross-links were still present between the glycan chains,

disrupting the regularity of migration of distinct lengths of glycan chains (Figure 4.8). This could suggest that the cross-links themselves are resistant to cleavage, and that they may be able to slow glycan chain cleavage, suggesting an evolutionary reason why peptidoglycan may be cross-linked.

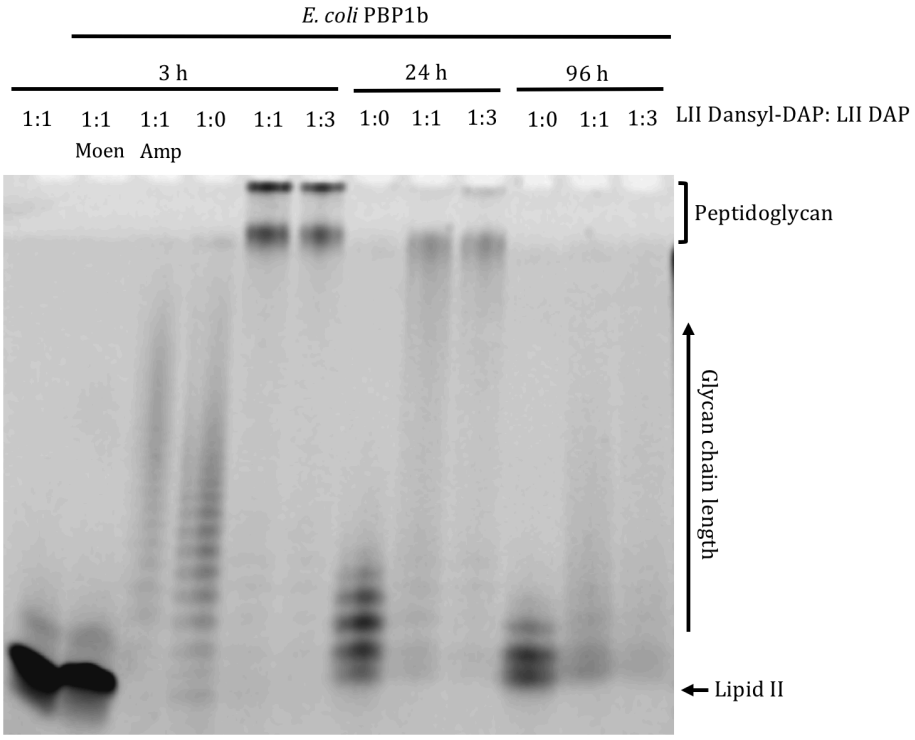

Figure 4.8 Cross-linking reduces glycan chain cleavage.
E. coli PBP1b activity was assayed by the polymerisation and transpeptidation of Lipid II *in vitro,* where the reaction products were separated by SDS-PAGE and visualised using the fluorescence of the dansyl group labelling the stem peptide. Reactions consisted of 50 mM Bis-Tris propane pH 8.5, 15 mM NaCl, 2 mM $MgCl_2$, 10% (v/v) DMSO, 1% (v/v) glycerol, 0.130% (v/v) Triton X-100, 10 μM Lipid II in varied ratios of (DAP) and (dansylated DAP), 50 nM *E. coli* PBP1b, 2 μM LpoB, 5 μM moenomycin (Moen) and 3 mM ampicillin (Amp) as controls. Representative gel of two independent experiments.

4.3.5 Establishing if glycan chain cleavage can be inhibited

While investigating the effect divalent metal ions had on the length of glycan chains polymerised by *E. coli* PBP1b (section 4.3.1), we also tested the effect of EDTA and observed EDTA to have an inhibitory effect on glycan chain cleavage (Figure 4.9A). When this was investigated in more detail, we found reduced glycan chain cleavage with increasing EDTA concentration (Figure 4.9B).

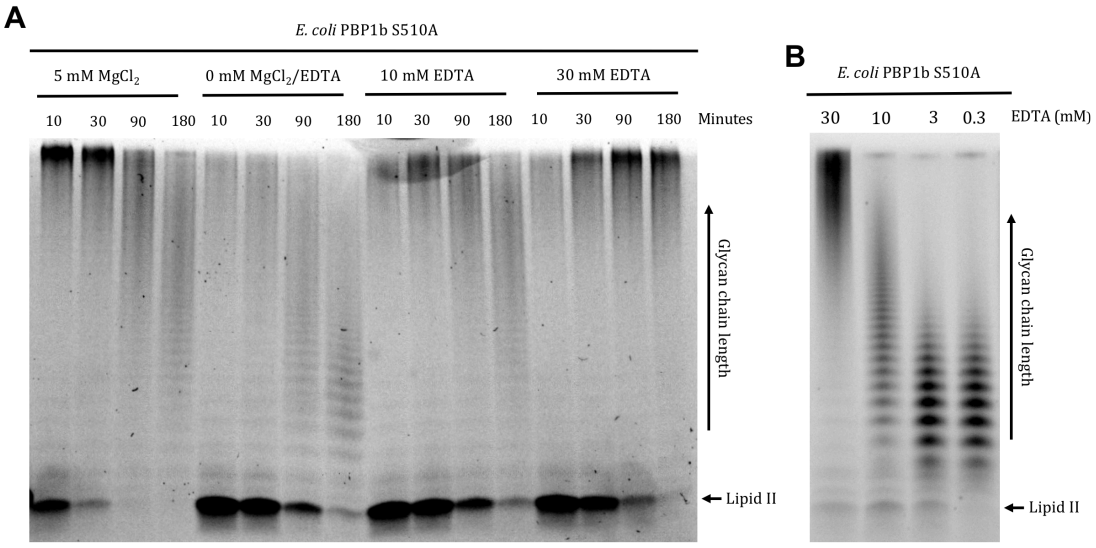

Figure 4.9 *E. coli* PBP1b glycan chain cleavage is reduced by EDTA.
E. coli PBP1b glycosyltransferase activity was assayed by the polymerisation of fluorescently labelled Lipid II *in vitro,* where the glycan chain products were separated by SDS-PAGE and visualised using the fluorescence of the dansyl group labelling the stem peptide. **(A)** Time course of glycan chain cleavage in varied $MgCl_2$ and EDTA concentrations. **(B)** Effect of varied EDTA concentrations on glycan chains cleavage in 4 hours. Reactions consisted of 50 mM Bis-Tris propane pH 8.5, 15 mM NaCl, varied $MgCl_2$ and EDTA concentrations, 10% (v/v) DMSO, 1% (v/v) glycerol, 0.130% (v/v) Triton X-100, 10 μM Lipid II (dansyl DAP), 50 nM *E. coli* PBP1b S510A and 2 μM LpoB. Representative gel of two independent experiments.

To investigate if EDTA inhibited glycan chain cleavage completely, glycan chains were polymerised for varying lengths of time, half the glycan chain sample was run on a gel, while the other half was treated with 30 mM EDTA and left for a reaction length total of 24 hours for cleavage to take place. Interestingly, the glycan chains treated with 30 mM EDTA, did not change in length, indicating 30 mM EDTA protected the chains from cleavage (Figure 4.10). This observation was

confirmed by LCMS of native glycan chains in the presence of 30 mM EDTA, as no m/z values were present for cleaved glycan chains (Table 4.2).

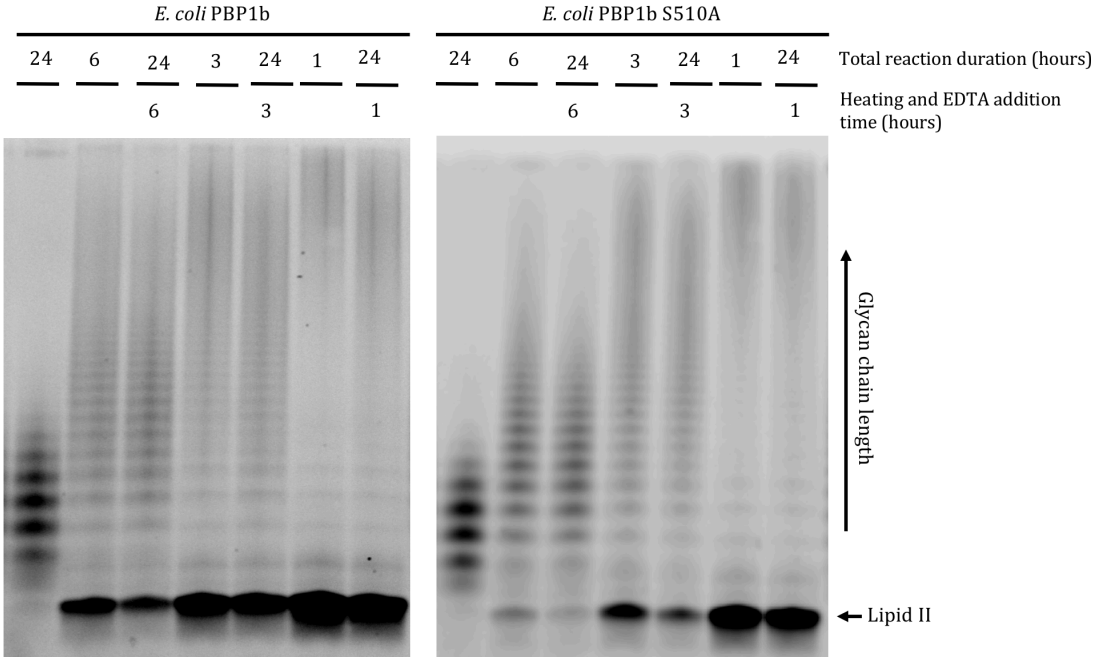

Figure 4.10 *E. coli* PBP1b glycan chain cleavage is inhibited by 30 mM EDTA.
E. coli PBP1b glycosyltransferase activity was assayed by the polymerisation of fluorescently labelled Lipid II *in vitro,* where the glycan chain products were separated by SDS-PAGE and visualised using the fluorescence of the dansyl group labelling the stem peptide. Effect of 30 mM EDTA on glycan chain cleavage. Reactions consisting of 50 mM Bis-Tris propane pH 8.5, 15 mM NaCl, 10% (v/v) DMSO, 1% (v/v) glycerol, 0.130% (v/v) Triton X-100, 10 μM Lipid II (dansyl DAP), 50 nM *E. coli* PBP1b or *E. coli* PBP1b S510A and 2 μM LpoB were allowed to polymerise for varying length of time. Reactions were split in two and half was heat treated at 95 °C for 10 mins to stop polymerisation, and 30 mM EDTA was added, before being left for a total reaction time of 24 hours. Representative gel of two independent experiments.

Due to this cleavage phenomenon all future SDS-PAGE analysis of glycan chains were carried out over various time points, so cleavage could be taken into consideration when conclusions were being made on glycan chain length.

4.4 Discussion and future work

4.4.1 Effect of metal ions on *E. coli* PBP1b glycan chain polymerisation

E. coli PBP1b glycosyltransferase activity has previously been reported to be affected by the concentration of divalent cation (Schwartz *et al.*, 2002; Barrett *et al.*, 2004; Walkowiak, 2017). In our hands *E. coli* PBP1b behaved similarly, with its activity being enhanced by cations such as Mg^{+}. As with Barret *et al*. we also found *E. coli* PBP1b to be active in the absence of metal ions (2004), but its activity extremely diminished. We also found divalent cations to increase the length of glycan chains polymerised by *E. coli* PBP1b, which to our knowledge has not been reported previously. We observed an increase in the length of glycan chains polymerised with increasing $MgCl_2$, $MnCl_2$ and $NiCl_2$ concentration, and hypothesise that this might be a consequence of the enhanced glycosyltransferase rate.

4.4.2 Glycan chain cleavage

This work also led to the observation of non-enzymatic glycan chain cleavage, involving hydrolysis of the glycosidic bond between the sugars, which to our knowledge has not been reported previously. This phenomenon has likely not been observed previously as most gel-based analysis of glycan chains reported to date have used ≥10 mM metal ion concentrations and visualised the glycan chains after an hour or less of polymerisation (Barrett *et al.*, 2007; Wang *et al.*, 2008; Paradis-Bleau *et al.*, 2010; Egan *et al.*, 2018; Pazos *et al.*, 2018), conditions which do not favour observation of glycan chain cleavage.

4.4.2.1 Effect of cross-links on glycan chain cleavage

As one of the many roles performed by peptidoglycan involves protecting the bacterial cell, it was disconcerting that native glycan chains could be so

susceptible to cleavage. We found that cross-linked glycan chains also underwent cleavage, but to a lesser extent than un-cross-linked glycan chains. To gain a more conclusive answer to whether cross-linking protects glycan chains from cleavage, the cross-links between the glycan chains would have to be broken to determine the length of the glycan chains within the cross-linked structure. However, finding an enzyme which only hydrolyses cross-links was problematic. *E. coli* PBP4 (DacB) (gifted by A. Lloyd (Warwick)), supposedly an D,D-carboxypeptidase and a D,D-endopeptidase (Korat *et al.*, 1991), was tested but appeared to only have carboxypeptidase activity, and *E. coli* MepA (1-274), supposedly an D,D-endopeptidase (Keck *et al.*, 1990), was purified and tested but it's cross-link hydrolysing efficiency was debatable, even after optimisation, so no conclusive result could be drawn.

Although the observation of cross-linked glycan chains cleavage was initially puzzling, the literature reports that newly synthesised glycan chains isolated from *E. coli* are longer than those from peptidoglycan of stationary phase *E. coli*, consistent with our results and time scales. Newly synthesised glycan chains from *E. coli* have been found to have a mean length of 50-60 disaccharide units, whereas in stationary phase bacteria they have a mean length of 17 disaccharide units (Glauner *et al.*, 1988; Glauner and Holtje, 1990). During exponential growth 25-30% of *E. coli* glycan chains are in the range of 30-80 disaccharides in length, with the remaining 70-75% of glycan chains being 1-30 disaccharides in length (Harz *et al.*, 1990). This shortening of newly synthesised glycan chains during *E. coli* growth has previously been reported to be a result of harsh sample preparation or *in vivo* processing by hydrolases, however it may be a natural cleavage process, as identified in this work.

4.4.2.2 Elucidating the mechanism of glycan chain cleavage

EDTA at a concentration of ≥ 30 mM was able to fully inhibit glycan chain cleavage, with lower concentrations having a decreasing inhibitory effect, indicating that metal ions must be involved in the catalysis of the cleavage reaction. It is well reported that *E. coli* peptidoglycan binds metal ions (Beveridge

and Koval, 1981; Hoyle and Beveridge, 1984), owing to the anionic carboxyl groups of the glutamic acid residues, DAP and D-ala, and to a lesser extent the hydroxyl groups of the sugars and amide groups of the peptide stem (Beveridge and Murray, 1976). The pyrophosphate moiety, nestling on the cell membrane *in vivo* and on the micelle in this *in vitro* situation, will also bind strongly to metal ions. We hypothesise a mechanism whereby a hydroxyl of GlcNAc comes into close proximity with a metal ion, likely bound to a pyrophosphate moiety or adjacent glycan chains, which coordinates and activates a water molecule for nucleophilic attack of the adjacent glycosidic bond, causing the bond to hydrolyse. This mechanism is not dissimilar to that of ribozymes, which have the ability to self-cleave their ribose backbones, catalysed by a metal ion (Doherty and Doudna, 2000; Wilson *et al.*, 2016).

4.4.3 Future work

Along with the future work already discussed, establishing if glycan chains produced by other bacterial PBPs also undergo cleavage, and investigating if glycan chain cleavage occurs in peptidoglycan produced *in vivo* would be invaluable. This could be investigated by extracting ^{14}C-labelled peptidoglycan from *E. coli*, treating it with amidases to cleave off the peptide stem and then measuring the length of the glycan chains over time by size exclusion chromatography (Turner *et al.*, 2018). These experiments could also be expanded to study the impact of metal ions on peptidoglycan stability. If glycan chain self-cleavage were to occur with peptidoglycan synthesised *in vivo*, deciphering the exact chemical mechanism would allow compounds to be developed that accelerate the natural process and act as antimicrobial agents.

4.5 Conclusions

To our knowledge this is the first study that has reported glycan chain cleavage *in vitro.* Glycan chains polymerised from Lipid II (dansylated and non-dansylated DAP) by *E. coli* PBP1b were observed to undergo cleavage by SDS-PAGE and LCMS analysis. We established that glycan chain cleavage was not due to enzymatic cleavage, occurred to a lesser extent when cross-links were present between the glycan chains, and required metal ions for catalysis. We propose a mechanism whereby a hydroxyl of GlcNAc comes into close proximity with a metal ion, likely bound to a pyrophosphate moiety or adjacent glycan chain, which coordinates and activates a water molecule for nucleophilic attack of the adjacent glycosidic bond, causing the bond to hydrolyse.

Chapter 5. Characterising the interaction between *E. coli* and *Y. pestis* PBP1b and LpoB, CpoB and FtsN

5.1 Introduction

Recent work has made advances in the knowledge of PBP1b-associated proteins and how these proteins interact with, and affect PBP1b activity *in vivo* and *in vitro*. This chapter characterises the interactions of known *E. coli* PBP1b associated proteins LpoB, CpoB and FtsN.

5.1.1 LpoB

Work has shown that *E. coli*, *P. aeruginosa* and presumably other Gram-negative bacterial peptidoglycan synthases are regulated from outside the sacculus by outer membrane-anchored lipoproteins. Lpo proteins reach through the peptidoglycan layer and are essential for the activity of their cognate bifunctional PBP *in vivo* (Paradis-Bleau *et al.*, 2010; Typas *et al.*, 2010). Indeed, deleting the lipoprotein, LpoA or LpoB/P, mimics the *in vivo* phenotype of deleting PBP1a or PBP1b respectively (Paradis-Bleau *et al.*, 2010; Typas *et al.*, 2010; Greene *et al.*, 2018). *E. coli* LpoB stimulates the glycosyltransferase and transpeptidase activities of PBP1b *in vitro* (Egan *et al.*, 2014; Egan *et al.*, 2018), however there are contradictory findings on the extent of stimulation *in vitro* and the consequences *in vivo* (Egan *et al.*, 2014; Egan *et al.*, 2018; Catherwood *et al.*, 2019).

5.1.2 CpoB

An additional elaboration of the regulation of PBP1b by LpoB was subsequently discovered in *E. coli*. The Tol-Pal complex is required for maintaining outer membrane integrity and ensuring proper invagination of the outer membrane during cell division (Gerding *et al.*, 2007). The Tol-Pal complex protein CpoB had

no defined functional role until recently (Gerding *et al.*, 2007), when it was shown to interact with PBP1b *in vivo*, and deletion of CpoB from *E. coli* which solely relies on PBP1b as its bifunctional PBP (PBP1a and LpoA deletion strain), caused severe growth defects, suggesting CpoB must modulate PBP1b function *in vivo* (Gray *et al.*, 2015). This interaction has also been confirmed *in vitro*, with SPR producing a K_D of 90-120 nM, and activity assay results suggesting that CpoB attenuates LpoB's activation of PBP1b by reducing transpeptidation activity (Gray *et al.*, 2015; Egan *et al.*, 2018).

5.1.3 FtsN

FtsN is an essential membrane protein which was thought to be the last essential protein recruited to the division site, but recent studies have shown that a portion of FtsN is also recruited at earlier stages through a cytosolic interaction with FtsA (Busiek and Margolin, 2014). FtsN is required for the recruitment of proteins to the cell division site: AmiC, a murein hydrolase that cleaves the septum (Heidrich *et al.*, 2001; Bernhardt and De Boer, 2003), and the Tol-Pal complex required for outer membrane invagination during cell constriction (Gerding *et al.*, 2007).

The C-terminal domain of FtsN has been shown to bind peptidoglycan, but this function is not essential (Ursinus *et al.*, 2004), instead the transmembrane helix plus the first ~80 periplasmic amino acids appear to make up the essential part of FtsN (Ursinus *et al.*, 2004). FtsN has also been found to interact with PBP1b *in vitro* and stimulate its activity in the absence of LpoB (Müller *et al.*, 2007; Pazos *et al.*, 2018; Boes *et al.*, 2019).

5.1.4 Analytical ultracentrifugation

Analytical ultracentrifugation (AUC) was selected to biophysically characterise *E. coli* and *Y. pestis* PBP1b, LpoB, CpoB and FtsN and their interactions. AUC is a well-established technique for characterising macromolecules and studying

protein-protein interactions, allowing determination of their molecular mass and size in solution. Proteins are subjected to a centrifugal force and their migration and hydrodynamic separation allows identification of different species by size (Schuck, 2013). Absorbance and/ or interference measurements taken along the length of the sample cell over time produce sedimentation profiles showing the evolution of a protein concentration gradient as it sediments (Ebel *et al.*, 2008). One of the useful properties of AUC is the measurement takes place with molecules free in solution, no immobilisation or chromatographic separation is required which may interfere with an interaction and the technique can measure homo- and hetero-interactions and their stoichiometry (Ebel *et al.*, 2008).

Membrane proteins require detergents to transfer them from their membranous environment to a micellar phase, and the effect detergent binding has on a protein size needs to be considered for AUC. Another problem can be that detergents like Triton X-100 have high absorbances at the wavelengths proteins are measured at for AUC (usually 280 nm). An attractive solution to these problems is to carry out sedimentation experiments under conditions where the detergent has minimal contributions to the buoyant molecular weight of the protein. This can be achieved by using a detergent that is neutrally buoyant, meaning it has a similar density to water (e.g. C_8E_5 which has a density of 0.993 g mL^{-1} compared to water 0.998 g mL^{-1} at 20°C). Due to the bound detergent now not contributing to the buoyant molecular weight of the protein, it's contribution can be ignored and data collection and analysis can be carried out in a manner identical to that for soluble proteins. Using a neutrally buoyant detergent also ensures that unbound detergent will undergo minimal sedimentation as it will float, making it unlikely to impact protein sedimentation (Fleming, 2016).

5.2 Experimental aims

- To biophysically characterise the size and interactions of *E. coli* and *Y. pestis* PBP1b, LpoB, CpoB and FtsN by AUC.

- To determine the effect of LpoB, CpoB and FtsN on *E. coli* and *Y. pestis* PBP1b activity.
- To determine any differences in *E. coli* and *Y. pestis* cross-linking activity.

5.3 Results

5.3.1 Oligomerisation and stoichiometry of *E. coli* and *Y. pestis* PBP1b, LpoB, CpoB and FtsN using analytical ultracentrifugation

AUC was carried out on *E. coli* and *Y. pestis* PBP1b, LpoB, CpoB and FtsN to determine their molecular weight, oligomeric state and confirm their interactions. AUC required all proteins to be in a specific detergent, C_8E_5 in this case: purifying the proteins in this detergent would be expensive, hence the membrane proteins were purified in CHAPS, concentrated to at least 25x the protein concentration needed for AUC and then diluted into the C_8E_5 AUC buffer. Although some CHAPS would still be present in the buffer, it would have been at 0.05x the CMC (Final CHAPS <0.025% (w/v), CHAPS CMC 0.48% (w/v)), hence no CHAPS micelles would have been able to form.

AUC experiments were performed with the proteins alone, as well as in pairs, with complex formation being determined by testing protein partners at different ratios and searching for a shift in the AUC peak sedimentation coefficient (S). All protein samples were found to be of a high purity, with little contamination or aggregates (Figure 5.1 and 5.2). *E. coli* and *Y. pestis* PBP1b and FtsN behaved predominantly as a single monomeric species, with a small proportion of the protein forming dimers (Figure 5.1A and F, 5.2A and F), with observed molecular weights close to their theoretical calculated molecular weight (Table 5.1). When *E. coli* or *Y. pestis* PBP1b and FtsN were run as a pair, the PBP1b peak broadened, which was consistent over different protein ratios. This feature is indicative of a PBP1b monomer, PBP1b-FtsN heterodimer equilibrium (Figure 5.1G and 5.2G).

E. coli and *Y. pestis* LpoB and CpoB behaved as a single species (Figure 5.1B and D, 5.2B and D) corresponding to molecular mass of a monomer for LpoB, and a trimer for CpoB (Table 5.1). *E. coli* or *Y. pestis* PBP1b and LpoB ran as a pair behaved as a stable heterodimer, observed by the shift in the PBP1b peak to a higher sedimentation coefficient (Figure 5.1C, and 5.2C), corresponding to the molecular mass of heterodimer (Table 5.1). Interestingly, when *E. coli* or *Y. pestis* PBP1b and CpoB were mixed, PBP1b was able to disrupt the stable CpoB trimer to form heterodimers, however the complex was not stable, seen by the broadening of the PBP1b peak, suggesting a PBP1b monomer CpoB trimer-PBP1b CpoB heterodimer equilibrium (Figure 5.1E and 5.2E).

The sedimentation process is dependent on the hydrodynamic friction and buoyancy of the protein, as well as the gravitational force. The frictional ratio (f/f0) extracted from the sedimentation data allows low resolution protein shape measurements to be made. An f/f0=1 would suggest the shape of the protein, with a particular mass and density, to be a smooth sphere, with increasing f/f0 values indicating greater asymmetry in the proteins shape, with many globular proteins have an f/f0= 1.05-1.35. *E. coli* and *Y. pestis* PBP1b have expected f/f0 values for membrane proteins in detergent micelles. While CpoB and FtsN are known to be more elongated proteins (Yang *et al.*, 2004; Krachler, Sharma, Cauldwell, *et al.*, 2010; Egan *et al.*, 2014) and this was reflected in their larger frictional ratio's (Table 5.1)

Table 5.1 Characterisation of *E. coli* and *Y. pestis* PBP1b, LpoB, CpoB and FtsN by analytical ultracentrifugation.

Sedimentation velocity analysis of *E. coli* and *Y. pestis* PBP1b, LpoB, CpoB and FtsN at varying concentrations. Absorption profiles were measured at 280 nm, at a rotor speed of 50 000 rpm at 20°C. Buffer conditions were 10 mM Tris, 500 mM NaCl, 0.35% (v/v) C_8E_5 and 0.025% (w/v) CHAPS pH 8.0, with a density of 1.0195 g/cm^3 and a viscosity of 1.0660 mPa. Molecular weight (MW), Sedimentation coefficient (Sed. Co) and frictional ratio (f/f0).

				AUC Species 1		AUC Species 2			
Organism	Protein/s	Theoretical MW (kDa)	Concentration (μM)	Observed MW (kDa)	Sed. Co (S)	Observed MW (kDa)	Sed. Co (S)	f/f0	Oligomeric state/ stoichiometry
E. coli	PBP1b (58-804)	83.7	10	114.0	5.53	192.0	7.54	1.37	Monomer and dimer
			5	99.6	5.13	198.0	7.44	1.35	
			2	89.6	4.82	-	-	1.35	
	LpoB (78-213)	14.4	50	13.7	1.46	-	-	1.25	Monomer
			30	14.0	1.46	-	-	1.27	
			10	14.0	1.46	-	-	1.27	
	CpoB (27-263)	25.7	30	74.8	3.12	-	-	1.88	Trimer
			10	68.5	3.17	-	-	1.75	
			5	74.1	3.17	-	-	1.85	
	FtsN (1-319)	36.2	20	40.6	2.11	107.0	4.12	1.69	Monomer and dimer
			10	34.5	2.01	90.3	3.62	1.83	
			5	32.3	1.91	88.8	3.42	1.95	
	PBP1b + LpoB	98.1	5 + 30	105	5.53	-	-	1.26	Heterodimer
			2 + 30	95.0	5.18	-	-	1.25	
	PBP1b + CpoB	109.4	5 + 10	115.0	4.77	-	-	1.52	Heterodimer-monomer/trimer equilibrium
			2 + 10	124.0	4.57	-	-	1.68	
	PBP1b + FtsN	119.9	5 + 10	159.0	5.43	-	-	1.59	Heterodimer-monomer equilibrium
			2 + 10	126.0	4.92	-	-	1.67	
Y. pestis	PBP1b (61-803)	82.7	10	125.0	5.53	251.0	8.54	1.38	Monomer and dimer
			5	101.0	5.03	190.0	7.34	1.35	
			2	94.9	4.92	-	-	1.36	
	LpoB (57-191)	14.9	30	16.1	1.46	-	-	1.38	Monomer
			10	15.9	1.41	-	-	1.37	
			5	15.7	1.43	-	-	1.34	
	CpoB (24-269)	26.8	30	75.4	3.21	-	-	1.86	Trimer
			10	73.9	3.27	-	-	1.81	
			5	78.5	3.27	-	-	1.88	
	FtsN (1-281)	30.9	20	30.3	1.81	69.2	3.32	1.66	Monomer and dimer
			10	31.4	1.61	70.1	2.61	1.88	
			5	29.3	1.51	70.5	2.61	1.95	
	PBP1b + LpoB	99.5	2 + 10	106.0	5.48	-	-	1.32	Heterodimer
	PBP1b + CpoB	111.4	5 + 10	149.0	5.48	-	-	1.64	Heterodimer-monomer/trimer equilibrium
			2 + 10	153.0	5.23	-	-	1.64	
	PBP1b + FtsN	115.5	5 + 10	156.0	5.08	-	-	1.73	Heterodimer-monomer equilibrium
			2 + 10	139.0	4.42	-	-	1.78	

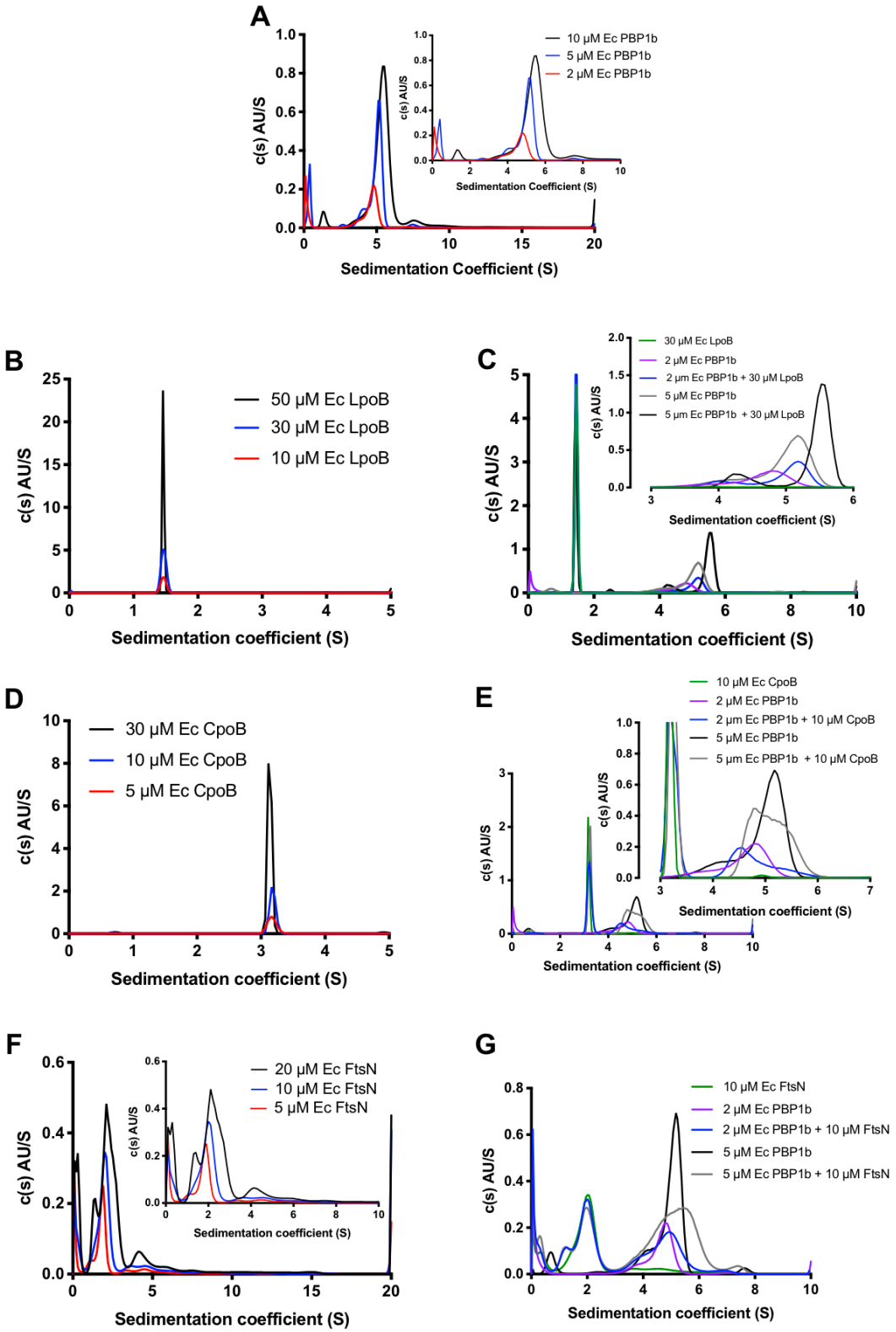

Figure 5.1 Characterisation of *E. coli* PBP1b, LpoB, CpoB and FtsN by analytical ultracentrifugation.

Sedimentation coefficient distribution of *E. coli* (Ec) PBP1b, LpoB, CpoB and FtsN at varying concentrations. Absorption profiles were measured at 280 nm, at a rotor speed of 50 000 rpm at 20°C. Buffer conditions were 10 mM Tris, 500 mM NaCl, 0.35% (v/v) C_8E_5 and 0.025% (w/v) CHAPS pH 8.0, with a density of 1.0195 g/cm^3 and a viscosity of 1.0660 mPa.

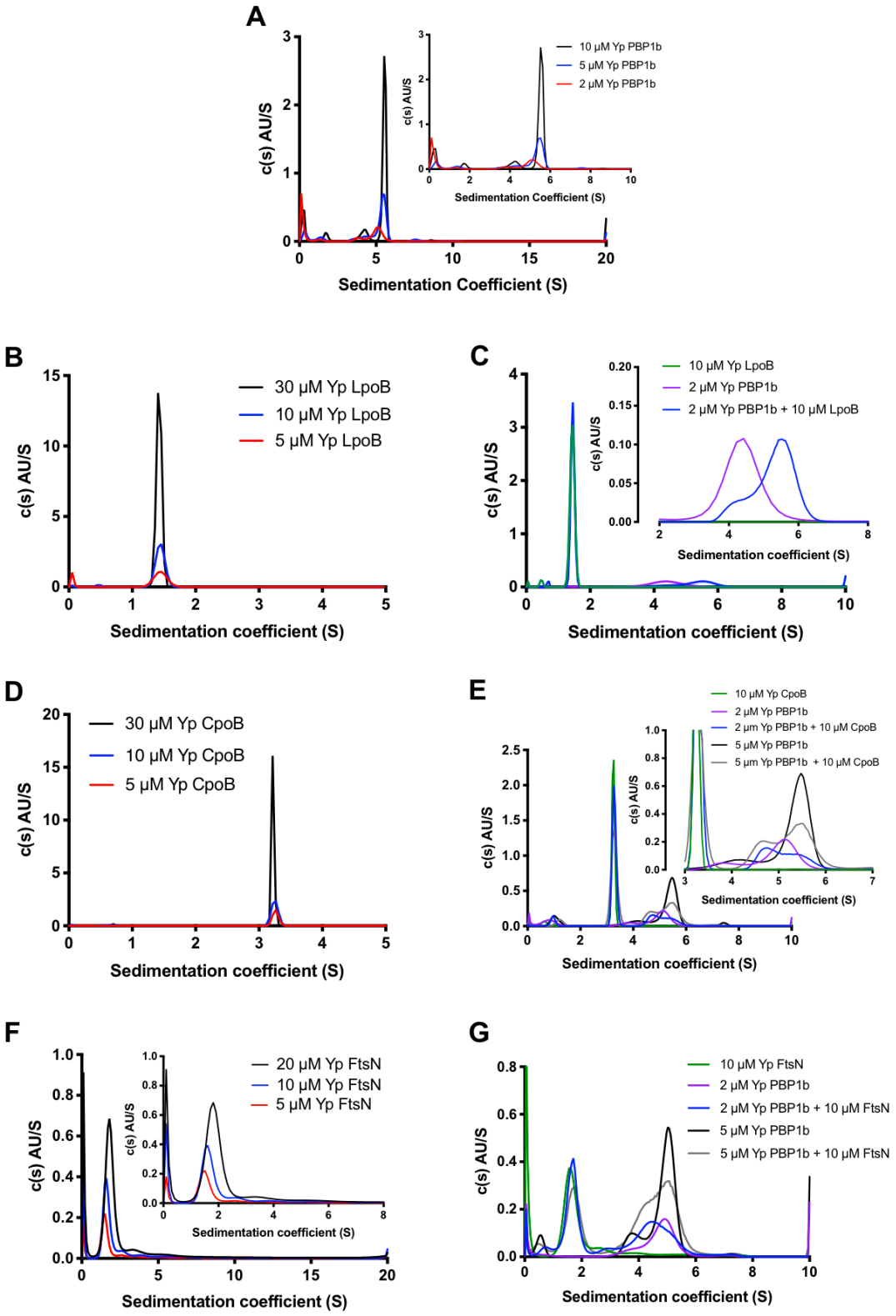

Figure 5.2 Characterisation of *Y. pestis* PBP1b, LpoB, CpoB and FtsN by analytical ultracentrifugation.

Sedimentation coefficient distribution of *Y. pestis* (Yp) PBP1b, LpoB, CpoB and FtsN at varying concentrations. Absorption profiles were measured at 280 nm, at a rotor speed of 50 000 rpm at 20°C. Buffer conditions were 10 mM Tris, 500 mM NaCl, 0.35% (v/v) C_8E_5 and 0.025% (w/v) CHAPS pH 8.0, with a density of 1.0195 g/cm^3 and a viscosity of 1.0660 mPa.

5.3.2 Effect of LpoB on *E. coli* and *Y. pestis* PBP1b activity

5.3.2.1 Effect of LpoB on *E. coli* and *Y. pestis* PBP1b initial rates

Chapter 3 established suitable substrates and assay conditions to measure *E. coli* and *Y. pestis* PBP1b activity using *in vitro* continuous glycosyltransferase and transpeptidase assays. Initial observations showed that LpoB significantly increased the activity of *E. coli* and *Y. pestis* PBP1b activity (sections 3.3.5.1, 3.3.6.1 and 3.3.6.3), and the effect of LpoB on PBP1b activity was characterised in more detail in this chapter. Comparison of the initial rates of *E. coli* and *Y. pestis* PBP1b activity determined that although PBP1b could carry out some glycan chain polymerisation in the absence of LpoB, there was little detectable transpeptidation activity (Figure 5.3), suggesting *E. coli* and *Y. pestis* PBP1b cannot carry out transpeptidation alone.

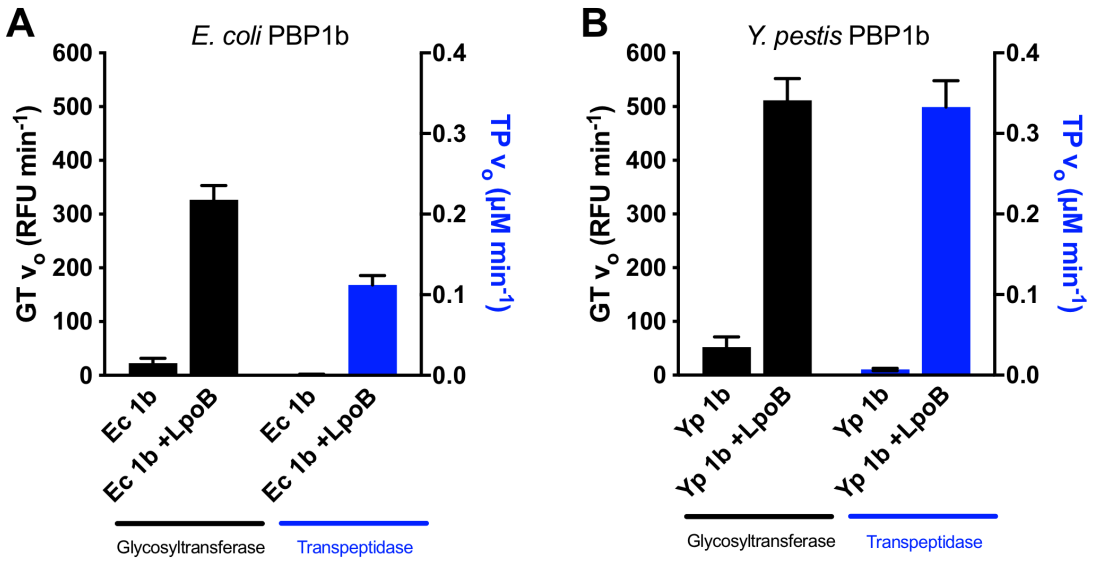

Figure 5.3 Dependency of *E. coli* and *Y. pestis* PBP1b on LpoB for activity.
(**A**) *E. coli* and (**B**) *Y. pestis* PBP1b *in vitro* activity, shown as initial rates. Glycosyltransferase rate was assayed by the consumption of fluorescently labelled Lipid II. Reactions consisted of 50 mM HEPES pH 7.5, 115 mM NaCl, 10 mM $MgCl_2$, 10% (v/v) DMSO, 1% (v/v) glycerol, 0.155% (v/v) Triton X-100, 0.1 mg ml^{-1} lysozyme, 5 μM Lipid II (dansyl DAP), 50 nM PBP1b and 2 μM LpoB. Transpeptidase rate was assayed using the amplex red assay for D-Ala release. Reactions consisted of 50 mM Bis-Tris propane pH 8.5, 6 mM NaCl, 20 mM $MgCl_2$, 1% (v/v) glycerol, 0.130% (v/v) Triton X-100, amplex red coupling reagents, 20 μM Lipid II- 5P (acetylated DAP), 50 nM PBP1b, 2 μM LpoB and 20 μM MurNac- 5P. Data is shown as mean $\pm$ SD (n=3).

LpoB was found to have similar stimulatory effects on *E. coli* and *Y. pestis* PBP1b glycosyltransferase activity, stimulating the glycosyltransferase rate 14.5 ± 1.2 and 8.8 ± 1.9-fold respectively compared to PBP1b alone (Figure 5.4). Interestingly, the effect of LpoB on the transpeptidation rate was more profound, stimulating the initial rate by 86.9 ± 8.9-fold for *E. coli* and 47.4 ± 4.7-fold for *Y. pestis* compared to PBP1b alone (figure 5.4), suggesting LpoB has a greater stimulatory effect on transpeptidase activity than glycosyltransferase activity.

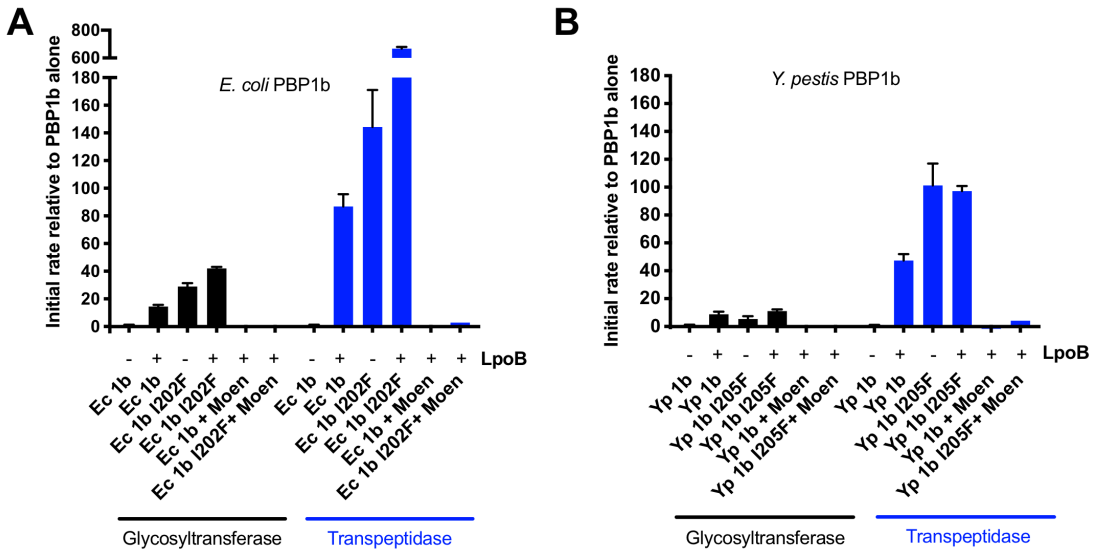

Figure 5.4 Effect of LpoB on *E. coli* and *Y. pestis* PBP1b initial rates of activity. (**A**) *E. coli* and (**B**) *Y. pestis* PBP1b and variants *in vitro* activity, shown as initial rates relative to PBP1b alone, in the presence and absence of LpoB. Glycosyltransferase rate was assayed by the consumption of fluorescently labelled Lipid II. Reactions consisted of 50 mM HEPES pH 7.5, 115 mM NaCl, 10 mM $MgCl_2$, 10% (v/v) DMSO, 1% (v/v) glycerol, 0.155% (v/v) Triton X-100, 0.1 mg ml^{-1} lysozyme, 5 μM Lipid II (dansyl DAP), 50 nM PBP1b and 2 μM LpoB. Transpeptidase rate was assayed using the amplex red assay for D-Ala release. Reactions consisted of 50 mM Bis-Tris propane pH 8.5, 6 mM NaCl, 20 mM $MgCl_2$, 1% (v/v) glycerol, 0.130% (v/v) Triton X-100, amplex red coupling reagents, 20 μM Lipid II- 5P (acetylated DAP), 50 nM PBP1b, 2 μM LpoB and 20 μM MurNac- 5P. Data is shown as mean ± SD (n=3).

Studies by Bernhardt *et al*. have identified four residues on *E. coli* PBP1b which are involved in LpoB stimulation, the mutation I202F mimicking LpoB stimulation most successfully (Markovski *et al.*, 2016; Egan *et al.*, 2018). Due to the homology between *Y. pestis* and *E. coli* PBP1b this mutation was easily mapped onto *Y. pestis* PBP1b (I205F) and its effect on PBP1b activity determined. Both *E. coli* and *Y. pestis* PBP1b mutants alone exhibited similar or greater glycosyltransferase and transpeptidase activity than wildtype with LpoB at the

same protein concentration (Figure 5.4). This indicates that the mutation does indeed mimic LpoB binding and that the intended function of *E. coli* and *Y. pestis* LpoB *in vivo* is to activate glycan chain polymerisation and transpeptidation. However, for *E. coli* PBP1b I202F the mutation did not fully mimic the absence of LpoB, as the presence of LpoB further increased the glycosyltransferase and transpeptidase activity of *E. coli* PBP1b I202F (Figure 5.4A), confirming that in *E. coli* LpoB induction of PBP1b activity is mechanistically different from *Y. pestis*. This data indicates that the difference in response of the mutants to LpoB is likely due to the affect LpoB has on their glycosyltransferase rates.

5.3.2.2 Effect of LpoB on *E. coli* and *Y. pestis* PBP1b glycan chain polymerisation

To investigate the effect of LpoB on the length of glycan chains produced by PBP1b, fluorescently labelled Lipid II was polymerised into glycan chains by PBP1b and separated by SDS-PAGE. The gel analysis showed that both *E. coli* and *Y. pestis* PBP1b produce very long glycan chains, shown by the unresolvable smear at the top of the gel, estimated to be longer than 14 disaccharides in length. The gel results also confirm the continuous assay results, showing that LpoB stimulates the glycosyltransferase rate of both *E. coli* and *Y. pestis* PBP1b, shown by the faster consumption of Lipid II over time in its presence (Figure 5.5). The presence of LpoB also increased the quantity of shorter glycan chains, which can be seen by the presence of bands lower down the gel. This was confirmed by the PBP1b mutants also producing shorter glycan chains (Figure 5.5)

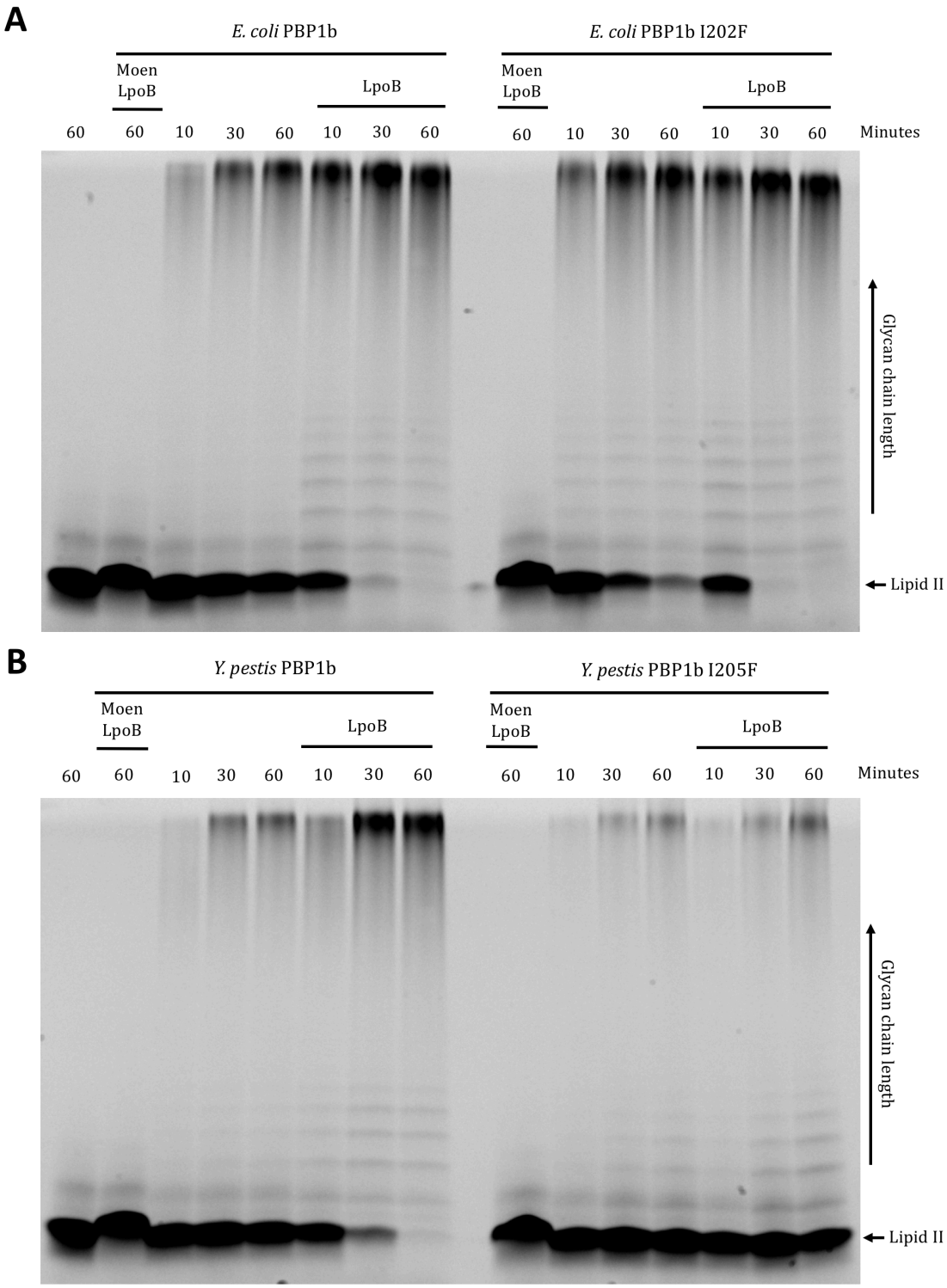

Figure 5.5 Effect of LpoB on *E. coli* and *Y. pestis* PBP1b glycan chain polymerisation.
(**A**) *E. coli* and (**B**) *Y. pestis* PBP1b and mutants *in vitro* glycosyltransferase activity was assayed by the consumption of fluorescently labelled Lipid II, in the presence and absence of LpoB, and visualised by SDS-PAGE analysis. Reactions consisted of 50 mM HEPES pH 7.5, 115 mM NaCl, 10 mM $MgCl_2$, 10% (v/v) DMSO, 1% (v/v) glycerol, 0.155% (v/v) Triton X-100, 10 μM Lipid II (dansyl DAP), 50 nM PBP1b, 2 μM LpoB and 5 μM moenomycin (Moen) as a control (n=2).

5.3.3 Interchangeability of *E. coli* and *Y. pestis* LpoB

The *E. coli* and *Y. pestis* PBP1b and LpoB proteins used in this study have a sequence identity of 72% and 57% respectively, and a sequence similarity of 82% and 70% respectively, indicating the proteins are relatively similar, so the specificity of LpoB for its cognate PBP1b was assessed. Interestingly, *Y. pestis* PBP1b was able to be stimulated just as effectively by *E. coli* LpoB as its cognate LpoB, however *Y. pestis* LpoB did little to stimulate *E. coli* PBP1b (Figure 5.6).

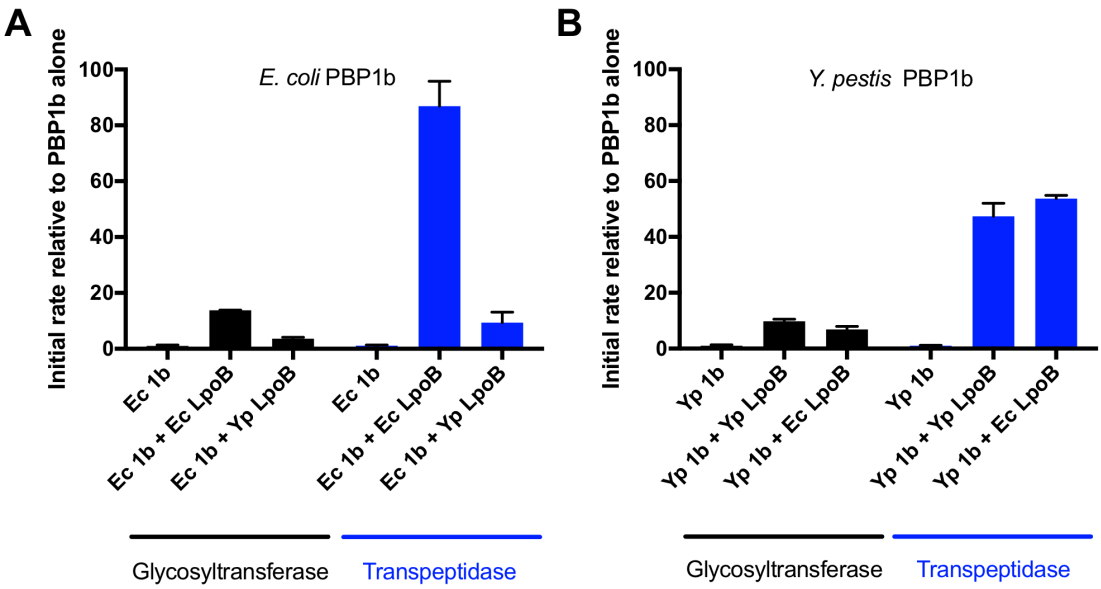

Figure 5.6 Interchangeability of *E. coli* and *Y. pestis* LpoB on PBP1b initial rates of activity.
(**A**) *E. coli* PBP1b and (**B**) *Y. pestis* PBP1b *in vitro* activity, shown as initial rates relative to PBP1b alone, in the presence and absence of LpoB. Glycosyltransferase rate was assayed by the consumption of fluorescently labelled Lipid II. Reactions consisted of 50 mM HEPES pH 7.5, 115 mM NaCl, 10 mM $MgCl_2$, 10% (v/v) DMSO, 1% (v/v) glycerol, 0.155% (v/v) Triton X-100, 0.1 mg ml^{-1} lysozyme, 5 μM Lipid II (dansyl DAP), 50 nM PBP1b and 2 μM LpoB. Transpeptidase rate was assayed using the amplex red assay for D-Ala release. Reactions consisted of 50 mM Bis-Tris propane pH 8.5, 6 mM NaCl, 20 mM $MgCl_2$, 1% (v/v) glycerol, 0.130% (v/v) Triton X-100, amplex red coupling reagents, 20 μM Lipid II- 5P (acetylated DAP), 50 nM PBP1b, 2 μM LpoB and 20 μM MurNac- 5P. Data is shown as mean $\pm$ SD (n=3).

5.3.4 Frequency of *E. coli* and *Y. pestis* PBP1b cross-linking

While carrying out the above experiments on *E. coli* and *Y. pestis* PBP1b it was noticeable from the end points of the transpeptidase assays that the

concentration of substrate consumed was different between the two organisms. This can be easily seen in Figure 3.13, where 100% substrate turnover would give an A_{555} of ~1.1, whereas the endpoint gave an A_{555} of ~0.15 for *E. coli* PBP1b and ~0.25 for *Y. pestis* PBP1b. When analysed the substrate consumption of *E. coli* PBP1b was only 9.7 ± 1.5% at its end point and 25.2 ± 2.8% for *Y. pestis* PBP1b (Figure 5.7). *Y. pestis* PBP1b had a higher consumption of substrate due to carboxypeptidation than *E. coli* PBP1b, where *Y. pestis* consumed 9.67 ± 1.94% of the donor substrate through carboxypeptidation compared to 1.53 ± 1.08% for *E. coli*. Interestingly this data suggests that *E. coli* and *Y. pestis* only cross-link

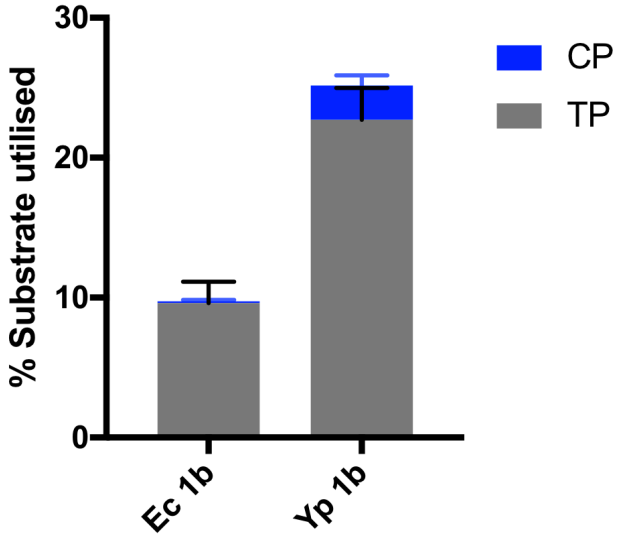

Figure 5.7 Percentage substrate utilisation of *E. coli* and *Y. pestis* PBP1b.
E. coli PBP1b (Ec 1b) and *Y. pestis* PBP1b (Yp 1b) *in vitro* activity, shown as percentage of substrate consumed at the end point of the assay by carboxypeptidation (CP) and transpeptidation (TP). Rates were assayed using the amplex red assay for D-Ala release. Reactions consisted of 50 mM Bis-Tris propane pH 8.5, 6 mM NaCl, 20 mM $MgCl_2$, 1% (v/v) glycerol, 0.130% (v/v) Triton X-100, amplex red coupling reagents, 20 μM Lipid II- 5P (acetylated DAP), 50 nM PBP1b, 2 μM LpoB and 20 μM MurNac- 5P. Data is shown as mean ± SD (n=3).

~9.5% and ~22.5% of their substrate respectively.

5.3.5 Effect of CpoB on *E. coli* and *Y. pestis* PBP1b activity

5.3.5.1 Effect of CpoB on *E. coli* and *Y. pestis* PBP1b initial rates

CpoB has previously been reported to interact with *E. coli* PBP1b through its UB2H domain, and modulate the extent of PBP1b cross-linking, by affecting LpoB

stimulation of transpeptidation (Gray *et al.*, 2015; Egan *et al.*, 2018). However, when tested in the continuous glycosyltransferase and transpeptidase assay CpoB was found to have no effect on the initial glycosyltransferase or transpeptidase rates of *E. coli* or *Y. pestis* PBP1b (Figure 5.8A and B). Gray *et al.* reported the inhibitory effect of CpoB on LpoB induced PBP1b transpeptidase activity to be greater at a higher salt concentration (Gray *et al.*, 2015). However, when tested at 150 mM NaCl, CpoB still had no effect on the initial transpeptidation rates of *E. coli* and *Y. pestis* PBP1b in the presence of LpoB (Figure 5.8C and D). These experiments highlighted the sensitivity of *E. coli* and *Y. pestis* PBP1b transpeptidase activity to NaCl, with their rates decreasing dramatically with increasing concentration of NaCl. The concentrations of NaCl tested were shown to have no effect on the assay enzyme converting system.

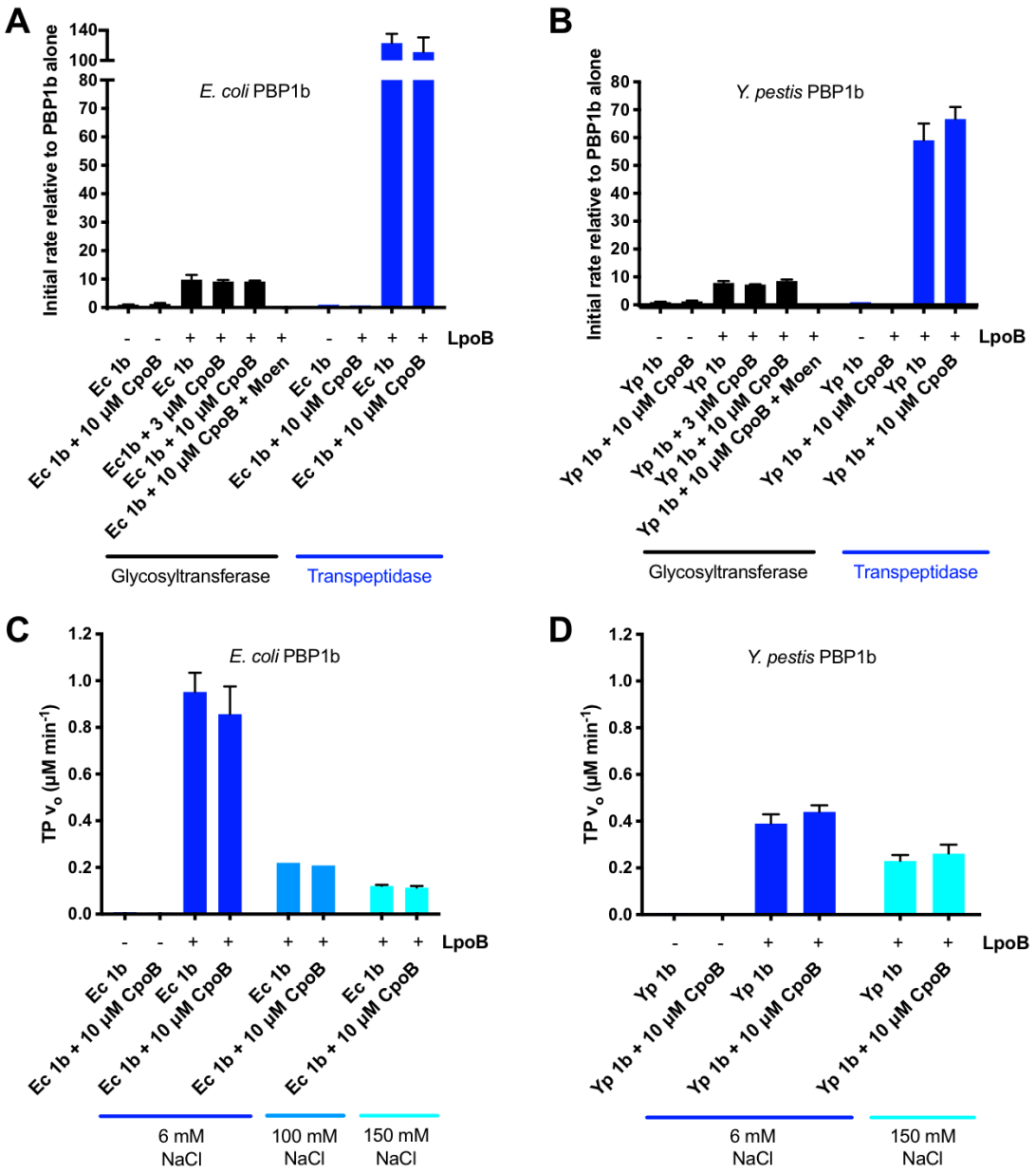

Figure 5.8 Effect of CpoB on *E. coli* and *Y. pestis* PBP1b initial rates of activity. (**A** and **C**) *E. coli* PBP1b and (**B** and **D**) *Y. pestis* PBP1b *in vitro* activity, shown as initial glycosyltransferase and transpeptidase rates relative to PBP1b alone (**A** and **B**) and initial transpeptidase rates (**C** and **D**), in the presence and absence of LpoB. Glycosyltransferase rate was assayed by the consumption of fluorescently labelled Lipid II at varying NaCl concentrations. Reactions consisted of 50 mM HEPES pH 7.5, 115 mM NaCl, 10 mM $MgCl_2$, 10% (v/v) DMSO, 1% (v/v) glycerol, 0.155% (v/v) Triton X-100, 0.1 mg ml^{-1} lysozyme, 5 μM Lipid II (dansyl DAP), 50 nM PBP1b, 2 μM LpoB and 3 or 10 μM CpoB. Data is shown as mean $\pm$ SD (n=3). Transpeptidase rate was assayed using the amplex red assay for D-Ala release. Reactions consisted of 50 mM Bis-Tris propane pH 8.5, 6 mM NaCl unless otherwise stated, 20 mM $MgCl_2$, 1% (v/v) glycerol, 0.130% (v/v) Triton X-100, amplex red coupling reagents, 20 μM Lipid II- 5P (acetylated DAP), 50 nM PBP1b, 2 μM LpoB, 3 or 10 μM CpoB and 20 μM MurNac- 5P. For 6 mM NaCl data is shown as mean $\pm$ SD (n=3), for 100 mM NaCl data is shown as a single value (n=1) and for 150 mM NaCl data is shown as mean and difference between the minimum and maximum values (n=2).

5.3.5.2 Effect of CpoB on *E. coli* and *Y. pestis* PBP1b glycan chain polymerisation

Due to LpoB affecting the length of glycan polymer produced and CpoB being thought to interfere with LpoB binding to PBP1b, the effect of CpoB on glycan chain length was investigated. However, CpoB was found to have no effect on the glycan chains produced by *E. coli* or *Y. pestis* PBP1b in the presence or absence of LpoB, nor the ability of LpoB to stimulate PBP1b transglycosylation activity (Figure 5.9).

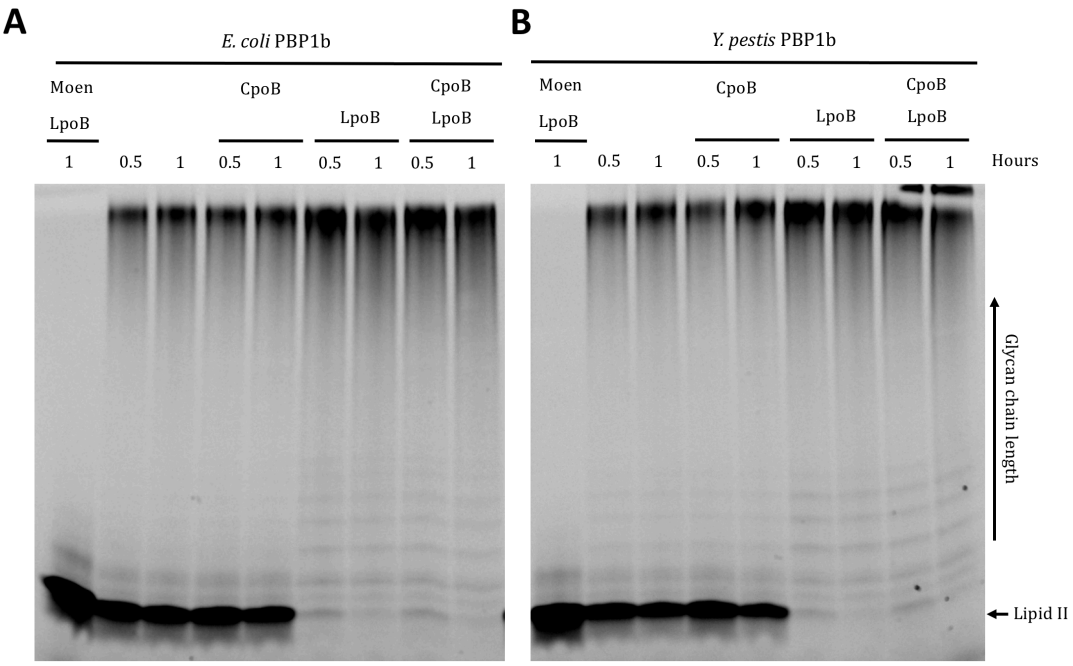

Figure 5.9 Effect of CpoB on *E. coli* and *Y. pestis* PBP1b glycan chain polymerisation.
(**A**) *E. coli* PBP1b and (**B**) *Y. pestis* PBP1b *in vitro* glycosyltransferase activity was assayed by the consumption of fluorescently labelled Lipid II, and visualised by SDS-PAGE analysis. Reactions consisted of 50 mM HEPES pH 7.5, 115 mM NaCl, 10 mM $MgCl_2$, 10% (v/v) DMSO, 1% (v/v) glycerol, 0.155% (v/v) Triton X-100, 10 μM Lipid II (dansyl DAP), 50 nM PBP1b, 2 μM LpoB, 10 μM CpoB and 5 μM moenomycin (Moen) as a control (n=2).

5.3.6 Effect of FtsN on *E. coli* and *Y. pestis* PBP1b activity

5.3.6.1 Effect of FtsN on *E. coli* and *Y. pestis* PBP1b initial rates

E. coli FtsN is a membrane protein that is essential for triggering active cell constriction (Liu *et al.*, 2015), and has been reported to interact with *E. coli* PBP1b *in vitro* (Müller *et al.*, 2007; Boes *et al.*, 2019). 10 μM FtsN was found to decrease the *E. coli* glycosyltransferase rate by 33.7% and transpeptidation rate by 67.3%. *Y. pestis* was similarly affected, with 10 μM FtsN reducing the glycosyltransferase rate by 75.3% and transpeptidation rate by 65.5%. While, FtsN had no significant effect on the glycosyltransferase or transpeptidase activity of *E. coli* or *Y. pestis* PBP1b alone, it did have a concentration dependent inhibitory effect on the initial rates of glycosyltransferation and transpeptidation in the presence in LpoB (Figure 5.10). This inhibitory effect was independent of the buffer FtsN was supplied in.

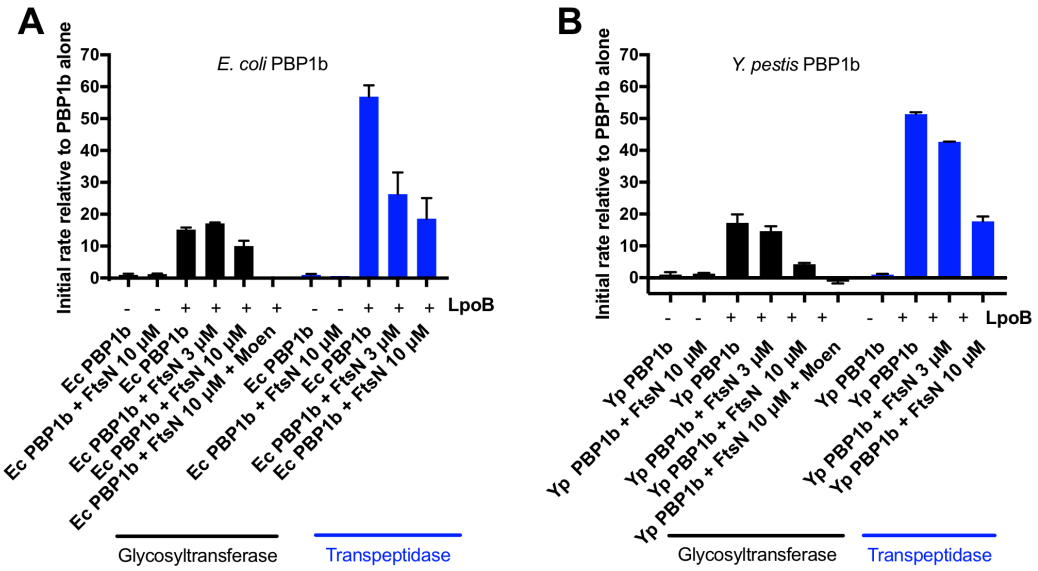

Figure 5.10 Effect of FtsN on *E. coli* and *Y. pestis* PBP1b initial rates of activity. (**A**) *E. coli* PBP1b and (**B**) *Y. pestis* PBP1b *in vitro* activity, shown as initial rates relative to PBP1b alone, in the presence and absence of LpoB. Glycosyltransferase rate was assayed by the consumption of fluorescently labelled Lipid II. Reactions consisted of 50 mM HEPES pH 7.5, 115 mM NaCl, 10 mM $MgCl_2$, 10% (v/v) DMSO, 1% (v/v) glycerol, 0.155% (v/v) Triton X-100, 0.1 mg ml^{-1} lysozyme, 5 μM Lipid II (dansyl DAP), 50 nM PBP1b, 2 μM LpoB and 3 or 10 μM FtsN. Transpeptidase rate was assayed using the amplex red assay for D-Ala release. Reactions consisted of 50 mM Bis-Tris propane pH 8.5, 6 mM NaCl, 20 mM $MgCl_2$, 1% (v/v) glycerol, 0.130% (v/v) Triton X-100, amplex red coupling reagents, 20 μM Lipid II- 5P (acetylated DAP), 50 nM PBP1b, 2 μM LpoB, 3 or 10 μM FtsN and 20 μM MurNac- 5P. Data is shown as mean $\pm$ SD (n=3).

5.3.6.2 Effect of FtsN on *E. coli* and *Y. pestis* PBP1b glycan chain polymerisation

Next the effect of FtsN on the glycan chains produced by PBP1b was assessed. Shorter glycan chains could be detected in its presence, with this observation being independent of LpoB. Although LpoB increased the quantity of shorter glycan chains, the presence of FtsN created an additive shortening affect (Figure 5.11). Interestingly, in the case of *Y. pestis* PBP1b the presence of FtsN appeared to increase the rate of transglycosylation, seen by the increased consumption of Lipid II compared to *Y. pestis* PBP1b alone (Figure 5.11B), even though the increase in initial glycosyltransferase rate was not significant (Figure 5.10B). Distortion of the Lipid II bands (Figure 5.11) was also likely due to the presence of CHAPS detergent, which the FtsN was supplied in. Although at a low final concentration in the assay (0.086%, 0.176x CMC), CHAPS has previously been observed to affect the migration of Lipid II in this manner (C. Rowland, personal communication.).

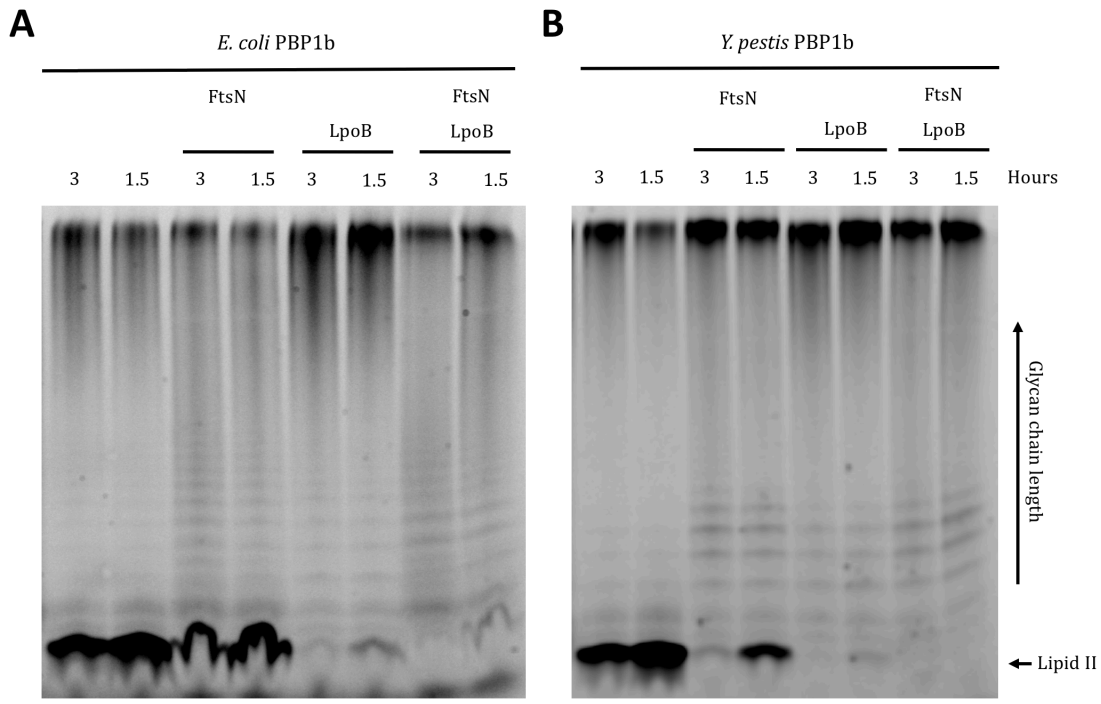

Figure 5.11 Effect of FtsN on *E. coli* and *Y. pestis* PBP1b glycan chain polymerisation.
(**A**) *E. coli* PBP1b and (**B**) *Y. pestis* PBP1b *in vitro* glycosyltransferase activity was assayed by the consumption of fluorescently labelled Lipid II, and visualised by SDS-PAGE analysis. Reactions consisted of 50 mM HEPES pH 7.5, 115 mM NaCl, 10 mM $MgCl_2$, 10% (v/v) DMSO, 1% (v/v) glycerol, 0.155% (v/v) Triton X-100, 10 μM Lipid II (dansyl DAP), 100 nM PBP1b, 4 μM LpoB, 6 μM FtsN and 5 μM moenomycin (Moen) as a control (n=2).

5.4 Discussion and future work

5.4.1 AUC of *E. coli* and *Y. pestis* PBP1b, LpoB, CpoB and FtsN

AUC determined *E. coli* and *Y. pestis* PBP1b to be predominantly monomeric in solution. This agrees with seven crystal structures (Sung *et al.*, 2009; King *et al.*, 2017) but is contradictory to previous reports of *E. coli* PBP1b dimerising with a K_D of 127 $\pm$96 nM (Bertsche *et al.*, 2005). This discrepancy may be due to differences in experimental conditions, e.g. buffer conditions (i.e. Triton X-100 vs C_8E_5 detergent) or construct length (this study: *E. coli* PBP1b 58-804, SPR dimerisation study: *E. coli* PBP1b 46-844 (Bertsche *et al.*, 2005)).

E. coli and *Y. pestis* LpoB were found to be monomeric by AUC, which also agrees with previous reports that found *E. coli* LpoB to be monomeric by size-exclusion

chromatography and AUC (Egan *et al.*, 2014). AUC was also able to determine that *E. coli* and *Y. pestis* PBP1b-LpoB interact as a stable heterodimer, which is consistent with previous pull-down assays, suggesting *E. coli* PBP1b-LpoB stoichiometry is close to 1:1 (Paradis-Bleau *et al.*, 2010). Indicating that LpoB may not stabilise the dimeric form of PBP1b, which is thought to be more active, as previously suggested (Bertsche *et al.*, 2005).

AUC determined *E. coli* and *Y. pestis* FtsN to be largely monomeric with an elongated shape, which is consistent with the NMR structure of *E. coli* FtsN, however no previous data has been published on its oligomeric state. The NMR structure determined *E. coli* FtsN to have a long flexible region with no detectable secondary stricture, connecting the transmembrane helix and the peptidoglycan-binding domain (Yang *et al.*, 2004). Yang *et al*. found the length of this unstructured region to be ~180 residues, contributing to more than half the proteins length (full length protein 319 residues) (2004), which clarifies why FtsN was found to have such an elongated shape. FtsN has previously been shown to interact with *E. coli* PBP1b *in vivo* by bacterial two-hybrid analysis (Müller *et al.*, 2007), however the interaction is not essential, as ponB (PBP1b) deletion from *E. coli* are still viable (Liu *et al.*, 2015). *In vitro* pull-down assays have also shown *E. coli* PBP1b to interact with FtsN, including truncated versions (58-319, 58-125 and 166-319). The interaction between *E. coli* PBP1b and full length FtsN (1-319) was also confirmed by SPR, however no interaction was seen with the truncated versions (Müller *et al.*, 2007), suggesting the interaction may be weak. AUC found both *E. coli* and *Y. pestis* PBP1b and FtsN to be in an equilibrium between bound complex and unbound monomers, suggesting a weak or transient interaction.

E. coli CpoB has previously been reported to form stable trimers in solutions (Krachler, Sharma, and Kleanthous, 2010), which is in agreement with the AUC findings in this study. AUC found *E. coli* and *Y. pestis* PBP1b able to disrupt the stable CpoB trimer to form heterodimers, seen previously with TolA, which was also able to disrupt the CpoB trimer to form a heterodimer (Krachler, Sharma, Cauldwell, *et al.*, 2010).

The differences between the observed molecular weights produced by AUC compared to the theoretical weights was more evident for the membrane proteins, and is likely due to the detergent micelles. Although C_8E_5 is neutrally buoyant and would not have affected the sedimentation of the membrane protein, the added size of the micelle would have affected its overall shape, therefore affecting the frictional ratio, which is used to compute the observed molecular mass. Only one frictional ratio is computed for a sample, so when the sample contains protein pairs an average frictional ratio is calculated, increasing the inaccuracy.

5.4.2 Effect of LpoB on *E. coli* and *Y. pestis* PBP1b initial rates

The results from section 5.3.2.1 indicate that LpoB is almost essential for *E. coli* and *Y. pestis* PBP1b transpeptidase activity *in vitro*, with it having less of a stimulatory effect on glycosyltransferase activity. It is well documented that LpoB is essential for *E. coli* PBP1b functionality *in vivo*, as cells lacking PBP1a (making PBP1b essential), require an active LpoB for viability (Paradis-Bleau *et al.*, 2010). However, this essentiality has not be replicated *in vitro*.

Previous findings found *E. coli* PBP1b to be active *in vitro* in the absence of LpoB, with LpoB having a greater stimulatory effect on PBP1b glycosyltransferase than transpeptidase activity. Studies using the same fluorescence based assay as used in this study found LpoB to stimulate *E. coli* PBP1b glycosyltransferase activity 8 to 11-fold (Egan *et al.*, 2014; Egan *et al.*, 2018), while assays using radioactive Lipid II found LpoB to only increase glycosyltransferase activity 1.5 to 3.6-fold (Paradis-Bleau *et al.*, 2010; Lupoli *et al.*, 2014). This discrepancy is likely due to the discontinuous radio-active assay missing the initial enhancement in rate LpoB causes. This study replicates the previous continuous assay findings showing that *E. coli* PBP1b can carry out transglycosylation in the absence of LpoB, but its presence increases the initial rate of transglycosylation by 15- fold, greater than previously seen. This study also found *Y. pestis* PBP1b to behave in a similar manner, with it being active alone, but LpoB stimulating its glycosyltransferase activity 9- fold.

The results from this study show *E. coli* PBP1b transpeptidase activity is negligible in the absence of LpoB, and LpoB stimulates the initial transpeptidation rate by ~90-fold. *Y. pestis* PBP1b was also found to act similarly, showing very little transpeptidase activity in the absence of LpoB, where LpoB stimulated its initial transpeptidase rate ~50-fold. Recently Catherwood *et al*. has also shown *E. coli* PBP1b transpeptidase activity to be almost dependent on the presence of LpoB, with LpoB increasing the initial transpeptidation rate by >100-fold, at PBP1b concentrations less than 1/10 of its dimerization K_D (2019). However, previous to this, others have found *E. coli* PBP1b able to carry out transpeptidation *in vitro* in the absence of LpoB, with PBP1b activity significantly increasing at concentrations above its dimerization K_D (Bertsche *et al.*, 2005). While the presence of LpoB only increased the rate of transpeptidation 1.5-fold (Lupoli *et al.*, 2014), and substrate cross-linking from 50-70%, even at concentrations of PBP1b that promote dimerization (Egan *et al.*, 2014; Egan *et al.*, 2018).

It is difficult to directly compare the findings in this study and those from Catherwood *et al.* (2019), to other previous findings due to major difference in the assaying methods. Catherwood *et al.* (2019) and this study use a continuous method to measure the transpeptidation rate directly, whereas other previous studies have measured the percentage of cross-linking at the end point of the assay. Therefore, negligible changes to the endpoint of the reaction may be preceded by large changes in the initial rate.

The results from this study shed light on the activation method of LpoB, and suggest that LpoB stimulates PBP1b glycosyltransferase and transpeptidase activity simultaneously, but to different extents, as suggested by recent structural and activity studies by Egan et al. (2018). The essentiality of LpoB for PBP1b transpeptidase activity *in vitro* also explains why LpoB is essential for PBP1b function *in vivo*.

Previous studies have found, residue 202 of *E. coli* PBP1b to be involved in the activation by LpoB's (Markovski *et al.*, 2016). In this study we confirmed this

observation by showing *E. coli* PBP1b I202F alone was significantly more active than wild type PBP1b in the presence of LpoB at the same concentration, however the presence of LpoB was still able to increase its activity further indicating a single mutation does not fully mimic LpoB binding. However, the same mutation in *Y. pestis* PBP1b I205F mimicked LpoB stimulation entirely, as the addition of LpoB did not increase the rate of transglycosylation or transpeptidation further. These differences may be explained by the sequence (Figure 1.3) and consequently structural differences in the UB2H domain of the proteins, changing how LpoB binds to PBP1b. In conclusion, although *E. coli* and *Y. pestis* PBP1b function very similarly, they do have some kinetic differences.

5.4.3 Effect of LpoB on *E. coli* and *Y. pestis* PBP1b glycan chain polymerisation

This study found *E. coli* and *Y. pestis* PBP1b to produce glycan chains of >14 disaccharide units in length which is consistent with previous reports of *E. col*i PBP1b polymerisation (Bertsche *et al.*, 2005; Barrett *et al.*, 2007; Paradis-Bleau *et al.*, 2010; Egan *et al.*, 2018). Although most chains are longer than this (estimated >50 disaccharides), their exact lengths are unknown due to insufficient separation of high molecular weight products by SDS-PAGE and the lack of high molecular weight glycan chain standards. The absence of any short glycan chains suggests *E. coli* and *Y. pestis* PBP1b produce glycan chains of a characteristic intrinsic length distribution, which is consistent with previous reports from *E. coli* PBP1b (Wang *et al.*, 2008).

The presence of LpoB was found to stimulate the production of shorter glycan chains, increasing the quantity of shorter glycan chains. These findings are consistent with previous studies that have investigated *E. coli* PBP1b glycan chain production *in vitro* (Wang *et al.*, 2008; Paradis-Bleau *et al.*, 2010; Markovski *et al.*, 2016). In comparison with *in vivo* findings, glycan chains extracted from *E. coli* are found to be greater than 200 nm in length (Turner *et al.*, 2018). As one GlcNAc-MurNAc 5P disaccharide has been estimated by solution NMR and computational modelling to have a length of ~1-1.5 nm (Meroueh *et al.*, 2006;

Kim *et al.*, 2018), a 200 nm glycan chain would be made up of >130 disaccharide units *in vivo*. Other studies have extracted glycan chains from *E. coli* which are ~20-80 disaccharides in length (Glauner *et al.*, 1988; Glauner and Holtje, 1990; Harz *et al.*, 1990), which are consistent with the *in vitro* findings from this study.

Egan *et al*. have suggested LpoB shortening of glycan chains is an artefact of DMSO, and show in the absence of DMSO LpoB induces *E. coli* PBP1b to produce longer glycan chains (2018). However, these findings are contradictory to previous studies which have also carried out the *in vitro* reactions in the absence of DMSO and have still found glycan chain shortening (Markovski *et al.*, 2016). Unfortunately, the effect of DMSO on glycan chain length could not be tested in this study, as DMSO was needed for visualisation of the fluorescent Lipid II and glycan chains (discussed in section 3.4.5). Although DMSO could not be removed completely, the concentration was kept low at 10% (v/v). The findings in this study also support the glycan chain shortening effect of LpoB, as the LpoB bypass mutants also produced shorter glycan chains than wildtype PBP1b, indicating that LpoB induced glycan polymer shortening maybe a relevant function of LpoB *in vivo*.

5.4.4 Frequency of *E. coli* and *Y. pestis* PBP1b cross-linking

The findings reported here indicate that *E. coli* PBP1b only cross-links ~9.5% of its substrate in the presence of LpoB. Previous findings on the cross-linking frequency of *E. coli* PBP1b are contradictory. *In vitro* studies using radio-labelled Lipid II found *E. coli* PBP1b in the presence of LpoB to cross-link ~70% of its substrates (Bertsche *et al.*, 2005; Egan *et al.*, 2014; Egan *et al.*, 2018; Pazos *et al.*, 2018), studies measuring the incorporation of D-ala showed PBP1b-LpoB to cross-link ~19% of its substrate, (Lupoli *et al.*, 2014), whereas studies using unlabelled Lipid II found *E. coli* PBP1b in the presence of LpoB to cross-link 15% of its substrate (Catherwood *et al.*, 2019). The findings from this study agree with the latter two *in vitro* studies, which are most similar to *E. coli* cross-linking *in vivo*, found to be 33-40% (Glauner *et al.*, 1988; Quintela *et al.*, 1995). Interestingly the data from this study suggests that *Y. pestis* PBP1b has a higher percentage of

cross-linking ~25%, which is similar to *in vivo* data showing 34% of *Y. pestis's* peptidoglycan is cross-linked (Quintela *et al.*, 1995). The lower cross-linking activity *in vitro* may be due to the use of non-native or modified substrates, or the use of other types of cross-linking in peptidoglycan e.g. 3-3 cross-links.

5.4.5 Effect of CpoB on *E. coli* and *Y. pestis* PBP1b activity

This study found the rate of *E. coli* and *Y. pestis* PBP1b transglycosylation and transpeptidation to be unaffected by CpoB in the absence or presence of LpoB, and found CpoB to have no effect on the glycan chains produced by *E. coli* or *Y. pestis* PBP1b. Although these findings differ from previous studies which have shown CpoB to inhibit LpoB stimulation of *E. coli* PBP1b transpeptidation, the discrepancies in the results may be due to different assaying methods. Previous studies have quantified the percentage of peptides cross-linked at the end point of a reaction, whereas this study measured the initial rate of transpeptidation. CpoB may alter the extent of PBP1b cross-linking by sensitising PBP1b to product inhibition, therefore the transpeptidation rate would not change until sufficient product had accumulated.

Previous experiments have determimed a CpoB copy number of 4550 ± 540 in growing *E. coli* cells (Gray *et al.*, 2015), in comparison to 1000 for PBP1b and 2300 for LpoB (Typas *et al.*, 2010). Considering we found LpoB needed to be at 40x excess to PBP1b to gain maximum stimulation, this study used CpoB in 200x excess to PBP1b (and a 5-fold excess over LpoB) to account for the abundance of CpoB to PBP1b in the cell, however it was still found to have no effect.

5.4.6 Effect of FtsN on *E. coli* and *Y. pestis* PBP1b activity

This study found FtsN to have an inhibitory effect on *E. coli* and *Y. pestis* glycosyltransferase and transpeptidase rates, only in the presence of LpoB. Most studies have measured the affect FtsN had on *E. coli* PBP1b activity alone, with FtsN increasing the basal rate of PBP1b glycosyltransferase rate by ~2.5-fold (Müller *et al.*, 2007; Egan *et al.*, 2015; Pazos *et al.*, 2018) and increasing

transpeptidation 5-fold, with the effect on transpeptidation only being seen at PBP1b concentrations below its dimerization K_D (Müller *et al.*, 2007; Pazos *et al.*, 2018).

Egan *et al*. have compared the stimulatory effects of FtsN and LpoB on *E. coli* PBP1b glycosyltransferase activity (at a PBP1b concentration above its dimerization K_D), and found LpoB was able to stimulate PBP1b by twice as much as FtsN, and the presence of both proteins had an additive stimulatory effect on (2015). Yet at lower PBP1b concentrations (38 nM, compared with 500 nM (Egan *et al.*, 2015)) Pazos *et al*. found FtsN to have a greater stimulatory effect than LpoB (2018), hence there are many contradictory findings among the results of previous studies. The finding of FtsN reducing PBP1b cross-linking activity align with its *in vivo* function of recruiting amidases to the division site to cleave the peptidoglycan layer.

The protein ratios used in this study were based on the copy numbers found in *E. coli* cells. PBP1b is found at 1000 copies per cell, LpoB 2300 (Typas *et al.*, 2010) and FtsN 3000-6000 (Ursinus *et al.*, 2004), and considering LpoB was needed in 40x excess to PBP1b to gain full stimulation, FtsN was used at 60x and 200x excess of PBP1b, due to it being expressed in higher quantities in the cell than LpoB.

We also found FtsN to have an effect on the length of glycan chains produced by *E. coli* and *Y. pestis* PBP1b. We found FtsN to decrease the length of glycan chains produced by PBP1b in the absence and presence of LpoB. Although a previous study has found the presence of FtsN to increase the length of glycan chains produced by *E. coli* PBP1b further than those produced in the presence of LpoB (Pazos *et al.*, 2018), the results are tenuous due to the reactions being at differing stages of completion.

5.4.7 Future work

In addition to the further work that has been generated from the results in this chapter discussed above, recent advances in periplasmic FRET would allow the *Y. pestis* protein-protein interaction to be tested *in situ* in *E. coli,* by expressing the proteins fused to FRET capable fluorescent proteins (Meiresonne *et al.*, 2019). Meiresonne *et al.* developed fluorescent proteins capable of FRET in the periplasm, which has long been difficult due to issues with fluorescent protein folding in the periplasm and non-fluorescent protein dimer formation.

One of the major drawbacks to using detergents in *in vitro* assays is poor mimicry of a single lipid bilayer comprising all the proteins and substrates needed for peptidoglycan synthesis, as *in vivo*. In order to better recreate the membrane environment *in vitro*, the interacting proteins could be reconstituted into nanodiscs or nanobodies, or extracted by SMALP. SMALP allows membrane proteins in their protein complexes to be extracted directly from native membranes. In contrast to detergents, SMALP extracts proteins within the portion of the membrane that surrounds them, thereby preserving the native lipid environment and removing the need for detergents, while maintaining protein in complexes (Teo *et al.*, 2019). Although the Lipid II substrates could not be delivered in SMALP at this stage, delivering the protein complexes in SMALP would bring the *in vitro* assays one step closer to reconstituting the *in vivo* complex. This would also allow the effect of the phospholipid environment on PBP1b to be investigated.

5.5 Conclusions

In this work we have demonstrated *E. coli* and *Y. pestis* PBP1b, LpoB and FtsN proteins to all be monomeric in solution and *E. coli* and *Y. pestis* CpoB to be trimeric in solution. AUC also confirmed the direct interaction between *E. coli* and *Y. pestis* PBP1b and LpoB, CpoB and FtsN. This study shows the first observations of the effect interacting partners LpoB, CpoB and FtsN have on *Y. pestis* PBP1b glycosyltransferase and transpeptidase rates *in vitro*. LpoB stimulated the *in vitro* initial glycosyltransferation and transpeptidation rates of *E. coli* and *Y. pestis* PBP1b, while CpoB was shown to have no effect on either activities. However, FtsN inhibited the initial glycosyltransferase and transpeptidase rates of both *E. coli* and *Y. pestis* PBP1b *in vitro*.

Chapter 6. Development of a functional *in vitro* assay to measure *P. aeruginosa* PBP3 activity

6.1 Introduction

6.1.1 PBP3

E. coli PBP3 is the only essential class B PBP (mono-transpeptidase) involved in cell division, catalysing the peptide cross-links between glycan chains. PBP3 is a membrane protein, comprising of a short cytoplasmic peptide, followed by a single transmembrane helix and a periplasmic domain, containing the transpeptidase active site (Sauvage *et al.*, 2014).

PBP3 is involved in many interactions within the divisome complex, including with FtsW. The localisation of PBP3 to the division site is reported to be dependent on the presence of FtsW (Pastoret *et al.*, 2004; Piette *et al.*, 2004), and they have been reported to directly interact *in vivo* and *in vitro* (Fraipont *et al.*, 2011). FtsW was one of the candidates for the Lipid II flippase (Mohammadi *et al.*, 2011), but has recently been shown to have Lipid II polymerisation activity *in vitro* (Taguchi *et al.*, 2019). Interestingly, FtsW was shown to only polymerase Lipid II in the presence of its cognate class B PBP, PBP3 (Taguchi *et al.*, 2019). This led to the proposal that FtsW-PBP3 forms a two-component peptidoglycan synthase, with FtsW carrying out the glycosyltransferase activity and PBP3 the transpeptidase activity (Taguchi *et al.*, 2019). This complex would mirror the RodA-PBP2 complex which has been reported to synthesise peptidoglycan during cell elongation (Meeske *et al.*, 2016; Cho *et al.*, 2016; Rohs *et al.*, 2018). PBP3 is also necessary for midcell localisation of PBP1b (Bertsche *et al.*, 2006), and they have been shown to interact directly *in vivo* and *in vitro* (Bertsche *et al.*, 2006). FtsW, PBP3 and PBP1b have subsequently been reported to form a trimeric complex *in vitro* (Leclercq *et al.*, 2017).

6.1.2 Class B PBP *in vitro* activity

In vitro class A PBP transpeptidase activity is well documented, however the same is not true for Class B PBPs. Although the cognate polymerases have been identified for PBP2 and PBP3 there have been very few reports of Gram-positive or -negative class B PBP *in vitro* transpeptidase activity in the literature. *Streptococcus thermophilus* PBP2x has been shown to cross-link glycan polymers produced by its cognate polymerase FtsW *in vitro*, as well polymers produced by *Staphylococcus aureus* monofunctional glycosyltransferase SgtB and transpeptidase inactive *Streptococcus pneumoniae* PBP1a (Taguchi *et al.*, 2019). These reports suggest that class B PBPs do not need to interact with their cognate polymerase for activity, and can use substrates produced by a non-cognate polymerase. *E. coli* PBP2 has also been reported to attach Lipid II to sacculi *in vitro* (Banzhaf *et al.*, 2012). Whereas *in vitro* PBP3 transpeptidase activity with natural substrate has never been reported, even though it has been shown to bind β-lactams and to catalyse the hydrolysis of simple thioester substrates *in vitro* (Adam *et al.*, 1991; Papp-Wallace *et al.*, 2012; Boes *et al.*, 2019).

6.2 Experimental aims

- To investigate if *P. aeruginosa* PBP3 is active in the D-Ala release assay and validate the assay with appropriate controls.
- To confirm *P. aeruginosa* PBP3 carboxypeptidation and transpeptidation by LCMS.
- To investigate *P. aeruginosa* PBP3 inhibition by ampicillin.
- To determine the substrate specificity of *P. aeruginosa* PBP3.
- To test other Gram negative PBP3's for activity in the D-Ala release assay.

6.3 Results

6.3.1 *P. aeruginosa* PBP3 assay rationale

Preliminary data from our laboratory concluded that *P. aeruginosa* PBP3 had a greater bocillin acylation (Shapiro *et al.*, 2013) and nitrocefin deacylation rate than PBP3 homologues from *E. coli*, *Y. pestis*, *Burkholderia pseudomallei, Haemophilus influenza* and *Acinetobacter baumannii* (Newman H and Bellini D, unpublished). Both bocillin and nitrocefin are fluorescent and chromogenic mimics of β-lactams respectively, that can acylate to the PBP3 transpeptidase active site, and in the case of nitrocefin, release of the hydrolysed product as a chromophore (Lloyd A. and Bellini D., unpublished). As bocillin and nitrocefin structurally mimic the terminal D-Ala-D-Ala peptides of the natural substrate of PBP3 and given the above data, it was hypothesised that *P. aeruginosa* PBP3 was the most likely out of all the PBP3 homologues tested to acylate and cross-link native substrates.

A transpeptidase inactive mutant of *E. coli* PBP1b (kindly gifted by D. Bellini (Warwick)) was used to produce the polymeric donor substrate for *P. aeruginosa* PBP3 (Matsuhashi *et al.*, 1990), as previous reports have suggested class B PBPs can utilise glycan chains produced by a non-cognate polymerase (Taguchi *et al.*, 2019; Boes *et al.*, 2019). The transpeptidase inactive mutant was produced by mutating the transpeptidase active site serine to an alanine (*E. coli* PBP1b S510A). The continuous D-Ala release assay (detailed in 3.1.4) was then used to measure PBP3 carboxypeptidase and transpeptidase activity (Figure 6.1).

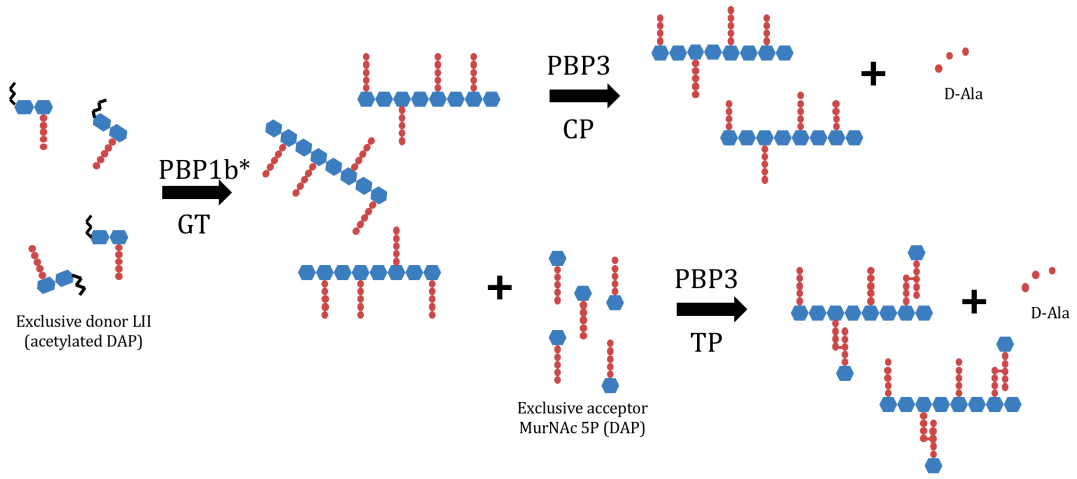

Figure 6.1. *In vitro* continuous PBP3 D-Ala release assay principle.
Lipid II (acetylated DAP) (rendered donor only substrate by acetylating the ε-amino group of the third DAP residue in the stem peptide) is polymerised into glycan chains (GT) by transpeptidase inactive *E. coli* PBP1b S510A (PBP1b*). The glycan polymer acylates to the active site serine of PBP3 releasing D-Ala. Upon addition of MurNAc 5P (DAP) (an exclusive acceptor substrate) transpeptidation (TP) occurs releasing the transpeptidation product. If water is used in the place of acceptor substrate carboxypeptidation (CP) occurs releasing the stem tetrapeptide. The release of D-Ala is monitored via a coupled enzyme detection system.

6.3.2 Initial observations of *P. aeruginosa* PBP3 activity and assay controls

To establish if *P. aeruginosa* PBP3 could utilise glycan chains produced by *E. coli* PBP1b S510A, PBP3 carboxypeptidase and transpeptidase activity was measured in the continuous D-Ala release assay with various substrates. Firstly, it was confirmed that *E. coli* PBP1b S510A was indeed transpeptidase inactive, which was established by the lack of D-ala release after its addition in the presence of Lipid II (acetylated DAP) (Figure 6.2A, B and D). Only on the addition of *P. aeruginosa* PBP3 was D-ala release detected (Figure 6.2A, B and D), suggesting *P. aeruginosa* PBP3 was active. To confirm *P. aeruginosa* PBP3 was using the glycan polymers rather than the Lipid II substrate *E. coli* PBP1b S510A was omitted from the reaction and no D-ala release was seen (Figure 6.2A), suggesting *P. aeruginosa* PBP3 was only able to utilise the polymeric substrate produced from Lipid II (acetylated DAP). As expected *P. aeruginosa* PBP3 D-ala release was also inhibited by ampicillin (transpeptidase inhibitor), and moenomycin (glycosyltransferase inhibitor) due to the lack of polymeric

substrate being produced (Figure 6.2B). *P. aeruginosa* PBP3 D-ala release initial rate was also linearly dependent on PBP3 concentration (Figure 2.6C).

P. aeruginosa PBP3 was able to utilise glycan polymers produced from Lipid II (DAP) and (acetylated DAP), but interestingly not from Lipid II (Lys) (Figure 6.2D), suggesting that *P. aeruginosa* PBP3 could only utilise glycan polymers with its native DAP in the 3rd position of the peptide stem. As Lipid II (acetylated DAP) can only be a transpeptidase donor substrate, the D-Ala release observed using this substrate can only be attributed to carboxypeptidation. On addition of acceptor only substrate MurNAc 5P (DAP) transpeptidation can be initiated, however no detectable change in D-Ala release rate was observed (Figure 6.2D), suggesting there was either no switch from carboxypeptidation to transpeptidation, or the D-Ala release rate from transpeptidation was far slower than that of carboxypeptidation. To determine this the reaction products were analysed by LCMS (detailed in 6.3.3).

Interestingly, the D-Ala release rate observed using native glycan polymers produced from Lipid II (DAP) was less than that with Lipid II (acetylated DAP) (Figure 6.2D). This may simply be a substrate preference, or may be due to the D-Ala production being from transpeptidation rather than carboxypeptidation, as the glycan polymers produced from Lipid II (DAP) can be both donor and acceptor transpeptidase substrates (investigated in 6.3.3).

Catherwood *et al.* have shown that the stereochemical orientation of the DAP *ε*-amino group with the pentapeptide stem biased *E. coli* PBP1b towards transpeptidation or carboxypeptidation (2019). Therefore, we determined if Lipid II (L,L-acetylated DAP), the stereoisomer of Lipid II (acetylated DAP), was also a donor substrate for *P. aeruginosa* PBP3. Lipid II (L,L-acetylated DAP) supported D-Ala release, however, it was not as well utilised as meso-acetylated DAP. *E. coli* sacculi also mainly contain tetrapeptides (Glauner and Entwi, 1988), which can act as acceptor but not donors substrates for transpeptidation. When we tested polymeric tetrapeptide substrates containing meso- or L,L-DAP as

transpeptidase acceptors they caused no change in the D-Ala release rate, however this should be investigated by LCMS.

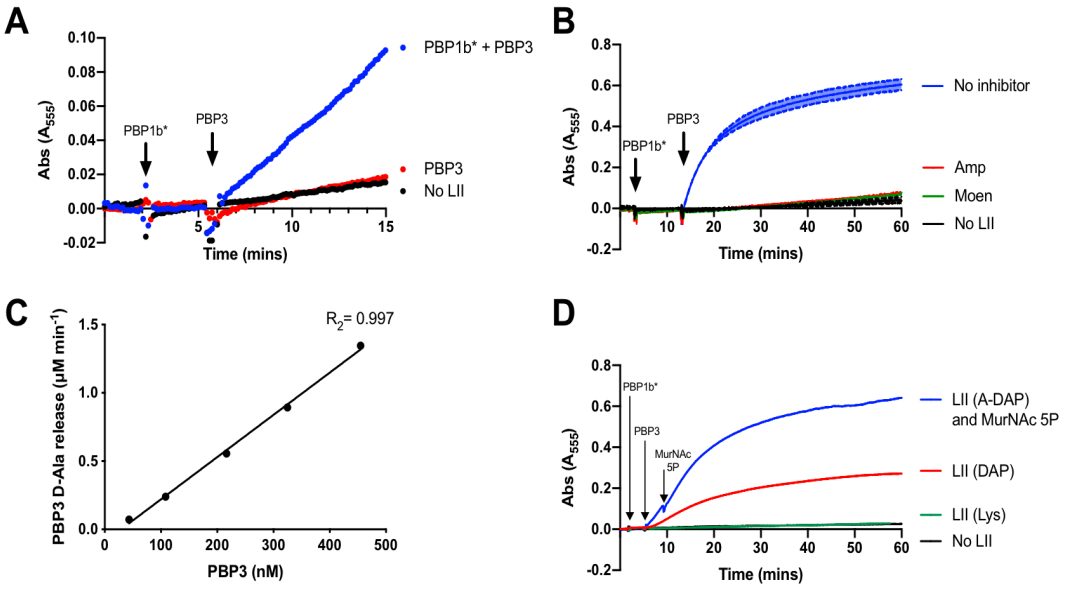

Figure 6.2 Initial observations of *P. aeruginosa* PBP3 activity and controls.
P. aeruginosa PBP3 activity was assayed using the amplex red assay for D-Ala release *in vitro.* **(A)** dependency on glycan polymer substrate, **(B)** inhibition, **(C)** linear dependency of initial rate on PBP3 concentration, and **(D)** substrate utilisation. Reactions consisted of 50 mM Bis-Tris propane pH 8.5, 6 mM NaCl, 2 mM $MgCl_2$, 1% (v/v) glycerol, 0.130% (v/v) Triton X-100 (0.0468% (v/v) E_6C_{12} for Lipid II (DAP) reaction), amplex red coupling reagents, 20 μM Lipid II (acetylated DAP) if not stated, 50 nM *E. coli* PBP1b S510A (PBP1b*), 20 μM MurNac 5P (DAP) only where stated, 2 μM LpoB, 325 nM *P. aeruginosa* PBP3 unless otherwise stated, 5 μM Moenomycin (Moen) and 3 mM Ampicillin (Amp) as controls. A, C and D: data is shown as n=1, and B: mean, maximum and minimum (n=2).

6.3.3 LCMS of *P. aeruginosa* PBP3 assay products

To determine if *P. aeruginosa* PBP3-catalysed D-ala release from Lipid II (acetylated DAP) and MurNAc 5P (DAP) was transpeptidation, the reaction products were digested with mutanolysin and analysed by LCMS (Figure 6.5A). LCMS detected m/z values for the Lipid II substrate or it's polymer, GlcNAc MurNAc 5P (acetylated DAP) (expected (m+1)/1: 1053.447, observed: 1053.448) (Figure 6.3A and Bi), the carboxypeptidase product GlcNAc MurNAc (acetylated DAP 4P) (expected (m+1)/1: 982.410, observed 982.412) (Figure 6.3Bi), the transpeptidase product GlcNAc MurNAc (acetylated DAP 4P) bonded via the carbonyl of its D-ala to the DAP ε-amino group within MurNAc 5P (DAP) (expected (m+2)/2: 886.378, observed: 886.378) (Figure 6.3Bii). Consistent with

these observations, there were no m/z values for any of these products in the absence of Lipid II, no m/z values for the transpeptidase product in the absence of MurNAc 5P (DAP) (Appendix 9.6), and no carboxypeptidase products in the absence of *P. aeruginosa* PBP3 (Figure 6.3A).

For *P. aeruginosa* PBP3-catalysed reaction products from Lipid II (DAP) LCMS detected m/z values for the Lipid II substrate or it's polymer GlcNAc MurNAc 5P (DAP) (expected (m+1)/1: 1011.436, observed: 1011.436) (Figure 6.4A), the carboxypeptidase product GlcNAc MurNAc (DAP 4P) (expected (m+1)/1: 940.399, observed: 940.398) (Figure 6.4B), and the transpeptidase product GlcNAc MurNAc (DAP 4P) bonded via the carbonyl of the donor D-ala to the DAP ε-amino group within the GlcNAc MurNAc 5P acceptor (DAP) (expected (m+2)/2: 966.913, observed: 966.912) (Figure 6.4C). These products were absent in the absence of Lipid II.

LCMS detected the carboxypeptidase product from Lipid II (DAP) as two anomer peaks (Figure 6.5C) of ~10% of the abundance of the carboxypeptidase product formed in the presence of Lipid II (acetylated DAP) and MurNAc 5P (DAP) (Figure 6.5B and C), also detected as two anomer peaks (Figure 6.5B). Concurrently Lipid II (acetylated DAP) produced a transpeptidase product peak (Figure 6.5B) of ~30% of the abundance of the transpeptidase product peak formed from Lipid II (DAP) (Figure 6.5B and C). If acetylating the DAP on the donor substrate biases *P. aeruginosa* PBP3 towards carboxypeptidation, this may suggest that PBP3 preferentially carboxypeptidates substrates that have previously been used as transpeptidase acceptors and are therefore acylated, mimicked by the acetylation.

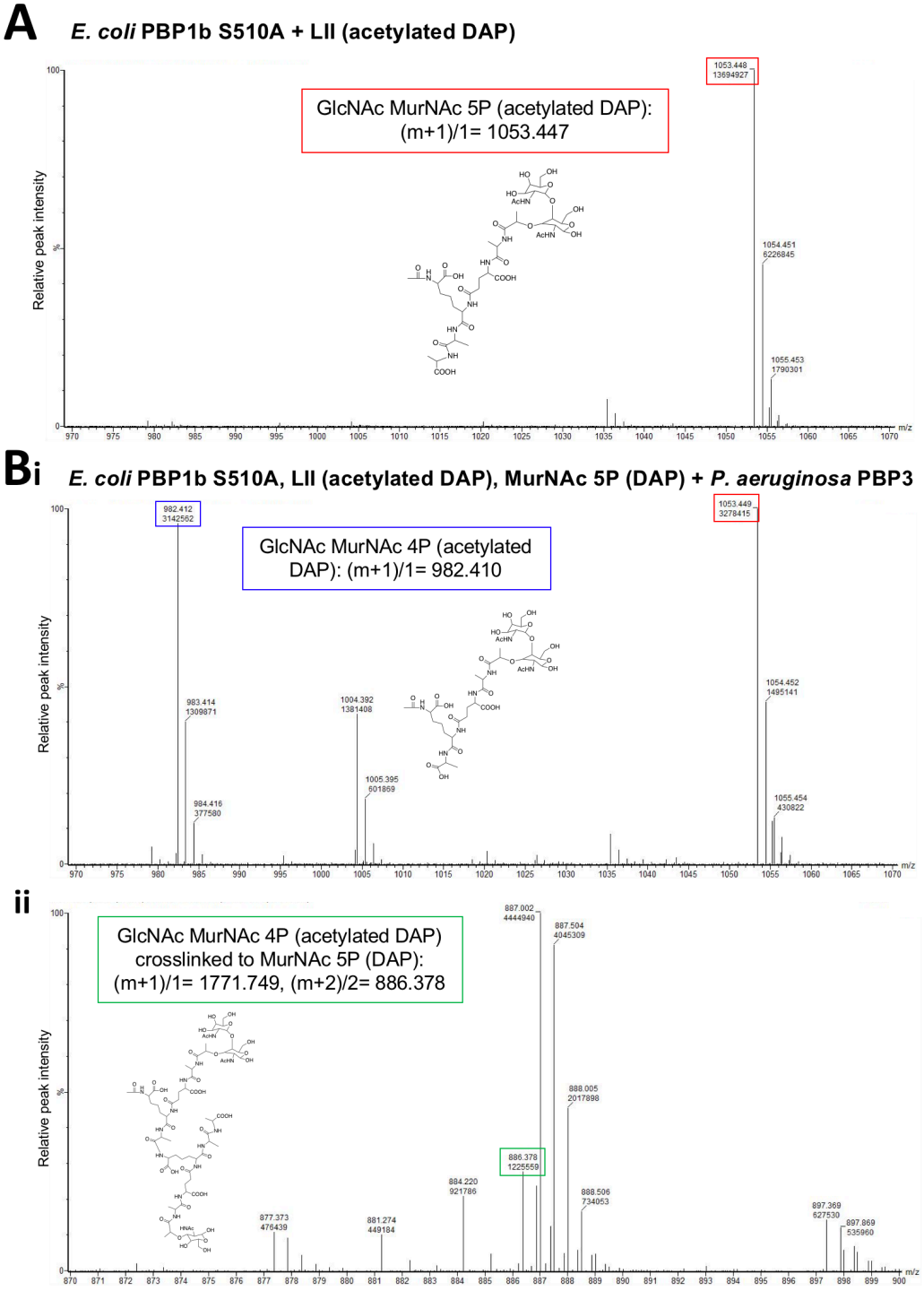

Figure 6.3 LCMS analysis of *P. aeruginosa* PBP3 reaction products from pentapeptide (acetylated DAP) glycan polymers and MurNAc 5P (DAP).
Positive ion LCMS analysis of **(A)** *E. coli* PBP1b S510A reaction products from Lipid II (acetylated DAP), and **(B)** *E. coli* PBP1b S510A and *P. aeruginosa* PBP3 reaction products from Lipid II (acetylated DAP) and MurNAc 5P (DAP). Reactions consisted of 50 mM Bis-Tris propane pH 8.5, 6 mM NaCl, 2 mM $MgCl_2$, 1% (v/v) glycerol, 0.0468% (v/v) E_6C_{12}, amplex red coupling reagents, 20 μM Lipid II (acetylated DAP), 50 nM *E. coli* PBP1b S510A, 20 μM MurNAc 5P (DAP), 2 μM LpoB and 430 nM *P. aeruginosa* PBP3. Prepared for LCMS by mutanolysin digestion, and the addition of $NaBH_4$ and phosphoric acid. Major peaks are annotated as m/z and ion count, determined by combining the spectrums of the peak relating to the ion of interest.

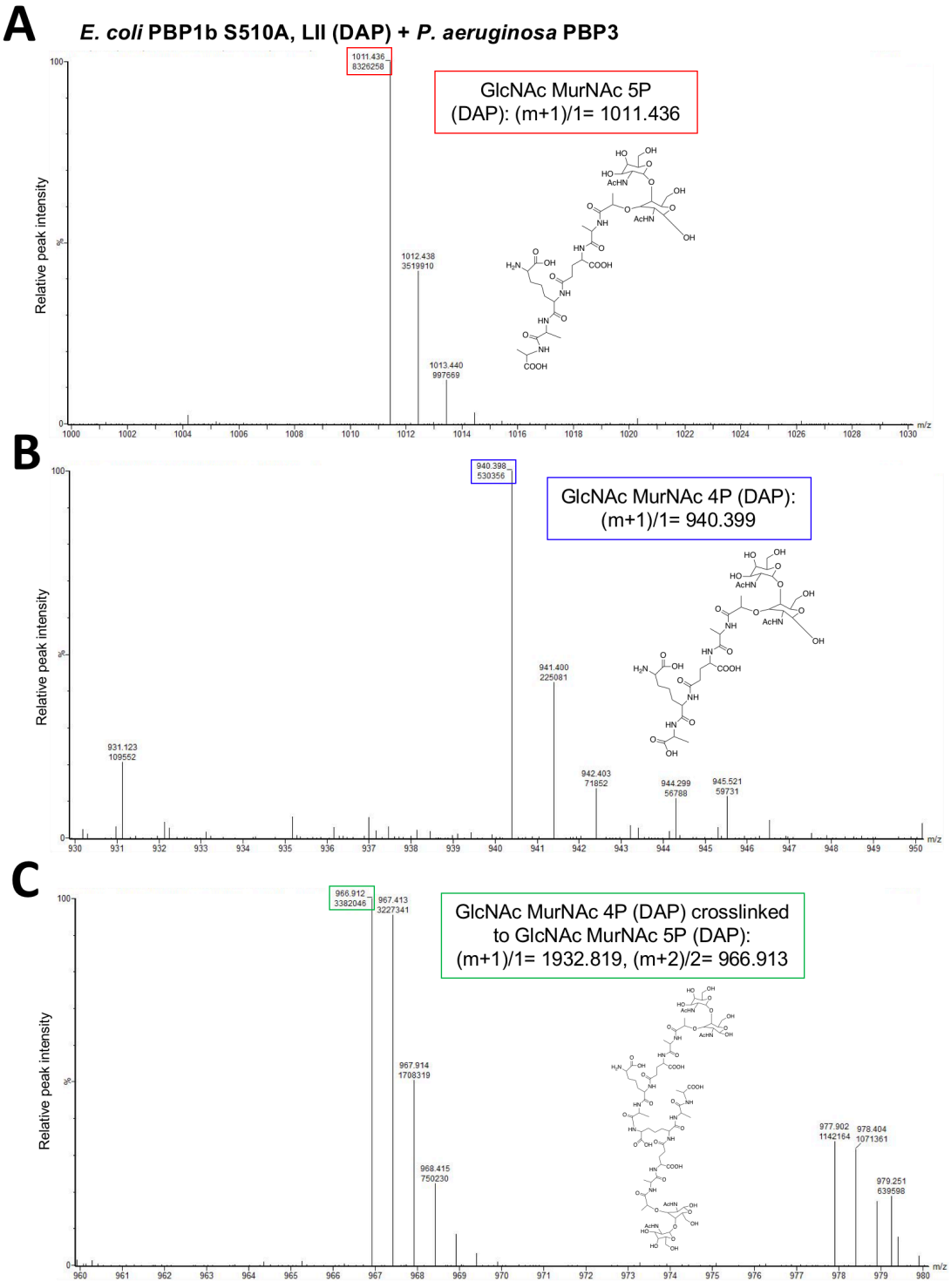

Figure 6.4 LCMS analysis of *P. aeruginosa* PBP3 reaction products from pentapeptide (DAP) glycan polymers.
Positive ion LCMS analysis of *E. coli* PBP1b S510A and *P. aeruginosa* PBP3 reaction products from Lipid II (DAP). Reactions consisted of 50 mM Bis-Tris propane pH 8.5, 6 mM NaCl, 2 mM $MgCl_2$, 1% (v/v) glycerol, 0.0468% (v/v) E_6C_{12}, amplex red coupling reagents, 20 μM Lipid II (DAP), 50 nM *E. coli* PBP1b S510A, 2 μM LpoB and 430 nM *P. aeruginosa* PBP3. Prepared for LCMS by mutanolysin digestion, and the addition of $NaBH_4$ and phosphoric acid. Major peaks are annotated as m/z and ion count, determined by combining the spectrums of the peak relating to the ion of interest.

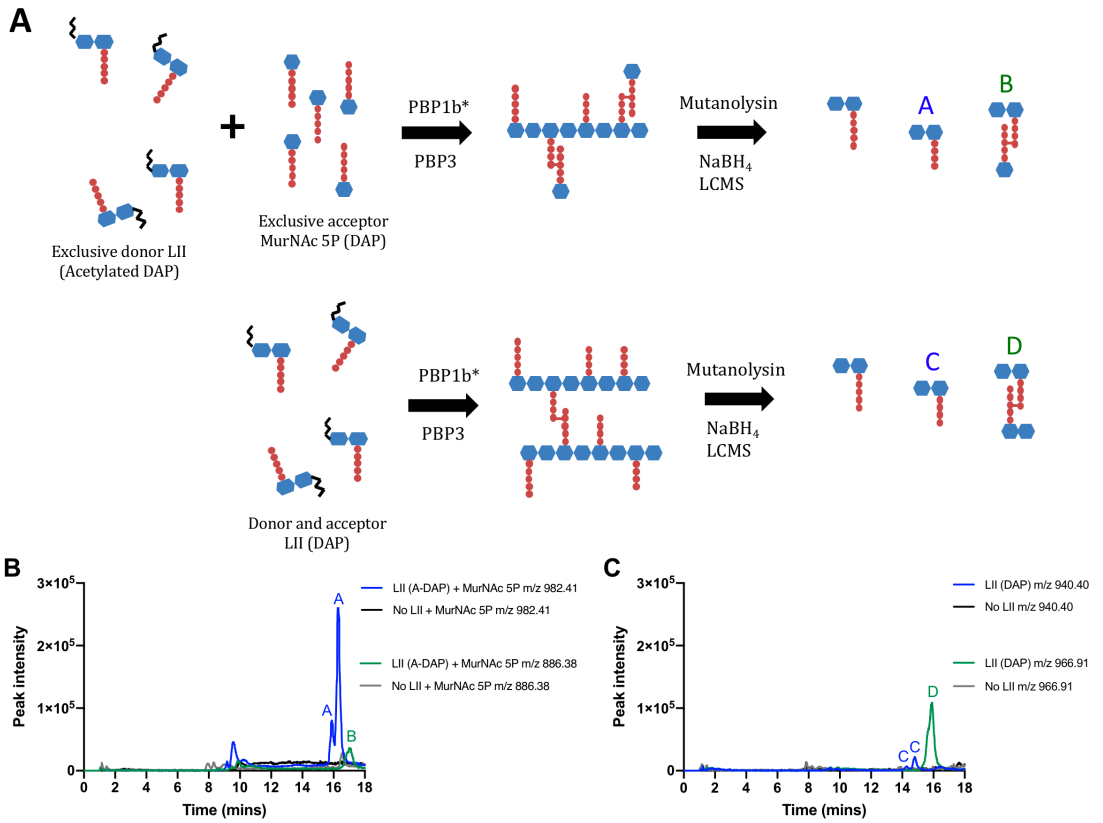

Figure 6.5 Extracted ion chromatograms of LCMS analysis of *P. aeruginosa* PBP3 reaction products.
(A) Schematic showing the detection of PBP3 reaction products by LC-MS. Positive ion LCMS analysis of **(B)** *E. coli* PBP1b S510A and *P. aeruginosa* PBP3 reaction products from Lipid II (acetylated DAP) and MurNAc 5P (DAP) and **(C)** *E. coli* PBP1b S510A and *P. aeruginosa* PBP3 reaction products from Lipid II (DAP). Blue and black traces follow the elution of carboxypeptidase products with m/z values of 982.41 and 940.40, and green and grey traces follow the elution of transpeptidase products with m/z values of 886.38 and 966.91. Reactions consisted of 50 mM Bis-Tris propane pH 8.5, 6 mM NaCl, 2 mM $MgCl_2$, 1% (v/v) glycerol, 0.0468% (v/v) E_6C_{12}, amplex red coupling reagents, 20 μM Lipid II (acetylated DAP), 50 nM *E. coli* PBP1b S510A, 20 μM MurNAc 5P (DAP), 2 μM LpoB and 430 nM *P. aeruginosa* PBP3. Prepared for LCMS by mutanolysin digestion, and the addition of $NaBH_4$ and phosphoric acid.

6.3.4 Inhibition of *P. aeruginosa* PBP3 carboxypeptidase activity by ampicillin

The sensitivity of *P. aeruginosa* PBP3 activity to ampicillin was investigated using the D-Ala release assay. Incubation of PBP3 with various ampicillin concentrations gave an estimation of the IC_{50} to be near half the PBP3 concentration, suggesting *P. aeruginosa* PBP3 is very sensitive to ampicillin. To gain an accurate IC_{50}, experiments were carried out without PBP3 incubation with ampicillin and gave an IC_{50} of 1.496 $\pm$ 0.083 μM with 20 μM Lipid II

(acetylated DAP), and when the substrate concentration was reduced to 8 μM the IC_{50} reduced to 0.803 $\pm$ 0.083 μM (Figure 6.6). This indicated *P. aeruginosa* PBP3 is very sensitive to ampicillin and glycan 5P (acetylated DAP) polymers can compete with ampicillin for transpeptidase active site binding.

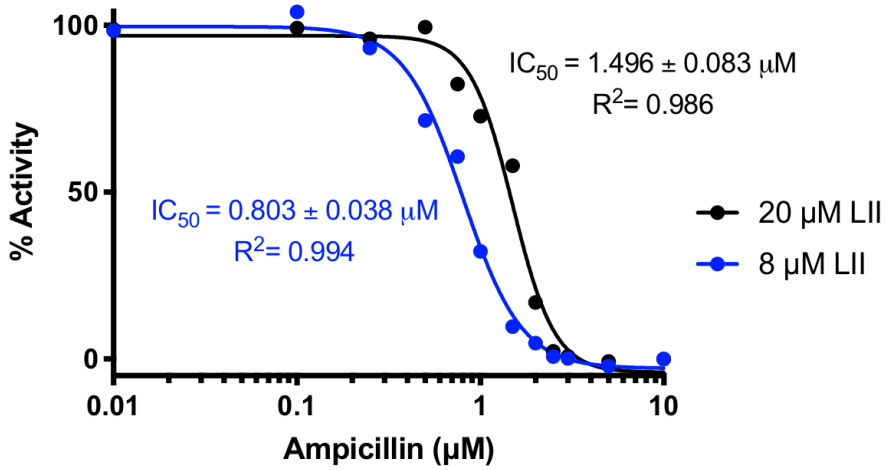

Figure 6.6 Inhibition of *P. aeruginosa* PBP3 activity by ampicillin.
P. aeruginosa PBP3 activity was assayed using the amplex red assay for D-Ala release *in vitro,* shown as percentage activity relative to the no inhibitor control and fitted to a four-parameter dose-response curve model. Reactions consisting of 50 mM Bis-Tris propane pH 8.5, 6 mM NaCl, 2 mM $MgCl_2$, 1% (v/v) glycerol, 0.130% (v/v) Triton X-100, amplex red coupling reagents, 8 or 20 μM Lipid II (acetylated DAP), 50 nM *E. coli* PBP1b S510A (PBP1b*) and 2 μM LpoB. Glycan chain accumulation was stopped after 10 mins with 5 μM moenomycin, and varied ampicillin concentrations and 325 nM *P. aeruginosa* PBP3 were added (n=1).

6.3.5 Effect of divalent cations and EDTA on *P. aeruginosa* PBP3 activity

During the initial experiments to establish *P. aeruginosa* PBP3 activity it was observed that D-Ala release was severely affected by the $MgCl_2$ concentration. To investigate this further, the sensitivity of *P. aeruginosa* PBP3 D-Ala release was measured in the presence of various concentrations of divalent metal ions, $MgCl_2$, $MgSO_4$ and $CaCl_2$. *P. aeruginosa* PBP3 was found to be active from 0-10 mM $MgCl_2$, with optimum activity found around 2 mM $MgCl_2$, however it was inactive at 20 mM $MgCl_2$ (Figure 6.7A). Similar trends were also observed for $MgSO_4$ and $CaCl_2$ (Figure 6.7A).

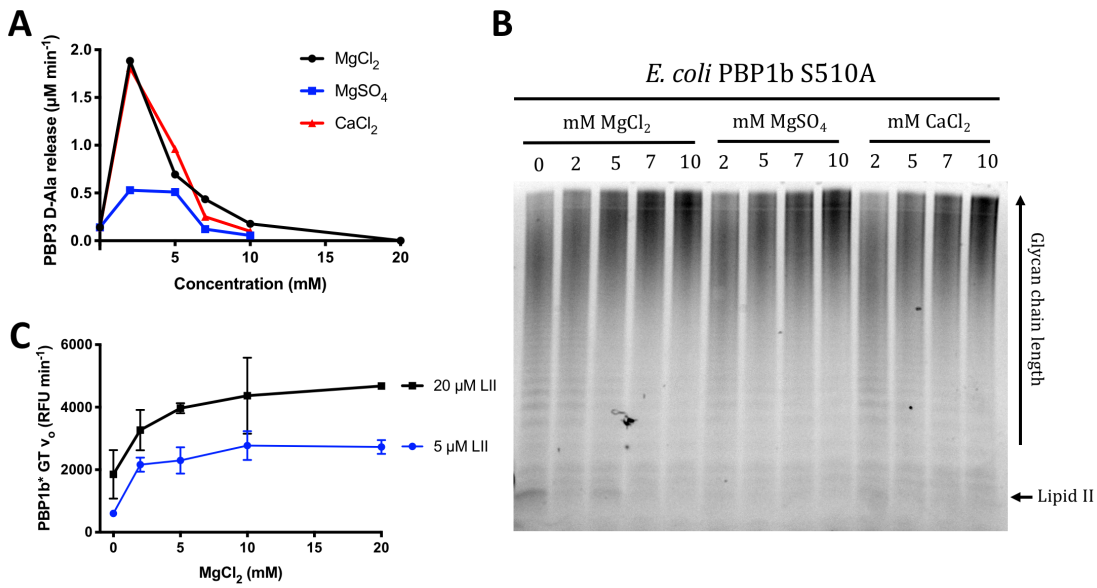

Figure 6.7 Effect of divalent cations on *P. aeruginosa* PBP3 and *E. coli* PBP1b S510A activity.
(A) Effect of divalent cation concentration on *P. aeruginosa* PBP3 activity, assayed using the amplex red assay for D-Ala release *in vitro,* shown as initial rates. **(B)** Effect of divalent cation concentration on *E. coli* PBP1b S510A glycan chain length, assayed by the polymerisation of fluorescently labelled Lipid II and visualised by SDS-PAGE analysis. **(C)** Effect of divalent cation concentration on *E. coli* PBP1b S510A glycosyltransferase activity, assayed by the consumption of fluorescently labelled Lipid II *in vitro,* shown as initial rates. PBP3 activity reactions consisted of 50 mM Bis-Tris propane pH 8.5, 6 mM NaCl, varied $MgCl_2$, $MgSO_4$ and $CaCl_2$ concentrations, 1% (v/v) glycerol, 0.130% (v/v) Triton X-100, amplex red coupling reagents, 20 μM Lipid II (acetylated DAP), 50 nM *E. coli* PBP1b S510A (PBP1b*), 2 μM LpoB and 325 nM *P. aeruginosa* PBP3. 1 hour glycan chain analysis reactions consisted of 50 mM HEPES pH 7.5, 115 mM NaCl, varied $MgCl_2$, $MgSO_4$ and $CaCl_2$ concentration, 10% (v/v) DMSO, 1% (v/v) glycerol, 0.155% (v/v) Triton X-100, 10 μM lipid II- 5P (dansyl DAP), 100 nM *E. coli* PBP1b S510A and 4 μM LpoB. Continuous glycosyltransferase (GT) assay reactions consisted of 50 mM HEPES pH 7.5, 115 mM NaCl, varied $MgCl_2$, 10% (v/v) DMSO, 1% (v/v) glycerol, 0.155% (v/v) Triton X-100, 0.1 mg ml^{-1} lysozyme, 5 or 20 μM Lipid II (dansyl DAP), 50 nM *E. coli* PBP1b S510A and 2 μM LpoB. A and B n=1, and C: data is shown as mean $\pm$ SD (n=3).

To determine if this sensitivity to divalent metal ions was a direct effect on PBP3 or an effect on PBP1b, and therefore, substrate availability for PBP3, the effect of divalent metal ions on *E. coli* PBP1b S510A glycosyltransferase activity was investigated. Using the continuous fluorescent glycosyltransferase assay the glycosyltransferase rate of *E. coli* PBP1b S510A was found to increase hyperbolically from 0 to 20 mM $MgCl_2$ (Figure 6.7C), and this increase in rate was combined with an increase in the length of glycan chains (Figure 6.7B). These results indicate that the increase in PBP3's activity from 0 to 2 mM $MgCl_2$ is likely due to the increased rate of glycan chain polymerisation by PBP1b, but as the

PBP1b polymerisation rate continues to increase up to 20 mM $MgCl_2$, the decrease in *P. aeruginosa* PBP3 activity after 2 mM $MgCl_2$ cannot be explained by a decrease in abundance of substrate, and therefore suggests divalent metal ion concentrations >2 mM negatively affects PBP3 activity.

Interestingly, EDTA, a metal ion chelator, also had an adverse negative effect on *P. aeruginosa* PBP3 D-ala release, as *P. aeruginosa* PBP3 activity declined with increasing EDTA concentration, until it was inactive at 12 mM EDTA (Figure 6.8A). It was confirmed that 12 mM EDTA did not affect the D-Ala release assay converting enzyme system. EDTA also had no adverse effect on the glycosyltransferase rate of *E. coli* PBP1b S510A, and PBP1b was found to still be active at 12 mM EDTA (Figure 6.8C), as well as EDTA not affecting the length of glycan chains produced by PBP1b (Figure 6.8B). This indicates that EDTA also negatively affects *P. aeruginosa* PBP3 activity.

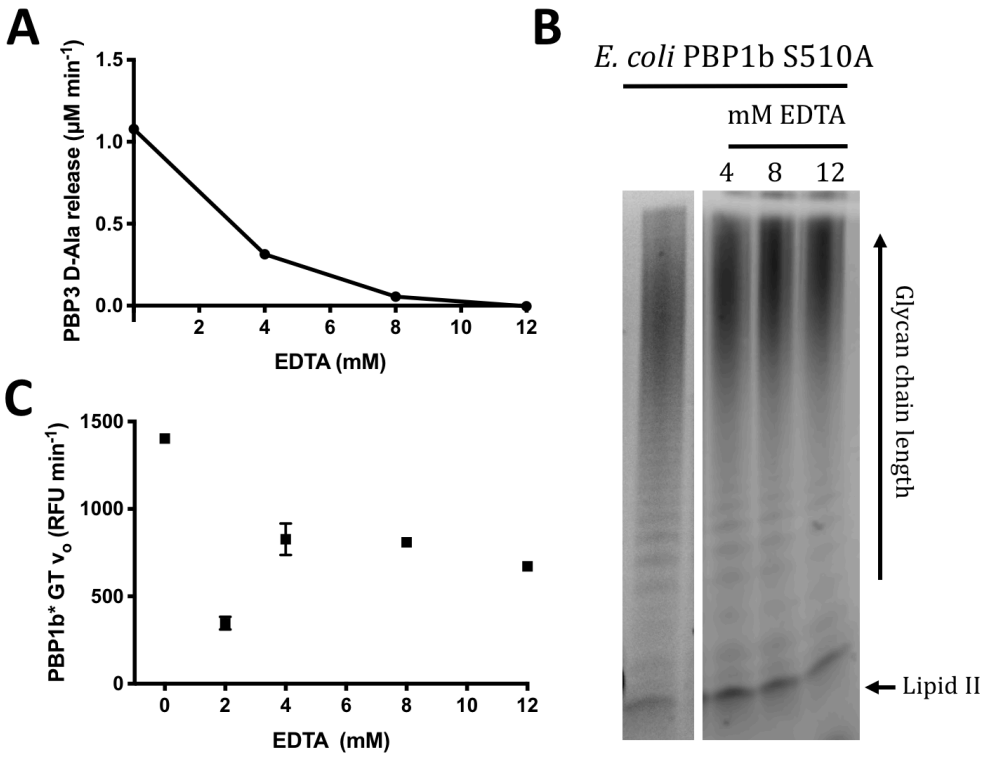

Figure 6.8 Effect of EDTA on *P. aeruginosa* PBP3 and *E. coli* PBP1b S510A activity. **(A)** Effect of EDTA concentration on *P. aeruginosa* PBP3 activity, assayed using the amplex red assay for D-Ala release *in vitro,* shown as initial rates. **(B)** Effect of EDTA concentration on *E. coli* PBP1b S510A glycan chain length, assayed by the polymerisation of fluorescently labelled Lipid II and visualised by SDS-PAGE analysis. **(C)** Effect of EDTA concentration on *E. coli* PBP1b S510A glycosyltransferase activity, assayed by the consumption of fluorescently labelled Lipid II *in vitro,* shown as initial rates. PBP3 activity reactions consisted of 50 mM Bis-Tris propane pH 8.5, 6 mM NaCl, varied EDTA concentration, 1% (v/v) glycerol, 0.130% (v/v) Triton X-100, amplex red coupling reagents, 20 μM Lipid II (acetylated DAP), 50 nM *E. coli* PBP1b S510A (PBP1b*), 2 μM LpoB and 325 nM *P. aeruginosa* PBP3 added after an hour of glycan chain accumulation. 1 hour glycan chain analysis reactions consisted of 50 mM HEPES pH 7.5, 115 mM NaCl, varied EDTA concentration, 10% (v/v) DMSO, 1% (v/v) glycerol, 0.155% (v/v) Triton X-100, 10 μM lipid II- 5P (dansyl DAP), 100 nM *E. coli* PBP1b S510A and 4 μM LpoB. Continuous glycosyltransferase (GT) assay reactions consisted of 50 mM HEPES pH 7.5, 115 mM NaCl, varied EDTA concentration, 10% (v/v) DMSO, 1% (v/v) glycerol, 0.155% (v/v) Triton X-100, 0.1 mg ml^{-1} lysozyme, 20 μM Lipid II (dansyl DAP), 50 nM *E. coli* PBP1b S510A and 2 μM LpoB. A n=1, B n=2, and C: data is shown as mean $\pm$ SD (n=3).

6.3.6 Effect of the glycan polymer substrate and *E. coli* PBP1b interaction on *P. aeruginosa* PBP3 activity

We next assessed if *P. aeruginosa* PBP3 had a preference of length of glycan chain substrate. Glycan chains of varying lengths were produced by allowing glycan chain polymerisation to occur for varying lengths of time, as well as in the

presence of various $MgCl_2$ concentrations. The accumulated glycan chains were run on an SDS-PAGE gel to determine their length (Figure 6.9B), and were used as substrates for *P. aeruginosa* PBP3 (Figure 6.9A). Although this method produced varying quantities of glycan chains, their abundance could be qualitatively estimated by the SDS-PAGE analysis.

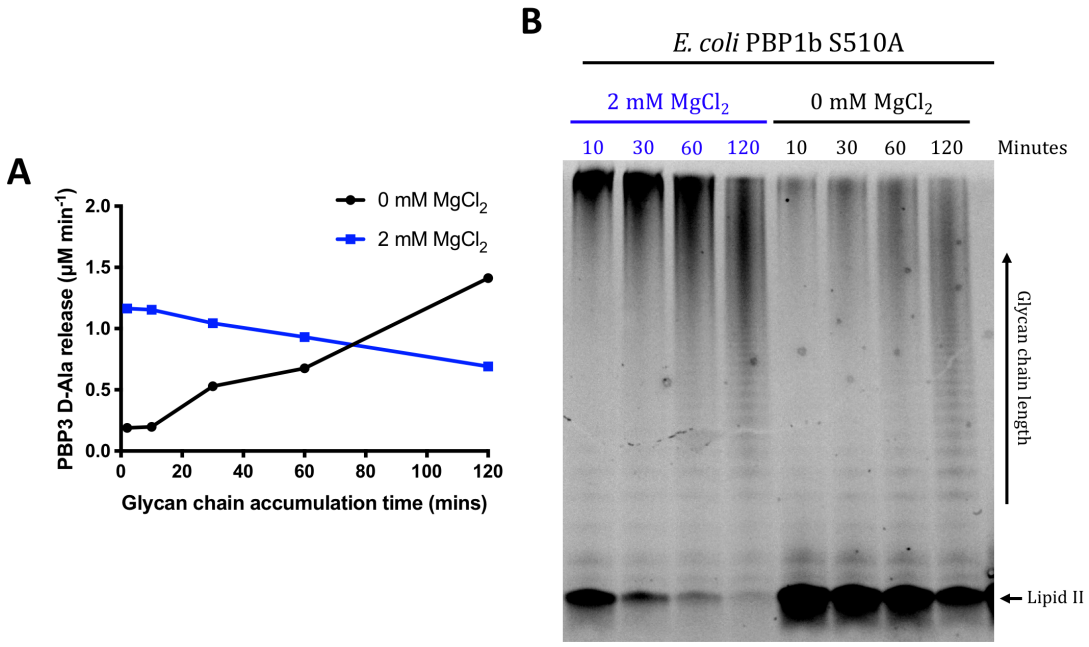

Figure 6.9 Effect of glycan chain accumulation on *P. aeruginosa* PBP3 activity. **(A)** Effect of glycan chain accumulation on *P. aeruginosa* PBP3 activity, assayed using the amplex red assay for D-Ala release *in vitro*, shown as initial rates. **(B)** Glycan chain length analysis of polymers produced by *E. coli* PBP1b S510A, used as *P. aeruginosa* PBP3 substrates, assayed by the polymerisation of fluorescently labelled Lipid II and visualised by SDS-PAGE analysis. PBP3 activity reactions consisted of 50 mM Bis-Tris propane pH 8.5, 6 mM NaCl, varied $MgCl_2$, 1% (v/v) glycerol, 0.130% (v/v) Triton X-100, amplex red coupling reagents, 20 μM Lipid II (acetylated DAP), 50 nM *E. coli* PBP1b S510A (PBP1b*), 2 μM LpoB and 325 nM *P. aeruginosa* PBP3. Glycan chain analysis reactions consisted of 50 mM Bis-Tris-propane pH 8.5, 15 mM NaCl, varied $MgCl_2$, 10% (v/v) DMSO, 1% (v/v) glycerol, 0.130% (v/v) Triton X-100, 10 μM lipid II-5P (dansyl DAP), 50 nM *E. coli* PBP1b S510A and 2 μM LpoB. A n=1, B n=2

From the glycan chains produced in the presence of 2 mM $MgCl_2$, *P. aeruginosa* PBP3 activity declined as the abundance of glycan chains increased with time, seen by the disappearance of the Lipid II band (Figure 6.9B). This is likely due to the increase in abundance of cleaved glycan chains over time, suggesting *P. aeruginosa* PBP3 cannot use the cleaved glycan chains as a substrate. While using the glycan chains accumulated in the presence of no $MgCl_2$, *P. aeruginosa* PBP3 activity increased as the abundance of glycan chains accumulated (Figure 6.9).

However, the results suggested that PBP3 could utilise glycan chains of varying length as substrates.

As it was not clear from the previous experiment whether *P. aeruginosa* PBP3 required actively polymerising glycan chains as a substrate, PBP3 activity was tested using glycan chains of different lengths (as produced earlier in this section) (Figure 6.10E), however active polymerisation was stopped with the addition of moenomycin. Glycan chains that had been treated with moenomycin were found to be similarly active as polymerising glycan chains (Figure 6.10A-D), indicating *P. aeruginosa* PBP3 does not require actively polymerising chains as a substrate.

The possibility of *P. aeruginosa* PBP3 requiring an interaction with PBP1b for activity was also investigated. Again, varying lengths of glycan chains were produced, but before being used as a substrate for PBP3 the glycan chains were boiled for 10 minutes to denature the *E. coli* PBP1b S510A and prevent an interaction with PBP3. *P. aeruginosa* PBP3 was found to be active with boiled chains, however its activity was less than with untreated chains (Figure 6.10A-D), suggesting that either an interaction with PBP1b is not essential but does increase PBP3 activity, or boiling the glycan chains affects their specificity as substrates for PBP3. Although boiling the glycan chains has no detectable effect by SDS-PAGE analysis, it may hydrolyse off the undecaprenyl pyrophosphate at the end of the glycan chain or promote the formation of glycan chain conformations which are unfavourable substrates for PBP3.

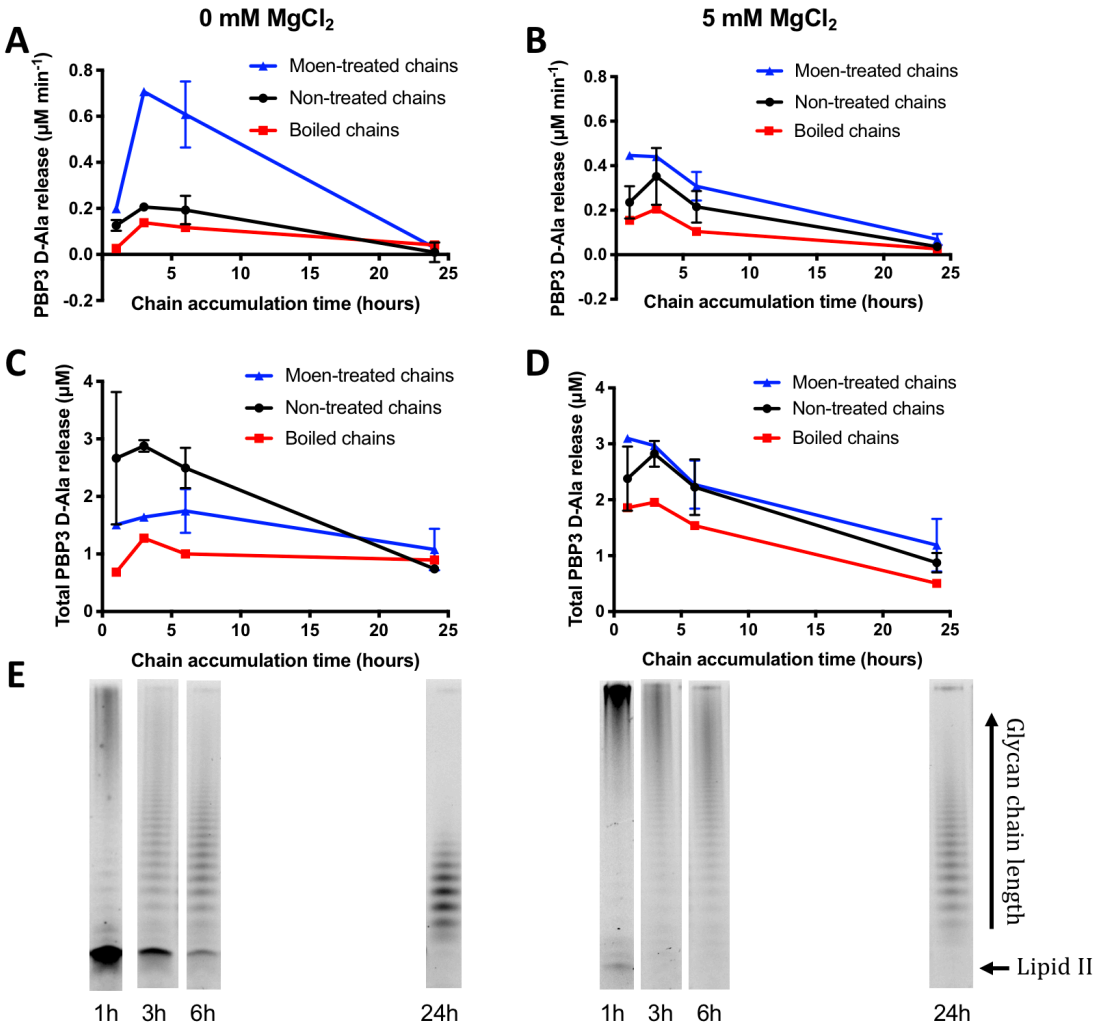

Figure 6.10 Effect of glycan chain treatment on *P. aeruginosa* PBP3 activity. Effect of glycan chains treated with 5 μM moenomycin (moen) or boiling for 10 minutes, on *P. aeruginosa* PBP3 activity at varying $MgCl_2$ concentrations, assayed using the amplex red assay for D-Ala release *in vitro*, **(A** and **B)** shown as initial rates and **(C** and **D)** shown as total D-Ala released. **(E)** glycan chain length analysis of polymers produced by *E. coli* PBP1b S510A, used as *P. aeruginosa* PBP3 substrates, assayed by the polymerisation of fluorescently labelled Lipid II and visualised by SDS-PAGE analysis. PBP3 activity reactions consisted of 50 mM Bis-Tris propane pH 8.5, 6 mM NaCl, varied $MgCl_2$, 1% (v/v) glycerol, 0.130% (v/v) Triton X-100, amplex red coupling reagents, 10 μM Lipid II (acetylated DAP), 50 nM *E. coli* PBP1b S510A (PBP1b*), 2 μM LpoB and 325 nM *P. aeruginosa* PBP3. Glycan chain analysis reactions consisted of 50 mM Bis-Tris-propane pH 8.5, 15 mM NaCl, varied $MgCl_2$, 10% (v/v) DMSO, 1% (v/v) glycerol, 0.130% (v/v) Triton X-100, 10 μM lipid II- 5P (dansyl DAP), 50 nM *E. coli* PBP1b S510A and 2 μM LpoB. A-D data is shown as mean, maximum and minimum (n=1-2), and E n=2.

6.3.7 Other Gram-negative bacterial PBP3 *in vitro* activity

As *P. aeruginosa* PBP3 was found to be active, other Gram-negative PBP3 homologues which shared a high sequence homology with *P. aeruginosa* PBP3 were also tested for activity (Figure 6.11).

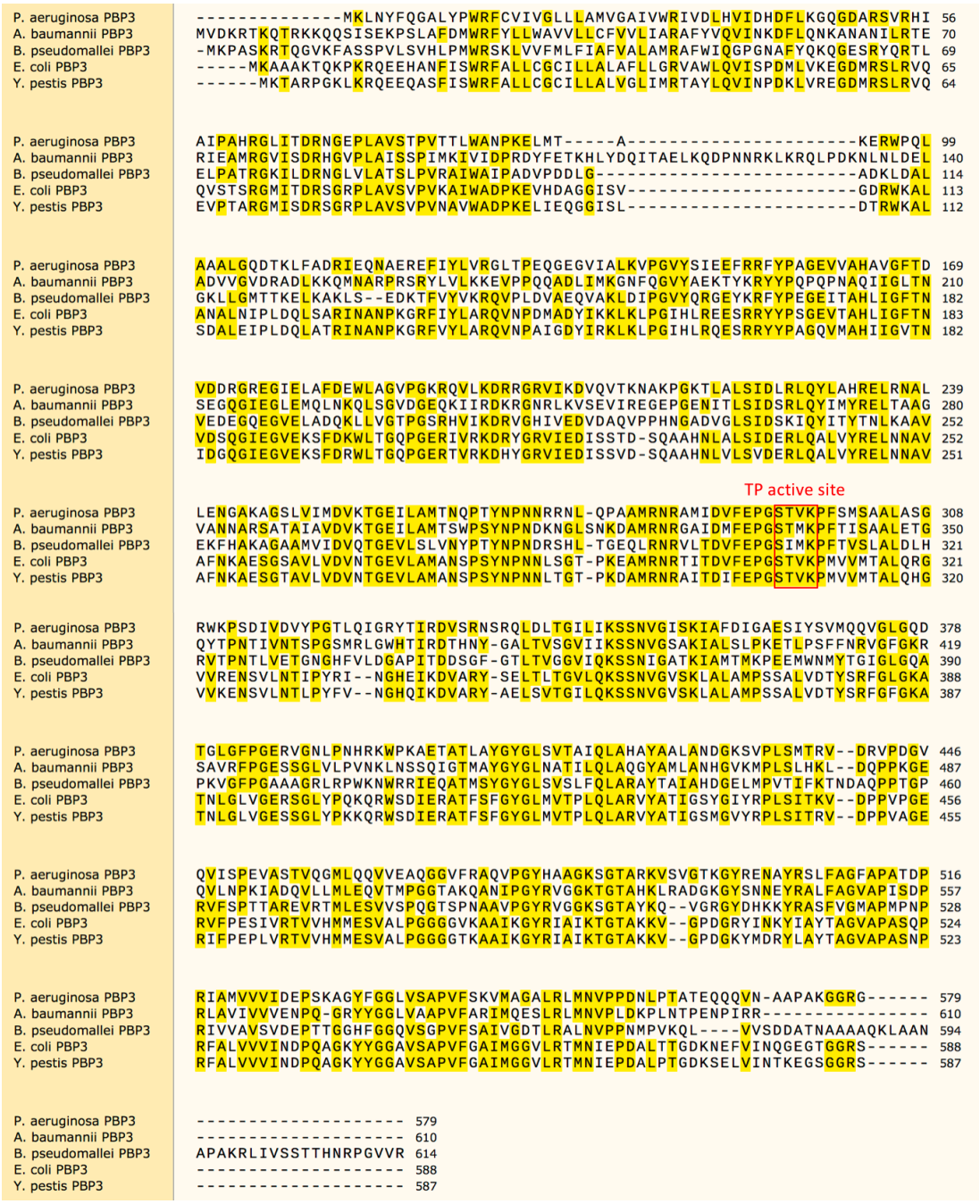

Figure 6.11 Gram-negative PBP3 sequence alignment.
Sequence alignment between PBP3 homologues in *P. aeruginosa*, *A baumannii*, *B. pseudomallei*, *E. coli* and *Y. pestis.* Identical residues between the homologues are highlighted in yellow and the transpeptidase active site is boxed in red.

Only *Acinetobacter baumannii* was found to have any PBP3 activity in the D-Ala release assay, although it was considerably less active in the same conditions than *P. aeruginosa* PBP3. *Burkholderia pseudomallei, E. coli* and *Y. Pestis* PBP3 homologues were all found to be inactive in the conditions tested (Figure 6.12).

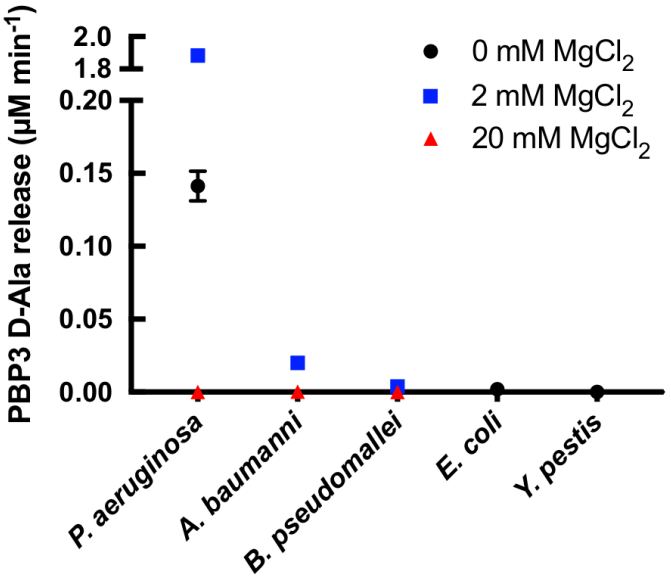

Figure 6.12 Gram-negative PBP3 activity.
PBP3 activity was assayed using the amplex red assay for D-Ala release *in vitro,* shown as initial rates. Reactions consisting of 50 mM Bis-Tris propane pH 8.5, 6 mM NaCl, varied $MgCl_2$, 1% (v/v) glycerol, 0.130% (v/v) Triton X-100, amplex red coupling reagents, 20 μM Lipid II (acetylated DAP), 50 nM *E. coli* PBP1b S510A (PBP1b*) and 2 μM LpoB. Glycan chain accumulation was allowed to proceed for 5 mins before the addition of 325 nM PBP3 homologue (n=1, apart from *P. aeruginosa* where n=3).

6.4 Discussion and future work

6.4.1 *P. aeruginosa* PBP3 substrate utilisation

P. aeruginosa PBP3 was successfully able to utilise glycan polymers produced by *E. coli* PBP1b S510A, a non-cognate polymerase from another Gram-negative organism. Other class B PBPs have similarly been reported to utilise glycan polymers produced by non-cognate polymerases: *S. thermophilus* PBP2x has been reported to utilise glycan polymers produced by *S. aureus* SgtB and *S. pneumoniae* PBP1a (Taguchi *et al.*, 2019), and *E. coli* PBP2 has been shown to use polymers produced by *E. coli* PBP1a (Banzhaf *et al.*, 2012). From these reports

and the data here, it is likely that class B PBP activity is not dependent on its cognate polymerase partner, but dependent on substrate recognition.

P. aeruginosa PBP3 activity was only detected in the presence of glycan polymers produced by *E. coli* PBP1b S510A, and not in its absence, confirming *P. aeruginosa* PBP3 is indeed a monofunctional enzyme that requires a polymeric donor substrate. *P. aeruginosa* PBP3 was able to utilise glycan polymers containing DAP as well as acetylated DAP, but not Lys in the third position of the pentapeptide stem. In the presence of a substrate with DAP in the third position of the pentapeptide stem *P. aeruginosa* PBP3 primarily carried out transpeptidation, but interestingly acetylating the DAP peptide biased *P. aeruginosa* PBP3 towards carboxypeptidation. This suggested PBP3 may preferentially carboxypeptidate over transpeptidate substrates that have previously been used as transpeptidase acceptors and are therefore acylated, a situation mimicked by the acetylation of the Lipid II donor.

Further work could be done on investigating if other substrates also bias *P. aeruginosa* PBP3 for a particular activity. We found Lipid II (L,L-acetylated DAP) was also a donor substrate utilised by *P. aeruginosa* PBP3, however it was not as well utilised as meso-acetylated DAP. It would be invaluable to assess if L,L-acetylated DAP donors biased PBP3 back towards transpeptidation, as seen by Catherwood *et al*. with *E. coli* PBP1b, who has proposed the orientation of the amine group and/or water might control the PBP1b transpeptidation:carboxypeptidation ratio (2019). Catherwood *et al.* also found *E. coli* PBP1b to discriminate against L,L-DAP containing acceptors (2019). Although we found glycan chains containing meso or L,L-DAP tetrapeptides used as acceptors caused no change to the D-Ala release rate, the reaction products should be investigated by LCMS to explore if a switch from carboxypeptidation to transpeptidation was made.

6.4.2 Ampicillin inhibition of *P. aeruginosa* PBP3

Peptidoglycan synthesis is targeted by β-lactam acylation of PBPs (Sauvage and Terrak, 2016). Here, pentapeptide (acylated DAP) glycan chains protected *P. aeruginosa* PBP3 from ampicillin, suggesting they competed for the transpeptidation site. Exposure of *P. aeruginosa* PBP3 to ampicillin inhibited carboxypeptidation with an IC_{50} of 1.496 ± 0.083 μM, similar to previous reports from other PBP3s (Papp-Wallace *et al.*, 2012), but ~20-fold lower than the ampicillin IC_{50} for *E. coli* and *Y. pestis* PBP1b (this work, and Lloyd A., personal communication).

6.4.3 Effect of divalent cations and EDTA on *P. aeruginosa* PBP3 activity

P. aeruginosa PBP3 D-Ala release was found to be adversely affected by divalent metal ion concentrations above 2 mM and EDTA. This was found not to be due to substrate availability by *E. coli* PBP1b S510A, as PBP1b was not negatively affected by increasing divalent metal ion concentrations up to 20 mM and still polymerising glycan chains at 12 mM EDTA. This indicated that *P. aeruginosa* PBP3 activity is directly sensitive to divalent metal ions or their absence. Divalent metal ions may affect PBP3 catalysis directly or affect the specificity of PBP3 for its substrate. Given transpeptidation has not been found to require the presence of a metal ion (Nagarajan and Pratt, 2004; Kumar and Pratt, 2005), and peptidoglycan is known to bind metal ions like Mg^{+} (Beveridge and Koval, 1981; Hoyle and Beveridge, 1984; Kern *et al.*, 2010), it is likely that metal ions alter the availability of the glycan polymer substrate to PBP3, by altering the structure of the substrate.

Although unlikely to contribute, the effect of the anion should be ruled out, for example by determining the effect of NaCl of *P. aeruginosa* PBP3 activity.

6.4.4 Effect of the glycan polymer substrate and *E. coli* PBP1b interaction on *P. aeruginosa* PBP3 activity

P. aeruginosa PBP3 had no clear preference for a particular length of glycan chain substrate, however it appeared unable to use very short cleaved glycan chains. Glycan chains also did not have to be actively polymerising to be a substrate for PBP3, suggesting it does not have to function in concert with a polymerase. This was also confirmed by PBP3 activity not being dependent on an interaction with a polymerase. Reports of other monofunctional transpeptidase *in vitro* activity have also found them to be active with glycan chain substrates produced by multiple polymerases (Banzhaf *et al.*, 2012; Taguchi *et al.*, 2019), supporting the case that PBP3 does not require an interaction with a polymerase for activity.

6.4.5 Other Gram-negative bacterial PBP3 *in vitro* activity

A. baumannii, B. pseudomallei, E. coli and *Y. Pestis* PBP3 homologues were also tested for their *in vitro* activity, as all have been shown to acylate nitrocefin and bocillin (Newman H. and Bellini D., unpublished)(Shapiro *et al.*, 2013) and share sequence homology with *P. aeruginosa* PBP3 (Figure 6.11). However only *A. baumannii* PBP3 was shown to have any activity in the D-ala release assay. This indicates that although the PBP3 proteins share a high sequence homology, they must differ in substrate specificity or buffer conditions for activity. Investigating *A. baumannii* PBP3 activity further would elucidate if the metal ion sensitivity and substrate specificity of *P. aeruginosa* PBP3 was specific to *P. aeruginosa* or a more generalised phenomenon.

6.4.6 Future work

As well as the future work already described from the results in this chapter confirming if *P. aeruginosa* PBP3 activity is affected by the polymerase producing its substrate would be valuable. Purifying *P. aeruginosa* PBP1b and LpoP was attempted: LpoP (123-259 (equivalent length of *E. coli* LpoB (78-213)) was

successfully purified, however *P. aeruginosa* PBP1b (16-740 equivalent length of *E. coli* PBP1b (58-804)) was more difficult, and found to be insoluble. However, with optimisation *P. aeruginosa* PBP1b and LpoP could be purified, as previously reported (Greene *et al.*, 2018), and its effects on *P. aeruginosa* PBP3 activity established. This could be compared to the effect it's cognate polymerase, FtsW (Taguchi *et al.*, 2019), has on its activity *in vitro*.

6.5 Conclusions

To our knowledge this study reports the first observation of PBP3 carboxypeptidase and transpeptidase activity *in vitro* using native substrates. *P. aeruginosa* PBP3 was shown to cross-link glycan polymers produced by a transpeptidase inactive *E. coli* PBP1b S510A. *P. aeruginosa* PBP3 activity was detected provided PBP1b had polymerised the glycan chain substrates, however neither active polymerisation, or an interaction with PBP1b was required for PBP3 activity. With glycan chains containing DAP in the 3rd position of the pentapeptide stem *P. aeruginosa* PBP3 was primarily a transpeptidase, however upon acetylating the DAP, PBP3 activity switched to primarily carboxypeptidation.

7. General conclusions

The discovery of penicillin and its ability to inhibit PBPs and cause bacterial lysis commenced the golden age of antibiotic discovery. Since then, PBPs have proven to be one of the most important antibiotic targets identified. Drug resistant bacteria threaten the effectiveness of our current antibiotics and could reverse the advances medicine has achieved. Therefore, in addition to a coordinated effort to increase awareness of antibiotic resistance, reduce inappropriate use of current antibiotics and improve infection diagnosis, it is vital new antibiotics are developed. A better understanding of the function and regulation of PBPs in different organisms is required to reveal novel ways to inhibit these validated targets. This study elucidates the enzymology and regulation of PBP1b and PBP3 from Gram-negative organisms *E. coli*, *Y. pestis* and *P. aeruginosa*.

Proteins of the divisome complex are thought to interact with PBP1b to coordinate its peptidoglycan synthesising activity (Müller *et al.*, 2007; Paradis-Bleau *et al.*, 2010; Gray *et al.*, 2015). The direct protein-protein interactions between *E. coli* and *Y. pestis* PBP1b and divisome proteins LpoB, CpoB and FtsN were confirmed by AUC in this study (Figure 7.1). Using a novel *in vitro* continuous transpeptidase assay developed by Catherwood *et al.* (2019), the essentiality of LpoB for PBP1b transpeptidase activity was demonstrated, replicating findings by Catherwood *et al.* (2019) with *E. coli* PBP1b, and showing this level of regulation also applies to *Y. pestis* PBP1b (Figure 7.1). The essentiality of LpoB for PBP1b activity has previously only been demonstrated *in vivo* (Paradis-Bleau *et al.*, 2010; Typas *et al.*, 2010) and was inconsistent with its modest impact *in vitro* (Egan *et al.*, 2014; Lupoli *et al.*, 2014; Egan *et al.*, 2018). These findings highlight the importance of continuous *in vitro* assays for assessing the effect of regulators on PBP activity, and reveals novel ways to block PBP function for therapeutic purposes. The demonstration of *Y. pestis* PBP1b *in vitro* activity also enables the development of inhibitor screening platforms against this bacterial target.

This study also found the *E. coli* and *Y. pestis* FtsN-PBP1b interaction to inhibit activated PBP1b activity (Figure 7.1). Where exactly a reduction in peptidoglycan synthesis fits into the cell division process is yet to be determined. It may be implemented during hydrolase cleavage of the septum. This study also demonstrates that not all proteins found to interact with PBP1b have a role affecting its activity, as we found with *E. coli* and *Y. pestis* CpoB (Figure 7.1). The function of a link between PBP1b and the outer membrane through CpoB is therefore yet to be fully understood, but it reveals an important additional layer in the intricate network of interactions in the divisome. Further study of the mechanisms by which accessory factors influence PBP activity is likely to reveal novel ways to target PBP activity. Importantly, PBP regulation appears to have a high degree of homology among different Gram-negative organisms, which would allow for the development of broad-spectrum inhibitors.

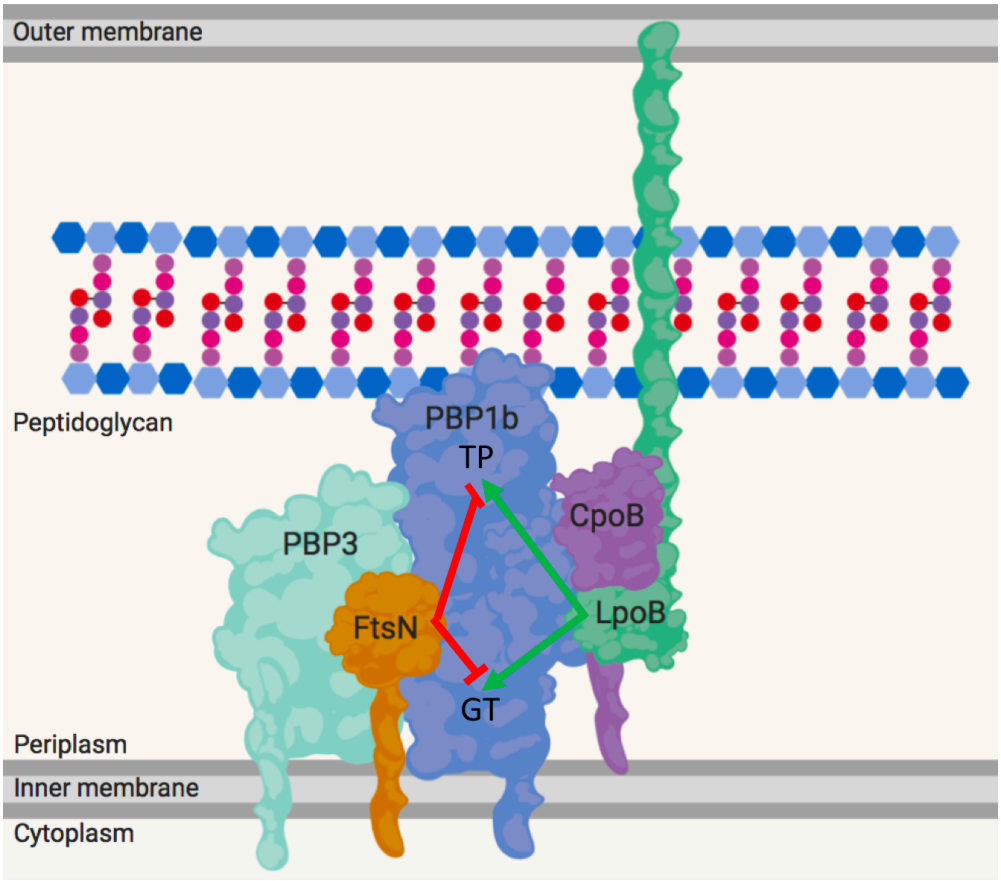

Figure 7.1 Regulation of *E. coli* and *Y. pestis* PBP1b through protein-protein interactions.
Scheme of the direct interactions of the peptidoglycan synthetase PBP1b in *E. coli* and *Y. pestis* and their effects on PBP1b activity. Green lines: stimulation of LpoB on PBP1b activity and red lines: negative modulation of FtsN on PBP1b enzyme activity.

The work in this study also led to the observation of non-enzymatic glycan chain cleavage, involving hydrolysis of the glycosidic bond between MurNAc and GlcNAc, catalysed by metal ions. This phenomenon highlights the stabilising influence cross-linking has on the peptidoglycan structure.

The recent discovery of SEDS protein RodA and FtsW as glycosyltransferases (Meeske *et al.*, 2016; Taguchi *et al.*, 2019) has elucidated the importance of the FtsW-PBP3 interaction, suggesting they act as a peptidoglycan synthase complex, mirroring the RodA-PBP2 complex. However, even with this knowledge *in vitro* PBP3 activity with native substrates is elusive. We demonstrate the first observations of *P. aeruginosa* PBP3 *in vitro* activity, and show it can utilise native glycan chains produced by PBP1b, with substrate modifications biasing PBP3 towards transpeptidation or carboxypeptidation. Continued dissection of the dynamic, multi-enzyme complex that is the divisome, including investigation of which interactions occur simultaneously and their impact on the enzymology of the complex, will provide greater understanding of the molecular mechanisms that govern divisome functions, underpinning bacterial proliferation and pathogenesis.

8. Bibliography

Adam, M., Damblon, C., Jamin, M., Zorzi, W., Dusart, V., Galleni, M., *et al.* (1991) Acyltransferase activities of the high-molecular-mass essential penicillin-binding proteins. *Biochem J* **279**: 601–604.

Alm, R.A., Johnstone, M.R., and Lahiri, S.D. (2015) Characterization of *Escherichia coli* NDM isolates with decreased susceptibility to aztreonam/avibactam: role of a novel insertion in PBP3. *J Antimicrob Chemother* **70**: 1420–1428.

Álvarez, R., López Cortés, L.E., Molina, J., Cisneros, J.M., and Pachón, J. (2016) Optimizing the Clinical Use of Vancomycin. *Antimicrob Agents Chemother* **60**: 2601–2609.

Aminov, R.I. (2010) A Brief History of the Antibiotic Era: Lessons Learned and Challenges for the Future. *Front Microbiol* **1**: 1–7.

Baisa, G., Stabo, N.J., and Welch, R.A. (2013) Characterization of *Escherichia coli* D-cycloserine transport and resistant mutants. *J Bacteriol* **195**: 1389–1399.

Banzhaf, M., Berg van Saparoea, B. van den, Terrak, M., Fraipont, C., Egan, A., Philippe, J., *et al.* (2012) Cooperativity of peptidoglycan synthases active in bacterial cell elongation. *Mol Microbiol* **85**: 179–194.

Barreteau, H., Kovač, A., Boniface, A., Sova, M., Gobec, S., and Blanot, D. (2008) Cytoplasmic steps of peptidoglycan biosynthesis. *FEMS Microbiol Rev* **32**: 168–207.

Barrett, D., Leimkuhler, C., Chen, L., Walker, D., Kahne, D., and Walker, S. (2005) Kinetic characterization of the glycosyltransferase module of *Staphylococcus aureus* PBP2. *J Bacteriol* **187**: 2215–2217.

Barrett, D., Wang, T.S.A., Yuan, Y., Zhang, Y., Kahne, D., and Walker, S. (2007) Analysis of glycan polymers produced by peptidoglycan glycosyltransferases. *J Biol Chem* **282**: 31964–31971.

Barrett, D.S., Chen, L., Litterman, N.K., and Walker, S. (2004) Expression and characterization of the isolated glycosyltransferase module of *Escherichia coli* PBP1b. *Biochemistry* **43**: 12375–12381.

Bassetti, M., Vena, A., Croxatto, A., Righi, E., and Guery, B. (2018) How to manage *Pseudomonas aeruginosa* infections. *Drugs Context* **7**: 212527.

Bellido, F., Veuthey, C., Blaser, J., Banernfeind, A., and Pechére, J.C. (1990) Novel resistance to imipenem associated with an altered PBP-4 in a *Pseudomonas aeruginosa* clinical isolate. *J Antimicrob Chemother* **25**: 57–68.

Bernhardt, T.G., and Boer, P.A.J. De (2003) The *Escherichia coli* amidase AmiC is a periplasmic septal ring component exported via the twin-arginine transport pathway. *Mol Microbiol* **48**: 1171–1182.

Bertsche, U., Breukink, E., Kast, T., and Vollmer, W. (2005) *In vitro* murein (peptidoglycan) synthesis by dimers of the bifunctional transglycosylase-transpeptidase PBP1B from *Escherichia coli*. *J Biol Chem* **280**: 38096–38101.

Bertsche, U., Kast, T., Wolf, B., Fraipont, C., Aarsman, M.E.G., Kannenberg, K., *et al.* (2006) Interaction between two murein (peptidoglycan) synthases, PBP3 and PBP1B, in *Escherichia coli*. *Mol Microbiol* **61**: 675–690.

Beveridge, T.J., and Koval, S.F. (1981) Binding of metals to cell envelopes of *Escherichia coli* K-12. *Appl Environ Microbiol* **42**: 325–335.

Beveridge, T.J., and Murray, R.G.E. (1976) Uptake and Retention of Metals by cell Walls of *Bacillus subtilis*. *J Bacteriol* **127**: 1502–1518.

Bhullar, K., Waglechner, N., Pawlowski, A., Koteva, K., Banks, E.D., Johnston, M.D., *et al.* (2012) Antibiotic resistance is prevalent in an isolated cave microbiome. *PLoS One* **7**: e34953.

Bibi, S. (2010) Fabrication and use of D-serine biosensors for characterising D-serine signalling in rat brain. .

Blaauwen, T. Den, Aarsman, M.E.G., Vischer, N.O.E., and Nanninga, N. (2003) Penicillin-binding protein PBP2 of *Escherichia coli* localizes preferentially in the lateral wall and at mid-cell in comparison with the old cell pole. *Mol Microbiol* **47**: 539–547.

Blair, J.M.A., Webber, M.A., Baylay, A.J., Ogbolu, D.O., and Piddock, L.J. V (2015) Molecular mechanisms of antibiotic resistance. *Nat Rev Microbiol* **13**: 42–51.

Blaskovich, M.A.T., Butler, M.S., and Cooper, M.A. (2017) Polishing the tarnished silver bullet: the quest for new antibiotics. *Essays Biochem* **61**: 103–114.

Boes, A., Olatunji, S., Breukink, E., and Terrak, M. (2019) Regulation of the Peptidoglycan Polymerase Activity of PBP1b by Antagonist Actions of the Core Divisome Proteins FtsBLQ and FtsN. *MBio* **10**: e01912-18.

Born, P., Breukink, E., and Vollmer, W. (2006) *In vitro* synthesis of cross-linked murein and its attachment to sacculi by PBP1A from *Escherichia coli*. *J Biol Chem* **281**: 26985–26993.

Bottat, G.A., Park, J.T., Botta, G.A., and Park, J.T. (1981) Evidence for involvement of penicillin-binding protein 3 in murein synthesis during septation but not during cell elongation. *J Bacteriol* **145**: 333–340.

Bouhss, A., Trunkfield, A.E., Bugg, T.D.H., and Mengin-Lecreulx, D. (2008) The biosynthesis of peptidoglycan lipid-linked intermediates. *FEMS Microbiol Rev* **32**: 208–233.

Breukink, E., Heusden, H.E. Van, Vollmerhaus, P.J., Swiezewska, E., Brunner, L., Walker, S., *et al.* (2003) Lipid II is an intrinsic component of the pore induced by nisin in bacterial membranes. *J Biol Chem* **278**: 19898–19903.

Budd, A., Blandin, S., Levashina, E.A., and Gibson, T.J. (2004) Bacterial α2-macroglobulins: colonization factors acquired by horizontal gene transfer from the metazoan genome? *Genome Biol* **5**: R38.

Bury, D., Dahmane, I., Derouaux, A., Dumbre, S., Herdewijn, P., Matagne, A., *et al.* (2015) Positive cooperativity between acceptor and donor sites of the peptidoglycan glycosyltransferase. *Biochem Pharmacol* **93**: 141–150.

Bush, L.M., and Perez, M.T. (2012) The Anthrax Attacks 10 years Later. *Ann Intern Med* **157**: 41–44.

Busiek, K.K., and Margolin, W. (2014) A role for FtsA in SPOR-independent localization of the essential *Escherichia coli* cell division protein FtsN. *Mol Microbiol* **92**: 1212–1226.

Butler, T. (2009) Plague into the 21st Century. *Clin Infect Dis* **49**: 736–742.

Byrne, W.R., Welkos, S.L., Pitt, M.L., Davis, K.J., Brueckner, R.P., Ezzell, J.W., *et al.* (1998) Antibiotic Treatment of Experimental Pneumonic Plague in Mice. *Antimicrob Agents Chemother* **42**: 675–681.

Campoli-Richards, D.M., Brogden, R.N., and Faulds, D. (1990) Teicoplanin. *Drugs* **40**: 449–486.

Canton, J., Khezri, R., Glogauer, M., and Grinstein, S. (2014) Contrasting phagosome pH regulation and maturation in human M1 and M2 macrophages. *Mol Biol Cell* **25**: 3330–3341.

Castañeda-García, A., Blázquez, J., and Rodríguez-Rojas, A. (2013) Molecular mechanisms and clinical impact of acquired and intrinsic fosfomycin resistance. *Antibiotics* **2**: 217–236.

Catherwood, A.C., Lloyd, A.J., Tod, J.A., Chauhan, S., Susan, E., Walkowiak, G., *et al.* (2019) Substrate and stereochemical control of peptidoglycan crosslinking by *Escherichia coli* penicillin-binding protein 1B. *(submitted)* .

Centre for Disease Control and Prevention (2000) Biological and chemical terrorism: strategic plan for preparedness and response. Recommendations of the CDC Strategic Planning Workgroup. *MMWR Recomm reports* **49**: 1–14.

Chen, L., Walker, D., Sun, B., Hu, Y., Walker, S., and Kahne, D. (2003) Vancomycin analogues active against vanA-resistant strains inhibit bacterial transglycosylase without binding substrate. *Proc Natl Acad Sci U S A* **100**: 5658–63.

Cho, H., Wivagg, C.N., Kapoor, M., Barry, Z., Rohs, P.D.A., Suh, H., *et al.* (2016) Bacterial cell wall biogenesis is mediated by SEDS and PBP polymerase families functioning semi-autonomously. *Nat Microbiol* **1**: 16172.

Clark, S.T., Sinha, U., Zhang, Y., Wang, P.W., Donaldson, S.L., Coburn, B., *et al.* (2019) Penicillin-binding protein 3 is a common adaptive target among *Pseudomonas aeruginosa* isolates from adult cystic fibrosis patients treated with β-lactams. *Int J Antimicrob Agents* **53**: 620–628.

Clarke, T.B., Kawai, F., Park, S.Y., Tame, J.R., Dowson, C.G., and Roper, D.I. (2009) Mutational analysis of the substrate specificity of *Escherichia coli* penicillin-binding protein 4. *Biochemistry* **48**: 2675–2683.

Coates, A., Hu, Y., Bax, R., and Page, C. (2002) The future challenges facing the development of new antimicrobial drugs. *Nat Rev Drug Discov* **1**: 895–910.

Dawson, R.M.C., Elliot, D.C., Elliot, W.H., and Jones, K.M. (1986) *DATA for Biochemical Research*. 3rd ed., Clarendon Press, Oxford.

Derouaux, A., Wolf, B., Fraipont, C., Breukink, E., Nguyen-Distèche, M., and Terrak, M. (2008) The monofunctional glycosyltransferase of *Escherichia coli* localizes to the cell division site and interacts with penicillin-binding protein 3, FtsW, and FtsN. *J Bacteriol* **190**: 1831–1834.

Doherty, E.A., and Doudna, J.A. (2000) Ribozyme Structures and Mechanisms. *Annu Rev Biophys Biomol Struct* **69**: 597–615.

Du, S., and Lutkenhaus, J. (2017) Assembly and activation of the *Escherichia coli* divisome. *Mol Microbiol* **105**: 177–187.

Easterday, W.R., Kausrud, K.L., Star, B., Heier, L., Haley, B.J., Ageyev, V., *et al.*

(2012) An additional step in the transmission of *Yersinia pestis*? *ISME J* **6**: 231–236.

Ebel, C., Møller, J. V., and Maire, M. le (2008) Analytical Ultracentrifugation: Membrane Protein Assemblies in the Presence of Detergent. In *Biophysical Analysis of Membrane Proteins: Investigating Structure and Function*. pp. 89–120.

Egan, A.J.F., Biboy, J., van't Veer, I., Breukink, E., and Vollmer, W. (2015) Activities and regulation of peptidoglycan synthases. *Philos Trans R Soc Biol Sci* **370**: 20150031.

Egan, A.J.F., Jean, N.L., Koumoutsi, A., Bougault, C.M., Biboy, J., Sassine, J., *et al.* (2014) Outer-membrane lipoprotein LpoB spans the periplasm to stimulate the peptidoglycan synthase PBP1B. *Proc Natl Acad Sci* **111**: 8197–8202.

Egan, A.J.F., Maya-Martinez, R., Ayala, I., Bougault, C.M., Banzhaf, M., Breukink, E., *et al.* (2018) Induced conformational changes activate the peptidoglycan synthase PBP1B. *Mol Microbiol* **110**: 335–356.

Egan, A.J.F., and Vollmer, W. (2016) Continuous Fluorescence Assay for Peptidoglycan Glycosyltransferases. In *Bacterial Cell Wall Homeostatsis*. Humana Press, New York, NY, pp. 171–184.

European Centre for Disease Prevention and Control (2017) Surveillance of antimicrobial resistance in Europe. *Annu Rep Eur Antimicrob Resist Surveill Netw* 1–97.

Ferreira, R.C., Park, J.T., Camelo, D., Almeida, D.F. De, and Ferreira, L.C. (1995) Interactions of *Yersinia pestis* penicillin-binding proteins with beta-lactam antibiotics. *Antimicrob Agents Chemother* **39**: 1853–5.

Ferreira, R.C.C., Park, J.T.J., and Ferreira, L.C.S. (1994) Plasmid regulation and temperature-sensitive behaviour of the *Yersinia pestis* penicillin-binding proteins. *Infect Immun* **62**: 2404–2408.

Fleming, A. (1929) On the antibacterial action of cultures of a penicillium, with special reference to their use in the isolation of *B. influenzae*. *Br J Exp Pathol* **10**: 226–236.

Fleming, A. (1945) Nobel Lecture: Penicillin. *Nobel Lect Physiol or Med 1942-1962* 83–93.

Fleming, K.G. (2016) Applications of analytical ultracentrifugation to membrane proteins. In *Analytical Ultracentrifugation: Instrumentation, Software, and Applications*. pp. 311–327.

Fraipont, C., Alexeeva, S., Wolf, B., Ploeg, R. Der, Schloesser, M., Blaauwen, T. Den, and Nguyen-Distèche, M. (2011) The integral membrane FtsW protein and peptidoglycan synthase PBP3 form a subcomplex in *Escherichia coli*. *Microbiology* **157**: 251–259.

Galimand, M., Carniel, E., and Courvalin, P. (2006) Resistance of *Yersinia pestis* to antimicrobial agents. *Antimicrob Agents Chemother* **50**: 3233–6.

Galimand, M., Guiyoule, A., Gerbaud, G., Rasoamanana, B., Chanteau, S., Carniel, E., and Courvalin, P. (1997) Multidrug Resistance in *Yersinia pestis* Mediated by a Transferable Plasmid. *N Engl J Med* **337**: 677–681.

Galley, N.F., O'Reilly, A.M., and Roper, D.I. (2014) Prospects for novel inhibitors of peptidoglycan transglycosylases. *Bioorg Chem* **55**: 16–26.

Garcia, F., Portillo, D., and Pedro, M.A. De (1991) Penicillin-Binding Protein 2 Is Essential for the Integrity of Growing Cells of *Escherichia coli* ponB Strains. *J Bacteriol* **173**: 4530–4532.

Garcia, F., Portillo, D., Pedro, Miguel A De, Garcia Del Portillo, F., Pedro, M A De, Joseleau-Petit, D., *et al.* (1990) Differential Effect of Mutational Impairment of Penicillin-Binding Proteins lA and 1B on *Escherichia coli* Strains Harboring Thermosensitive Mutations in the Cell Division Genes ftsA, ftsQ, ftsZ, and pbpB. *J Bacteriol* **172**: 5863–5870.

Gerding, M.A., Liu, B., Bendezú, F.O., Hale, C.A., Bernhardt, T.G., and Boer, P.A.J. De (2009) Self-enhanced accumulation of FtsN at division sites and roles for other proteins with a SPOR domain (DamX, DedD, and RlpA) in *Escherichia coli* cell constriction. *J Bacteriol* **191**: 7383–7401.

Gerding, M.A., Ogata, Y., Pecora, N.D., Niki, H., and Boer, P.A.J. De (2007) The trans-envelope Tol-Pal complex is part of the cell division machinery and required for proper outer-membrane invagination during cell constriction in *E. coli*. *Mol Microbiol* **63**: 1008–1025.

Ghuysen, J.M. (1991) Serine beta-lactamases and penicillin-binding proteins. *Annu Rev Microbiol* **45**: 37–67.

Glauner, B., and Entwi, iir (1988) Separation and Quantification of Muropeptides with High-Performance Liquid Chromatography. *Anal Biochem* **172**: 451–464.

Glauner, B., and Holtje, J. V. (1990) Growth pattern of the murein sacculus of *Escherichia coli*. *J Biol Chem* **265**: 18988–18996.

Glauner, B., Holtje, J. V., and Schwarz, U. (1988) The composition of the murein of *Escherichia coli*. *J Biol Chem* **263**: 10088–10095.

Goffin, C., and Ghuysen, J.M. (1998) Multimodular penicillin-binding proteins: an enigmatic family of orthologs and paralogs. *Microbiol Mol Biol Rev* **62**: 1079–93.

Goffin, C., and Ghuysen, J.M. (2002) Biochemistry and comparative genomics of SxxK superfamily acyltransferases offer a clue to the mycobacterial paradox: presence of penicillin-susceptible target proteins versus lack of efficiency of penicillin as therapeutic agent. *Microbiol Mol Biol Rev* **66**: 702–738.

Gotoh, N., Nunomura, K., and Nishino, T. (1990) Resistance of *Pseudomonas aeruginosa* to cefsulodin: modification of penicillin-binding protein 3 and mapping of its chromosomal gene. *J Antimicrob Chemother* **25**: 513–523.

Gram, H.C. (1884) Über die isolierte Färbung der Schizomyceten in Schnitt- und

Trockenpräparaten. *Fortschr Med* **2**: 185–189.

Gray, A.N., Egan, A.J.F., van't Veer, I.L., Verheul, J., Colavin, A., Koumoutsi, A., *et al.* (2015) Coordination of peptidoglycan synthesis and outer membrane constriction during *Escherichia coli* cell division. *Elife* **4**: 1–29.

Greene, N.G., Fumeaux, C., and Bernhardt, T.G. (2018) Conserved mechanism of cell-wall synthase regulation revealed by the identification of a new PBP activator in *Pseudomonas aeruginosa*. *Proc Natl Acad Sci* **115**: 3150–3155.

Guiyoule, A., Gerbaud, G., Buchrieser, C., Galimand, M., Rahalison, L., Chanteau, S., *et al.* (2001) Transferable plasmid-mediated resistance to streptomycin in a clinical isolate of *Yersinia pestis*. *Emerg Infect Dis* **7**: 43–8.

Hancock, R.E.W. (1998) Resistance Mechanisms in *Pseudomonas aeruginosa* and Other Nonfermentative Gram-Negative Bacteria. *Clin Infect Dis* **27**: S93–S99.

Harz, H., Burgdorf, K., and Hijltje, J.V. (1990) Isolation and Separation of the Glycan Strands from Murein of *Escherichia coli* by Reversed-Phase High-Performance Liquid Chromatography. *Anal Biochem* **190**: 120–128.

Hawkey, P.M., Warren, R.E., Livermore, D.M., McNulty, C.A.M., Enoch, D.A., Otter, J.A., and Wilson, A.P.R. (2018) Treatment of infections caused by multidrug-resistant Gram-negative bacteria: report of the British Society for Antimicrobial Chemotherapy/Healthcare Infection Society/British Infection Association Joint Working Party. *J Antimicrob Chemother* **73**: iii2–iii78.

Heidrich, C., Templin, M.F., Ursinus, A., Merdanovic, M., Berger, J., Schwarz, H., *et al.* (2001) Involvement of N-acetylmuramyl-l-alanine amidases in cell separation and antibiotic-induced autolysis of *Escherichia coli*. *Mol Microbiol* **41**: 167–178.

Heijenoort, J. van (2011) Peptidoglycan Hydrolases of *Escherichia coli*. *Microbiol Mol Biol Rev* **75**: 636–663.

Heijenoort, Y. Van, Gomez, M., Derrien, M., Ayala, J., and Heijenoort, J. Van (1992)

Membrane intermediates in the peptidoglycan metabolism of *Escherichia coli*: Possible roles of PBP 1b and PBP 3. *J Bacteriol* **174**: 3549–3557.

Helassa, N., Vollmer, W., Breukink, E., Vernet, T., and Zapun, A. (2012) The membrane anchor of penicillin-binding protein PBP2a from *Streptococcus pneumoniae* influences peptidoglycan chain length. *FEBS J* **279**: 2071–2081.

Hernandez, E., Girardet, M., Ramisse, F., Vidal, D., and Cavallo, J.D. (2003) Antibiotic susceptibilities of 94 isolates of *Yersinia pestis* to 24 antimicrobial agents. *J Antimicrob Chemother* **52**: 1029–1031.

Holtje, J. V., and Tuomanen, E.I. (1991) The murein hydrolases of *Escherichia coli*: Properties, functions and impact on the course of infections *in vivo*. *J Gen Microbiol* **137**: 441–454.

Holtje, J. V, Mirelman, D., Sharon, N., and Schwarz, U. (1975) Novel Type of Murein Transglycosylase in *Escherichia coli*. *J Bacteriol* **124**: 1067–1076.

Höltje, J.V. (1995) From growth to autolysis: the murein hydrolases in *Escherichia coli*. *Arch Microbiol* **164**: 243–254.

Höltje, J.V., and Holtje, J. V (1998) Growth of the stress-bearing and shape-maintaining murein sacculus of *Escherichia coli*. *Microbiol Mol Biol Rev* **62**: 181–203.

Hoyle, B.D., and Beveridge, T.J. (1984) Metal binding by the peptidoglycan sacculus of *Escherichia coli* K-12. *Can J Microbiol* **30**: 204–211.

Inglesby, T. V., Dennis, D.T., Henderson, D.A., Bartlett, J.G., Ascher, M.S., Eitzen, E., *et al.* (2000) Plague as a biological weapon: medical and public health management. *JAMA* **283**: 2281–2290.

Jonge, R., Takumi, K., Ritmeester, W.S., and Leusden, F.M. (2003) The adaptive response of *Escherichia coli* O157 in an environment with changing pH. *J Appl Microbiol* **94**: 555–560.

Jovetic, S., Zhu, Y., Marcone, G.L., Marinelli, F., and Tramper, J. (2010) β-Lactam and glycopeptide antibiotics: First and last line of defense? *Trends Biotechnol* **28**: 596–604.

Kaper, J.B., Nataro, J.P., and Mobley, H.L.T. (2004) Pathogenic *Escherichia coli*. *Nat Rev Microbiol* **2**: 123–140.

Keck, W., Leeuwen, A.M. Van, Huber, M., and Goodell, E.W. (1990) Cloning and characterization of mepA, the structural gene of the penicillin-insensitive murein endopeptidase from *Escherichia coli*. *Mol Microbiol* **4**: 209–219.

Kern, T., Giffard, M., Hediger, S., Amoroso, A., Giustini, C., Bui, N.K., *et al.* (2010) Dynamics characterization of fully hydrated bacterial cell walls by solid-state NMR: Evidence for cooperative binding of metal ions. *J Am Chem Soc* **132**: 10911–10919.

Khomenko, V.A., Solovieva, T.F., and Ovodov, Y.S. (1980) Peptidoglycan from *Yersinia pseudotuberculosis*: isolation and general characterization. *Microbios* **27**: 15–8.

Kim, S., Pires, M.M., and Im, W. (2018) Insight into Elongation Stages of Peptidoglycan Processing in Bacterial Cytoplasmic Membranes. *Sci Rep* **8**: 17704.

King, D.T., Wasney, G.A., Nosella, M., Fong, A., and Strynadka, N.C.J. (2017) Structural Insights into Inhibition of *Escherichia coli* Penicillin-binding Protein 1B. *J Biol Chem* **292**: 979–993.

Koirala, J. (2006) Plague: Disease, Management, and Recognition of Act of Terrorism. *Infect Dis Clin North Am* **20**: 273–287.

Konovalova, A., Kahne, D.E., and Silhavy, T.J. (2017) Outer Membrane Biogenesis. *Annu Rev Microbiol* **71**: 539–556.

Korat, B., Mottl, ' H, and Keck^, W. (1991) Penicillin-binding protein 4 of *Eschenchia coli*: molecular cloning of the dacB gene, controlled overexpression,

and alterations in murein composition. .

Krachler, A.M., Sharma, A., Cauldwell, A., Papadakos, G., and Kleanthous, C. (2010) TolA Modulates the Oligomeric Status of YbgF in the Bacterial Periplasm. *J Mol Biol* **403**: 270–285.

Krachler, A.M., Sharma, A., and Kleanthous, C. (2010) Self-association of TPR domains: Lessons learned from a designed, consensus-based TPR oligomer. *Proteins Struct Funct Bioinforma* **78**: 2131–2143.

Kumar, I., and Pratt, R.F. (2005) Transpeptidation reactions of a specific substrate catalyzed by the *Streptomyces* R61 DD-peptidase: The structural basis of acyl acceptor specificity. *Biochemistry* **44**: 9961–9970.

Leclercq, S., Derouaux, A., Olatunji, S., Fraipont, C., Egan, A.J.F., Vollmer, W., *et al.* (2017) Interplay between Penicillin-binding proteins and SEDS proteins promotes bacterial cell wall synthesis. *Sci Rep* **7**: 43306.

Lee, D.S., Lee, S.J., Choe, H.S., and Giacobbe, D.R. (2018) Community-Acquired Urinary Tract Infection by *Escherichia coli* in the Era of Antibiotic Resistance. *Biomed Res Int* **2018**: 7656752.

Leeb, M. (2004) A shot in the arm. *Nature* **431**: 892–893.

Legaree, B.A., Daniels, K., Weadge, J.T., Cockburn, D., and Clarke, A.J. (2007) Function of penicillin-binding protein 2 in viability and morphology of *Pseudomonas aeruginosa*. *J Antimicrob Chemother* **59**: 411–424.

Lessard, I.A.D., Pratt, S.D., McCafferty, D.G., Bussiere, D.E., Hutchins, C., Wanner, B.L., *et al.* (1998) Homologs of the vancomycin resistance D-Ala-D-Ala dipeptidase VanX in *Streptomyces toyocaensis, Escherichia coli* and *Synechocystis*: Attributes of catalytic efficiency, stereoselectivity and regulation with implications for function. *Chem Biol* **5**: 489–504.

Lessard, I.A.D., and Walsh, C.T. (1999) VanX, a bacterial D-alanyl-D-alanine

dipeptidase: Resistance, immunity, or survival function? *Proc Natl Acad Sci U S A* **96**: 11028–11032.

Liu, B., Persons, L., Lee, L., and Boer, P.A.J. de (2015) Roles for both FtsA and the FtsBLQ subcomplex in FtsN-stimulated cell constriction in *Escherichia coli*. *Mol Microbiol* **95**: 945–970.

Lloyd, A.J., Gilbey, A.M., Blewett, A.M., Pascale, G. De, Zoeiby, A. El, Levesque, R.C., *et al.* (2008) Characterization of tRNA-dependent peptide bond formation by MurM in the synthesis of *Streptococcus pneumoniae* peptidoglycan. *J Biol Chem* **283**: 6402–6417.

Lloyd, A.J., Thomann, H.-U., Ibba, M., and Soil, D. (1995) A broadly applicable continuous spectrophotometric assay for measuring aminoacyl-tRNA synthetase activity. *Nucleic Acids Res* **23**: 2886–2892.

Lovering, A.L., Castro, L.H. de, Lim, D., and Strynadka, N.C.J. (2007) Structural Insight into the Transglycosylation Step of Bacterial Cell-Wall Biosynthesis. *Science* **315**: 1402–1405.

Lupoli, T.J., Lebar, M.D., Markovski, M., Bernhardt, T., Kahne, D., and Walker, S. (2014) Lipoprotein Activators Stimulate *Escherichia coli* Penicillin-Binding Proteins by Different Mechanisms. *J Am Chem Soc* **136**: 52–55.

Lupoli, T.J., Tsukamoto, H., Doud, E.H., Wang, T.-S.A.S.A., Walker, S., and Kahne, D. (2011) Transpeptidase-mediated incorporation of d-amino acids into bacterial peptidoglycan. *J Am Chem Soc* **133**: 10748–10751.

Magnet, S., Dubost, L., Marie, A., Arthur, M., and Gutmann, L. (2008) Identification of the L,D-Transpeptidases for Peptidoglycan Cross-Linking in *Escherichia coli*. *J Bacteriol* **190**: 4782–4785.

Markovski, M., Bohrhunter, J.L., Lupoli, T.J., Uehara, T., Walker, S., Kahne, D.E., and Bernhardt, T.G. (2016) Cofactor bypass variants reveal a conformational control mechanism governing cell wall polymerase activity. *Proc Natl Acad Sci* **113**:

4788–4793.

Matsuhashi, M., Wachi, M., and Ishino, F. (1990) Machinery for cell growth and division: Penicillin-binding proteins and other proteins. *Res Microbiol* **141**: 89–103.

Meeske, A.J., Riley, E.P., Robins, W.P., Uehara, T., Mekalanos, J.J., Kahne, D., *et al.* (2016) SEDS proteins are a widespread family of bacterial cell wall polymerases. *Nature* **537**: 634–638.

Meiresonne, N.Y., Consoli, E., Mertens, L.M.Y., Chertkova, A.O., Goedhart, J., and Blaauwen, T. den (2019) Superfolder mTurquoise2 ^{ox} optimized for the bacterial periplasm allows high efficiency *in vivo* FRET of cell division antibiotic targets. *Mol Microbiol* **111**: 1025–1038.

Meroueh, S.O., Bencze, K.Z., Hesek, D., Lee, M., Fisher, J.F., Stemmler, T.L., and Mobashery, S. (2006) Three-dimensional structure of the bacterial cell wall peptidoglycan. *Proc Natl Acad Sci* **103**: 4404–4409.

Mesleh, M.F., Rajaratnam, P., Conrad, M., Chandrasekaran, V., Liu, C.M., Pandya, B.A., *et al.* (2016) Targeting Bacterial Cell Wall Peptidoglycan Synthesis by Inhibition of Glycosyltransferase Activity. *Chem Biol Drug Des* **87**: 190–199.

Mohammadi, T., Dam, V. Van, Sijbrandi, R., Vernet, T., Zapun, A., Bouhss, A., *et al.* (2011) Identification of FtsW as a transporter of lipid-linked cell wall precursors across the membrane. *EMBO J* **30**: 1425–1432.

Moradali, M.F., Ghods, S., and Rehm, B.H.A. (2017) *Pseudomonas aeruginosa* lifestyle: A paradigm for adaptation, survival, and persistence. *Front Cell Infect Microbiol* **7**: 1–29.

Mueller, E.A., Egan, A.J., Breukink, E., Vollmer, W., and Levin, P.A. (2019) Plasticity of *Escherichia coli* cell wall metabolism promotes fitness and antibiotic resistance across environmental conditions. *Elife* **8**: e40754.

Müller, P., Ewers, C., Bertsche, U., Anstett, M., Kallis, T., Breukink, E., *et al.* (2007) The essential cell division protein FtsN interacts with the murein (peptidoglycan) synthase PBP1B in *Escherichia coli*. *J Biol Chem* **282**: 36394–36402.

Nagarajan, R., and Pratt, R.F. (2004) Synthesis and evaluation of new substrate analogues of *Streptomyces* R61 DD-peptidase: Dissection of a specific ligand. *J Org Chem* **69**: 7472–7478.

Nakayama, H., Kurokawa, K., and Lee, B.L. (2012) Lipoproteins in bacteria: structures and biosynthetic pathways. *FEBS J* **279**: 4247–4268.

Nelson, D.E., and Young, K.D. (2000) Penicillin Binding Protein 5 Affects Cell Diameter, Contour, and Morphology of *Escherichia coli*. *J Bacteriol* **182**: 1714–1721.

Nguyen-Disteche, M., Ghujysen, J.M., Coyette, J., Pollock, J.J., Reynolds, P., Perkins, H.R., and Salton, M.R.J. (1974) Enzymes Involved in Wall Peptide Crosslinking in *Escherichia coli* K12, Strain 44. *Eur J Biochem* **41**: 447–455.

Nozaki, Y., Katayama, N., Harada, S., Ono, H., and Okazaki, H. (1989) Lactivicin, a naturally occurring non-β-lactam antibiotic having β-lactam-like action: Biological activities and mode of action. *J Antibiot (Tokyo)* **42**: 84–93.

O'Neill, J. (2016) Tackling drug-resistant infections globally: Final report and recommendations. *Rev Antimicrob Resist* 1–81.

Offant, J., Terrak, M., Derouaux, A., Breukink, E., Nguyen-Distèche, M., Zapun, A., and Vernet, T. (2010) Optimization of conditions for the glycosyltransferase activity of penicillin-binding protein 1a from *Thermotoga maritima*. *FEBS J* **277**: 4290–4298.

Ostash, B., and Walker, S. (2010) Moenomycin family antibiotics: Chemical synthesis, biosynthesis, and biological activity. *Nat Prod Rep* **27**: 1594–1617.

Palumbi, S.R. (2001) Humans as the World's Greatest Evolutionary Force. *Science*

293: 1786–1790.

Papp-Wallace, K.M., Senkfor, B., Gatta, J., Chai, W., Taracila, M.A., Shanmugasundaram, V., *et al.* (2012) Early insights into the interactions of different β-lactam antibiotics and β-lactamase inhibitors against soluble forms of *Acinetobacter baumannii* PBP1a and *Acinetobacter* sp. PBP3. *Antimicrob Agents Chemother* **56**: 5687–5692.

Paradis-Bleau, C., Markovski, M., Uehara, T., Lupoli, T.J., Walker, S., Kahne, D.E., and Bernhardt, T.G. (2010) Lipoprotein cofactors located in the outer membrane activate bacterial cell wall polymerases. *Cell* **143**: 1110–1120.

Parkhill, J., Wren, B.W., Thomson, N.R., Titball, R.W., Holden, M.T.G., Prentice, M.B., *et al.* (2001) Genome sequence of *Yersinia pestis*, the causative agent of plague. *Nature* **413**: 523–527.

Pastoret, S., Fraipont, C., Blaauwen, T. Den, Wolf, B.B., Aarsman, M.E.G., Piette, A., *et al.* (2004) Functional Analysis of the Cell Division Protein FtsW of *Escherichia coli*. *J Bacteriol* **186**: 8370–8379.

Pazos, M., Peters, K., Casanova, M., Palacios, P., VanNieuwenhze, M., Breukink, E., *et al.* (2018) Z-ring membrane anchors associate with cell wall synthases to initiate bacterial cell division. *Nat Commun* **9**: 5090.

Pechous, R.D., Sivaraman, V., Stasulli, N.M., and Goldman, W.E. (2016) Pneumonic Plague: The Darker Side of *Yersinia pestis*. *Trends Microbiol* **24**: 190–197.

Perlstein, D.L., Zhang, Y., Wang, T.S., Kahne, D.E., and Walker, S. (2007) The direction of glycan chain elongation by peptidoglycan glycosyltransferases. *J Am Chem Soc* **129**: 12674–12675.

Peters, K., Pazos, M., Edoo, Z., Hugonnet, J.-E., Martorana, A.M., Polissi, A., *et al.* (2018) Copper inhibits peptidoglycan LD-transpeptidases suppressing β-lactam resistance due to bypass of penicillin-binding proteins. *Proc Natl Acad Sci* **115**: 10786–10791.

Piette, A., Fraipont, C., Blaauwen, T. Den, Aarsman, M.E.G., Pastoret, S., and Nguyen-Distèche, M. (2004) Structural determinants required to target penicillin-binding protein 3 to the septum of *Escherichia coli*. *J Bacteriol* **186**: 6110–7.

Pollock, T.J., Thorne, L., Yamazaki, M., Mikolajczak, M.J., and Armentrout, R.W. (1994) Mechanism of Bacitracin Resistance in Gram-Negative Bacteria That Synthesize Exopolysaccharides. *J Bacteriol* **176**: 6229–6237.

Pompliano, D., Gomez, R., and Anthony, N. (1992) Intramolecular Fluorescence Enhancement: A Continuous Assay of Ras Farnesyl:Protein Transferase. *J Am Chem Soc* **114**: 7945–7946.

Punekar, A.S., Samsudin, F., Lloyd, A.J., Dowson, C.G., Scott, D.J., Khalid, S., and Roper, D.I. (2018) The role of the jaw subdomain of peptidoglycan glycosyltransferases for lipid II polymerization. *Cell Surf* **2**: 54–66.

Qiao, Y., Srisuknimit, V., Rubino, F., Schaefer, K., Ruiz, N., Walker, S., and Kahne, D. (2017) Lipid II overproduction allows direct assay of transpeptidase inhibition by beta-lactams. *Nat Chem Biol* **13**: 793–798.

Quintela, J., Caparrós, M., and Pedro, M.A. de (1995) Variability of peptidoglycan structural parameters in Gram-negative bacteria. *FEMS Microbiol Lett* **125**: 95–100.

Reddy Bolla, J., Sauer, J.B., Wu, D., Mehmood, S., Allison, T.M., and Robinson, C. V (2018) Direct observation of the influence of cardiolipin and antibiotics on lipid II binding to MurJ. *Nat Chem* **10**: 363–371.

Rice, L.B. (2008) Federal Funding for the Study of Antimicrobial Resistance in Nosocomial Pathogens: No ESKAPE. *J Infect Dis* **197**: 1079–1081.

Rohs, P.D.A., Buss, J., Sim, S.I., Squyres, G.R., Srisuknimit, V., Smith, M., *et al.* (2018) A central role for PBP2 in the activation of peptidoglycan polymerization by the bacterial cell elongation machinery. *PLOS Genet* **14**: e1007726.

Rojas, E.R., Billings, G., Odermatt, P.D., Auer, G.K., Zhu, L., Miguel, A., *et al.* (2018) The outer membrane is an essential load-bearing element in Gram-negative bacteria. *Nature* **559**: 617–621.

Ropy, A., Cabot, G., Sánchez-Diener, I., Aguilera, C., Moya, B., Ayala, J.A., and Oliver, A. (2015) Role of *Pseudomonas aeruginosa* low-molecular-mass penicillin-binding proteins in AmpC expression, β-lactam resistance, and peptidoglycan structure. *Antimicrob Agents Chemother* **59**: 3925–3934.

Sarkar, P., Yarlagadda, V., Ghosh, C., and Haldar, J. (2017) A review on cell wall synthesis inhibitors with an emphasis on glycopeptide antibiotics. *Med Chem Commum* **8**: 516–533.

Sauvage, E., Derouaux, A., Fraipont, C., Joris, M., Herman, R., Rocaboy, M., *et al.* (2014) Crystal structure of penicillin-binding protein 3 (PBP3) from *Escherichia coli*. *PLoS One* **9**: e98042.

Sauvage, E., Kerff, F., Terrak, M., Ayala, J.A., and Charlier, P. (2008) The penicillin-binding proteins: Structure and role in peptidoglycan biosynthesis. *FEMS Microbiol Rev* **32**: 234–258.

Sauvage, E., and Terrak, M. (2016) Glycosyltransferases and Transpeptidases/Penicillin-Binding Proteins: Valuable Targets for New Antibacterials. *Antibiotics* **5**: 12.

Schägger, H., and Jagow, G. von (1987) Tricine-sodium dodecyl sulfate-polyacrylamide gel electrophoresis for the separation of proteins in the range from 1 to 100 kDa. *Anal Biochem* **166**: 368–379.

Schiffer, G., and Höltje, J.V. (1999) Cloning and characterization of PBP 1C, a third member of the multimodular class A penicillin-binding proteins of *Escherichia coli*. *J Biol Chem* **274**: 32031–32039.

Schmidt, L.S., Botta, G., and Park, J.T. (1981) Effects of furazlocillin, a β-lactam antibiotic which binds selectively to penicillin-binding protein 3, on *Escherichia*

coli mutants deficient in other penicillin-binding proteins. *J Bacteriol* **145**: 632–637.

Schuck, P. (2000) Size-Distribution Analysis of Macromolecules by Sedimentation Velocity Ultracentrifugation and Lamm Equation Modeling. .

Schuck, P. (2013) Analytical ultracentrifugation as a tool for studying protein interactions. *Biophys Rev* **5**: 159–171.

Schwartz, B., Markwalder, J.A., Seitz, S.P., Wang, Y., and Stein, R.L. (2002) A kinetic characterization of the glycosyltransferase activity of *Escherichia coli* PBP1b and development of a continuous fluorescence assay. *Biochemistry* **41**: 12552–12561.

Sham, L.-T., Butler, E.K., Lebar, M.D., Kahne, D., Bernhardt, T.G., and Ruiz, N. (2014) MurJ is the flippase of lipid-linked precursors for peptidoglycan biogenesis. *Science* **345**: 220–222.

Shapiro, A.B., Gu, R.F., Gao, N., Livchak, S., and Thresher, J. (2013) Continuous fluorescence anisotropy-based assay of BOCILLIN FL penicillin reaction with penicillin-binding protein 3. *Anal Biochem* **439**: 37–43.

Spratt, B.G. (1975) Distinct penicillin binding proteins involved in the division, elongation, and shape of *Escherichia coli* K12. *Proc Natl Acad Sci* **72**: 2999–3003.

Spratt, B.G. (1977) Temperature-sensitive cell division mutants of *Escherichia coli* with thermolabile penicillin-binding proteins. *J Bacteriol* **131**: 293–305.

Stenseth, N.C., Atshabar, B.B., Begon, M., Belmain, S.R., Bertherat, E., Carniel, E., *et al.* (2008) Plague: Past, present, and future. *PLoS Med* **5**: 9–13.

Sung, M.-T., Lai, Y.-T., Huang, C.-Y., Chou, L.-Y., Shih, H.-W., Cheng, W.-C., *et al.* (2009) Crystal structure of the membrane-bound bifunctional transglycosylase PBP1b from *Escherichia coli*. *Proc Natl Acad Sci* **106**: 8824–8829.

Suzuki, H., Nishimura, Y., and Hirota, Y. (1978) On the process of cellular division

in *Escherichia coli*: a series of mutants of *E. coli* altered in the penicillin-binding proteins. *Proc Natl Acad Sci* **75**: 664–668.

Tacconelli, E., Carrara, E., Savoldi, A., Harbarth, S., Mendelson, M., Monnet, D.L., *et al.* (2018) Discovery, research, and development of new antibiotics: the WHO priority list of antibiotic-resistant bacteria and tuberculosis. *Lancet Infect Dis* **18**: 318–327.

Taguchi, A., Welsh, M.A., Marmont, L.S., Lee, W., Kahne, D., Bernhardt, T.G., and Walker, S. (2019) FtsW is a peptidoglycan polymerase that is activated by its cognate penicillin-binding protein. *Nat Microbiol* **4**: 587–594.

Teo, A.C.K., Lee, S.C., Pollock, N.L., Stroud, Z., Hall, S., Thakker, A., *et al.* (2019) Analysis of SMALP co-extracted phospholipids shows distinct membrane environments for three classes of bacterial membrane protein. *Sci Rep* **9**: 1813.

Terrak, M., Ghosh, T.K., Heijenoort, J. van, Beeumen, J. Van, Lampilas, M., Aszodi, J., *et al.* (1999) The catalytic, glycosyl transferase and acyl transferase modules of the cell wall peptidoglycan-polymerizing penicillin-binding protein 1b of *Escherichia coli*. *Mol Microbiol* **34**: 350–364.

Terrak, M., and Nguyen-Distèche, M. (2006) Kinetic characterization of the monofunctional glycosyltransferase from *Staphylococcus aureus*. *J Bacteriol* **188**: 2528–2532.

Thulin, E., and Andersson, D.I. (2019) Upregulation of PBP1B and LpoB in cysB mutants confers mecillinam resistance in *Escherichia coli*. *Antimicrob Agents Chemother* AAC.00612-19.

Tipper, D.J., and Strominger, J.L. (1965) Mechanism of action of penicillins: a proposal based on their structural similarity to acyl-D-alanyl-D-alanine. *Proc Natl Acad Sci U S A* **54**: 1133–1141.

Turner, R.D., Mesnage, S., Hobbs, J.K., and Foster, S.J. (2018) Molecular imaging of glycan chains couples cell-wall polysaccharide architecture to bacterial cell

morphology. *Nat Commun* **9**: 1263.

Typas, A., Banzhaf, M., Berg van Saparoea, B. van den, Verheul, J., Biboy, J., Nichols, R.J., *et al.* (2010) Regulation of peptidoglycan synthesis by outer membrane proteins. *Cell* **143**: 1097–1109.

Typas, A., Banzhaf, M., Gross, C.A., and Vollmer, W. (2012) From the regulation of peptidoglycan synthesis to bacterial growth and morphology. *Nat Rev Microbiol* **10**: 123–136.

Ursinus, A., Ent, F. van den, Brechtel, S., Pedro, M. de, Höltje, J., Löwe, J., and Vollmer, W. (2004) Murein (Peptidoglycan) Binding Property of the Essential Cell Division Protein FtsN from *Escherichia coli*. *J Bacteriol* **186**: 6728–6737.

Venter, H., Mowla, R., Ohene-Agyei, T., and Ma, S. (2015) RND-type drug efflux pumps from Gram-negative bacteria: molecular mechanism and inhibition. *Front Microbiol* **6**: 377.

Vila, J., Sáez-López, E., Johnson, J.R., Römling, U., Dobrindt, U., Cantón, R., *et al.* (2016) *Escherichia coli*: An old friend with new tidings. *FEMS Microbiol Rev* **40**: 437–463.

Vocadlo, D.J., Davies, G.J., Laine, R., and Withers, S.G. (2001) Catalysis by hen egg-white lysozyme proceeds via a covalent intermediate. *Nature* **412**: 835–838.

Vollmer, W., and Bertsche, U. (2008) Murein (peptidoglycan) structure, architecture and biosynthesis in *Escherichia coli*. *Biochim Biophys Acta - Biomembr* **1778**: 1714–1734.

Vollmer, W., Blanot, D., and Pedro, M.A. De (2008) Peptidoglycan structure and architecture. *FEMS Microbiol Rev* **32**: 149–167.

Vollmer, W., Joris, B., Charlier, P., and Foster, S. (2008) Bacterial peptidoglycan (murein) hydrolases. *FEMS Microbiol Rev* **32**: 259–286.

Walburger, A., Lazdunski, C., and Corda, Y. (2002) The Tol/Pal system function requires an interaction between the C-terminal domain of TolA and the N-terminal domain of TolB. *Mol Microbiol* **44**: 695–708.

Walkowiak, G.P. (2017) The development of high-throughput assays and screening to enable the discovery of class A penicillin-binding proteins inhibitors. *Univ Warwick* .

Walsh, C.T., and Wencewicz, T.A. (2014) Prospects for new antibiotics: A molecule-centered perspective. *J Antibiot (Tokyo)* **67**: 7–22.

Wang, T.S.A., Manning, S.A., Walker, S., and Kahne, D. (2008) Isolated peptidoglycan glycosyltransferases from different organisms produce different glycan chain lengths. *J Am Chem Soc* **130**: 14068–14069.

Waxman, D.J., and Strominger, J.L. (1983) Penicillin-Binding Proteins and the Mechanism of Action of Beta-Lactam Antibiotics. *Annu Rev Biochem* **52**: 825–869.

Weidel, W., and Pelzer, H. (1964) Bagshaped macromolecules - a new outlook on bacterial cell walls. *Adv Enzymol* **26**: 193–232.

Weiss, D.S., Pogliano, K., Carson, M., Guzman, L., Fraipont, C., Nguyen-Distèche, M., *et al.* (1997) Localization of the *Escherichia coli* cell division protein FtsI (PBP3) to the division site and cell pole. *Mol Microbiol* **25**: 671–681.

Welsh, M.A., Schaefer, K., Taguchi, A., Kahne, D., and Walker, S. (2019) The direction of chain growth and substrate preferences of SEDS-family peptidoglycan glycosyltransferases. *J Am Chem Soc* jacs.9b06358.

WHO (2015) Global action plan on antimicrobial resistance. *WHO Press* 1–28.

Wilks, J.C., and Slonczewski, J.L. (2007) pH of the cytoplasm and periplasm of *Escherichia coli*: Rapid measurement by green fluorescent protein fluorimetry. *J Bacteriol* **189**: 5601–5607.

Wilson, T.J., Liu, Y., and Lilley, D.M.J. (2016) Ribozymes and the mechanisms that underlie RNA catalysis. *Front Chem Sci Eng* **10**: 178–185.

Wong, J.D., Barash, J.R., and Sandfort, R.F. (2000) Susceptibilities of *Yersinia pestis* Strains to 12 Antimicrobial Agents. *Antimicrob Agents Chemother* **44**: 1995–1997.

Yang, J.C., Ent, F. Van Den, Neuhaus, D., Brevier, J., and Löwe, J. (2004) Solution structure and domain architecture of the divisome protein FtsN. *Mol Microbiol* **52**: 651–660.

Yang, R. (2018) Plague: Recognition, Treatment, and Prevention. *J Clin Microbiol* **56**: e01519-17.

Yousif, S., Broome-Smith, J., and Spratt, B. (1985) Lysis of *Escherichia coli* by beta-lactam antibiotics: deletion analysis of the role of penicillin-binding proteins 1A and 1B. *J Gen Microbiol* **131**: 2839–45.

Zervosen, A., Sauvage, E., Frère, J.M., Charlier, P., and Luxen, A. (2012) Development of new drugs for an old target - The penicillin binding proteins. *Molecules* **17**: 12478–12505.

Zhang, Y., Fechter, E.J., Wang, T.S.A., Barrett, D., Walker, S., and Kahne, D.E. (2007) Synthesis of heptaprenyl-lipid IV to analyze peptidoglycan glycosyltransferases. *J Am Chem Soc* **129**: 3080–3081.

Zhang, Y., Kashikar, A., Brown, C.A., Denys, G., and Bush, K. (2017) Unusual *Escherichia coli* PBP 3 Insertion Sequence Identified from a Collection of Carbapenem-Resistant *Enterobacteriaceae* Tested *In Vitro* with a Combination of Ceftazidime-, Ceftaroline-, or Aztreonam-Avibactam. *Antimicrob Agents Chemother* **61**: e00389-17.

Zhou, M., Diwu, Z., Panchuk-Voloshina, N., and Haugland, R.P. (1997) A Stable Nonfluorescent Derivative of Resorufin for the Fluorometric Determination of Trace Hydrogen Peroxide: Applications in Detecting the Activity of Phagocyte

NADPH Oxidase and Other Oxidases. *Anal Biochem* **253**: 162–168.

9. Appendix

9.1 Extinction coefficient of resorufin over pH 7.5-11.0

pH	Extinction coefficient $\pm$ SD
7.5	21313 ± 4685
8.0	26188 ± 5922
8.5	52563 ± 5392
9.0	63487 ± 5535
9.5	71502 ± 7612
10.0	77938 ± 2386
10.5	78534 ± 1779
11.0	78438 ± 1326

Appendix 9.1 Extinction coefficient of resorufin over pH 7.5-11.0.
D-Ala release rate was assayed using the amplex red assay for D-Ala release. Reactions consisted of 50 mM buffer, 6 mM NaCl, 20 mM $MgCl_2$, 1% (v/v) glycerol, 0.130% (v/v) Triton X-100, amplex red coupling reagents and 8 or 34 μM H_2O_2. Buffers used were Bis-Tris propane pH 7.5-8.5, CHES pH 9.0-9.5, CAPS pH 10.0-11.0. Data is shown as mean $\pm$ SD (n=3).

9.2 *E. coli* PBP1b glycan chain polymerisation in the presence of varied metal ions

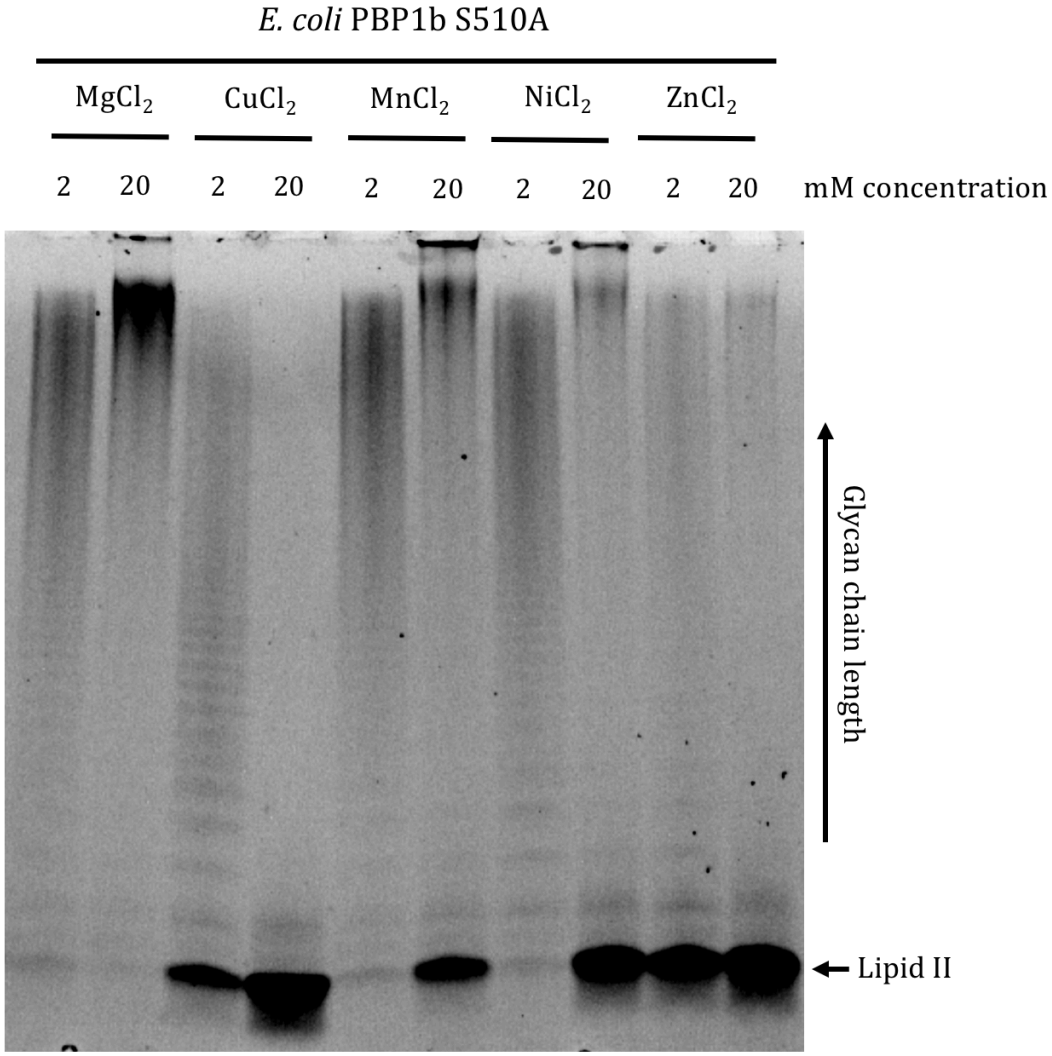

Appendix 9.2 *E. coli* PBP1b glycan chain polymerisation in the presence of varied metal ions.
E. coli PBP1b glycosyltransferase activity was assayed by the polymerisation of fluorescently labelled Lipid II *in vitro,* where the glycan chain products were separated by SDS-PAGE and visualised using the fluorescence of the dansyl group labelling the stem peptide. 1 hour reactions consisted of 50 mM Bis-Tris propane pH 8.5, 15 mM NaCl, varied divalent metal ion concentration, 10% (v/v) DMSO, 1% (v/v) glycerol, 0.130% (v/v) Triton X-100, 10 μM Lipid II (dansyl DAP), 50 nM *E. coli* PBP1b S510A and 2 μM LpoB (n=1).

9.3 Effect of moenomycin on the migration of Lipid II by SDS-PAGE

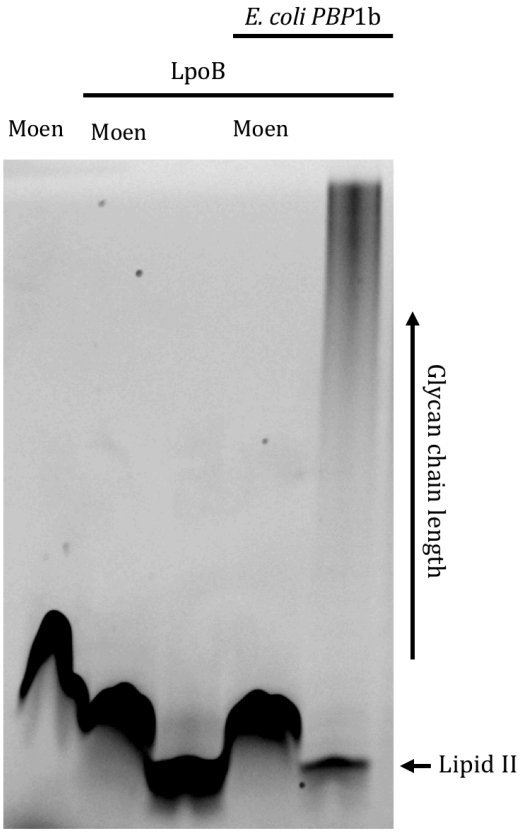

Appendix 9.3 Effect of moenomycin on the migration of Lipid II by SDS-PAGE
E. coli PBP1b glycosyltransferase activity was assayed by the polymerisation of fluorescently labelled Lipid II *in vitro,* where the glycan chain products were separated by SDS-PAGE and visualised using the fluorescence of the dansyl group labelling the stem peptide. 2 hour reactions consisted of 50 mM HEPES pH 7.5, 115 mM NaCl, 10 mM $MgCl_2$, 10% (v/v) DMSO, 1% (v/v) glycerol, 0.155% (v/v) Triton X-100, 10 μM Lipid II (dansyl DAP), 100 nM *E. coli* PBP1b, 4 μM LpoB and 5 μM moenomycin (Moen) (n=1).

9.4 LCMSMS of *E. coli* PBP1b S510A recombinant protein

Appendix 9.4 LCMSMS of *E. coli* PBP1b S510A.

LCMSMS analysis identifying all the proteins in the *E. coli* PBP1b S510A purified protein sample. The identified peptides were searched against the *Escherichia coli* database (www.uniprot.org/proteomes) and the common contaminant database from MaxQuant. Protein sample was prepared for LCMSMS by reduction with TCEP, trypsin digestion and C18 membrane clean-up.

Protein name	Protein accession numbers	MW (Da)	Protein probability	Peptide count	Spectrum count	% total spectra	% sequence coverage
Penicillin-binding protein 1B OS=Escherichia coli (strain K12) GN=mrcB PE=1 SV=2	PBPB_ECOLI	94295	100.00%	71	151	33.90%	62.00%
CON__P00761= Trypsin, Sus scrofa (Pig)	CON__P00761	-	100.00%	11	19	3.97%	-
Peptidoglycan synthase FtsI OS=Escherichia coli (strain K12) GN=ftsI PE=1 SV=1	FTSI_ECOLI	63878	100.00%	27	37	3.97%	43.20%
Chaperone protein DnaJ OS=Escherichia coli (strain K12) GN=dnaJ PE=1 SV=3	DNAJ_ECOLI	41100	100.00%	18	24	2.50%	45.20%
ATP synthase subunit b OS=Escherichia coli (strain K12) GN=atpF PE=1 SV=1	ATPF_ECOLI	17265	100.00%	18	24	2.07%	72.40%
Phage shock protein B OS=Escherichia coli (strain K12) GN=pspB PE=1 SV=1	PSPB_ECOLI	8764	100.00%	9	16	1.90%	56.80%
50S ribosomal protein L2 OS=Escherichia coli (strain K12) GN=rplB PE=1 SV=2	RL2_ECOLI	29860	100.00%	14	19	1.73%	52.70%
50S ribosomal protein L5 OS=Escherichia coli (strain K12) GN=rplE PE=1 SV=2	RL5_ECOLI	20303	100.00%	14	18	1.55%	92.70%
Ferric uptake regulation protein OS=Escherichia coli (strain K12) GN=fur PE=1 SV=1	FUR_ECOLI	16795	100.00%	12	16	1.47%	60.80%
Major outer membrane lipoprotein Lpp OS=Escherichia coli (strain K12) GN=lpp PE=1 SV=1	LPP_ECOLI	8324	100.00%	11	15	1.29%	48.70%
Outer membrane protein A OS=Escherichia coli (strain K12) GN=ompA PE=1 SV=1	OMPA_ECOLI	37201	100.00%	10	15	1.29%	24.00%
CON__P04264= Keratin, type II cytoskeletal 1, Human	CON__P04264	-	100.00%	11	12	1.21%	-
Inner membrane protein YhcB OS=Escherichia coli (strain K12) GN=yhcB PE=1 SV=2	YHCB_ECOLI	14961	100.00%	7	9	1.04%	51.50%
50S ribosomal protein L6 OS=Escherichia coli (strain K12) GN=rplF PE=1 SV=2	RL6_ECOLI	18904	100.00%	10	11	0.95%	53.70%
Elongation factor Tu 1 OS=Escherichia coli (strain K12) GN=tufA PE=1 SV=1	EFTU1_ECOLI,EFTU2_ECOLI	43314	100.00%	11	11	0.95%	24.90%
50S ribosomal protein L14 OS=Escherichia coli (strain K12) GN=rplN PE=1 SV=1	RL14_ECOLI	13541	100.00%	8	10	0.86%	50.40%
Chaperone protein DnaK OS=Escherichia coli (strain K12) GN=dnaK PE=1 SV=2	DNAK_ECOLI	69116	100.00%	9	10	0.86%	15.50%
30S ribosomal protein S5 OS=Escherichia coli (strain K12) GN=rpsE PE=1 SV=2	RS5_ECOLI	17603	100.00%	8	9	0.78%	51.50%
Uncharacterized protein YqjD OS=Escherichia coli (strain K12) GN=yqjD PE=1 SV=1	YQJD_ECOLI	11052	100.00%	8	9	0.78%	64.40%
Uncharacterized protein YgiM OS=Escherichia coli (strain K12) GN=ygiM PE=3 SV=1	YGIM_ECOLI	23077	100.00%	5	7	0.69%	36.40%
Uncharacterized protein YibN OS=Escherichia coli (strain K12) GN=yibN PE=1 SV=1	YIBN_ECOLI	15596	100.00%	6	7	0.69%	28.00%
30S ribosomal protein S4 OS=Escherichia coli (strain K12) GN=rpsD PE=1 SV=2	RS4_ECOLI	23470	100.00%	7	8	0.69%	40.30%
30S ribosomal protein S12 OS=Escherichia coli (strain K12) GN=rpsL PE=1 SV=2	RS12_ECOLI	13737	100.00%	6	8	0.69%	40.30%
50S ribosomal protein L17 OS=Escherichia coli (strain K12) GN=rplQ PE=1 SV=1	RL17_ECOLI	14365	100.00%	6	6	0.52%	37.80%
Outer membrane lipoprotein SlyB OS=Escherichia coli (strain K12) GN=slyB PE=2 SV=1	SLYB_ECOLI	15601	100.00%	4	4	0.43%	38.10%
CON__P35908= Keratin, type II cytoskeletal 2, epidermal, Human	CON__P35908	-	100.00%	5	5	0.43%	-
30S ribosomal protein S2 OS=Escherichia coli (strain K12) GN=rpsB PE=1 SV=2	RS2_ECOLI	26744	100.00%	4	5	0.43%	18.70%
30S ribosomal protein S10 OS=Escherichia coli (strain K12) GN=rpsJ PE=1 SV=1	RS10_ECOLI	11736	100.00%	4	5	0.43%	38.80%
Phage shock protein C OS=Escherichia coli (strain K12) GN=pspC PE=1 SV=1	PSPC_ECOLI	13518	100.00%	4	5	0.43%	32.80%
30S ribosomal protein S11 OS=Escherichia coli (strain K12) GN=rpsK PE=1 SV=2	RS11_ECOLI	13845	100.00%	4	5	0.43%	24.80%
CON__P35527= Keratin, type I cytoskeletal 9, Human	CON__P35527	-	100.00%	5	5	0.43%	-
Glutamate/aspartate import solute-binding protein OS=Escherichia coli (strain K12) GN=gltI PE=1 SV=2	GLTI_ECOLI	33421	100.00%	3	4	0.35%	12.30%
CON__P02538= Keratin, type II cytoskeletal 6A, Human	CON__P02538	-	99.90%	1	1	0.35%	0.00%
Periplasmic serine endoprotease DegP OS=Escherichia coli (strain K12) GN=degP PE=1 SV=1	DEGP_ECOLI	49355	100.00%	3	3	0.35%	9.49%
Protein HemY OS=Escherichia coli (strain K12) GN=hemY PE=1 SV=1	HEMY_ECOLI	45246	100.00%	4	4	0.35%	11.60%
Maltose-binding periplasmic protein OS=Escherichia coli (strain K12) GN=malE PE=1 SV=1	MALE_ECOLI	43390	100.00%	4	4	0.35%	15.90%
CON__P04259= Cluster of Keratin, type II cytoskeletal 6B, Human	CON__P04259	-	99.90%	1	1	0.35%	-
CON__P13645= Keratin, type I cytoskeletal 10, Human	CON__P13645	-	100.00%	4	4	0.35%	-
CON__P02768-1= Serum albumin, Human	CON__P02768-1	-	100.00%	3	3	0.26%	-
Penicillin-binding protein activator LpoB OS=Escherichia coli (strain K12) GN=lpoB PE=1 SV=1	LPOB_ECOLI	22515	100.00%	3	3	0.26%	23.50%
30S ribosomal protein S14 OS=Escherichia coli (strain K12) GN=rpsN PE=1 SV=2	RS14_ECOLI	11581	100.00%	3	3	0.26%	35.60%
ATP-dependent zinc metalloprotease FtsH OS=Escherichia coli (strain K12) GN=ftsH PE=1 SV=1	FTSH_ECOLI	70710	100.00%	3	3	0.26%	5.90%
50S ribosomal protein L10 OS=Escherichia coli (strain K12) GN=rplJ PE=1 SV=2	RL10_ECOLI	17712	100.00%	3	3	0.26%	21.80%
Multidrug efflux pump subunit AcrA OS=Escherichia coli (strain K12) GN=acrA PE=1 SV=1	ACRA_ECOLI	42197	100.00%	3	3	0.26%	12.60%
Succinate dehydrogenase flavoprotein subunit OS=Escherichia coli (strain K12) GN=sdhA PE=1 SV=1	SDHA_ECOLI	64422	100.00%	3	3	0.26%	6.46%
CON__P13647= Keratin, type II cytoskeletal 5, Human	CON__P13647	-	100.00%	3	3	0.26%	-
30S ribosomal protein S21 OS=Escherichia coli (strain K12) GN=rpsU PE=1 SV=2	RS21_ECOLI	8500	99.90%	2	2	0.17%	31.00%
30S ribosomal protein S17 OS=Escherichia coli (strain K12) GN=rpsQ PE=1 SV=2	RS17_ECOLI	9704	100.00%	2	2	0.17%	20.20%
30S ribosomal protein S3 OS=Escherichia coli (strain K12) GN=rpsC PE=1 SV=2	RS3_ECOLI	25984	100.00%	2	2	0.17%	9.87%
Protease HtpX OS=Escherichia coli (strain K12) GN=htpX PE=1 SV=1	HTPX_ECOLI	31924	99.90%	2	2	0.17%	4.78%
Ribonuclease E OS=Escherichia coli (strain K12) GN=rne PE=1 SV=6	RNE_ECOLI	118194	100.00%	2	2	0.17%	2.45%
50S ribosomal protein L13 OS=Escherichia coli (strain K12) GN=rplM PE=1 SV=1	RL13_ECOLI	16019	98.90%	2	2	0.17%	18.30%
GTP cyclohydrolase 1 OS=Escherichia coli (strain K12) GN=folE PE=1 SV=2	GCH1_ECOLI	24831	99.90%	2	2	0.17%	7.66%
50S ribosomal protein L1 OS=Escherichia coli (strain K12) GN=rplA PE=1 SV=2	RL1_ECOLI	24729	100.00%	2	2	0.17%	12.80%
30S ribosomal protein S18 OS=Escherichia coli (strain K12) GN=rpsR PE=1 SV=2	RS18_ECOLI	8987	99.70%	1	2	0.17%	16.00%
Outer membrane lipoprotein RcsF OS=Escherichia coli (strain K12) GN=rcsF PE=1 SV=1	RCSF_ECOLI	14164	100.00%	2	2	0.17%	26.90%
ATP-dependent protease ATPase subunit HslU OS=Escherichia coli (strain K12) GN=hslU PE=1 SV=1	HSLU_ECOLI	49595	99.70%	2	2	0.17%	6.32%
Osmotically-inducible lipoprotein E OS=Escherichia coli (strain K12) GN=osmE PE=2 SV=1	OSME_ECOLI	12021	97.60%	1	1	0.09%	9.82%
50S ribosomal protein L11 OS=Escherichia coli (strain K12) GN=rplK PE=1 SV=2	RL11_ECOLI	14876	97.60%	1	1	0.09%	7.04%
UPF0265 protein YeeX OS=Escherichia coli (strain K12) GN=yeeX PE=1 SV=1	YEEX_ECOLI	12779	80.80%	1	1	0.09%	7.34%
30S ribosomal protein S9 OS=Escherichia coli (strain K12) GN=rpsI PE=1 SV=2	RS9_ECOLI	14857	91.70%	1	1	0.09%	6.15%
Succinate--CoA ligase [ADP-forming] subunit beta OS=Escherichia coli (strain K12) GN=sucC PE=1 SV=1	SUCC_ECOLI	41393	92.10%	1	1	0.09%	2.32%
60 kDa chaperonin OS=Escherichia coli (strain K12) GN=groL PE=1 SV=2	CH60_ECOLI	57329	90.40%	1	1	0.09%	2.19%
Peptidyl-prolyl cis-trans isomerase D OS=Escherichia coli (strain K12) GN=ppiD PE=1 SV=1	PPID_ECOLI	68151	97.20%	1	1	0.09%	1.61%
CON__P15636= Protease 1, Achromobacter lyticus	CON__P15636	-	87.00%	1	1	0.09%	-
Uncharacterized protein YobH OS=Escherichia coli (strain K12) GN=yobH PE=3 SV=1	YOBH_ECOLI	8515	97.40%	1	1	0.09%	13.90%
Translation initiation factor IF-2 OS=Escherichia coli (strain K12) GN=infB PE=1 SV=1	IF2_ECOLI	97349	95.10%	1	1	0.09%	1.35%
FKBP-type peptidyl-prolyl cis-trans isomerase FkpA OS=Escherichia coli (strain K12) GN=fkpA PE=1 SV=1	FKBA_ECOLI	28883	89.60%	1	1	0.09%	4.07%
Toxin CptA OS=Escherichia coli (strain K12) GN=cptA PE=1 SV=1	CPTA_ECOLI	16065	97.60%	1	1	0.09%	6.67%
Lipopolysaccharide assembly protein A OS=Escherichia coli (strain K12) GN=lapA PE=1 SV=1	LAPA_ECOLI	11352	82.00%	1	1	0.09%	22.50%
Glycerol dehydrogenase OS=Escherichia coli (strain K12) GN=gldA PE=1 SV=1	GLDA_ECOLI	38713	97.60%	1	1	0.09%	2.45%
CON__P05787= Keratin, type II cytoskeletal 8, Human	CON__P05787	-	97.60%	1	1	0.09%	-
CON__Q3SX09= Hemoglobin fetal subunit beta, Bos taurus (Bovine)	CON__Q3SX09	-	80.10%	1	1	0.09%	-
Succinate--CoA ligase [ADP-forming] subunit alpha OS=Escherichia coli (strain K12) GN=sucD PE=1 SV=2	SUCD_ECOLI	29778	96.70%	1	1	0.09%	3.11%
ATP synthase subunit alpha OS=Escherichia coli (strain K12) GN=atpA PE=1 SV=1	ATPA_ECOLI	55223	91.70%	1	1	0.09%	1.56%
CON__P07477= Trypsin 1, Human	CON__P07477	-	92.80%	1	1	0.09%	-
Integration host factor subunit beta OS=Escherichia coli (strain K12) GN=ihfB PE=1 SV=1	IHFB_ECOLI	10652	82.90%	1	1	0.09%	9.57%
UPF0352 protein YejL OS=Escherichia coli (strain K12) GN=yejL PE=1 SV=1	YEJL_ECOLI	8289	81.60%	1	1	0.09%	16.00%
HTH-type transcriptional regulator GntR OS=Escherichia coli (strain K12) GN=gntR PE=1 SV=1	GNTR_ECOLI	36423	91.70%	1	1	0.09%	2.42%
50S ribosomal protein L15 OS=Escherichia coli (strain K12) GN=rplO PE=1 SV=1	RL15_ECOLI	14981	95.30%	1	1	0.09%	9.72%
50S ribosomal protein L28 OS=Escherichia coli (strain K12) GN=rpmB PE=1 SV=2	RL28_ECOLI	9007	97.60%	1	1	0.09%	12.80%
Isocitrate dehydrogenase [NADP] OS=Escherichia coli (strain K12) GN=icd PE=1 SV=1	IDH_ECOLI	45758	97.00%	1	1	0.09%	2.88%
Uncharacterized protein YgaM OS=Escherichia coli (strain K12) GN=ygaM PE=1 SV=2	YGAM_ECOLI	11847	94.50%	1	1	0.09%	8.26%
Undecaprenyl-phosphate 4-deoxy-4-formamido-L-arabinose transferase OS=Escherichia coli (strain K12) GN=arnC PE=1 SV=1	ARNC_ECOLI	36340	95.00%	1	1	0.09%	4.66%

9.5 LCMSMS of *E. coli* LpoB recombinant protein

Appendix 9.5 LCMSMS of *E. coli* LpoB.

LCMSMS analysis identifying all the proteins in the *E. coli* LpoB purified protein sample. The identified peptides were searched against the *Escherichia coli* database (www.uniprot.org/proteomes) and the common contaminant database from MaxQuant. Protein sample was prepared for LCMSMS by reduction with TCEP, trypsin digestion and C18 membrane clean-up.

Protein name	Protein accession numbers	MW (Da)	Protein probability	Peptide count	Spectrum count	% total spectra	% sequence coverage
Penicillin-binding protein activator LpoB OS=Escherichia coli (strain K12) GN=lpoB PE=1 SV=1	LPOB_ECOLI	22,515.20	100.00%	15	38	49.00%	54.90%
CON__P00761= Trypsin, Sus scrofa (Pig)	CON__P00761	-	100.00%	10	16	4.78%	-
CON__P08779= Cluster of Keratin, type I cytoskeletal 16, Human	CON__P08779	-	100.00%	7	8	2.22%	-
CON__P04259= Cluster of Keratin, type II cytoskeletal 6B, Human	CON__P04259	-	100.00%	2	2	1.54%	-
CON__P02533= Keratin, type I cytoskeletal 14, Human	CON__P02533	-	100.00%	2	2	1.54%	-
CON__P02538= Keratin, type II cytoskeletal 6A, Human	CON__P02538	-	100.00%	1	1	1.37%	-
Cell division protein FtsN OS=Escherichia coli (strain K12) GN=ftsN PE=1 SV=3	FTSN_ECOLI	35,792.30	100.00%	8	8	1.37%	23.50%
CON__P04264= Keratin, type II cytoskeletal 1, Human	CON__P04264	-	100.00%	7	7	1.37%	-
Chaperone protein DnaK OS=Escherichia coli (strain K12) GN=dnaK PE=1 SV=2	DNAK_ECOLI	69,116.10	100.00%	6	6	1.19%	8.46%
CON__P13645= Keratin, type I cytoskeletal 10, Human	CON__P13645	-	100.00%	4	4	1.02%	-
CON__P35908= Keratin, type II cytoskeletal 2 epidermal, Human	CON__P35908	-	100.00%	3	3	1.02%	-
50S ribosomal protein L2 OS=Escherichia coli (strain K12) GN=rplB PE=1 SV=2	RL2_ECOLI	29,860.30	100.00%	5	6	1.02%	19.40%
Ferric uptake regulation protein OS=Escherichia coli (strain K12) GN=fur PE=1 SV=1	FUR_ECOLI	16,795.00	100.00%	5	5	0.85%	37.20%
CON__P35527= Keratin, type I cytoskeletal 9, Human	CON__P35527	-	100.00%	4	4	0.68%	-
GTP cyclohydrolase 1 OS=Escherichia coli (strain K12) GN=folE PE=1 SV=2	GCH1_ECOLI	24,831.00	100.00%	3	4	0.68%	18.90%
CON__P13647= Keratin, type II cytoskeletal 5, Human	CON__P13647	-	100.00%	2	2	0.68%	-
50S ribosomal protein L15 OS=Escherichia coli (strain K12) GN=rplO PE=1 SV=1	RL15_ECOLI	14,981.10	100.00%	4	4	0.68%	34.70%
Uncharacterized protein YqjD OS=Escherichia coli (strain K12) GN=yqjD PE=1 SV=1	YQJD_ECOLI	11,051.70	100.00%	4	4	0.68%	39.60%
Iron-sulfur cluster assembly scaffold protein IscU OS=Escherichia coli (strain K12) GN=iscU PE=1 SV=1	ISCU_ECOLI	13,848.90	100.00%	2	3	0.51%	10.90%
D-alanyl-D-alanine carboxypeptidase DacB OS=Escherichia coli (strain K12) GN=dacB PE=1 SV=2	DACB_ECOLI	51,799.40	100.00%	2	2	0.34%	5.24%
CON__Q14532= Keratin, type I cuticular Ha2, Human	CON__Q14532,CON__Q15323	-	96.80%	1	1	0.34%	-
30S ribosomal protein S12 OS=Escherichia coli (strain K12) GN=rpsL PE=1 SV=2	RS12_ECOLI	13,736.80	100.00%	2	2	0.34%	16.90%
Peptidoglycan synthase FtsI OS=Escherichia coli (strain K12) GN=ftsI PE=1 SV=1	FTSI_ECOLI	63,878.40	100.00%	2	2	0.34%	3.74%
CON__Q6ISB0= Keratin, type II cuticular Hb4, Human	CON__Q6ISB0,CON__Q9NSB2	-	99.60%	1	1	0.34%	-
Elongation factor Tu 1 OS=Escherichia coli (strain K12) GN=tufA PE=1 SV=1	EFTU1_ECOLI,EFTU2_ECOLI	43,313.80	100.00%	2	2	0.34%	5.33%
Universal stress protein UP12 OS=Escherichia coli (strain K12) GN=uspG PE=1 SV=2	USPG_ECOLI	15,934.80	94.10%	1	1	0.17%	7.04%
60 kDa chaperonin OS=Escherichia coli (strain K12) GN=groL PE=1 SV=2	CH60_ECOLI	57,328.90	97.30%	1	1	0.17%	2.19%
Maltose-binding periplasmic protein OS=Escherichia coli (strain K12) GN=malE PE=1 SV=1	MALE_ECOLI	43,389.90	93.20%	1	1	0.17%	2.78%
3-ketoacyl-CoA thiolase OS=Escherichia coli (strain K12) GN=fadA PE=1 SV=3	FADA_ECOLI	40,876.40	97.30%	1	1	0.17%	2.84%
P0A9B6= D-erythose-4-phosphate dehydrogenase, Escherichia coli (strain K12)	P0A9B6-DECOY	-	95.90%	1	1	0.17%	-
Ribonuclease E OS=Escherichia coli (strain K12) GN=rne PE=1 SV=6	RNE_ECOLI	118,194.00	99.00%	1	1	0.17%	1.60%
30S ribosomal protein S14 OS=Escherichia coli (strain K12) GN=rpsN PE=1 SV=2	RS14_ECOLI	11,581.00	99.10%	1	1	0.17%	9.90%
Acyl carrier protein OS=Escherichia coli (strain K12) GN=acpP PE=1 SV=2	ACP_ECOLI	8,639.40	89.90%	1	1	0.17%	10.30%

9.6 LCMS analysis of *P. aeruginosa* PBP3 reaction products from pentapeptide (acetylated DAP) glycan polymers

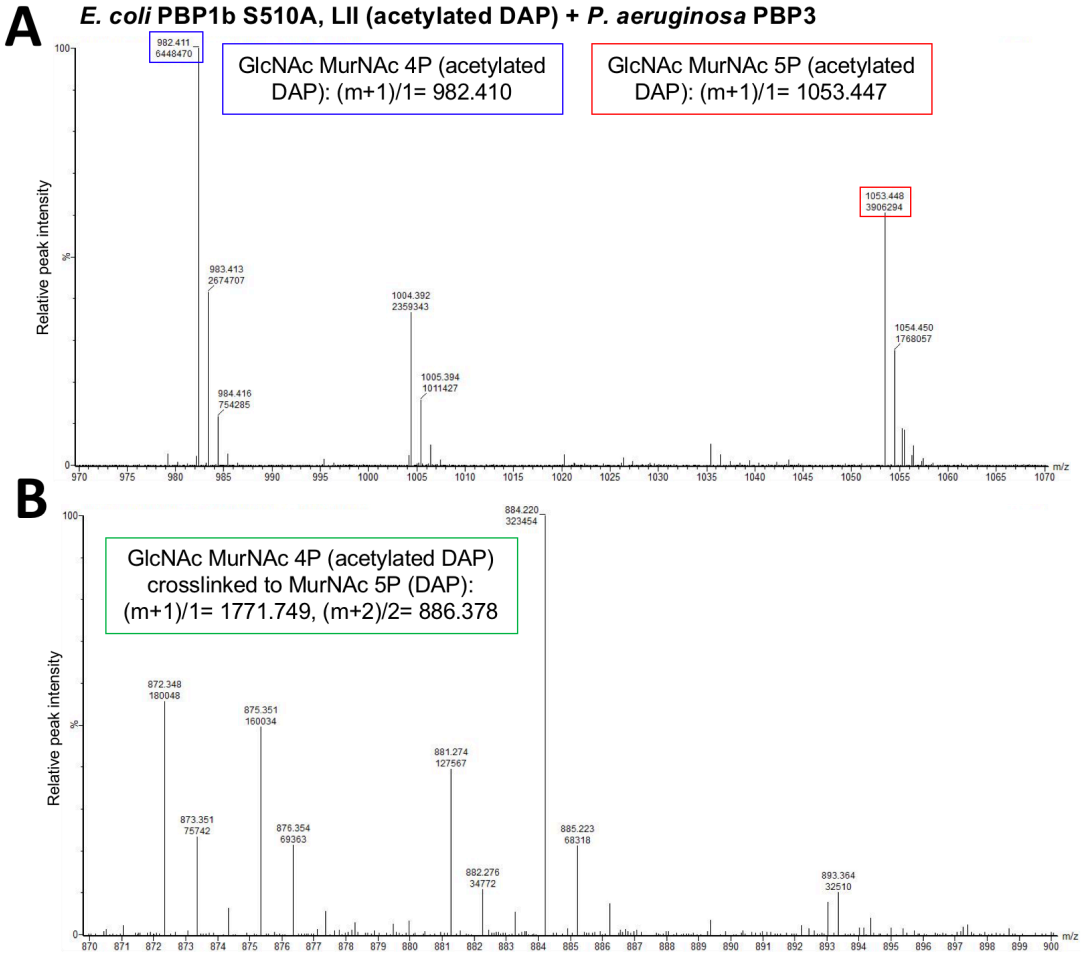

Appendix 9.6 LCMS analysis of *P. aeruginosa* PBP3 reaction products from pentapeptide (acetylated DAP) glycan polymers.
Positive ion LCMS analysis of *E. coli* PBP1b S510A and *P. aeruginosa* PBP3 reaction products from Lipid II (acetylated DAP). Reactions consisted of 50 mM Bis-Tris propane pH 8.5, 6 mM NaCl, 2 mM $MgCl_2$, 1% (v/v) glycerol, 0.0468% (v/v) E_6C_{12}, amplex red coupling reagents, 20 μM Lipid II (acetylated DAP), 50 nM *E. coli* PBP1b S510A, 2 μ M LpoB and 430 nM *P. aeruginosa* PBP3. Prepared for LCMS by mutanolysin digestion, and the addition of $NaBH_4$ and phosphoric acid. Major peaks are annotated as m/z and ion count, determined by combining the spectrums of the peak relating to the ion of interest.